THE VIBRATION CHARACTERISTICS OF PIEZOELECTRIC DISCS

by

Ningqun Guo

A thesis submitted to the University of London

for the degree of Doctor of Philosophy

and for the Diploma of Imperial College

Department of Mechanical Engineering

Imperial College of Science, Technology and Medicine

London SW7

October 1989

Abstract

Most of the techniques to analyse the vibration characteristics of piezoelectric discs are one dimensional, which assumes that the piezoelectric disc vibrates in the thickness direction only (piston-like motion) and is applicable to discs with either very large diameter to thickness ratio (D/T ratio) or very small D/T ratio. However, it cannot predict other modes of vibration of the piezoelectric disc, which may affect the transducer behaviour in the frequency range of interest, especially for those discs with finite D/T ratios.

Finite element methods and modal analysis techniques have been used to predict the vibration characteristics of piezoelectric discs. The modal constant has been employed to evaluate the strength of excitation of the modes which can be excited by applying voltages across the disc.

The finite element study of piezoelectric discs shows that many modes including radial, edge, thickness shear, thickness extensional, and high frequency radial modes are predicted in the frequency range of interest. However, no mode has been predicted having piston-like motion assumed by the one dimensional model. The most strongly excited modes of the discs are the thickness extensional modes, which are in the frequency range of the first through thickness mode predicted by the one dimensional model, and have non-zero mean value of the axial displacement over the surface of the disc, and the number of thickness extensional modes is reduced with increasing the D/T ratio. It has been shown that the thickness extensional modes have much larger modal constants than the other modes especially in discs with D/T ratio larger than 5. When the D/T ratio is very large, one single thickness extensional mode which has a very large modal constant occurs and dominates the response, this is analogous to the one dimensional assumption. The finite element model has been validated by the excellent agreement between the predicted and measured electrical impedance responses and by the qualitative agreement between the predicted and measured mode shapes.

The predicted transient mechanical displacement over the surface of the piezoelectric disc when it is excited by voltage pulses across the two electrodes shows that the disc may display piston-like motion over the first few periods of the through thickness mode due to high modal density and modal coupling effects. The surface motion then becomes more complicated since other lower frequency modes come into effect. Finally the surface motion tends to gradually approach that of the first radial mode, which is the last mode to be damped out.

The application of the three dimensional model to analyse piezoelectric discs with an elastic addition and partially electroded discs has demonstrated the potential of the techniques for use in the design of transducers of more complicated structure, and transducers with non-uniformly distributed electrodes. However, further work is required if more practical aspects of transducers, such as backing and interaction with mounting structures and the surrounding fluid are considered.

Acknowledgements

First of all, I would like to thank Dr. Peter Cawley for his encouragement and guidance throughout the course of the research. I am particularly indebted to Mr. Denis Hitchings for many useful discussions and helps. Thanks are also due to the acadamic and technical staffs in the Dynamic section of the mechanical department for their assitance.

Finally, I would also like to thank both the Chinese Education Commission and British Council for their support for providing the scholarship.

Contents

List of Tables

List of Figures

Nomenclature

Symbols for material properties are listed in Appendix A. In some cases multiple definitions have been made due to the large nunmber of parameters used, but they can be easily identified from the context.

1. Normal letters

a	Thickness of a piezoelectric element
A	Area; Amplitude
[B]	Strain matrix
c	Elastic constants, longitudinal velocity
[C]	Generalised material constants matrix
c_1	Mechanical viscous damping coefficient
C_0	Static capacitance by the 1D model
D	Diameter of the piezoelectric discs
D/T	Diameter to thickness ratio
e	Piezoelectric coupling constants
E	Electric fields
f	Frequency
f_a, f_r,	Anti-resonant, resonant frequencies
f_{max}, f_{min}	Frequencies at maximum and minimum impedances
f_p, f_s	Parallel and series frequencies
f_1, f_2	mechanical force and electrical force
{f}	Mechanical displacement vector, = {u, v, w}
$\{f_G\}$	The generalised displacement vector, = $\{f, \phi\}$ = {u, v, w, ϕ}
fT	Product of frequency and thickness
F	Force
F_1, F_2	Amplitudes of the mechanical force and electrical force
[G]	Damping matrix
h	piezoelectric coupling factor
H(t)	Heverside function
$\{H_F\}$	Equivalent nodal force vector
H_r	Product of the equivalent nodal force vector and r'th eigenvector
$H_{\phi\phi}$	Static capacitance of piezoelectric discs predicted by FE analysis
i	imaginary part
k_{ij}	Piezoelectric coupling factors
[K]	Stiffness matrix

[M]	Mass matrix
[N]	Displacement shape function
l	Harmonic number
P	Pressure
Q	Electrical charge, Mechanical quality factor
r	Subscript to denote mode r; Radius
$_rA$	Modal constants = H_r^2
r_0, r_a	Reflection coefficients
r, z, θ	Polar coordinates
S	Mechanical strain; Area
T	Thickness of the piezoelectric discs; mechanical stress
T_0, T_a	Transmission coefficients
U	Strain energy,
W	Potential energy of external loads
u, v, w	Mechanical displacement components in x, y, z directions
v, v_1, v_2	velocity of waves in the piezoelectric material, media 1 and 2
V	Voltage; Volume
x, y, z	Cartesian coordinates
x_1, x_2	Mechanical displacement and electrical potential of piezoelectric discs
X_1, X_2	Amplitudes of the mechanical displacement and electrical potential of piezoelectric discs
z_r	modal amplitude vector
Z(ω)	Electrical impedance of the piezoelectric disc
Z_c, Z_1, Z_2	Acoustic impedance of the piezoelectric material, media 1 and 2

2. Greek letters

α	Time factor
χ	Total energy
{δ}	Generalised nodal displacement vector, = {f, ϕ} = {u, v, w, ϕ}
ε	Dielectric constants
{ε}	Generalised strain vector
ϕ	Electrical potential at nodes
η	Structural damping factor, coupling factor
η, ξ	Local coordinates
φ	Electrical potential at non-zero electrodes
κ	Wavenumbers
λ	Wavelength; Eigenvalue = ω^2
ν	Poisson's ratio

ρ	Density
τ	Time for wave travelling through the thickness of the disc
ω	Angular frequency = $2\pi f$
ψ	Eigenvector
$[\Psi]$	Eigenvector matrix

3. Brackets

$[\,]$	Matrix
$[\,]^T$	Transpose of a matrix
$[\,]^{-1}$	Inverse of a matrix
$\{\,\}$	Vector
$\{\,\}^T$	Transpose of a vector, or an one column vector

CHAPTER 1

INTRODUCTION

1.1 Piezoelectricity and piezoelectric transducers

Piezoelectricity is a phenomenon which allows electric polarisation to be produced by mechanical strains in certain materials. This is defined as the direct piezoelectric effect. The indirect piezoelectric effect is the inverse process, in which mechanical strain in the material may be induced by electrical polarisation. The variables are in linear relationship to one another in both direct and indirect processes.

Piezoelectricity was first found in crystals by the Pierre and Curie brothers in 1880 (Mason, 1948). The piezoelectric effect is a property of the crystal structure, and a necessary condition for the existence of piezoelectricity is a certain type of asymmetry in the material. Piezoelectric materials are therefore inherently anisotropic. Three groups of piezoelectric materials may be classified as indicated below.

The first group of materials are crystals, which are usually inherently piezoelectric to some extent and whose properties are determined by their crystallographic structure. Crystals are characterised by having one or more polar axes. The mechanical strain due to any pressure on the crystal can shift the electrically charged elements of the crystal lattice, which results in electrical charges appearing on the surface of the material due to the asymmetry. When crystals are placed in an electric field, the electrically charged elements of the crystal are distorted due to the asymmetry, which results in deformation of the crystals. Crystals which exhibit this effect strongly include sodium potassium tartrate (Rochelle salt), ammonium dihydrogen phosphate (ADP), and quartz.

The second group of piezoelectric materials are piezoelectric ceramics, such as barium titanate ($BaTiO_3$), lead zirconate titanate ($Pb(Zr.Ti)O_3$, trademark PZT) and lead metaniobate ($PbNb_2O_6$). Ceramics are initially isotropic materials and are subsequently polarised above the Curie temperature by applying strong electric fields to induce anisotropy or asymmetry in certain directions. After the ceramic is cooled down within the electric field, the anisotropic structure and the polarisation responsible for their piezoelectric properties remain even after the electric field is removed. Usually ceramics exhibit strong piezoelectric effects, have a high dielectric constant and their properties are essentially independent of humidity and temperature (Allocca and Stuart, 1983).

Polymers are another group of materials which exhibit piezoelectric effects. However, in most polymers the piezoelectric effect is very weak though recently polyvinylidenefluoride (PVDF) has demonstrated promising potential; it has comparable piezoelectric properties to the conventional materials and and has the advantage of a relatively low acoustic impedance.

Piezoelectric materials are widely used in hydro- and electro-acoustics, electro-optics and communications. The piezoelectric transducers, which are the electromechanical devices used in transformation of electrical energy to mechanical energy and vice versa, have found wide application particularly in underwater sonar, hydrophones, non-destructive testing (NDT), medical diagnosis, high power cleaning, mechanical filters and resonators.

Among the piezoelectric transducers used in NDT, particularly in ultrasonic testing, the piezoelectric elements may be made from all the type of material mentioned above, including traditional crystals (quartz) and novel plastics, such as PVDF, but the majority of transducers are made of piezoelectric ceramics, among which PZT is the type of material most commonly used. The geometry of the transducers is varied according to the application, and plates, bars, rings, and discs are sometimes used. However, a circular disc is the most commonly used geometry (Bond *et al.*, 1982), and this thesis investigates the properties of piezoelectric ceramic discs.

1.2 Vibration modes of piezoelectric discs

1.2.1 The thickness mode vibration of the piezoelectric disc

The vibration characteristics of piezoelectric discs can be very complicated, and they depend on not only the operational mode in which the piezoelectric transducers work but also the deformation pattern when the disc vibrates, i.e, the vibration modes of the piezoelectric disc.

The basic transducer structure, in which the piezoelectric disc is of most interest in this thesis, is illustrated in Fig 1.1. The piezoelectric disc, which is usually sandwiched between a backing part and face layer (sometimes called matching layer), serves as the active element. The acoustic impedance of the backing and face are chosen to control the signal produced. This entire assembly is then housed in a metal case as shown in Fig 1.1. Two electrodes on the top and bottom surfaces of the disc are connected to signal generators or signal receivers.

Piezoelectric transducers may be used to operate in two modes as shown in Fig 1.2; one is transmission mode in which an ultrasonic wave is generated by an applied electrical

voltage or current and the other is receiver mode in which an electrical signal is generated by an incoming mechanical wave. Frequently, in pulse echo testing systems, the same transducer is used to perform both functions.

When an elastic disc*, which may also be piezoelectric, has a very large D/T ratio, it is usually assumed to vibrate only in the thickness direction if subjected to an axisymmetrical loading. Therefore the lowest thickness mode frequency of mechanical vibration is such that the disc is half a wavelength thick, so

$$T = \frac{\lambda}{2} = \frac{c}{2f_1}$$

which gives

$$f_1 = \frac{c}{2T} \tag{1.1}$$

where λ is the wavelength of the resonant mode, T is the thickness of a piezoelectric disc, c is the longitudinal wave velocity in the piezoelectric material, and f_1 is the fundamental thickness frequency.

The frequency defined by (1.1) is usually termed the mechanical resonant frequency of the piezoelectric disc since it is a property of elasticity and geometry only. Other vibration modes may exist, for example, radial modes (sometimes called radial extensional modes, or contour modes), which are negligible in thin discs with large D/T ratios, and high order through thickness modes, they are multiples of the first thickness mode determined by (Silk, 1984),

$$f_n = n\frac{c}{2T} \qquad n = 1, 2, 3, ..., \text{ integer} \tag{1.2}$$

It can be seen that the family of the through thickness modes is equally spaced in the frequency domain. The mode shapes of the first four thickness modes are shown schematically in Fig 1.3(a). It is evident that when the disc vibrates in odd integer modes, the upper and lower faces move in opposite directions which results in large strain deformation in the through thickness direction, and the whole body vibrates in a so called "stretching" or "piston-like" mode to produce a compressional ultrasonic wave if it is coupled to other loading media, Fig 1.3(b) shows the piston-like mode shape of the first through thickness mode. The modes which are even multiples of the first through thickness mode, n = 2, 4, ..., in equation (1.2), have in phase deformation for upper and lower faces of a disc, and the distance between the faces of the disc remains constant.

* All discs studied in this thesis have stress free boundary conditions except where otherwise specified.

For discs with piezoelectricity, there is another resonant frequency of the through thickness mode due to the piezoelectric coupling effect, which is often called the electrical resonant frequency as opposed to the mechanical frequency. The value of this resonant frequency is smaller than the one given in (1.1), and the corresponding frequencies of the higher order thickness modes are not multiples of the fundamental one as is the case given in (1.2). Tiersten (1969) showed that these frequencies of the thickness modes are given by the roots of

$$\frac{\omega}{2c}T = k_t^2 \tan\left(\frac{\omega}{2c}T\right) \tag{1.3}$$

where k_t is the piezoelectric thickness coupling factor, which will be discussed later.

Equation (1.3) may be solved by plotting the two curves (Onoe *et al.*, 1963),

$$y = \frac{\omega}{2c}T \quad \text{and} \quad y = k_t^2 \tan\left(\frac{\omega}{2c}T\right)$$

The intersections of these two curves give the solutions for the electrical thickness mode frequencies. It can be shown that the piezoelectric effects are different in different modes, the higher order modes being less affected than the lower ones, and when k_t is small (less than 0.1), the first mode approaches f_1 given by (1.1). The frequency value defined by the first root of the equation (1.3) is often specified by manufacturer in terms of the thickness frequency constant, $N_{3,t}$, which is the product of this resonant frequency and the thickness of the piezoelectric disc.

1.2.2 Vibration modes other than the thickness modes

There have been many experimental reports which show that a variety of vibration modes exist in piezoelectric discs (Shaw, 1956; Ikegami *et al.*, 1974 and Ueha *et al.*, 1983). The experimental studies were usually carried out by measuring the frequency spectrum, which is defined as the relationship between the product of resonant frequencies and the thickness of the piezoelectric disc (fT) and the diameter to thickness ratio (D/T).

Ikegami *et al.* (1974) made extensive measurements of the frequency spectrum with $PbTiO_3$ piezoelectric discs in the D/T range 5 to 28 as shown in Fig 1.4. It was shown that the vibration behaviour of a piezoelectric disc is very complicated. Five groups of modes were classified by careful inspection of the measured frequency spectrum. The first group is the thickness extensional mode or TE-1 mode, which is the main resonance of the response; the second group are the T modes, which exist below the TE-1 mode and

are weakly excited, and converge monotonically to the TE-1 mode as the D/T ratio is increased; the third group is the edge mode or E mode, which is almost independent of the D/T ratio; the fourth group is the radial modes, R-modes, which are strongly dependent upon the D/T ratio and exist across the whole frequency spectrum; the final group are the high frequency radial modes, A-modes, which are only observed near to and above the TE-1 mode, and have stronger D/T dependence than the T-modes.

Similar experimental results were found by other researchers. Shaw (1956) measured the resonant frequencies and mode shapes of vibration of piezoelectric discs of $BaTiO_3$ in the D/T range 1 to 6.6, as shown in Fig 1.5. The so-called "edge mode" in which large axial displacement occurred at the edge of the disc was found, together with the radial modes and thickness extensional modes. It was also found that more than two modes can be equally strongly excited by a voltage across the disc for discs in the D/T range from 3 to 6, and neither of them has a uniform displacement over the surface of the disc.

Ueha *et al.* (1983) measured the vertical velocity distributions on the surface of the disc and the vibration modes as a function of the diameter to thickness ratio (D/T). The frequency spectrum was measured with the piezoelectric material $Pb(Zr.Ti)O_3$ in the D/T range from 2 to 12 as shown in Fig 1.6. Four types of modes were classified by the measured vibration patterns of flat discs, which are the thickness extensional mode (TE-1 mode), the edge mode (E-mode), the radial modes (R-modes) and the high frequency radial modes (A-modes).

It is evident from the above experimental results that the vibration characteristics of piezoelectric discs are very complicated. In general, five mode types have been found in the frequency range of interest, so it is therefore necessary to analyse the piezoelectric disc by using three dimensional methods.

The vibration characteristics of piezoelectric structures are completely determined from the three dimensional equations of linear elasticity, the Maxwell equations, and the piezoelectric constitutive equations. Solutions may be obtained from these general equations with appropriate boundary conditions. However, even for the simplest geometries and isotropic materials the solutions are very complicated. In general, it is impossible to solve these equations in a closed form except for the infinite plate. Two alternatives are usually employed. One is to use a numerical solution, and the other is to derive approximate equations which model the disc's behaviour under certain conditions.

Techniques available to analyse the piezoelectric transducers are reviewed in following sections both in one dimensional and three dimensional.

1.3 One dimensional analyses of piezoelectric transducers

The one dimensional model has been used for almost 40 years in the analysis and design of piezoelectric transducers, and is still the most commonly used technique. Since the lateral dimension of the piezoelectric disc is usually much larger than the thickness, the lateral effects can often be ignored, and the motion of the disc may be considered to be one dimensional provided that the ratio of the diameter of the disc to its thickness is large enough. A number of approximate methods have been employed to analyse the response of transducers using this type of model.

1.3.1 Simple acoustic transmission method

One simple method which was described in detail by Krautkramer (1983) is to ignore the piezoelectric effects in the transducer. The distribution of ultrasonic wave amplitudes may be used to construct the pulse shape produced by the transducer, which could be represented by two stress waves generated at each face of the transducer as shown in Fig 1.7. The remaining problem is to consider the propagation of ultrasonic waves within the layered devices and the wave reflection and transmission at the boundaries of the system, such as boundaries between the piezoelectric element and backing, and between piezoelectric element and the loading medium. This method may give reasonable pulse shapes for materials of weak piezoelectric effect, and when the backing is approximately matched, i.e. the acoustic impedance of the piezoelectric element is equal to that of backing, but it cannot be widely used. Nevertheless, it has been used to help the understanding of the transducer behaviour and in simple ultrasonic transducer design (Silk, 1983; Smith and Awojobi, 1979; Low and Jones, 1984), and construct roughly the response shape of a transducer-specimen-transducer system (Williams and Doll, 1982).

1.3.2 Equivalent circuits

From the end of 1940s the analogue approach (Barker, 1964) of representing mechanical properties by their electrical analogues has been widely used to investigate transducer behaviour. In this method an electric circuit analogue of a mechanical system may be used to analyse and predict the properties of the mechanical system. For a piezoelectric transducer this method is particularly useful since the transducer has both mechanical and electrical properties.

1. Mason's model

Mason (1948) first introduced the equivalent electrical circuit to model the properties of the transducer by using the above technique. The transducer was modelled as a three port electrical circuit, one pair representing the electrical properties and the other two representing the boundary conditions on the two faces of the piezoelectric disc. The acoustic wave propagation within the transducer was modelled as a transmission line, and an electromechanical transformer (1:N) was used to connect the mechanical and electrical properties, see Fig 1.8. However, a negative capacitance had to appear in the circuit in order to satisfy the constitutive equations, which does not have an obvious physical interpretation.

2. KLM model

The KLM model developed by Krimholtz *et al.* (1970) represented the mechanical properties of the piezoelectric element as a lossless acoustic transmission line and the electrical properties as a lumped network as shown in Fig 1.9. Each half of the thickness of the piezoelectric disc is represented as a transmission line, and they are coupled together at their middle point instead of being distributed in the network as in Mason's model. The mechanical transmission lines are then coupled to the electrical network via an electromechanical transformer (different ratio from the one in the Mason's model). The KLM model also provides an easy way to deal with any extra layers such as backing and facing attached to the element by adding corresponding acoustic transmission lines.

Within the limitations of one dimensional modelling, the equivalent circuit approach (via either Mason's model or the KLM model) can provide an accurate prediction of transducer performance. However, the negative capacitance in the circuit shown in Fig 1.8, which has a significant effect for materials with high piezoelectric coupling, has no obvious physical significance.

The negative capacitance in the equivalent circuit represents the intercoupling effect or secondary piezoelectric action between the mechanical and electrical properties. For example, when an ultrasonic wave strikes a piezoelectric plate on its front face, an electric field will be built up and a resulting voltage across the element will be produced due to the direct piezoelectricity. However, this electric field generates another ultrasonic wave (Jacobsen, 1960) which propagates within the plate; an extra electric field will then be built up, so the resulting voltage form will be modified by this extra electric field. This process may be regarded as the intercoupling effect or secondary piezoelectric action between the mechanical and electrical properties. This process continues and must be

taken into account if the voltage response is to be predicted accurately. Similar phenomena occur when a mechanical response is produced by electrical excitation.

The equivalent circuit model has found wide application by a number of workers. Mason's model has been used to analyse the effect of backing and matching on the performance of piezoelectric ceramic transducers (Kossoff, 1966). For the mechanical response of transducers, the equivalent circuit of the transducer at resonance was used by Redwood (1963, 1964) to model the behaviour of transducer, and an Impulse Diagram was used to form the shape of response for arbitrary boundary conditions shown in Fig 1.10. For an applied voltage V, the waves are generated at the boundaries with the amplitudes shown in Fig 1.10(a), these waves then propagate inside the piezoelectric element, and reflection and transmission occur when the waves reach the boundaries, and are decided by the acoustic impedance of the materials, see Fig 1.10(b) and (c). This method is essentially the same as the simple wave propagation method shown in Fig 1.7, and ignores the negative capacitance, so it is only valid for a material with very weak a piezoelectric coupling effect.

Since the KLM transmission line model is very flexible, it has been used to predict the effect of some design parameters on the performance of ultrasonic transducers, such as the quarter-wave matching layer (Desilets, 1978), backing, bond-line thickness, and the thickness of the matching layer (Silk, 1983), cable length and conductive layer thickness (Wustenberg *et al.*, 1989), and allowable tolerances in design parameters (Kwun *et al.*, 1988),

The electrical equivalent circuit normally represents the frequency behaviour of the piezoelectric element and therefore yields solutions in terms of angular frequency ω. To get the time domain response, either inverse Fourier Transformation has to be used, or an analytical method based on the constitutive equation of piezoelectricity must be employed. However the former may fail due to the existence of infinite values (poles) in some of the equivalent circuit elements at resonant frequencies (Challis, 1983), and the latter may be restricted due to the complicated Laplace transform required (Zhang *et al.*, 1983).

1.3.3 Analytical methods

The Laplace transform has been used to study the transient response of piezoelectric transducers when the transducer is excited by mechanical and electrical pulses. Redwood (1961) formulated an analytical solution for the transient response of transducers for certain basic exciting function by a Laplace transform treatment. This method includes all the effects which were incorporated in Mason's equivalent circuit shown in Fig 1.8,

including those represented by the negative capacitance in this circuit. It was found that in an open circuit receiver, the voltage response of a transducer for a step function of force is a decaying repeated ramp function while when a step voltage is applied to the transducer it can produce a repeated step force into a load.

A free piezoelectric plate was investigated by Stuetzer (1967, 1968) and Filipczynski (1975) to study the effects of the piezoelectric intercoupling on the response shape. It was shown that for a step voltage excitation the stress response of the plate varies exponentially with time during each period τ, which is the time for an ultrasonic wave to travel through the plate, and there is a phase change when $t = n\tau$, n integer, see Fig 1.11. After a few periods the response approximates to a decaying sine wave with periodic sharp pulses.

Zhang *et al.* (1983) studied the transient response of a piezoelectric transducer in transmitting mode by the method of Laplace transforms, and the negative capacitance in the Mason equivalent circuit was interpreted as the acousto-electrical regenerative vibration.

1.3.4 Hayward's systems approach

Hayward *et al.*, (1981) recently developed a systems approach model which used a feedback loop to describe the piezoelectric action on transducer behaviour and more clearly interpreted the physical phenomena involved. The piezoelectric coupling effect (or negative capacitance) was interpreted as a feedback device in the loop. Originally the systems model was one dimensional, but Hossack and Hayward (1987) have recently extended it to solve the vibration problem of a piezoelectric bar element used in two dimensional array transducers by considering multiple feedback loops representing vibrations in different directions. However, the technique is much more difficult to apply to piezoelectric discs since they have many more modes than a bar, and the main resonances are often high order modes.

1.3.5 Other methods

In addition to the conventional equivalent methods mentioned some other techniques have also been proposed. The matrix formulation of transducers used by Sitting (1969) is particularly useful to analyse composite, multi-layered transducers. A transduction matrix relating the input and output of each individual part of the transducer can be formed from the fundamental equations of the material. The overall transduction matrix can then be obtained by multiplying the individual matrices. The final output is determined by the

overall matrix and the given input. The impulse response method (Stepanishen, 1971), which assume the piston motion of the transducer, has also been widely used in wave propagation and pressure field problem (Hayman and Weight, 1978).

Challis (1983) developed a Z-transform technique, which can be applied in the same manner as a digital filter to a variety of exciting functions. Martin *et al.* (1975) presented a Thevenin equivalent electrical circuit to simulate the thickness mode piezoelectric transducer under the condition that the transducer operates near resonance. Banah (1983) developed a reentrant transmission line model by Feynman diagrams, which provided a significant physical insight into transducer operation.

1.3.6 Discussion

All the one dimensional methods mentioned above have made the following fundamental assumptions:

(i) Through thickness vibration: the transducer only vibrates in its thickness direction; the motions of other directions are either ignored or restricted.

(ii) Planar wave propagation in the thickness direction of the transducer and unidirectional strain; the stress in the plane perpendicular to the thickness direction is uniform.

To satisfy the above assumptions, the piezoelectric elements considered must be either very thin plate or long rods (bars) (D/T in the region of 20:1 or greater for piezoelectric discs (Hayward, 1981)). Otherwise, radial modes are easily observed (Hayward, 1981) and can even be strongly excited and used as the operational modes in low frequency ultrasonic NDT (Guyott *et al.*, 1986).

The one dimensional analysis is also restricted to piezoelectric transducers with regular geometries and fully electroded surfaces, which may not be the case in complicated transducers.

1.4 Characteristic frequencies and electrical impedance of the piezoelectric transducers

1.4.1 The characteristic frequencies

The resonant frequencies given by (1.2) and (1.3) are usually defined as one pair of the characteristic frequencies of piezoelectric transducers working in the thickness modes (Hilke, 1973). The first frequency of the pair is known as the parallel frequency, f_p,

given by (1.2), and the second frequency is known as the series frequency, f_s, which is given by the roots of equation (1.3).

The interpretation of the 'series' and 'parallel' descriptions of these two frequencies can be seen from the approximate equivalent circuits of an unloaded piezoelectric disc as shown in Fig 1.12(a) (Mason, 1948; Berlincourt *et al.*, 1964), in which C_0 is the static capacitance of the transducer, R_1 accounts for the mechanical loss, C_1 and L_1 are the electrical equivalent components of the mass and stiffness of the disc, which can be derived from the first order power series approximation for a thin piezoelectric disc (Berlincourt *et al.*, 1964).

It can be shown that the branch circuit in which L_1, R_1 and C_1 are in series shown in Fig 1.12(a) has a resonant frequency close to the one given by (1.3), and the shunt circuit has a resonant frequency given by (1.2). For a one dimensional bar or rod vibrating in the longitudinal mode, a similar equivalent circuit can be obtained excepted that a different piezoelectric coupling factor, k_{33}, is used instead of k_t.

If the loss is not considered, the electrical impedance of the equivalent circuit shown in Fig 1.12(a) can be found as,

$$Z = -\frac{\omega L_1 - \dfrac{1}{\omega C_1}}{\omega C_0[\omega L_1 - \dfrac{1}{\omega}(\dfrac{1}{C_1} + \dfrac{1}{C_0})]} \tag{1.4}$$

This is illustrated schematically as a function of frequency in Fig 1.12(b). $Z = 0$ at the series frequency given by $f_s = 1/\sqrt{(L_1C_1)}$, and the transducer is then in short circuit, while $Z = \infty$ at the parallel frequency f_p given by $f_p = \sqrt{[(1+C_1/C_0)/(L_1C_1)]}$, and the transducer is then open circuit.

There are another two pairs of characteristic frequencies for a piezoelectric transducer: f_{max}, f_{min}, and f_a, f_r (Berlincourt *et al.*, 1964; and IRE Standard, 1957), which can be interpreted from the impedance circle (Nyquist plot) around the resonance as shown in Fig 1.13, and are listed in Table 1.1 for clarity. They should not be confused with the usual resonance definitions in vibration analysis. When loss is not considered, f_s, f_{min} and f_r are the same, as are f_p, f_{max} and f_a. In practice, if the losses are small, these assumptions are also sufficient.

If vibrations in other dimensions are considered, piezoelectric discs may have many more modes in the frequency range of interest, and two sets of the characteristic resonant frequencies of piezoelectric transducers, (f_p, f_{max}, f_a) and (f_s, f_{min}, f_r), are seen at each resonant mode. If the modal density is very high, i.e., they may be very close and coupled to each other, which tends to make them difficult to identify.

1.4.2 The electrical impedance

The electrical impedance of a piezoelectric disc vibrating in the thickness mode can be found analytically as (Meeker, 1972; Hilke, 1973),

$$Z = \frac{1}{i\,\omega C_0}\left(1 - \frac{k_t^2}{\phi \cot \phi}\right) \tag{1.5}$$

where

$$\phi = \frac{\pi}{2}\frac{f}{f_p}$$

Equation (1.5) can be used to calculate the electrical impedance function of piezoelectric discs and plates which work in the through thickness modes.

1.5 Two and three dimensional analyses of piezoelectric transducers

1.5.1 Mindlin's plate theory

Extensive efforts have been made by many authors since the 1950s to use classical elasticity theory for the analysis of the vibration behaviour of discs with finite D/T ratios. Kane and Mindlin (1956) introduced a correction factor to couple the first through thickness mode by thin plate theory and the radial extensional modes obtained from plane stress theory. Good agreement with Shaw's experiments was obtained as far as the first two modes are concerned as shown in Fig 1.14. Mindlin and Medick (1959) extended the plate theory and considered coupling between radial extensional, symmetric thickness-stretch and the first symmetric thickness shear modes. Furthermore Gazis and Mindlin (1960) considered the existence of the edge mode and took into account the influence of Poisson's ratio.

The plate theory developed by Mindlin and other authors is based on the power series expansion method. The mechanical displacement may be expanded in a power series of the thickness coordinate. By applying the variational principle followed by integration with respect to the thickness variable, the three dimensional equations of elasticity are converted to an infinite series of two dimensional equations, which are then truncated to

produce approximate first or second order equations. To correct for the truncation, additional constants are obtained by comparing the approximate equations with the full three dimensional equations. The number of terms which it is necessary to retain in the expansion depends on the problem to be analysed. Therefore, the zero order plate theory corresponds to the radial modes in the plate, the first order theory couples the first thickness mode and radial modes, and the second order theory takes into account the radial modes, the first thickness mode and the first symmetrical thickness shear mode. Details of the application of this theory to piezoelectric materials are given by Tiersten (1969). The mathematical effort involved in this theory is enormous, and some awkward mathematical forms may be encountered for second and higher order theory, which tend to obscure the physical interpretation of the solution.

The second order Mindlin's plate theory has been used by several researchers to compare with the measurements on the piezoelectric discs (Gazis and Mindlin, 1960; Ikegami *et al.*, 1974, 1976). For example, the lines in the frequency spectrum shown in Fig 1.4 by Ikegami *et al.* (1974) correspond to predictions by the second order plate theory. It can be seen that good agreement has been obtained between the experiment and prediction over most of the frequency spectra. However, the T-modes and the edge mode were not accurately predicted.

Although good agreement was generally obtained between the frequencies of the different modes and those predicted by the plate theory, the plate theory gives no information about the amplitude of each mode, so it is not possible to predict which mode is most strongly excited when the piezoelectric disc is subjected to, for example, voltage excitation.

1.5.2 Bogy's plate theory

Recently, Bugdayci and Bogy (1981) developed a two dimensional plate theory for piezoelectric layers. The procedure used is identical to Mindlin's plate theory except that trigonometric series expansions are used instead of power series expansions. The theory has been used to analyse the transient problem of piezoelectric discs subjected to an axisymmetrical load (Bogy and Miu, 1982), and a non-axisymmetrical load (Bogy and Bechtel, 1982). The first order theory has recently been extended to analyse the interaction of a piezoelectric transducer with the test medium, for example, a transducer coupled through its bottom surface to the testpiece surface via a viscous liquid (Bechtel and Bogy, 1984).

1.5.3 Aggarwal's three dimensional analytical solution

Aggarwal (1952a, 1952b) studied analytically the vibration of free elastic discs of finite thickness. The exact solution of a free disc should satisfy four boundary conditions: zero stress normal and tangential to the flat surfaces (major surfaces) of the disc and zero stress normal and tangential to the cylindrical surface of the disc. However, analytical solutions from the three dimensional wave equation can only satisfy three of them exactly and one approximately. Since wave propagation in the axial direction was of most interest, the two boundary conditions over the major surface and one over the cylindrical surface were used to solve the equation of the elastic disc. Two possible sets of boundary conditions were therefore specified:

Boundary condition set I (BC I): zero stress normal and tangential to the flat surfaces and zero stress normal to the cylindrical surface; boundary condition set II (BC II): zero stress normal and tangential to the flat surfaces and zero stress tangential to the cylindrical surface.

Two sets of solutions were found corresponding to BC I, and BC II. For example, for the solution corresponding to BC I, the following equation was obtained (Aggarwal, 1952a),

$$(1 - \upsilon)\, J_1\left(\frac{\kappa D}{2}\right) = \frac{\kappa D}{2} J_0\left(\frac{\kappa D}{2}\right) \tag{1.6}$$

where υ is Poisson's ratio, J_0, J_1 are Bessel functions of first kind (zero- and first-order), κ is the wave number, and D is the diameter of the disc.

The mode shapes of the modes obtained according to the two set of boundary conditions are shown in Fig 1.15. Fig 1.15(a) shows the mode shapes of the first symmetrical extensional modes according to BC I, which can be obtained from the lowest four roots of κ in equation (1.6). The mode shapes of the second symmetrical shear modes obtained from BC I are shown in Fig 1.15(b), in which the radial deformation varies greatly along the thickness in the disc. Fig 1.15(c) shows the mode shapes for both extensional and shear modes when BC II is satisfied.

Although the Aggarwal's analytical solutions were approximate and ambiguous due to the fourth boundary condition not being satisfied, they may be useful in understanding the physics of the vibration of piezoelectric discs (Ueha *et al.*, 1983).

1.5.4 The finite element method

An alternative to the development of approximate analytical solutions is to use a numerical solution such as the finite element method. The finite element method (FEM) has been well developed and extensively used in structural mechanics. Although the variational principle has already been used to analyse the vibration of piezoelectric discs (EerNisse, 1967b), the general finite element formulation for a piezoelectric material was first given by Allik and Hughes (1970). Since then it has been widely used for the vibration analysis of many electromechanical devices at both low and high frequencies, such as electromechanical filters (Kagawa, 1971), sonar transducers (Smith *et al.*, 1973; Allik *et al.*, 1974; Armstrong and McMahon, 1984), surface-wave devices (Kagawa and Yamabuchi, 1976a), hydrophones (Winnicki and Auyer, 1977), and array transducers (Boucher *et al.*, 1981; Naillon *et al.*, 1983; Lerch and Kaarmann, 1987).

The finite element method has great flexibility for the analysis of composite structures which consist of different geometries and materials, and can also be used to study the coupling between the transducer and test structure. Kagawa and Yamabuchi (1976b) calculated the vibration modes of a composite transducer (Langevin type) by an axisymmetrical two dimensional model. Ostergaard and Pawlak (1986) studied a piezoelectric disc sandwiched between two aluminium discs, and calculated the natural frequency of the first mode of the structure by a three dimensional model. Smith *et al.* (1973) took into consideration the coupling effects between a piezoelectric structure and the loading medium, in this case a sonar transducer in water.

However, very few authors have used the finite element method to study piezoelectric discs, and the studies have been limited to the low order modes or the piezoelectric discs with small D/T ratios. Kagawa and Yamabuchi (1976b) studied the natural frequencies of a piezoelectric circular rod with height to diameter ratio of 1 to 5 (equivalent D/T of 0.2 to 1). Jensen (1986) calculated the natural frequencies and mode shapes of the vibration of piezoelectric discs. Recently Locke *et al.* (1987) calculated the frequency spectrum of piezoelectric discs of PZT5H in the D/T range 0.2 to 10, in which the radial R modes, the edge mode, the thickness shear modes and the thickness extensional mode were clearly defined.

1.5.5 Discussion

It is evident that the plate theory may give good results as far as the natural frequency of the piezoelectric disc is concerned. However, it cannot predict the frequency response function when the disc is subjected to an electrical excitation. The finite element method

shows great potential for modelling piezoelectric discs with finite D/T ratios, and has great flexibility to accommodate the severe demands of the design of complicated advance transducers. Three dimensional studies of piezoelectric discs have been limited to the classification of the natural frequencies of the disc. The physical interpretation of some resonant modes, such as the thickness extensional modes and the edge mode, have not been well clarified.

1.6 Strength of excitation at resonant frequencies

An important parameter in modelling a piezoelectric disc's performance is to estimate the strength of each resonance when a voltage is applied across the electrodes of the disc. From the literature available so far, most investigations have used an electromechanical coupling coefficient or piezoelectric coupling factor, k, to estimate the strength of a mode.

The piezoelectric coupling factor is defined as the ratio of the mutual elastic and dielectric energy density to the geometric mean of the elastic and dielectric self-energy density (Berlincourt *et al.*, 1963):

$$k^2 = \frac{U_m^2}{U_e U_d} \tag{1.7}$$

where U_m = mutual energy, U_e = elastic energy, and U_d = dielectric energy.

In practice, equation (1.7) is much more complicated than it looks. However, a simple expression can be derived for transducers whose motion is one dimensional. In the thickness mode this piezoelectric coupling factor can be derived as (Berlincourt *et al.*, 1964)

$$k_t^2 = h_{33}^2 \frac{\varepsilon_{33}^S}{c_{33}^D} \tag{1.8}$$

where subscript t denotes the thickness mode, h is the piezoelectric coupling constant, ε^S is dielectric constant, and c^D is the elastic constant. The thickness mode piezoelectric coupling factor is a very important parameter for the thickness mode transducer since it quantifies the degree of piezoelectricity of different materials. It can vary from 0.1 for Quartz to 0.5 - 0.7 for PZT piezoelectric ceramics.

It is also possible to calculate piezoelectric coupling factors for other simple modes. For example, in the longitudinal mode of a piezoelectric bar, the piezoelectric coupling factor is given by (Berlincourt *et al.*, 1964)

$$k_{33}^2 = \frac{d_{33}^2}{\varepsilon_{33}^T s_{33}^E} \tag{1.9}$$

where d_{33} is the coupling constant, e_{33} is the dielectric constant, s_{33} is the elastic constant.

These coupling factors can also be obtained from the resonance frequency f_r of the appropriate mode and the corresponding anti-resonance frequency f_a as (Hilke, 1973)

$$k^2 = \frac{\pi}{2}\frac{f_r}{f_a}\cot\left(\frac{\pi}{2}\frac{f_r}{f_a}\right) \tag{1.10}$$

Equation (1.10) can be approximately written as

$$k = \sqrt{\frac{f_a^2 - f_r^2}{f_a^2}} \tag{1.11}$$

Equation (1.11) is usually used to calculate the coupling factor by measuring the resonant frequency and corresponding anti-resonant frequency of the mode.

In the experimental work on piezoelectric discs with finite D/T ratios by Shaw (1956), the electro-mechanical coupling coefficient k_m was used to evaluate the strength of each resonance. This was defined as

$$k_m^2 = \frac{\pi^2}{4}\frac{\Delta_m}{f_m}\left[\, 1 + \left(1 - \frac{\pi^2}{4}\right)\frac{\Delta_m}{f_m} + \ \ldots\ \right] \tag{1.12}$$

where f_m is the resonant frequency of the mode and Δ_m is the difference between the frequencies of the resonance of that mode and that of the corresponding anti-resonance.

It was found that the first radial mode and the thickness extensional modes had the largest electro-mechanical coefficients and more than two thickness modes were found with similar values of coefficients in the D/T range 3 to 5 (Shaw, 1956). Similar experiment were done by Ueha *et al.* (1983) for piezoelectric discs with the D/T range 2 to 12, and same result was obtained by using formula (1.12).

Naillon *et al.* (1983) applied the finite element method to a piezoelectric bar used in array transducers, and an effective piezoelectric coupling factor similar to that in (1.11) was derived to relate to the anti-resonant and resonant frequencies of the piezoelectric structure, which was then used to estimate the strength of each mode as,

$$k_{eff} = \sqrt{\frac{f_a^2 - f_r^2}{f_r^2}} \tag{1.13}$$

Piezoelectric coupling factors are best used in characterising the piezoelectricity of a material, and unidirectional motion of a piezoelectric structure. Therefore, they are widely used in the one dimensional analysis of the transducers, and in two dimensional analysis of bars provided that the modes are well separated each other.

Apart from various piezoelectric coupling factors discussed so far, Ikegami *et al.* (1974) used a dynamic range to determine the intensity of each resonance, which was defined as the ratio of the maximum admittance to the lowest admittance of the two minima on either side of the maximum as illustrated in Fig 1.16.

However difficulties often arise in determining the above coupling factors or dynamic ranges when the frequency separation between successive modes is comparable to the typical separation between the resonance and anti-resonance frequencies. In these cases, a correction procedure had to be used (Shaw, 1956; Ueha *et al.*, 1983). This also occurred in the numerical study of piezoelectric discs by Locke *et al.* (1987) where the anti-resonant frequencies of some modes, f_a, were predicted to be smaller than the corresponding resonant frequencies, f_r, due to high modal density, particularly around the frequency of the first through thickness mode defined by the one dimensional model. The assumption that the resonance frequencies are followed by the corresponding anti-resonance frequencies may therefore be broken down for discs which have high modal density in the frequency range of interest.

It is therefore proposed in this thesis to use a new parameter, the modal constant (Ewins, 1984), to evaluate the intensity of the resonance. The advantage is that it only requires knowledge of the resonant frequencies. More details about the modal constant and its derivation will be given later in the thesis.

1.7 Aims and outline of the thesis

1.7.1 Limitation of previous research and aims of the thesis

It is evident from the above review and discussion that previous research has the following limitations:

(i) Although it has been known that the vibration modes of piezoelectric discs are very complicated, most modelling techniques have limitations, which result in inaccuracy of the predictions. No attempt has been made to predict the influence of the three

dimensional effects on the frequency response function and the electrical impedance characteristics of a disc.

(ii) The nature of some resonant modes of piezoelectric discs is not well understood. Although the radial modes have been well classified by the analytical approximate solution and plate theory, and experiments have shown good agreement with the predictions, other modes, such as the edge mode and the thickness shear modes are less well defined. It is also not clear whether piston-like motion should occur in three dimensional analyses.

(iii) There is a lack of parameters to evaluate the strength of excitation of each resonant mode in a three dimensional model. Although various electromechanical coupling factors and a dynamic range parameter have been used, all these parameters require clear identification of resonant frequency and anti-resonant frequency of the mode. This can only be obtained in the one dimensional analysis and in the two dimensional bar structure (Naillon *et al.*, 1983). For piezoelectric discs, the approach is problematic both in measurements and predictions since the modal density is very high in the frequency range of interest (Shaw, 1956; Locke *et al.*, 1987).

The current thesis attempts to eliminate these limitations.

(i) A finite element model is developed to analyse the vibration characteristics of piezoelectric structures.

(ii) The vibration characteristics of piezoelectric discs in D/T ratio from 0.5 to 20 are predicted, including resonant frequencies and corresponding mode shapes, mechanical frequency response functions and electrical impedance response of the discs. The model is then used to predict the transient mechanical response of piezoelectric discs with voltage excitation.

(iii) A new method is presented to evaluate the strength of excitation at each resonance by using the concept of the modal constant. It is then incorporated in calculation of the frequency spectrum of piezoelectric discs by using the finite element model.

(iv) The application of the FE model is presented to the analysis of the piezoelectric discs with elastic additions, and the analysis of piezoelectric discs with partial electrodes.

A one dimensional analytical method is also used to analyse the effect of backing on the behaviour of piezoelectric transducers.

1.7.2 Outline of the thesis

Following the above introduction of piezoelectricity and transducers, and the review of the techniques and previous researches in modelling piezoelectric discs in this chapter, this thesis is intended to cover two aspects of the vibration characteristics of piezoelectric discs. Since the one dimensional methods are the most commonly used techniques in the analysis and design of piezoelectric transducers, a one dimensional analytical method is used to calculate the transient response of transducers subjected to excitation with voltage pulses of various shapes, and then a degenerate two degree of freedom mechanical mass-spring system is developed to analyse a piezoelectric disc.

The three dimensional analysis of piezoelectric discs, which forms the bulk of the thesis, is then discussed. The finite element formulation for piezoelectric materials and the modal analysis of piezoelectric discs are first discussed in Chapter 3, and the mechanical frequency response functions and the electrical impedance function are formed. This is then followed in Chapter 4 by detailed numerical and experimental studies of the vibration characteristics of piezoelectric discs with D/T ratios between 0.5 and 20. The frequency spectrum of piezoelectric discs, and the influence of the piezoelectric effect on the different modes are studied in Chapter 5.

The transient mechanical response of a piezoelectric disc subjected to a voltage pulse across the electrodes is treated in Chapter 6, and the mode superposition method is used to calculate the surface motion of the disc. Chapter 7 is devoted to the application of the three dimensional FE model to analyse the vibration characteristics of other piezoelectric discs, such as the piezoelectric disc coupled with an elastic addition, piezoelectric discs in connection with an electrical resistor, and piezoelectric discs which are partially electroded on the major surfaces.

Finally, conclusions and suggestions for future work are made in Chapter 8.

Characteristic Frequencies	Definition	Condition
f_{min}	Frequency of minimum Z	$\frac{d\|Z\|}{d\omega} = 0$
f_s	Series frequency	$X_1 = 0$
f_r	Resonance frequency	$X_e = 0$
f_{max}	Frequency of maximum Z	$\frac{d\|Z\|}{d\omega} = 0$
f_p	Parallel frequency (lossless)	$X_e \|_{R_1=0} = \infty$
f_a	Antiresonance frequency	$X_e = 0$

Table 1.1 The various characteristic frequencies of a piezoelectric transducer (where X_1, R_1 are reactance and resistance in the series branch; X_e, R_e are reactance and resistance of the circuit; and Z is the electrical impedance, see Fig 1.12(a))

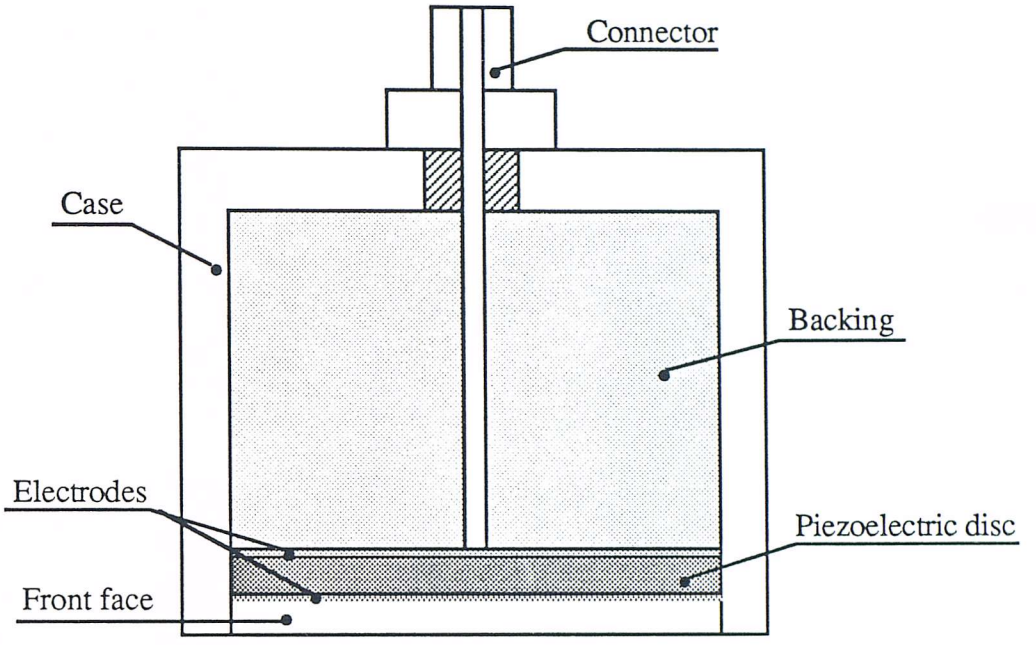

Fig 1.1 Basic structure of a piezoelectric transducer

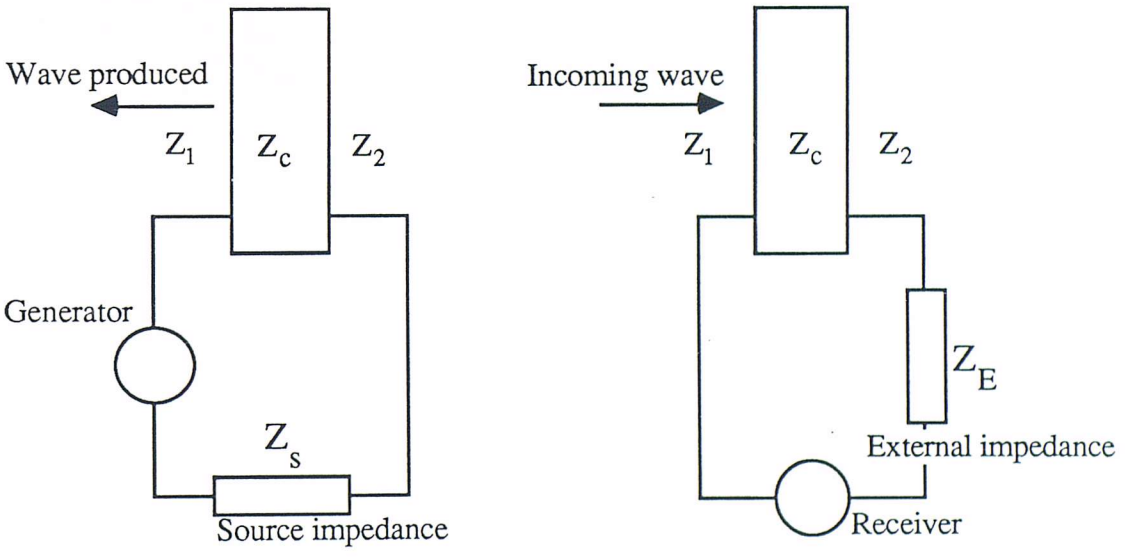

(a) Transmission mode (b) Receive mode

Fig 1.2 Electrical circuits of transducers as a transmitter and receiver (Z_c, Z_1 and Z_2 are acoustic impedances of the piezoelectric element, loading and backing)

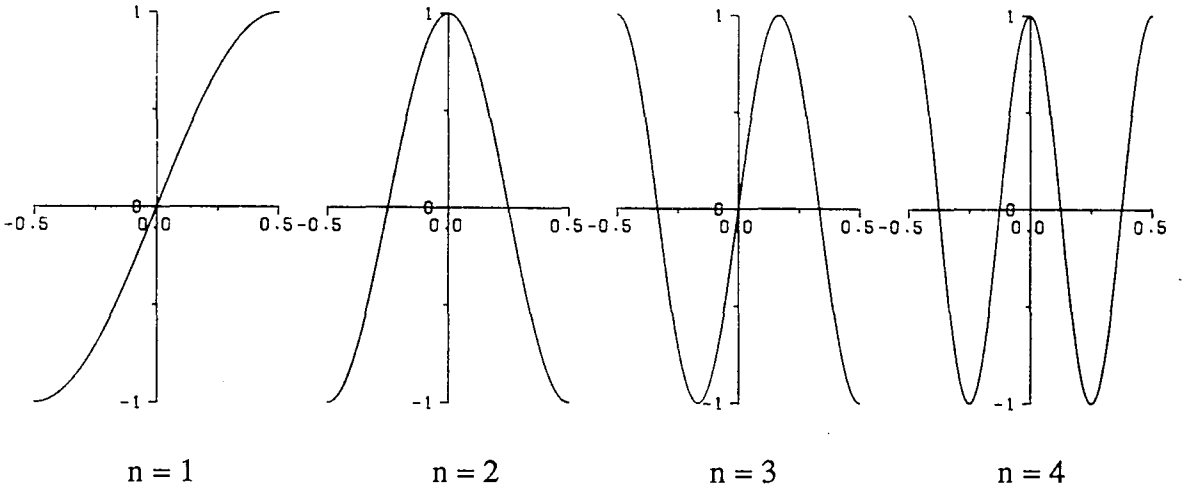

(a) the first four through thickness modes
(vertical coordinate: normalized displacement; horizontal coordinate: thickness position)

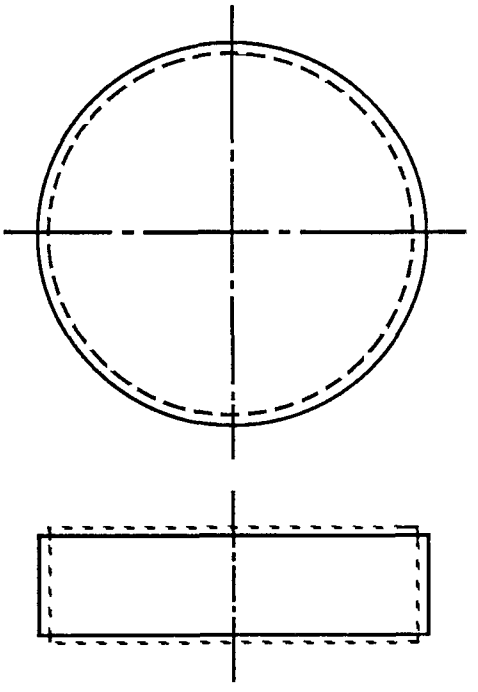

(b) the piston-like motion of the first through thickness mode

Fig 1.3 The mode shapes of the through thickness modes of piezoelectric discs assumed by the one dimensional model

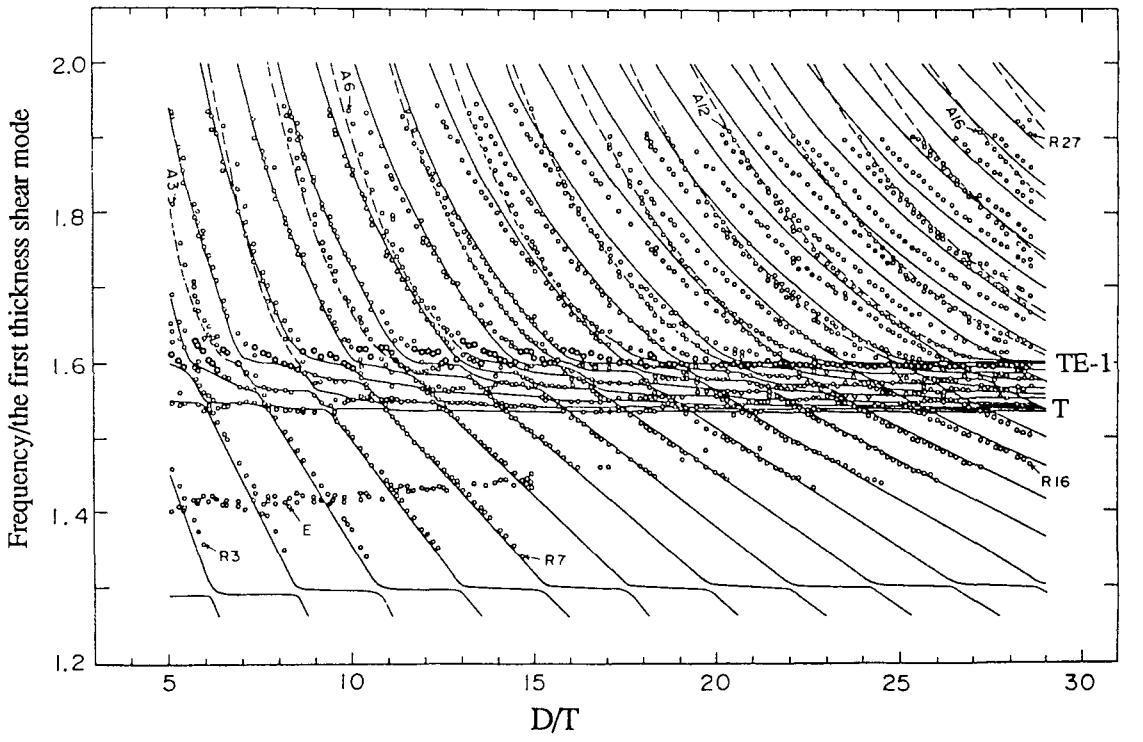

Fig 1.4 Comparison between frequency spectra by the experimental results (circles) and the plate theory (lines) (From Ikegami *et al.*, 1974)

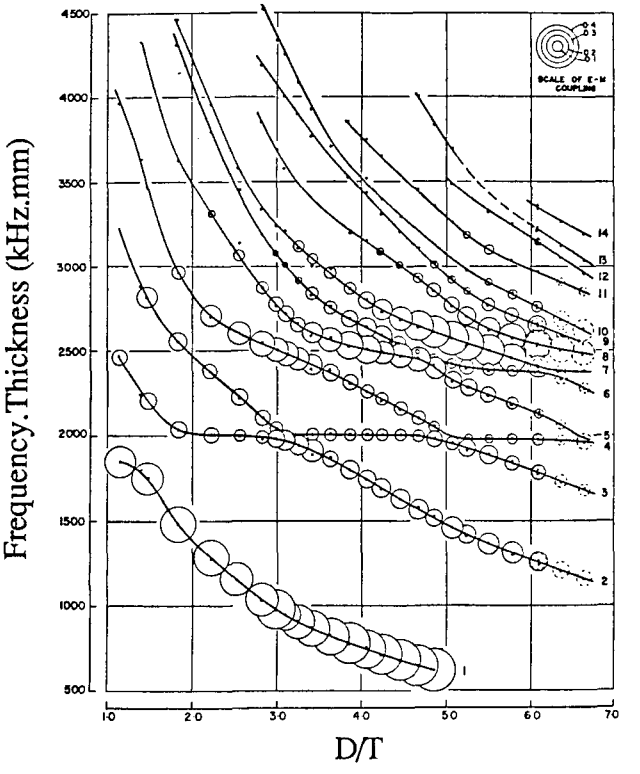

Fig 1.5 The measured frequency spectrum of BaTiO3 discs (From Shaw, 1956) (Circle diameters proportional to observed values of the coupling factors)

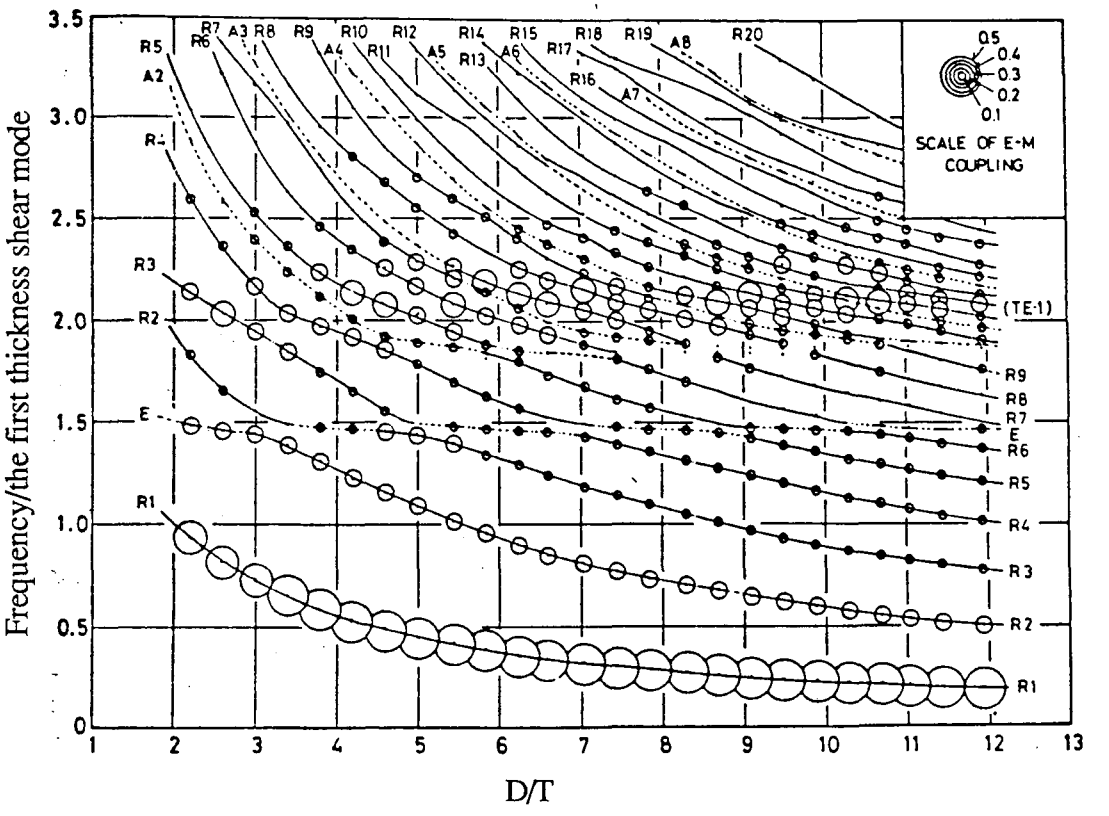

Fig 1.6 The measured frequency spectrum of Pb(ZrTi)O3 (From Ueha *et al.*,1983) (Circle diameters proportional to observed values of the coupling factors)

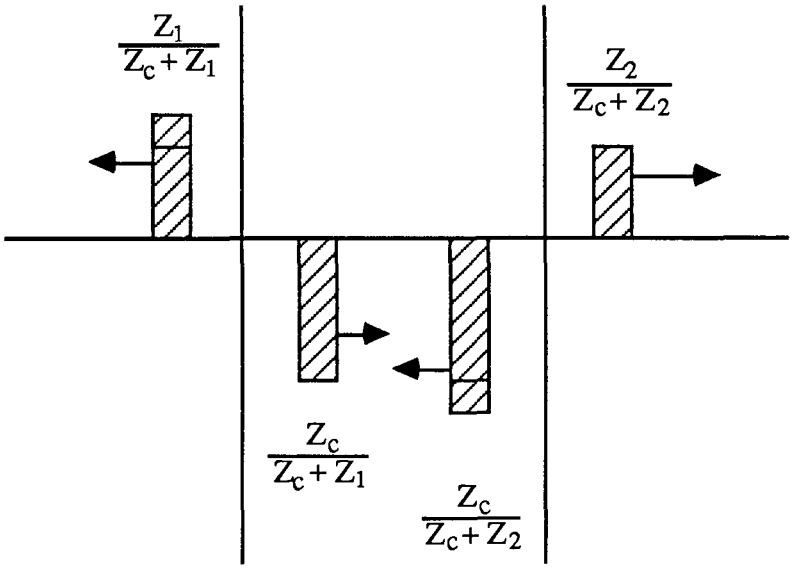

Fig 1.7 Ultrasonic wave amplitudes from a simple transmission model (Z_c, Z_1 and Z_2 are acoustic impedances of the piezoelectric element, loading medium and backing)

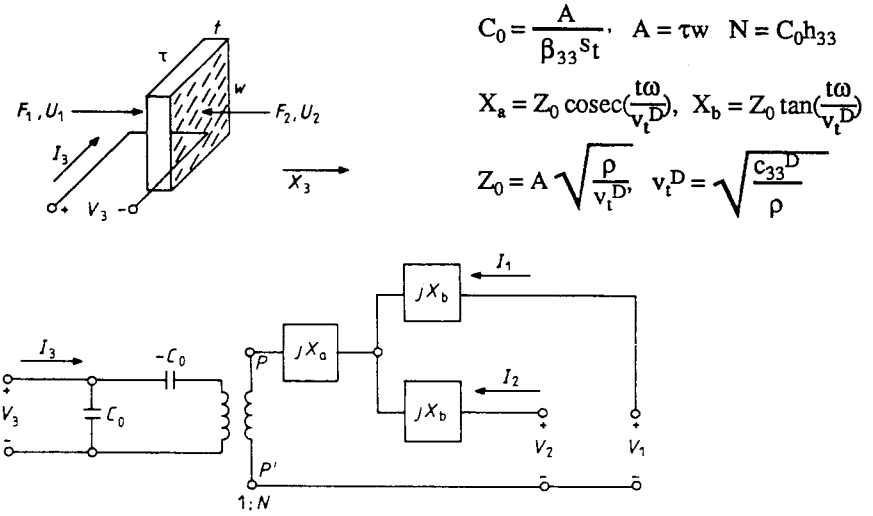

Fig 1.8 Mason's equivalent circuit for a thickness plate (From Silk, 1984)

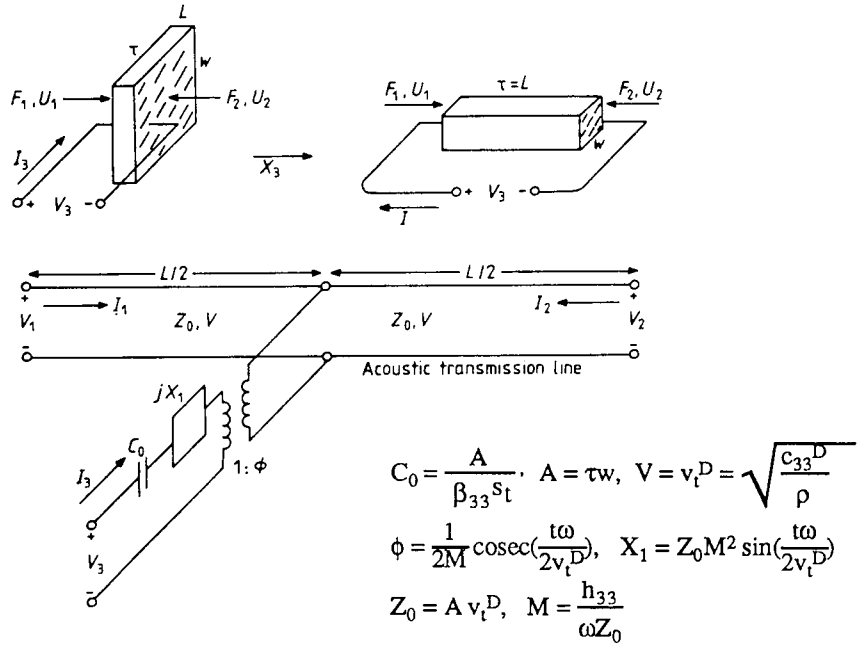

Fig 1.9 KLM equivalent circuit for a thickness plate and a length bar (From Silk, 1984)

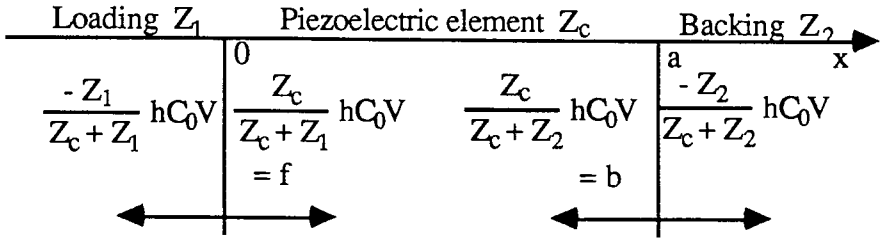

(a) wave amplitudes generated at front and back interfaces

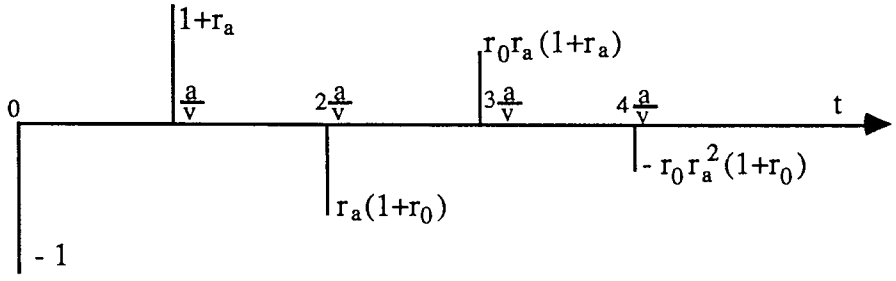

(b) the wave amplitude at the front face

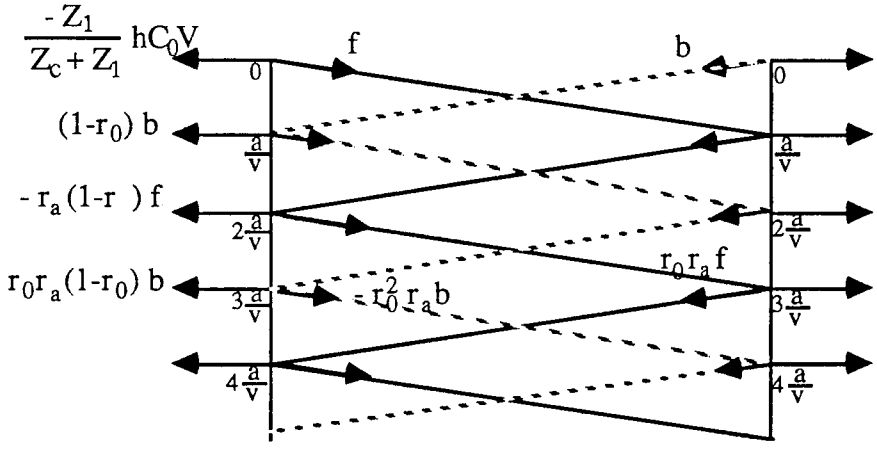

(c) reflections and transmission inside the piezoelectric element

Fig 1.10 The Impulse Diagram (From Redwood, 1963)

(Z_c, Z_1 and Z_2 are acoustic impedances of the piezoelectric element, loading medium and backing; h, C_0, and V are piezoelectric coupling constant, static capacitance and applied voltage; r_0, r_a are reflection and transmission coefficients at x = 0 and a; a/v is the time for an ultrasonic wave to travel through the element)

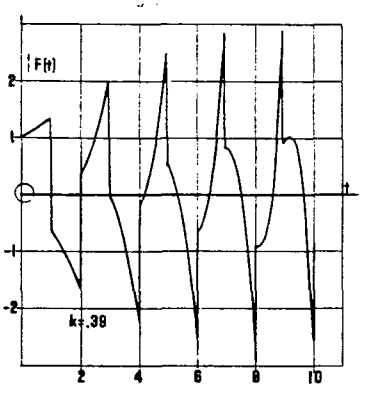

Fig 1.11 Short circuit mechanical response of a free piezoelectric plate when it is excited by a voltage pulse (From Stuetzer, 1967)
(t = nomalised to the time for wave to travel through the plate)

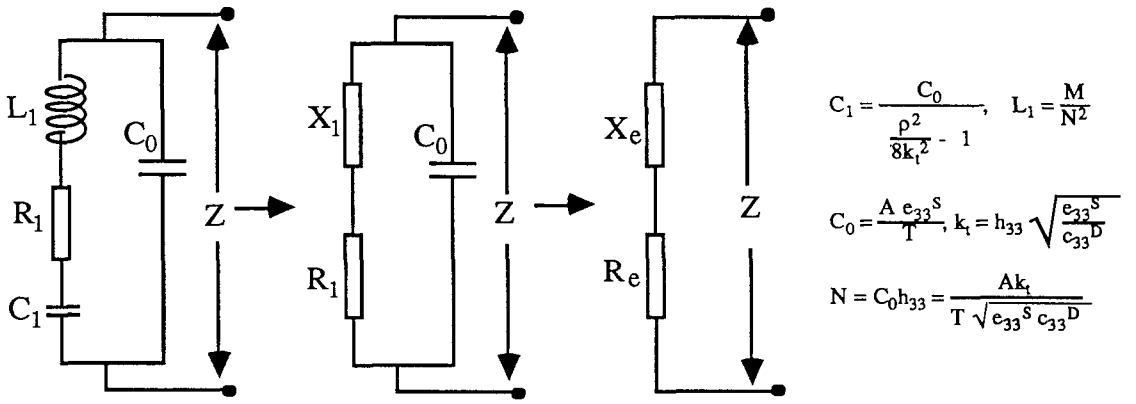

(a) the equivalent circuit around the resonance

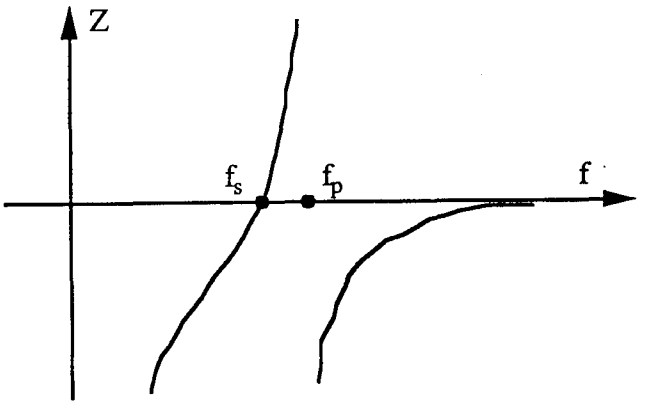

(b) the electrical impedance of the circuit

Fig 1.12 Approximate equivalent circuit of a piezoelectric disc

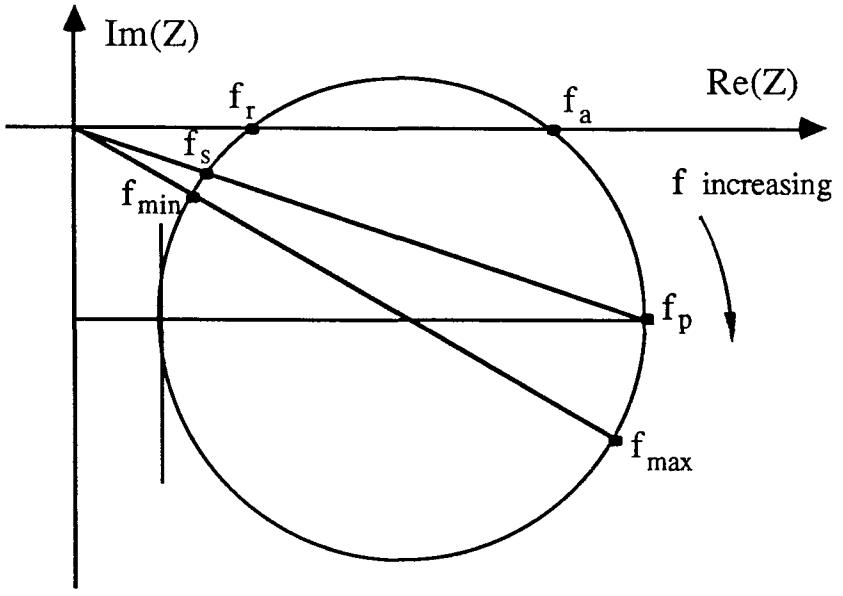

Fig 1.13 Nyquist plot of the electrical impedance of a piezoelectric disc around the thickness frequency

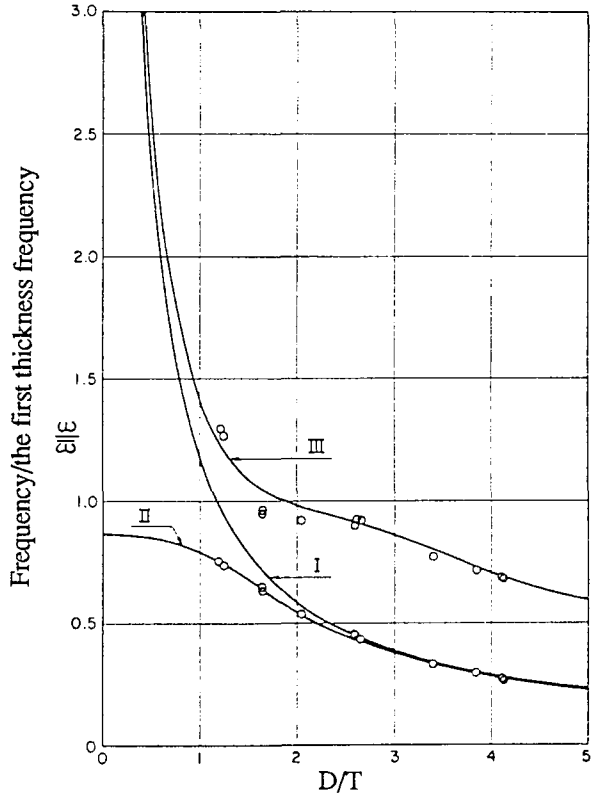

Fig 1.14 Normalised frequency spectrum of the first two radial modes as a function of D/T (From Kane and Mindlin, 1956)
Curve I: the first radial mode obtained by generalised plane stress theory;
Curve II: the first two radial modes by the first order plate theory;
Dots: Shaw's experimental results obtained

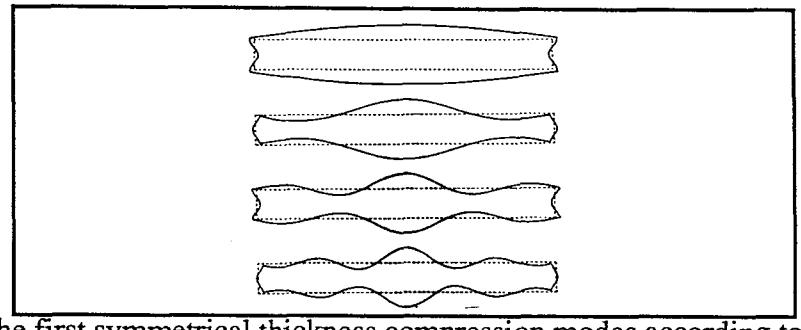

(a) the first symmetrical thickness compression modes according to BC I

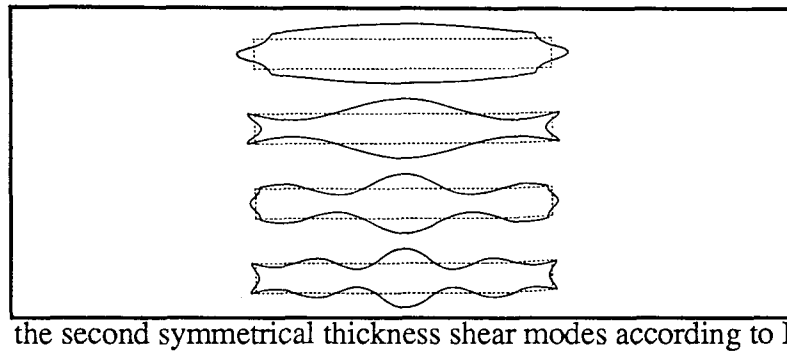

(b) the second symmetrical thickness shear modes according to BC I

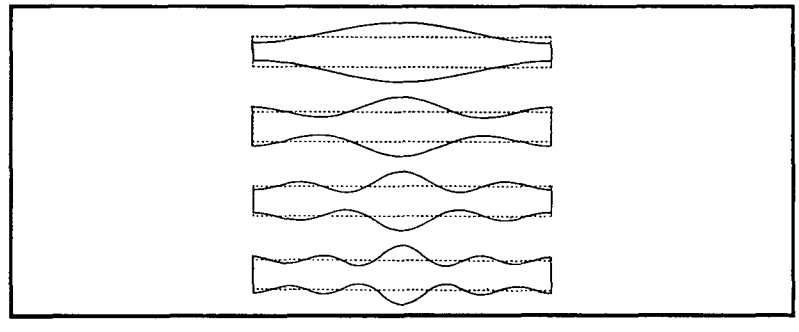

(c) the symmetrical thickness modes according to BC II

Fig 1.15 Mode shapes obtained by applying approximate boundary conditions (After Aggarwal, 1952b)

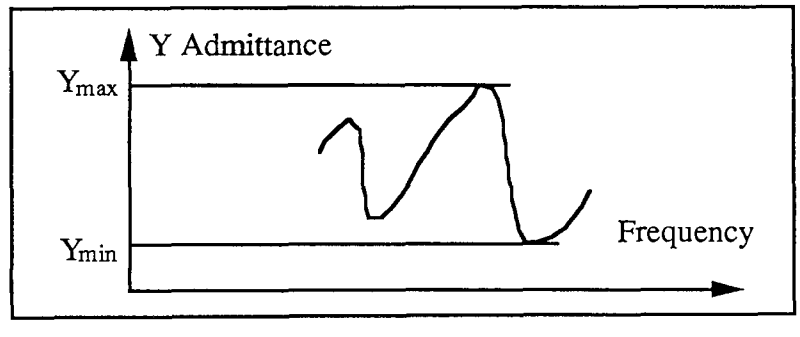

Fig 1.16 Schematic representation of the dynamic range defined by Ikegami

CHAPTER 2

ONE DIMENSIONAL ANALYSES OF VIBRATION CHARACTERISTICS OF PIEZOELECTRIC TRANSDUCERS

2.1 Introduction

Piezoelectric transducers are commonly analysed by one dimensional theory since the piezoelectric element usually has one dimension much different from the others. For instance, thin plates and discs which vibrate in their through thickness mode have lateral dimensions much larger than the thickness; and long bars and rods which vibrate in their longitudinal mode have lateral dimensions much smaller than the length.

It has been shown in Chapter 1 that a number of one dimensional techniques have been developed and they are still the most commonly used techniques in the analysis and design of piezoelectric transducers. It is therefore necessary to study the one dimensional analysis of the piezoelectric transducer in more detail.

In this chapter the vibration characteristics of piezoelectric transducers are studied in one dimension as a preliminary to further more complex analyses of transducers. The piezoelectric elements considered are thin discs. The transient response of the piezoelectric transducer is first studied in detail by the Laplace transformation method for open circuit and short circuit transducers, and the effect of backing on the response is discussed. A one dimensional mechanical model is then developed in which a piezoelectric structure is modelled as a degenerate two degree of freedom mass-spring system. The model is then applied to analyse the effects of mechanical damping and electric loss.

2.2 The one dimensional analysis of piezoelectric transducers

2.2.1 The constitutive equation and wave equations

The piezoelectric transducer working in the thickness mode is studied in this section. The piezoelectric disc is polarised parallel to the thickness direction, i.e., x direction as shown in Fig 2.1, and an electric field can exist only along the thickness direction (the wave front is an equipotential surface). In the thickness mode, the piezoelectric element dimensions in the plane perpendicular to the x axis are assumed to be infinite so that only through thickness vibration need be considered, and waves within the transducer propagate

without distortion in the x direction and remain plane whenever reflection and transmission occur.

If there are no magnetic field effects and adiabatic conditions are assumed, the constitutive equations which govern the plane compressional wave propagation in x direction (thickness direction) in piezoelectric materials are (Berlincourt *et al.*, 1964; Hilke, 1973),

$$T = c^D \frac{\partial u}{\partial x} - hD \tag{2.1}$$

$$E = -h \frac{\partial u}{\partial x} + \frac{D}{\varepsilon^S} \tag{2.2}$$

where u is the particle displacement in x direction, D is the electrical flux density or electrical displacement, T is the mechanical stress field, and E is the electric field. ε^S denotes the permittivity coefficient measured at constant strain S, c^D is the stiffness constant at constant charge density, h is the piezoelectric constant.

Applying Newton's second law to the transducer gives

$$\rho \frac{\partial u}{\partial x} = \frac{\partial T}{\partial x} \tag{2.3}$$

and Gauss' law, if there is no free charge inside the transducer, as for insulating crystals or ceramics gives

$$\text{div}\{D\} = 0 \tag{2.4}$$

Hence, since $\frac{\partial D}{\partial y} = \frac{\partial D}{\partial z} = 0$ from the previous assumptions,

$$\frac{\partial D}{\partial x} = 0 \tag{2.5}$$

Combining (2.1), (2.2), and (2.3) gives

$$\frac{\partial^2 u}{\partial t^2} = \frac{c^D}{\rho} \frac{\partial^2 u}{\partial x^2} - \frac{h}{\rho} \frac{\partial D}{\partial x} \tag{2.6}$$

Substitution of (2.5) into (2.6) gives

$$\frac{\partial^2 u}{\partial t^2} = v^2 \frac{\partial^2 u}{\partial x^2} \tag{2.7}$$

Equation (2.7) is the wave equation governing wave propagation in piezoelectric materials in which the polarisation direction is parallel to the direction of wave propagation, and the velocity of wave propagation is

$$v^2 = \frac{c^D}{\rho} \tag{2.8}$$

where $c^D = (\partial T/\partial S)_D$ is the elastic stiffness at constant flux density which should be distinguished from c^E, which is the elastic stiffness at constant electric field. The relationship between these two parameters is

$$c^D = c^E + \frac{h^2}{\varepsilon^S} \tag{2.9}$$

Hence the effective elastic stiffness increases due to the piezoelectricity; this phenomenon is known as stiffening effect of piezoelectricity.

The wave equation in non-piezoelectric elastic materials is (Auld, 1973),

$$\frac{\partial^2 u}{\partial t^2} = v^2 \frac{\partial^2 u}{\partial x^2}$$

but

$$v^2 = \frac{c^E}{\rho} \tag{2.10}$$

Hence, wave equations in piezoelectric and non-piezoelectric materials are identical, but the wave velocities are different. The solution of the wave equation can therefore be applied to both the piezoelectric element and the attached non-piezoelectric layers provided that the appropriate velocities are used.

2.2.2 Solutions by Laplace transformation

In order to solve the differential equation (2.7) the Laplace transform method is used in which,

$$f_L(s) = L[f(t)]$$

$$= \int_{-\infty}^{+\infty} e^{-st} f(t)\, dt \tag{2.11}$$

where $f_L(s)$ is the Laplace transform of f(t) and s is the Laplace operator. Having found the solution of the equation, the inverse Laplace transform must be employed to obtain the final analytical solution in the time domain.

The solution of the wave equation (2.7) obtained by applying the Laplace transform is

$$u_L = A\, e^{-\frac{x}{v}s} + B\, e^{+\frac{x}{v}s} \tag{2.13}$$

where A, B are constants to be determined by the boundary conditions. Equation (2.13) represents two waves which propagate in opposite directions with amplitude A and B,

and is valid for waves both in non-piezoelectric and piezoelectric material. The stress in non-piezoelectric materials can be found from the constitutive law and is given by,

$$T_L = c^E \frac{s}{v}[-A e^{-\frac{x}{v}s} + B e^{+\frac{x}{v}s}] \tag{2.14}$$

The force on the plane perpendicular to x direction is,

$$F_L = sZ_c[-A e^{-\frac{x}{v}s} + B e^{+\frac{x}{v}s}] \tag{2.15}$$

where F_L is the force applied on the surface, S is the area of the cross section, and

$$Z_c = \rho v S \tag{2.16a}$$

This is defined as the characteristic acoustic impedance of the material while the specific acoustic impedance is,

$$Z_s = \rho v \tag{2.16b}$$

For piezoelectric materials, an extra term hD is added to the stress due to the piezoelectric coupling shown in equation (2.1). Now $D_L = \frac{Q_L}{S}$, where Q is the electrical charge on the surfaces of the disc. Substitution of this and equation (2.15) into the constitutive equation (2.1) and (2.2) gives

$$F_L + hQ_L = sZ_c[-A e^{-\frac{x}{v}s} + B e^{+\frac{x}{v}s}] \tag{2.17}$$

With reference to Fig 2.1, if the thickness of piezoelectric element is a, the voltage across the transducer is

$$V_L = -[(V_a)_L - (V_0)_L] = \int_0^a E_L \, dx \tag{2.18}$$

Applying equation (2.2) and integrating with respect to x gives

$$V_L = -h[(u_L)_a - (u_L)_o] + \frac{Q_L}{C_0} \tag{2.19}$$

where $C_0 = \frac{\varepsilon^s S}{a}$ is the static capacitance of the piezoelectric element.

It can be seen that the voltage across the transducer is proportional to the change in thickness of the piezoelectric element.

2.2.3 Boundary conditions

As shown in Fig 1.1, the piezoelectric element is usually attached to other mechanical structures, such as a backing layer on one side, and a loading medium on the other side. The boundary conditions applied to the transducer are found by applying displacement continuity and force equilibrium on each interface as shown in Fig 2.1,

$$(u_1)_0 = (u)_0, \qquad (u_2)_a = (u)_a \tag{2.20}$$

and

$$(F_1)_0 + (F)_0 = 0 \qquad (F_2)_a + (F)_a = 0 \tag{2.21}$$

where subscripts 1 and 2 represent the load medium and backing respectively; subscripts '0' and 'a' outside the brackets refer to x = 0 and x = a.

In general, when the two electrodes on the surfaces of the piezoelectric material are connected to a electrical network, a current I(t) flowing through the network opposes the voltage building up, and an extra equation is therefore added,

$$V + I r = 0 \tag{2.22}$$

so

$$V_L + sQ_L r = 0 \tag{2.23}$$

where r is the external resistance. For simplicity, this is not considered here.

2.3 The transient response of a transducer as a receiver

2.3.1 The formulation of the solution

As discussed in the previous section there should be two waves in each layer travelling in opposite directions as shown in Fig 2.1. This can be simplified by considering different cases. The transducer is first considered as an open circuit receiver, which is a good approximation to practice because of the large impedance of the external device to which transducers are usually connected. The loading medium and backing layer are assumed to extend indefinitely away from the piezoelectric element, so no wave is reflected from the ends. An ultrasonic wave with amplitude A_1 coming from the loading medium is incident on the transducer. Since no wave comes from the backing, B_2 is zero.

Combining equations (2.13) to (2.19), the voltage response may be obtained as

$$V = \frac{A_1 h(1 - r_0)\,[1 - (1 + r_a)e^{-st} + r_a e^{-2st}]}{1 - r_0 r_a e^{-2st}} \tag{2.24}$$

where τ is time interval for a wave to travel through the piezoelectric element, thus,

$$\tau = \frac{a}{v}.$$

$$r_a = \frac{Z_c - Z_2}{Z_c + Z_2} \quad \text{and} \quad r_0 = \frac{Z_c - Z_1}{Z_c + Z_1}$$

are the reflection coefficients at the back (x = a) and front (x = 0) surfaces of the piezoelectric element. The corresponding transmission coefficients are defined as,

$$T_a = 1 + r_a = \frac{2Z_c}{Z_c + Z_2} \quad \text{and} \quad T_0 = 1 + r_0 = \frac{2Z_c}{Z_c + Z_1}$$

After expanding the denominator of equation (2.24) by the binomial theorem the final form is

$$V_L = A_1 h(1 - r_0)\,\Pi_V \tag{2.26}$$

where

$$\Pi_V = 1 - S_a + S_0 \tag{2.27}$$

$$S_a = (1 + r_a) \sum_{n=1}^{\infty} (r_0 r_a)^{n-1}\, e^{-(2n-1)st}$$

$$S_0 = r_0(1 + r_a) \sum_{n=1}^{\infty} (r_0 r_a)^{n-1}\, e^{-2nst}$$

A_1 depends on the input force applied to the front face of the transducer and from (2.15) is given by,

$$(F_1)_L = - A_1 s Z_1$$

Hence, the transfer function of a transducer as a receiver is

$$H_L(s) = \frac{V_L}{(F_1)_L} = C_V \frac{\Pi_V}{s} \tag{2.28}$$

where $C_V = -\dfrac{2h}{Z_c + Z_1}$ is the amplitude of the response.

From equations (2.27) it can be seen that in the open circuit receiver the voltage across the transducer generated by an incident ultrasonic wave consists of three parts: the unit term 1 represents the voltage generated at the instant when the incident mechanical force impinges on the front face of the piezoelectric element; the second term S_a is the voltage generated when the reverberating waves inside the element reach the back face of the element; the third term S_0 describes the voltage caused when the reverberating waves inside the element reach the front face of element. The equation (2.27) is independent of s;

it describes only the relative amplitude of the terms at different time intervals $e^{-ns\tau}$. Consequently, the voltage response depends only upon the form of the input force.

2.3.2 The solution for different forms of input force

Two kinds of input force, a Dirac pulse and a step function, are discussed, and the voltage response of transducers with different boundary conditions is predicted for these forces. The piezoelectric disc considered is made of PZT4 with a specific acoustic impedance of 345×10^5 kg/m^{2}s; its other properties can be found from Appendix A. For each force input, the voltage response is calculated for 5 different backing impedances 14.8×10^5, 115×10^5, 345×10^5, 1035×10^5 and 345000×10^5, which correspond to water, $r_a = 0.5$, matched backing, $r_a = -0.5$ and very rigid backing. In some case the responses for a free piezoelectric disc ($Z_1 = Z_2 = 0$) are discussed. Two loading media, with acoustic impedances of 14.8×10^5 (water) and 115×10^5 ($r_0 = 0.5$), are compared.

(i) Dirac pulse input $F_1 = \delta(t)$, and $(F_1)_L = 1$

By the inverse Laplace transform, the voltage in the time domain is given by,

$$V = C_V [\, H(t) - (1 + r_a)H(t - \tau) + r_a(1 + r_0)H(t - 2\tau) - ...] \qquad (2.29)$$

where H(t) is the Heaviside Function.

Fig 2.2(a) - (e) show plots of the voltage response of transducers for the above five kinds of backing. It can be seen that a voltage is produced across the transducer at the instant the Dirac pulse is applied; the voltage is then constant until the pulse reaches the back face of the disc; the voltage then changes phase due to the sign of the reflection coefficient at the back face provided that the backing is 'softer' than the disc (the impedance of the backing is smaller than that of the piezoelectric disc), see Fig 2.2(a) and (b). This kind of reverberation continues until the pulse dies away within the disc due to the transmission of waves into the loading and backing. The decay rate depends on the acoustic impedance of both the backing and loading; the rate increases as the impedance of backing approaches the matched case. If the transducer has no backing and air loading, the duration of the 'ringing' is a maximum as shown in Fig 2.2(f), while when the transducer has a matched backing, only one voltage pulse is produced, see Fig 2.2(c). If the backing is harder (the impedance of the backing is larger than that of the piezoelectric element) or rigid, the voltage does not change phase when the wave is reflected from the back face as shown in Fig 2.2(d). The front loading has a similar effect to that of the backing. The two curves in each figure show that the larger the acoustic impedance of the front loading, the less the voltage is obtained.

(ii) Step unit function $F_1 = H(t)$, and $(F_1)_L = \frac{1}{s}$

The voltage response is then,

$$V = C_V \left[t - H(t_{2n-1})(1+r_a) \sum_{n=1}^{\infty} (r_0 r_a)^{2n-1} t_{2n-1} + H(t_{2n}) r_a (1+r_0) \sum_{n=1}^{\infty} (r_0 r_a)^{2n} t_{2n} \right] \quad (2.30)$$

where $t_{2n-1} = t - (2n - 1)\tau$, and $t_{2n} = t - (2n)\tau$, n = 1, 2, 3, ... integer.

Hence the voltage response is proportional to t within each time interval τ for an applied step force. Fig 2.3 (a) - (f) show the response for different backings. It can be seen that when the force is applied to the front face of the transducer the voltage generated starts at zero, builds up linearly and then decreases when the wave reaches the back face; it then continues to reverberate until it dies away due to the damping effect of the backing and loading. Other features of the response are similar to the case of a Dirac impulse, except that after a period of reverberations the voltage approaches a constant dc value which is given by,

$$V = \frac{C_V \tau (1 - r_a)}{1 - r_a r_0} \quad (2.31)$$

2.4 The transient response of a transducer as a transmitter

2.4.1 The formulation of the general solution

In this section the transducer is considered as a transmitter whose function is to generate an ultrasonic wave when an external voltage is applied across it. The mechanical response of the transducer is more complicated than the voltage response, due to the interactive coupling of piezoelectricity (which is represented by the negative capacitance in the electrical analogue models as shown in Fig 1.8). If this effect is ignored, the mechanical response can be derived as an impulse diagram (Redwood 1963, 1964) as shown in Fig 1.10 of Chapter 1. A general solution has been obtained by Stuetzer (1967) for a free piezoelectric plate, which showed that for a step voltage excitation the stress response consists initially of alternating exponential pulses which decay to a form similar to a sine wave accompanied by a sequence of sharp spikes. This exponential alternation becomes more significant as the degree of piezoelectric intercoupling is increased. In this section, the general solution for the mechanical response of the transducer is obtained with arbitrary mechanical boundary conditions, and the response to different forms of applied voltage is discussed.

The transducer working in transmitter mode can be considered short circuited since the external energy source has very small resistance. The boundary conditions applied to the transducer are similar to those for a receiver, as the loading and backing are assumed to extend indefinitely away from the piezoelectric element, so no wave can come back, which results $A_1 = B_2 = 0$ in Fig 2.1.

The input voltage is assumed to be of the form $V = V(t)$, where $V(t)$ describes the input form and the amplitude is unity, and its Laplace transform is $V_L(s)$. From equations (2.13) to (2.15) the mechanical displacement at $x = 0$, the front face of the transducer, may be shown to be

$$(u_0)_L = C_u V_L(s) \frac{1 - (1 + r_a)e^{-s\tau} + r_a e^{-2s\tau}}{K(s - \alpha)} \tag{2.32}$$

where

$$C_u = -\frac{k_t^2 T_0}{2h\tau}$$

$$\alpha = \frac{k_t^2(T_0 + T_a)}{2\tau}$$

$$K = 1 + b_1 e^{-s\tau} + b_2 e^{-2s\tau}$$

$$b_1 = \frac{C_1}{s - \alpha} \text{ and } b_2 = k_r + \frac{C_2}{s - \alpha}$$

$$C_1 = \frac{k_t^2 T_0 T_a}{\tau} \text{ and } C_2 = \frac{k_t^2(r_a T_0^2 + r_0 T_a^2)}{2\tau}$$

$$k_r = r_0 r_a$$

Here, α is known as the time factor, and plays an important role in determining the form of the response; C_u determines the amplitude of the displacement response; C_1, C_2, k_r are constants in terms of k_t, τ and the reflection and transmission coefficients r_0, r_a, T_0, T_a; while b_1, b_2 and K are related to Laplace operator, s. The denominator K^{-1} can be expanded as follows,

$$\begin{aligned} K^{-1} &= (1 + b_1 e^{-s\tau} + b_2 e^{-2s\tau})^{-1} \\ &= 1 - (b_1 e^{-s\tau} + b_2 e^{-2s\tau}) + (b_1 e^{-s\tau} + b_2 e^{-2s\tau})^2 - (b_1 e^{-s\tau} + b_2 e^{-2s\tau})^3 + (b_1 e^{-s\tau} + b_2 e^{-2s\tau})^4 - \ldots \\ &= 1 - b_1 e^{-s\tau} + (b_1^2 - b_2)e^{-2s\tau} - (b_1^3 - 2b_1 b_2)e^{-3s\tau} \\ &\quad + (b_1^4 - 3b_1^2 b_2 + b_2^2)e^{-4s\tau} - (b_1^5 + 3b_1 b_2^2 + 4b_1^2 b_2)e^{-5s\tau} + \ldots\ldots \end{aligned}$$

Combining K^{-1} with $[1 - (1 + r_a)e^{-s\tau} + r_a e^{-2s\tau}]$ leads to a function $\Pi_u(s)$ in which the terms come into effect successively according to the delay factor $e^{-ns\tau}$

$$\begin{aligned}\Pi_u &= 1 \\ &- (b_1 + T_a)\, e^{-s\tau} \\ &+ (b_1^2 - b_2 + T_a b_1 + r_a)\, e^{-2s\tau} \\ &- [b_1^3 - 2b_1 b_2 + T_a(b_1^2 - b_2) + r_a b_1]\, e^{-3s\tau} \\ &+ [b_1^4 - 3b_1^2 b_2 + b_2^2 + T_a(b_1^3 - 2b_1 b_2) + r_a(b_1^2 - b_2)]\, e^{-4s\tau} \\ &- [b_1^5 + 3b_1 b_2^2 - 4b_1^3 b_2 + T_a(b_1^4 - 3b_1^2 b_2 + b_2^2) + r_a(b_1^3 - 2b_1 b_2)]\, e^{-5s\tau} \\ &+ \ldots \end{aligned} \tag{2.33}$$

Hence, equation (2.32) can be written as

$$(u_0)_L = V_L(s)\, C_u \frac{\Pi_u}{s - \alpha} \tag{2.34}$$

So the transfer function of the transducer as a transmitter is

$$F_L(s) = \frac{(u_0)_L}{V_L} = C_u \frac{\Pi_u}{s - \alpha} \tag{2.35}$$

The mechanical response in terms of force is then given by,

$$(F_0)_L = (u_0)_L\, sZ_1 \tag{2.36}$$

The physical meaning of equation (2.34) is much easier to see than that of equation (2.32). In the amplitude C_u, $\frac{1(\text{Volt})}{h}$ has the dimensions of displacement, and is the static mechanical response of the piezoelectric disc when the voltage is applied extremely slowly (Silk, 1984); k_t is the piezoelectric coupling factor which represents the effect of piezoelectricity and the power transduction; T_0 describes the effect of mechanical loading on the wave produced at x = 0, i.e the position of the ultrasonic sound source. These two factors show the effect of both the electrical and mechanical properties of the transducer on the static mechanical response. The remaining terms and the sequence function Π_u are involved with the transient part of the response. In contrast to the voltage response discussed in the last section, the sequence function, Π_u, given by (2.33), is very complicated and is dependent on both s and α. The terms involving α, C_1 and C_2 in the sequence function Π_u represent the intercoupling between the mechanical and electrical properties, i.e., the secondary action of piezoelectricity (Hayward, 1984) or acoustic regeneration (Zhang *et al.*, 1986). The shape of mechanical response depends not only on the input form but also on the sequence function.

If the coupling factor k_t is very small, α, C_1, C_2 can be ignored, and equation (2.34) reduces to the approximate solution obtained from the Impulse diagram as shown in Fig 1.10. In the following examples both the general and approximate solutions are used to predict the mechanical response of the transducer .

2.4.2 The solution for different forms of applied voltage

Four forms of voltage applied across the transducer are discussed: Dirac, step, sine wave, and pulsed sine wave. The complete solution is too complicated to list fully here, only the response $0 \le t \le \tau$, is given in detail, except that for the Dirac input the displacement response is listed up to the sixth term as an illustration. However, for all cases responses are predicted and plotted up to 10τ. The materials used and loading cases are similar to the previous section.

(i) Dirac pulse voltage $V = \delta(t)$, and $V_L = 1$

The displacement on the front face of transducer, u_0, $(0 \le t \le 5\tau)$ is given by

$$
\begin{aligned}
u_0 = C_u \{ & e^{\alpha t} \\
& - [(T_a + C_1 t_1) e^{\alpha t_1}] \\
& + [(k_r + r_a) + (C_2 + T_a C_1) t_2 + \frac{1}{2!} C_1^2 t_2^2] e^{\alpha t_2} \\
& - [T_a k_r + (2C_1 k_r + r_a C_1 + T_a C_2) t_3 + \frac{1}{2!} (2C_1 C_2 + T_a C_1^2) t_3^2 + \frac{1}{3!} C_1^3 t_3^3] e^{\alpha t_3} \\
& + [(k_r^2 + r_a k_r) + (2C_2 k_r + r_a C_2 + 2T_a k_r C_1) t_4 + \frac{1}{2!} (3C_1^2 k_r + C_2^2 + r_a C_1^2 + 2T_a C_1 C_2) t_4^2 \\
& + \frac{1}{3!} (3C_1^2 C_2 + T_a C_1^3) t_4^3 + \frac{1}{4!} C_1^4 t_4^4] e^{\alpha t_4} \\
& - [T_a k_r^2 + (3C_1 k_r^2 + 2r_a k_r C_1 + 2T_a k_r C_2) t_5 + \frac{1}{2!} (6C_1 C_2 k_r + 2r_a C_1 C_2 + 3T_a k_r C_1^2 + T_a C_2^2) t_5^2 \\
& + \frac{1}{3!} (3C_1 C_2^2 + 4C_1^3 k_r + r_a C_1^3 + 3T_a C_1^2 C_2) t_5^3 + \frac{1}{4!} (4C_1^3 C_2 + T_a C_1^4) t_5^4 + \frac{1}{5!} C_1^5 t_5^5] e^{\alpha t_5} \\
& + \ldots \} \qquad (2.37)
\end{aligned}
$$

where $t_n = t - n\tau \ge 0$ $n = 1, 2, 3, \ldots$, integer.

When the piezoelectric coupling factor is small, for example with Quartz, $k_t = 0.1$, the intercoupling effect can be ignored, α, C_1 and C_2 may be neglected compared with other terms, and $e^{at} \approx 1 + \alpha t \approx 1$, therefore only the first term in each transient term remains, and the solution becomes

$$u_0 = C_u[1 - H(t_1)T_a + H(t_2)(k_r + r_a) - H(t_3)T_a k_r + H(t_4)(k_r^2 + r_a k_r) - H(t_5)T_a k_r^2 + \ldots] \quad (2.38)$$

where $t_n = t - n\tau \ge 0$ $n = 1, 2, 3, \ldots$, integer. This is identical to the Impulse diagram given by Redwood (1963) as shown in Fig 1.10.

For a free piezoelectric plate, substituting $r_0 = r_a = 1$ into the solution (2.37), leads to

$$u_0 = C_u \{ e^{\alpha t}$$

$$
\begin{aligned}
&- 2\, e^{\alpha t_1}(1 + \alpha t_1) \\
&+ 2\, e^{\alpha t_2}(1 + 3\alpha t_2 + \alpha^2 t_2^2) \\
&- 2\, e^{\alpha t_3}(1 + 5\alpha t_3 + 4\alpha^2 t_3^2 + \tfrac{2}{3}\alpha^3 t_3^3) \\
&+ 2\, e^{\alpha t_4}(1 + 7\alpha t_4 + 9\alpha^2 t_4^2 + \tfrac{2}{3}\alpha^3 t_4^3 + \tfrac{1}{3}\alpha^4 t_4^4) \\
&- 2\, e^{\alpha t_5}(1 + 9\alpha t_5 + 16\alpha^2 t_5^2 + \tfrac{2}{3}\, 14\alpha^3 t_5^3 + \tfrac{1}{3}\, 6\alpha^4 t_5^4 + \tfrac{2}{15}\alpha^5 t_5^5) \\
&+ \ldots\}
\end{aligned}
\tag{2.39}
$$

where $t_n = t - n\tau \geq 0$ $n = 1, 2, 3, \ldots$, integer. This is identical with the solution given by Stuetzer (1967).

Fig 2.4 shows the displacement responses with varying mechanical boundary conditions for a Dirac input voltage. In each plot, the two curves show the general solution given by (2.37) and the approximate solution by (2.38) or the Impulse diagram as shown in Fig 1.10 of Chapter 1. It can been seen from these plots that the displacement response of a short circuited transmitter is very complicated. When a delta voltage pulse is applied across the transducer, waves are immediately generated at both front and back faces of the element with amplitudes A, B, B_1 and A_2. The waves represented by A and B propagate within the piezoelectric element, and reflection and transmission occur at each interface, and the secondary piezoelectric action takes place to modify the response. Obviously the response by the approximate solution (2.38) has no such feature.

It can be seen that the mechanical displacement generated instantaneously at t = 0 by the applied voltage varies exponentially within the first interval, τ, due to the effect of secondary piezoelectricity. At $t = \tau$, a spike appears when part of wave B is transmitted into the loading medium. This behaviour is repeated each time when the waves inside the element reach the two interfaces, and after several periods the displacement approaches a sinusoidal form while the amplitude decays gradually. It was shown by Stuetzer (1967) that for a free piezoelectric plate this response may decay to a sine wave; this feature may be seen from Fig 2.4(f) in which the piezoelectric element is free from any backing and loading. The decay rate depends on the impedances of the loading and backing as shown in Fig 2.4(a)-11(e); when the backing is matched, the shortest signal is generated as shown in Fig 2.4(c). When the backing has a higher impedance than the piezoelectric disc, the response does not change phase when the wave reaches the back interface, which can be seen from Fig 2.4(d) and (e).

(ii) Step function voltage, V = H(t), $t \geq 0$, and $V_L = \frac{1}{s}$

The transient displacement response in $0 \leq t \leq \tau$ is given as

$$u_0 = C_u(e^{\alpha t} - 1) \tag{2.40}$$

The responses for five different backing are shown in Fig 2.5(a) - (e), and that for a free piezoelectric disc in Fig 2.5(f). It can been seen that at the start, the displacement response builds up nearly linearly; after the first interval, it decreases but the relationship with time is no longer linear due to the intercoupling effect; the response oscillates with a period of 2τ until it approaches a constant value. The amplitude of the response predicted by the general equation is larger than that by the Impulse diagram; the difference between the two at the first interval is $C_u(e^{\alpha\tau} - 1 - \alpha\tau)$.

The mechanical loading and backing have a similar effect as in the response to a Dirac pulse. In the case of matched backing, the response reaches a dc value after time τ by the Impulse diagram, but the general solution predicts some overshooting as shown in Fig 2.5(c). For a free piezoelectric disc, the maximum reverberation occurs , see Fig 2.5(f).

(iii) Sine excitation with $V = \sin(\omega t)$, and $V_L = \dfrac{\omega}{s^2 + \omega^2}$

The transient response when $0 \le t \le \tau$ is

$$u_0 = C_u \left[e^{\alpha t} - \cos(\omega t) - \frac{\alpha}{\omega} \sin(\omega t) \right] \qquad (2.41)$$

Fig 2.6(a) - (e) compares the general solution with that from the Impulse diagram for different backing conditions. The driving frequency is the open circuit frequency defined by (1.1). It can been seen that there are significant differences between the two curves; the response by the impulse diagram oscillates at the resonant frequency and the amplitude tends to infinity, while the response by the general solution has finite amplitude and smaller frequency than the driving frequency. This demonstrates that the short circuit resonant frequency of a transducer with high piezoelectric coupling factor (0.51 for PZT4) is lower than the frequency of the thickness mode at open circuit. Therefore, if a transducer with high intercoupling effect is driven by a voltage at the open circuit frequency, the mechanical response at the start is dominated by the transient response, and after several periods it approaches the steady state response. This phenomenon corresponds to that reported by Onoe *et al.* (1963) in which it was shown that the resonant frequency of a thin piezoelectric plate is shifted lower than the thickness frequency.

The rate of increase of the response is affected by the mechanical loading and backing, see Fig 2.6(a), (b) and for matched backing the amplitude of the oscillations is constant after time τ as shown in Fig 2.6(c). When the backing is of higher impedance than the transducer, the response no longer tends to infinity; in particular for rigid backing, it decreases gradually, see Fig 2.6(d) and (e).

(iv) Pulsed sine voltage excitation $V = \sin(\omega t)$ $(0 \le t \le T, T = \frac{\pi}{\omega}$ or $\frac{2\pi}{\omega})$

The responses to sine voltage excitations with duration of a half cycle or one cycle are of interest since they are close to the pulse shape used to excite piezoelectric transducers. The responses to a half cycle sine voltage for $Z_2 = 115 \times 10^5$ and 345×10^5 are shown in Fig 2.7(a) and (b). It can be seen that with matched backing, the displacement response is close to the applied pulse form, see Fig 2.7(b), however, a small reverberation (overshooting) is seen in the general solution. The responses to one cycle sine voltage for both backings are shown in Fig 2.8.

2.4.3 Discussion

It has been shown that the piezoelectric coupling factor has a great effect on the transient response. When the coupling factor is large, the amplitude of response is increased and the response form is modified, and the difference between the open circuit frequency and the short circuit frequency is also increased. When the coupling factor is small, the approximate method or the impulse diagram gives good results.

The mechanical backing is an important factor in the control of the response level and the duration of the ringing (sensitivity and bandwidth). When the impedance of the backing is smaller than that of the piezoelectric element, the response changes phase each time the waves inside the element reach the front and back faces of the element, and gradually decreases. However, for the case of free loading and backing, the oscillation would not die away in the absence of mechanical damping in the piezoelectric element. When the backing impedance approaches the matched case, the response tends to die away rapidly. In the case of matched backing, only one signal is produced which is very close to the input form. When the backing is 'harder' than the transducer, the response only changes phase at intervals of 2τ and gradually decreases. When the backing is rigid, the wave is completely reflected at the back interface without changing phase.

2.5 A one dimensional mechanical model of piezoelectric transducers

A one dimensional mechanical vibration model of piezoelectric structures is presented in this section. It can be used to aid understanding of the mechanism of the vibration of piezoelectric transducers, particularly the interpretation of the characteristic frequencies of the transducers in the vibration viewpoint, and it may be useful for transducer design when both the mechanical damping and the electrical loss are considered. The piezoelectric

structure is assumed to vibrate in one dimension only, and the vibration and materials are linear.

The piezoelectric structures considered are mainly discs with large D/T ratios and rods with very small D/T ratios although it is also applicable to other structures vibrating in a one dimensional manner, such as spheres in pure radial vibration. The electrodes on the surfaces are considered to be very thin, and their mechanical properties, such as mass and stiffness are negligible.

2.5.1 A degenerate two degree of freedom mechanical vibration system

In mechanical vibration analysis a spring and a mass system can be used to model an elastic structure which vibrate around resonance. Similarly, a simple mechanical mass-spring system can be used to analyse the vibration characteristics of a piezoelectric structure. The following equations describe the degenerate two degree of freedom system in which has only one mass component as shown in Fig 2.9

$$m_1 \ddot{x}_1 + c_1 \dot{x}_1 + (k_1 + \eta^2 k_2) x_1 - \eta k_2 x_2 = f_1 \quad (2.42a)$$

$$-\eta k_2 x_1 + k_2 x_2 = f_2 \quad (2.42b)$$

where m_1, k_1, c_1 are the mechanical mass, stiffness and damping of the piezoelectric structure, and x_1, f_1 are the mechanical displacement and force respectively; k_2 is the electrical 'stiffness' (dielectric stiffness) which can be determined by the static capacitance of the structure, x_2 is the electrical displacement, which represents the voltage across the electrodes, and f_2 is the electrical force, which represents the total electrical charge on the electrode; η is a transformation factor between mechanical and electrical variables, which for a piezoelectric disc vibrating in the thickness mode is given by

$$\eta = \frac{e^{33}}{\varepsilon_{33}^S} \quad (2.43)$$

where e_{33} and ε_{33}^S are the piezoelectric and dielectric constant in the thickness direction.

Three cases of the solution are discussed according to excitation manners.

(i) Electrical excitation

If the transducer is excited by an electrical signal, and $f_1 = 0$, which is the case when transducers are used as transmitters, and if a voltage is applied across the electrodes of the transducer, then assuming harmonic excitation and vibration, $x_2 = X_2 e^{i\omega t}$, $f_2 = F_2 e^{i\omega t}$ and $x_1 = X_1 e^{i\omega t}$, from equation (2.42a)

$$m_1 \ddot{x}_1 + c_1 \dot{x}_1 + (k_1 + \eta^2 k_2)\, x_1 = \eta k_2\, x_2 \tag{2.44}$$

Since the RHS of the above equation is a known force, the natural frequency of this mass spring system is given by

$$\omega_s^2 = \frac{k_1 + \eta^2 k_2}{m_1} \tag{2.45}$$

This is defined as the series frequency of the transducer, so

$$X_1 = \frac{\eta k_2\, X_2}{k_1 + \eta^2 k_2 - m_1 \omega^2 + i\, c_1 \omega}$$

This is the mechanical displacement response when the piezoelectric structure is excited by applying a voltage, the mechanical frequency response function (FRF) for voltage excitation can therefore be written as

$$\frac{X_1}{X_2} = \frac{\eta k_2}{k_1 + \eta^2 k_2 - m_1 \omega^2 + i\, c_1 \omega} \tag{2.46a}$$

Substituting (2.46a) into (2.42b) gives

$$\frac{F_2}{X_2} = \frac{-(\eta k_2)^2}{k_1 + \eta^2 k_2 - m_1 \omega^2 + i\, c_1 \omega} + k_2$$

which can be written as

$$\frac{F_2}{X_2} = \frac{k_2(k_1 - m_1 \omega^2 + i\, c_1 \omega)}{k_1 + \eta^2 k_2 - m_1 \omega^2 + i\, c_1 \omega} \tag{2.46b}$$

This can be defined as the electrical frequency response function since it is the ratio of voltage to electrical charge.

The mechanical frequency response function for charge excitation can be found by dividing (2.46a) by (2.46b) and is given by

$$\frac{X_1}{F_2} = \frac{\eta}{k_1 - m_1 \omega^2 + i\, c_1 \omega} \tag{2.46c}$$

where the parallel resonant frequency of the transducer is defined as

$$\omega_p^2 = \frac{k_1}{m_1} \tag{2.47}$$

The electrical impedance of the transducer can easily be found from (2.46b) as

$$Z(\omega) = \frac{k_1 + \eta^2 k_2 - m_1 \omega^2 + i\, c_1 \omega}{i \omega k_2 (k_1 - m_1 \omega^2 + i\, c_1 \omega)} \tag{2.48}$$

Since the electrical stiffness k_2 is negative (dielectric property), the series frequency defined by (2.45) is smaller than the parallel frequency by (2.47). It can be seen from (2.46a) and (2.46c) that if there is no loss at the series frequency the mechanical response at constant voltage reaches a maximum, and the mechanical response at constant charge is a finite value, while at the parallel frequency, the mechanical response at constant charge reaches a maximum and the mechanical response at constant voltage is finite. However, the electrical response, which is usually expressed in terms of impedance in (2.48), drops to a minimum at the series frequency and reaches a maximum at the parallel frequency.

The mechanical stiffness and mass can be obtained approximately by expanding the one dimensional analytical solution in a similar way as to obtain the parameters of the equivalent electrical circuit as shown in Fig 1.12(a) (Berlincourt *et al.*, 1963). However, they may also be obtained by equating (2.45) and (2.47) to corresponding series and parallel frequencies obtained from the one dimensional analytical solution defined by (2.3) and (2.2).

(ii) Mechanical excitation

If the structure is excited by a mechanical force f_1, and $f_2 = 0$, which is the case for open circuit receivers, and assuming $f_1 = F_1 e^{i\omega t}$, from equations (2.42) the frequency response functions can be found as,

$$\frac{X_1}{F_1} = \frac{1}{k_1 - m_1\omega^2 + i\, c_1\omega} \tag{2.49a}$$

$$\frac{X_2}{F_1} = \frac{\eta}{k_1 - m_1\omega^2 + i\, c_1\omega} \tag{2.49b}$$

It can be seen that the transducer working as a receiver then vibrates at the parallel frequency as given by (2.47). The mechanical displacement and the electrical voltage reach maxima at the parallel frequency.

From the vibration point of view, it is evident from both cases that the system behaves like a resonator at the series frequency, and acts as an absorber at the parallel frequency. This is reasonable since the transducer is used as a transmitter at the series frequency and as a receiver at the parallel frequency.

(iii) Resistors

If the transducer is considered in connection with a voltage source with an internal resistor of R, then an extra equation is needed as,

$$x_2 + R\,\dot{f}_2 = E_V \tag{2.42c}$$

where E_V is the source voltage. However, this is not treated in the current thesis.

2.5.2 Application to thin piezoelectric discs

In this section some theoretical results are presented by applying the mechanical model to a thin piezoelectric disc.

In the approximate equivalent circuit as shown in Fig 1.12 in Chapter 1 the lumped electrical components are found from the first order approximation of the power series (Mason, 1948; Berlincourt *et al.*, 1964). Here, the lumped mass and stiffness in the mechanical model can be found in a similar way. However, for convenience and accuracy they can also be obtained directly from the series and parallel frequencies given by the one dimensional analytical method. The electrical impedance, and the mechanical frequency response functions at constant voltage and at constant charge defined in (2.48) and (2.46) are then computed in the frequency range of interest.

The prediction is made with a thin piezoelectric disc, PZT5A, a modified lead zircorate titanate; the material properties are listed in Table A.1 of Appendix A with a mechanical Q factor of 75. The disc is 40.10 mm in diameter and 2.03 mm thick, giving a D/T ratio of 20.

In Fig 2.10(a) the predicted electrical impedance of the disc by the mechanical model is shown as a solid line, together with the electrical impedance predicted by the one dimensional analytical theory given by equation (1.5) of Chapter 1 which is shown as a broken line. It can be seen that excellent agreement is obtained throughout the frequency range of interest. Fig 2.10(b) and (c) show the mechanical response function at constant voltage and the mechanical response function at constant charge predicted by the one dimensional mechanical model.

The effects of mechanical damping on the behaviour of the piezoelectric disc are clearly seen in Fig 2.11 where the mechanical structural damping factor is varied from 0.001 to 0.1. As expected, with increasing damping, the resonant frequencies shift slightly lower and the amplitudes at the resonant frequencies are reduced.

The superposition method can be used to calculate the response over a large frequency range which includes other thickness modes. In Fig 2.12(a) the electrical impedance response is predicted for the same disc in the frequency range 10 to 6500 kHz, which includes the first three through thickness modes (1st, 3rd, 5th thickness modes), and the electrical impedance response given by the analytical method is also shown in Fig 2.12(a) as a broken line. The structural damping factor of 0.0133 which corresponds to the mechanical Q factor of 75 for PZT5A is included in the prediction, so the response amplitudes at the resonant frequencies predicted by the mechanical model are finite and gradually decrease with increasing frequency. Fig 2.12(b) and (c) are the corresponding mechanical FRF at constant voltage and at constant charge respectively.

Piezoelectric elements are often connected with other electrical components. The electrical impedance response has been predicted for piezoelectric discs connected with resistors and inductors as shown in Fig 2.13. Fig 2.13(a) shows the response of a system in which the disc is in series with resistances of 0, 1, 5, 10, 20, 50 Ω. It can be seen that the impedance at the resonant frequency increases as the series resistance increases, which broadens the bandwidth over the resonant frequency range, while the impedance at the anti-resonant frequency remains unchanged.

Fig 2.13(b) shows the effect of a shunt inductance on the electrical impedance of piezoelectric discs as the inductance changes from 1 μH to 20 μH. It can be seen that the impedance in the low frequency range has been reduced by the shunt inductance.

In broadband transducers an inductor placed in parallel with the piezoelectric element is usually used as a tuning element for the system (O'Donnell *et al.*, 1981) together with a series resistor as shown in Fig 2.14(a). The corresponding electrical impedance response of such a system for a 10 Ω series resistor and a 5 μH shunt inductor is shown in Fig 2.14(b). It can be seen that the tuning system reduces the low frequency impedance and increases the bandwidth of the resonance.

It is evident from the above examples that the piezoelectric disc working in the thickness mode can be modelled by a simple mechanical mass and spring vibration system, and the model can be used to assist the understanding of the operating principles of piezoelectric transducers, and mechanical damping and electrical loss can easily be included.

2.6 Conclusions

The one dimensional analyses of vibration characteristics of piezoelectric discs have been studied in detail in this chapter in both the transient response and steady state response of piezoelectric transducers.

The transient study by the Laplace transform can be very tedious even for the simple cases. It has been shown that the short circuit mechanical response is much more complicated than the open circuit electrical response due to the secondary piezoelectric effect. The acoustic impedance of the backing has a great influence on the response of the transducers.

A simple mechanical vibration model of piezoelectric discs, which is based on a degenerate two degree of freedom mass-spring system, has been developed. It has been shown that the model can give easy interpretation of the characteristic frequencies of the piezoelectric transducers. The model has also been used to predict the electrical impedance response and the mechanical frequency response functions both with and without mechanical damping. Good agreement with the predictions by the analytical method have been obtained.

However, the above analyses are limited to one dimensional motion. To account for other vibration modes of piezoelectric discs, three dimensional models have to be used. This is discussed in the following chapters.

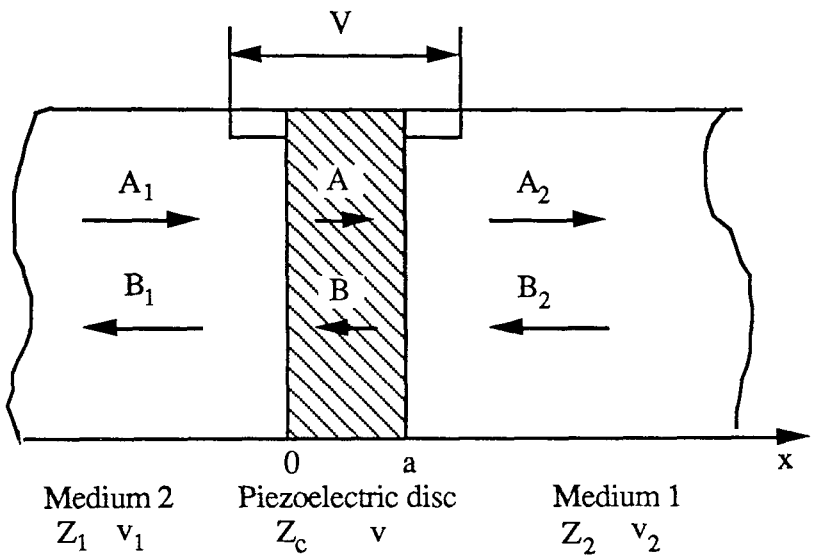

Fig 2.1 Boundary conditions and wave propagation in a transducer
(V: voltage; A and B are amplitudes of the waves in the piezoelectric element, v and Z are corresponding velocity and acoustic impedance; subscripts 1, 2 refer to parameters for media 1 (loading) and 2 (backing))

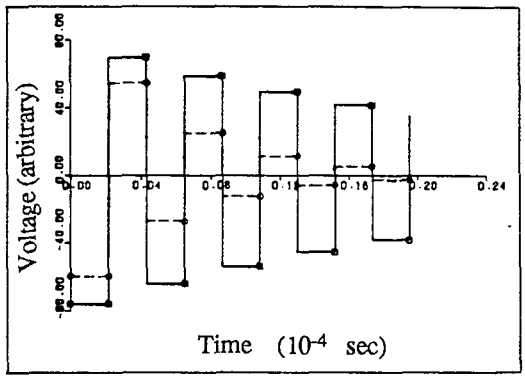

(a) $Z_2 = 14.8 \times 10^5$ kg/m^{2}s (water)

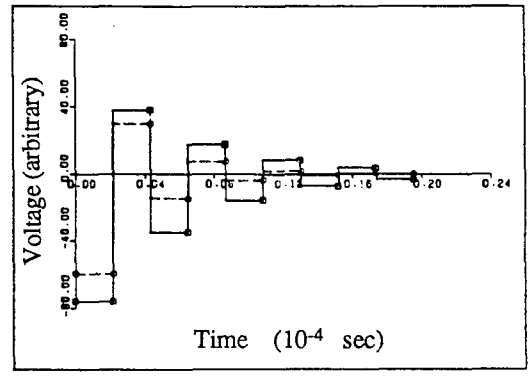

(b) $Z_2 = 115 \times 10^5$ kg/m^{2}s ($r_a = 0.5$)

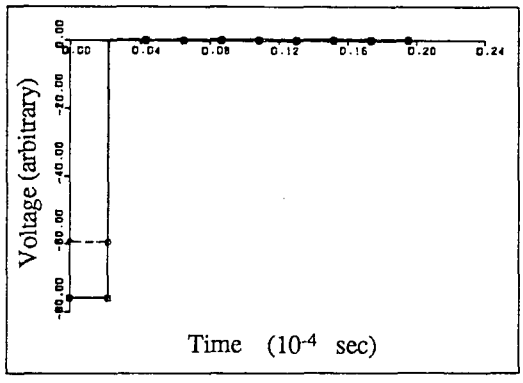

(c) $Z_2 = 345 \times 10^5$ kg/m^{2}s (matched backing)

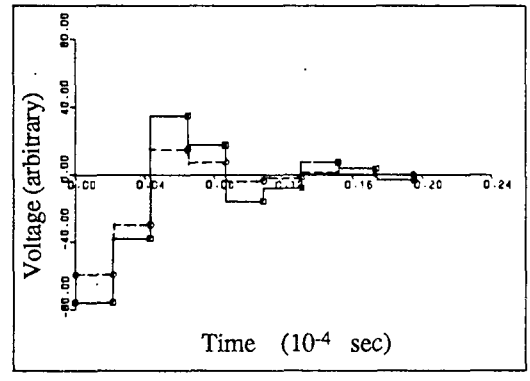

(d) $Z_2 = 1035 \times 10^5$ kg/m^{2}s ($r_a = -0.5$)

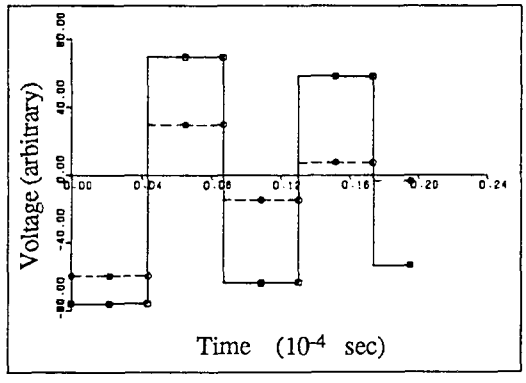

(e) $Z_2 = 345 \times 10^8$ kg/m^{2}s (rigid backing)

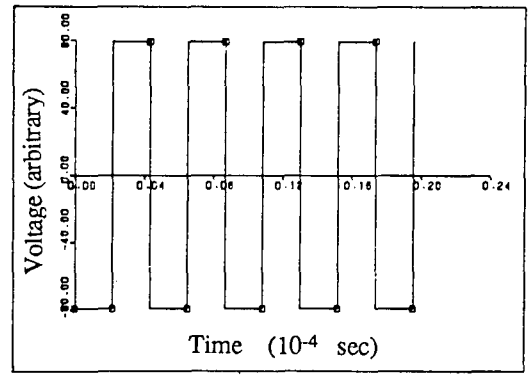

(f) free piezoelectric disc

Fig 2.2 The voltage response of a piezoelectric transducer when a Dirac force pulse is applied at the front face for different backing (Z_2) ($Z_c = 345 \times 10^5$ kg/m^{2}s (PZT4); front loading, solid lines: $Z_1 = 14.8 \times 10^5$; broken lines: $Z_1 = 115 \times 10^5$; ∘ and ▫ are positions at time interval = $n\tau$, τ is time for wave to travel through the disc, n is integer)

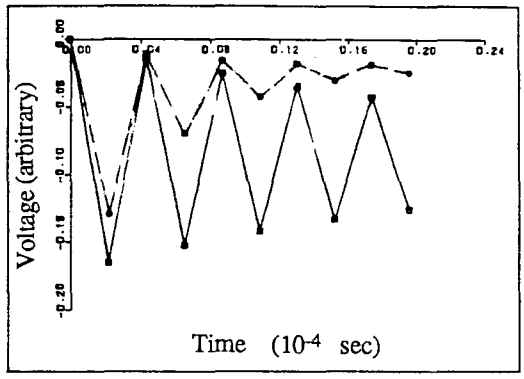

(a) $Z_2 = 14.8 \times 10^5$ kg/m^{2}s (water)

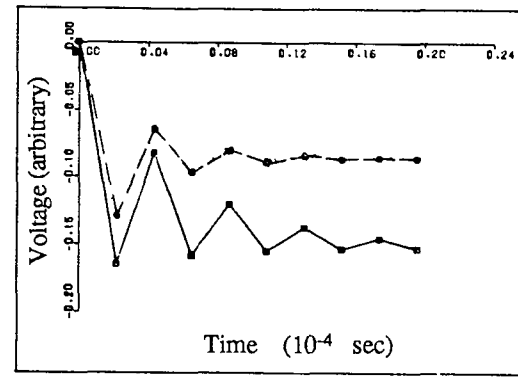

(b) $Z_2 = 115 \times 10^5$ kg/m^{2}s ($r_a = 0.5$)

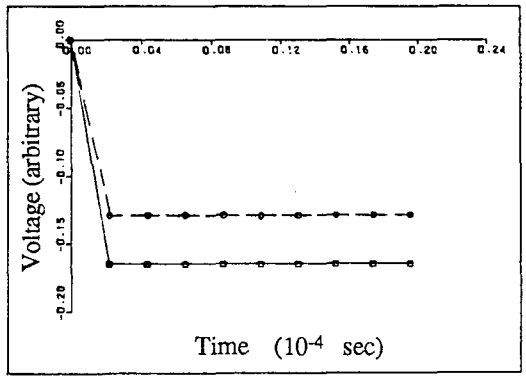

(c) $Z_2 = 345 \times 10^5$ kg/m^{2}s (matched backing)

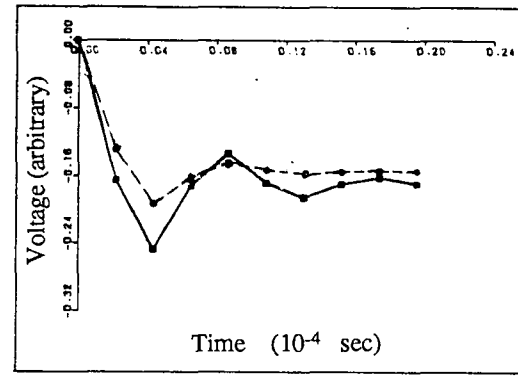

(d) $Z_2 = 1035 \times 10^5$ kg/m^{2}s ($r_a = -0.5$)

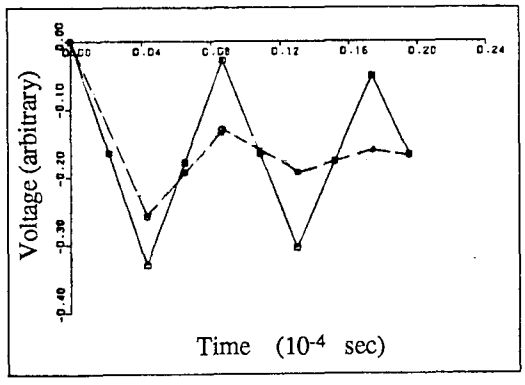

(e) $Z_2 = 345 \times 10^8$ kg/m^{2}s (rigid backing)

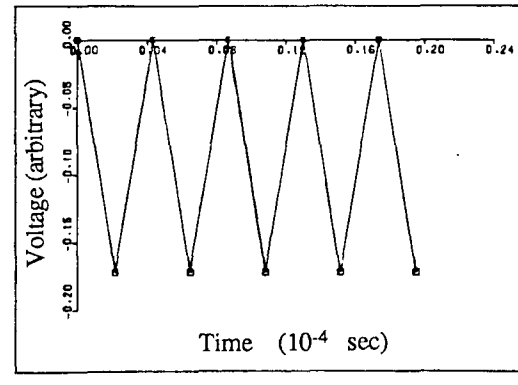

(f) free piezoelectric disc

Fig 2.3 The voltage response of a piezoelectric transducer when a step force pulse is applied at the front face for different backing (Z_2) ($Z_c = 345 \times 10^5$ kg/m^{2}s (PZT4); front loading, solid lines: $Z_1 = 14.8 \times 10^5$; broken lines: $Z_1 = 115 \times 10^5$; ∘ and □ are positions at time interval = $n\tau$, τ is time for wave to travel through the disc, n is integer)

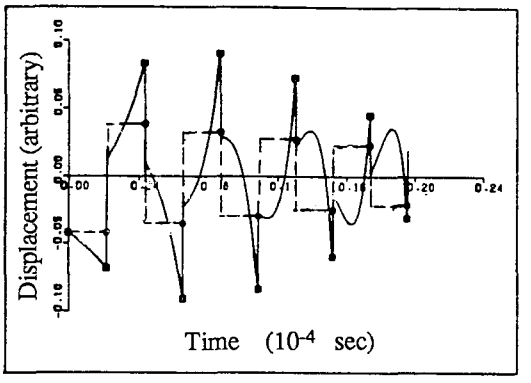

(a) $Z_2 = 14.8 \times 10^5$ kg/m^{2}s (water)

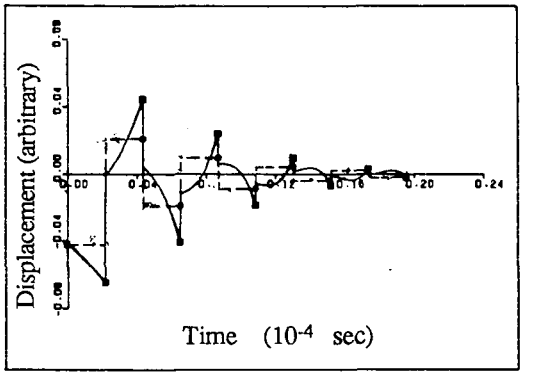

(b) $Z_2 = 115 \times 10^5$ kg/m^{2}s ($r_a = 0.5$)

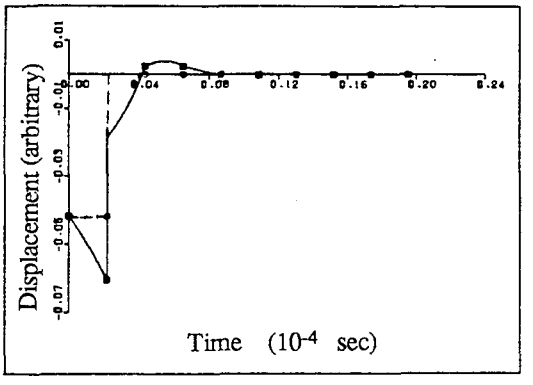

(c) $Z_2 = 345 \times 10^5$ kg/m^{2}s (matched backing)

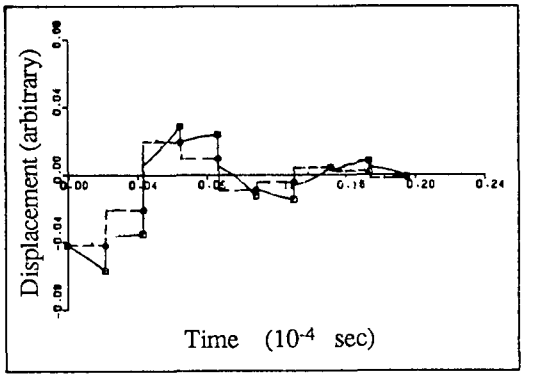

(d) $Z_2 = 1035 \times 10^5$ kg/m^{2}s ($r_a = -0.5$)

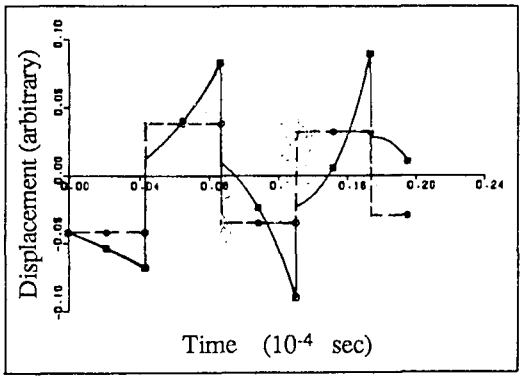

(e) $Z_2 = 345 \times 10^8$ kg/m^{2}s (rigid backing)

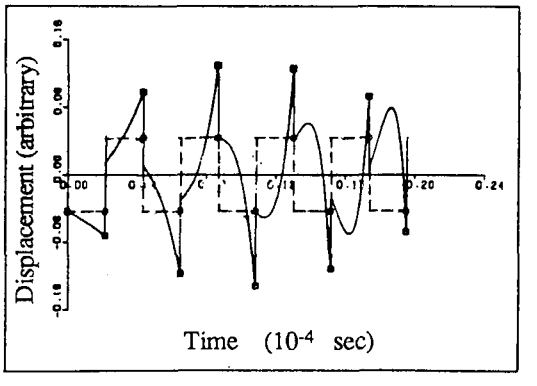

(f) free piezoelectric disc

Fig 2.4 The displacement response of a piezoelectric transducer when a Dirac voltage pulse is applied across the electrodes for different backing (Z_2) ($Z_c = 345 \times 10^5$ kg/m^{2}s (PZT4); $Z_1 = 14.8 \times 10^5$; solid lines by general solution; broken lines by Impulse diagram; ∘ and ▫ are positions at time interval = $n\tau$, τ is time for wave to travel through the disc, n is integer)

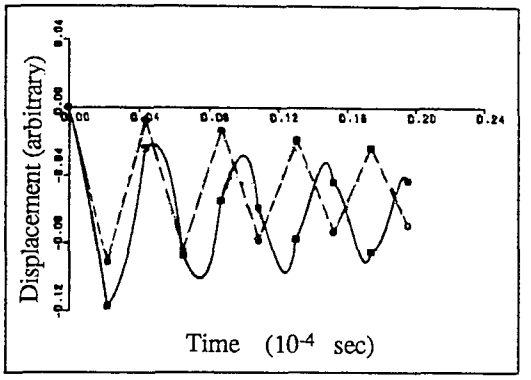

(a) $Z_2 = 14.8 \times 10^5$ kg/m^{2}s (water)

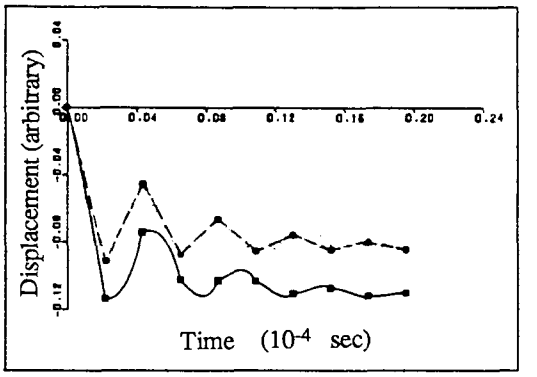

(b) $Z_2 = 115 \times 10^5$ kg/m^{2}s ($r_a = 0.5$)

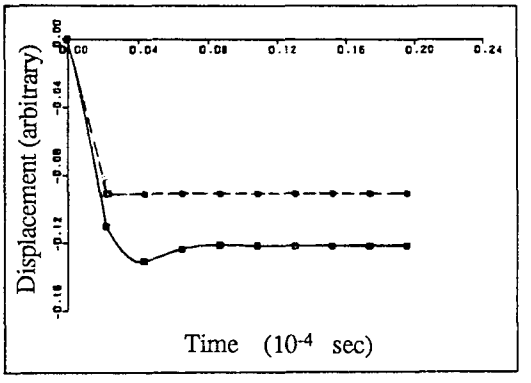

(c) $Z_2 = 345 \times 10^5$ kg/m^{2}s (matched backing)

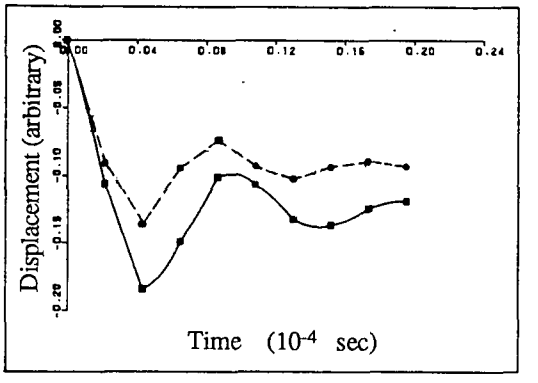

(d) $Z_2 = 1035 \times 10^5$ kg/m^{2}s ($r_a = -0.5$)

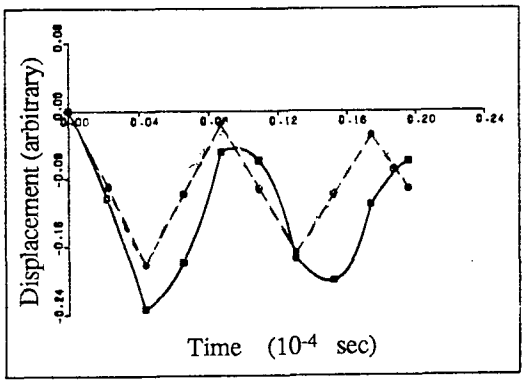

(e) $Z_2 = 345 \times 10^8$ kg/m^{2}s (rigid backing)

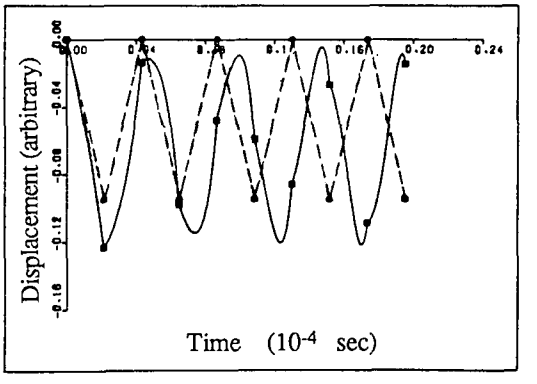

(f) free piezoelectric disc

Fig 2.5 The displacement response of a piezoelectric transducer when a step voltage pulse is applied across the electrodes for different backing (Z_2) ($Z_c = 345 \times 10^5$ kg/m^{2}s (PZT4); $Z_1 = 14.8 \times 10^5$; solid lines by general solution; broken lines by Impulse diagram; ◦ and ▫ are positions at time interval = $n\tau$, τ is time for wave to travel through the disc, n is integer)

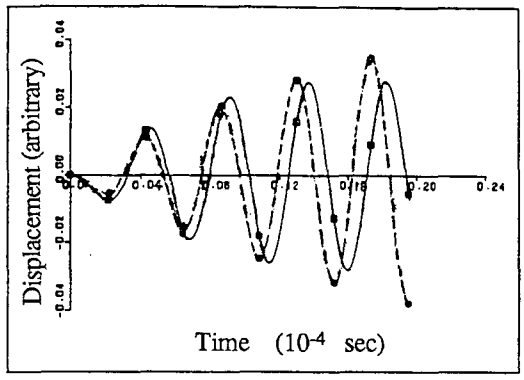

(a) $Z_2 = 14.8 \times 10^5$ kg/m^{2}s (water)

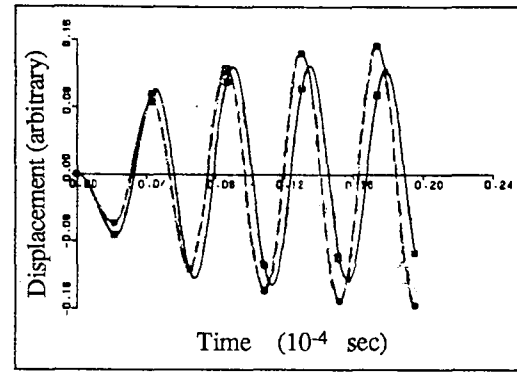

(b) $Z_2 = 115 \times 10^5$ kg/m^{2}s ($r_a = 0.5$)

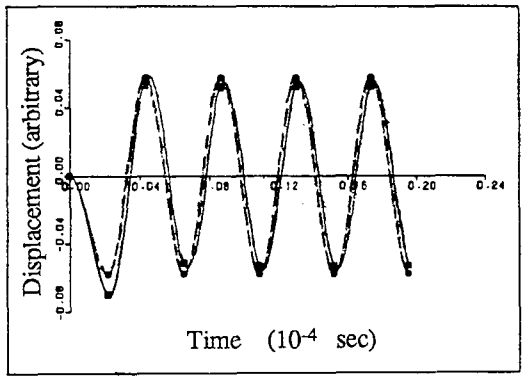

(c) $Z_2 = 345 \times 10^5$ kg/m^{2}s (matched backing)

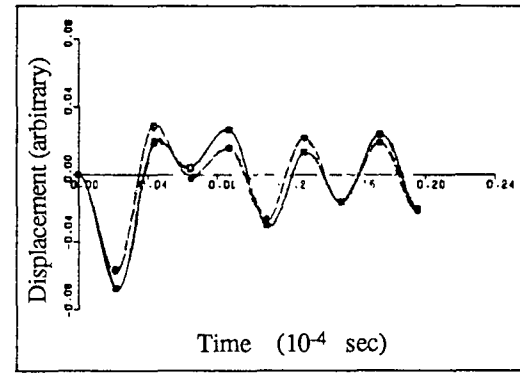

(d) $Z_2 = 1035 \times 10^5$ kg/m^{2}s ($r_a = -0.5$)

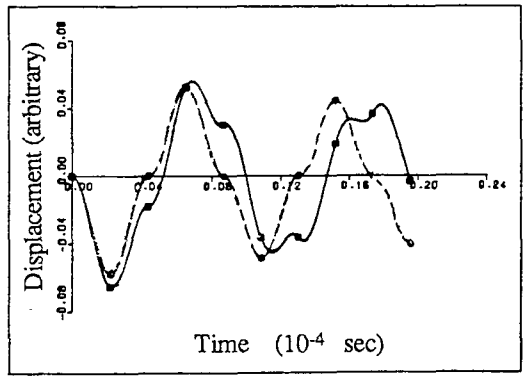

(e) $Z_2 = 345 \times 10^8$ kg/m^{2}s (rigid backing)

Fig 2.6 The displacement response of a piezoelectric transducer when a sine wave voltage is applied across the electrodes for different backing (Z_2) ($Z_c = 345 \times 10^5$ kg/m^{2}s (PZT4); $Z_1 = 14.8 \times 10^5$; solid lines by general solution; broken lines by Impulse diagram; ∘ and ▫ are positions at time interval = $n\tau$, τ is time for wave to travel through the disc, n is integer)

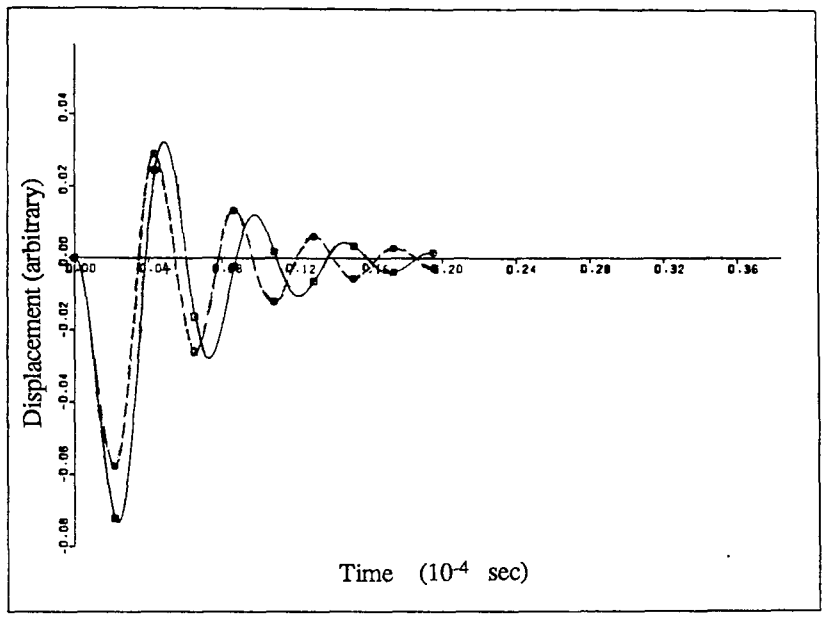

(a) $Z_2 = 115 \times 10^5$ kg/m^{2}s ($r_a = 0.5$)

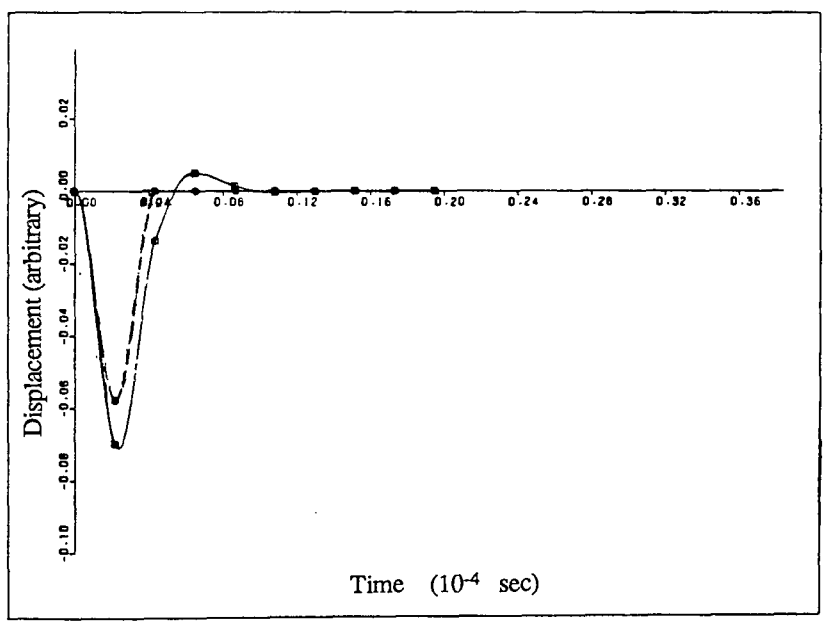

(b) $Z_2 = 345 \times 10^5$ kg/m^{2}s (matched backing)

Fig 2.7 The displacement response of a piezoelectric transducer when a half period of a sine voltage is applied across the electrodes for different backing (Z_2)
($Z_c = 345 \times 10^5$ kg/m^{2}s (PZT4); $Z_1 = 14.8 \times 10^5$; solid lines by general solution; broken lines by Impulse diagram; ∘ and ▫ are positions at time interval = $n\tau$, τ is time for wave to travel through the disc, n is integer)

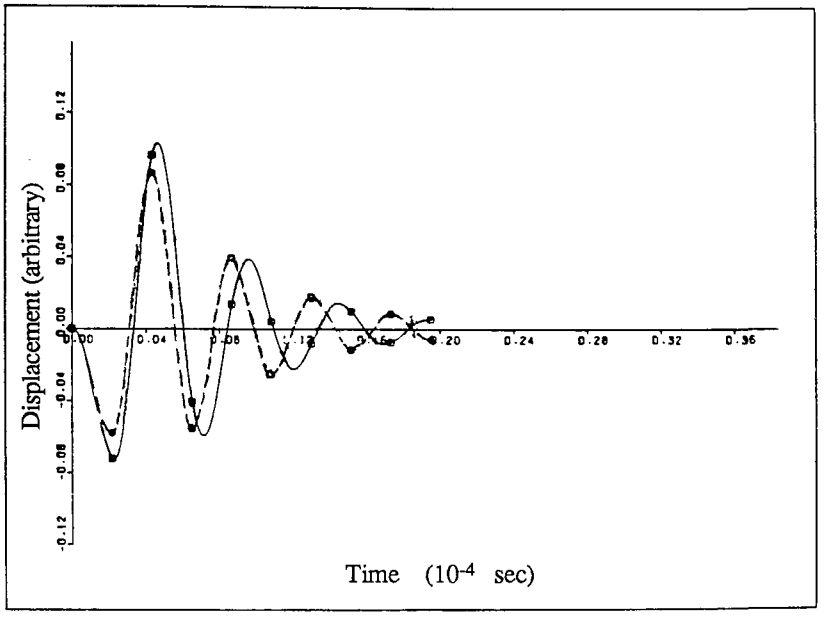

(a) $Z_2 = 115 \times 10^5$ kg/m^{2}s ($r_a = 0.5$)

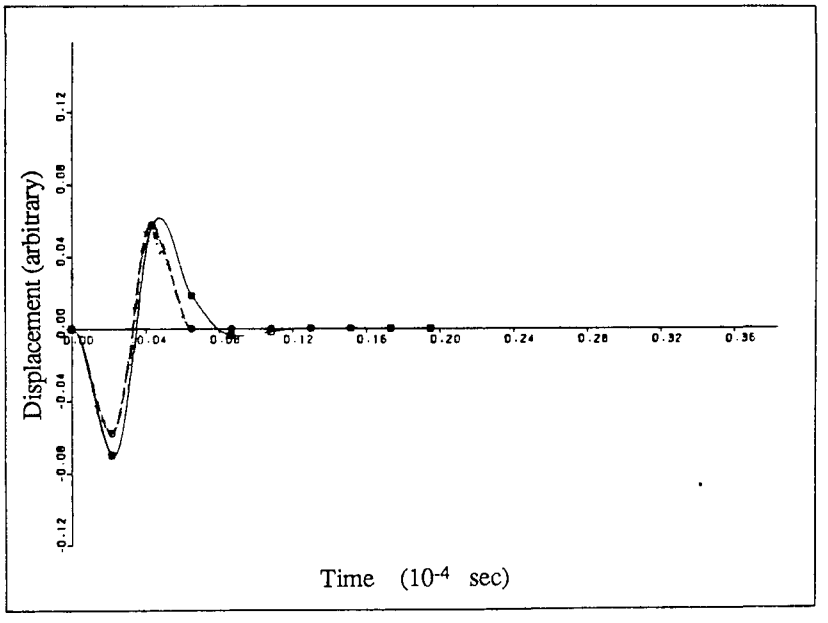

(b) $Z_2 = 345 \times 10^5$ kg/m^{2}s (matched backing)

Fig 2.8 The displacement response of a piezoelectric transducer when a period of sine voltage is applied across the electrodes for different backing (Z_2) ($Z_c = 345 \times 10^5$ kg/m^{2}s (PZT4); $Z_1 = 14.8 \times 10^5$; solid lines by general solution; broken lines by Impulse diagram; ○ and □ are positions at time interval = $n\tau$, τ is time for wave to travel through the disc, n is integer)

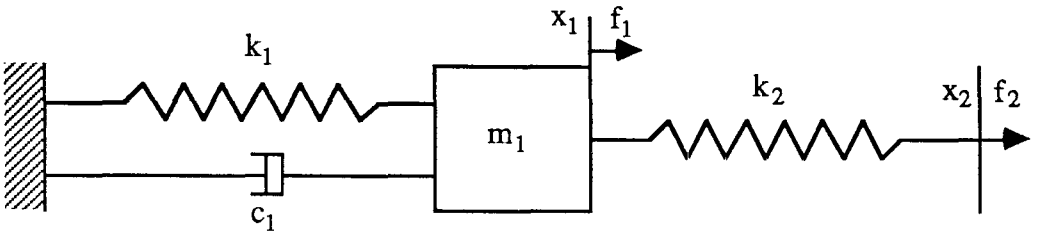

Fig 2.9 A degenerate two degree freedom of vibration model of a piezoelectric disc (m_1, k_1, c_1 are mechanical mass, stiffness and damping coefficient; x_1, f_1 are mechanical displacement and force; k_2 is the electrical capacitance; x_2, f_2 are electrical potential and charge; η is the coupling factor)

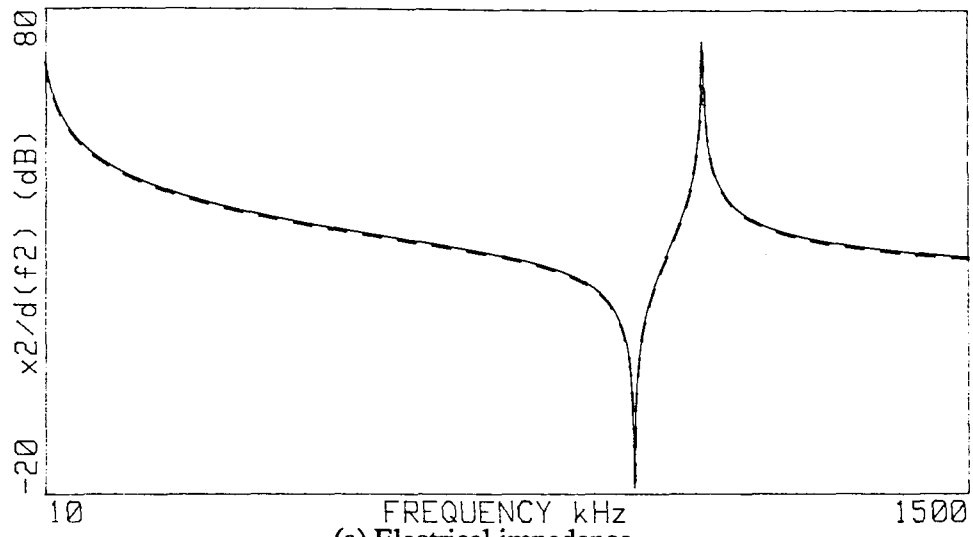

(a) Electrical impedance

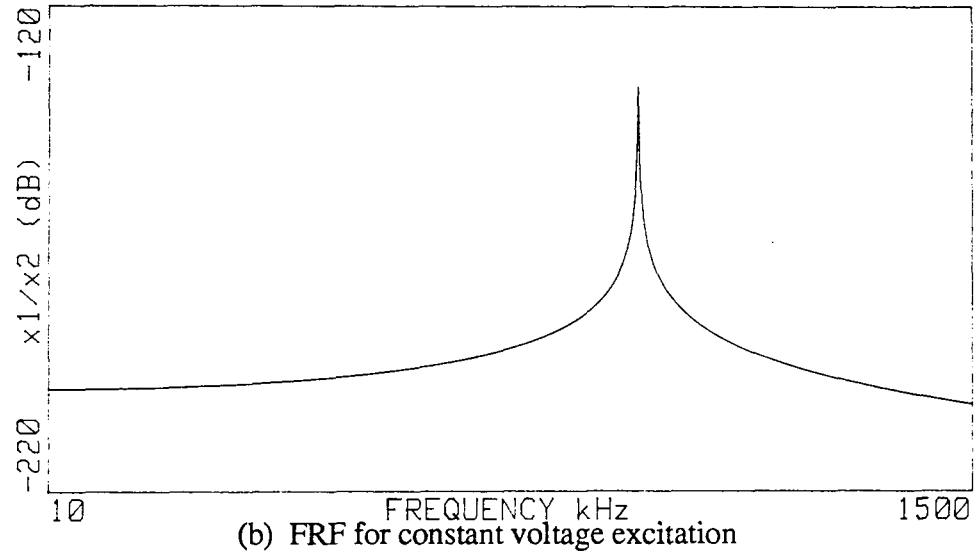

(b) FRF for constant voltage excitation

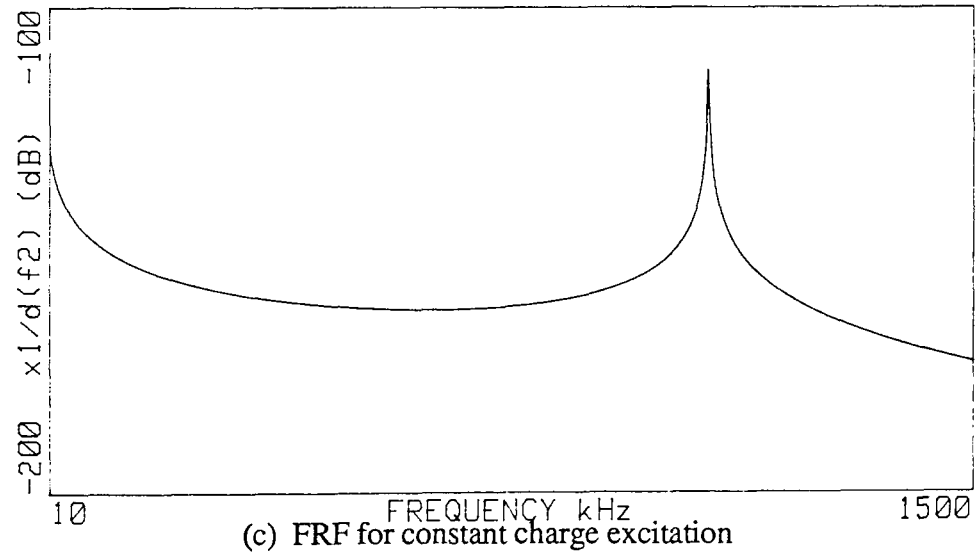

(c) FRF for constant charge excitation

Fig 2.10 The predicted electrical impedance response and frequency response functions of a piezoelectric disc with a D/T ratio of 20
(broken line: predicted by the analytical method; solid line: predicted by the mechanical model)

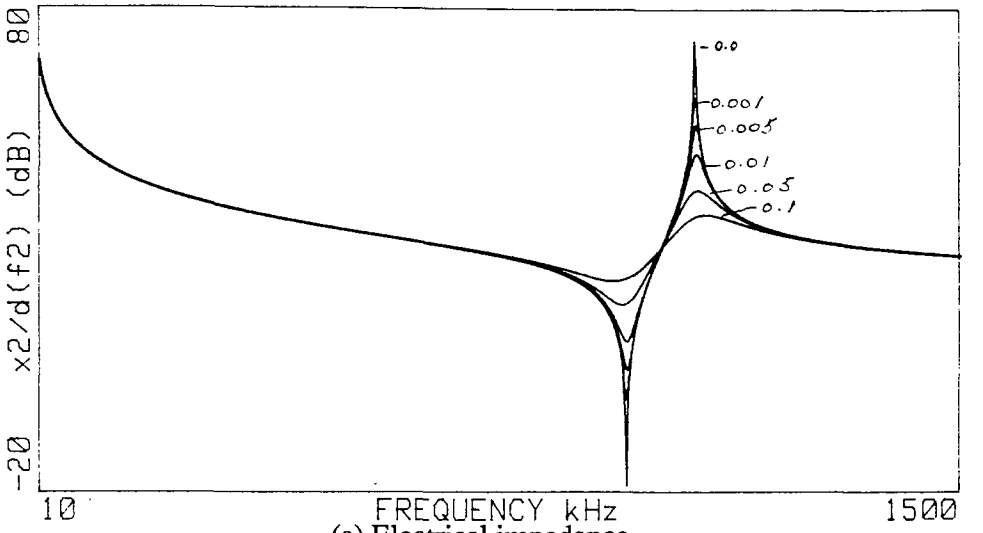

(a) Electrical impedance

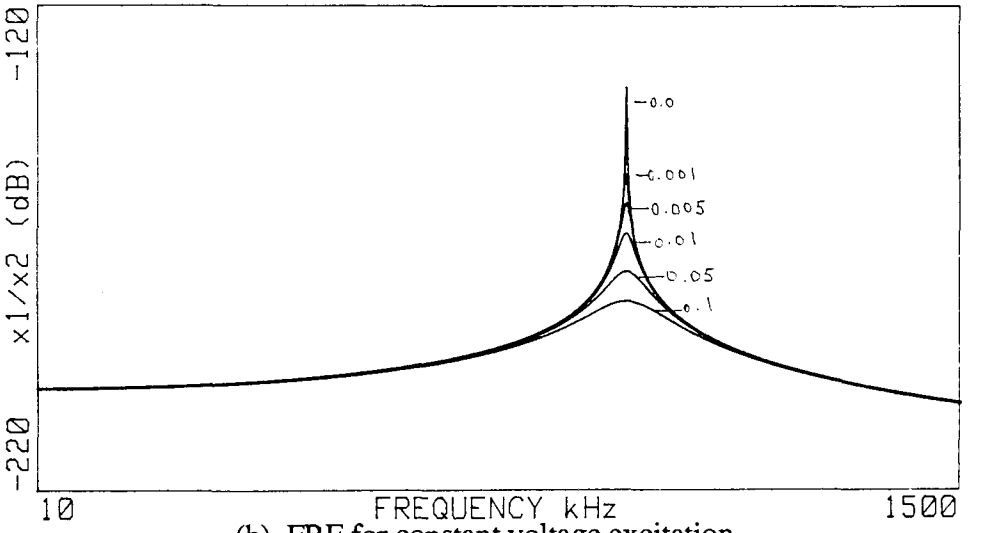

(b) FRF for constant voltage excitation

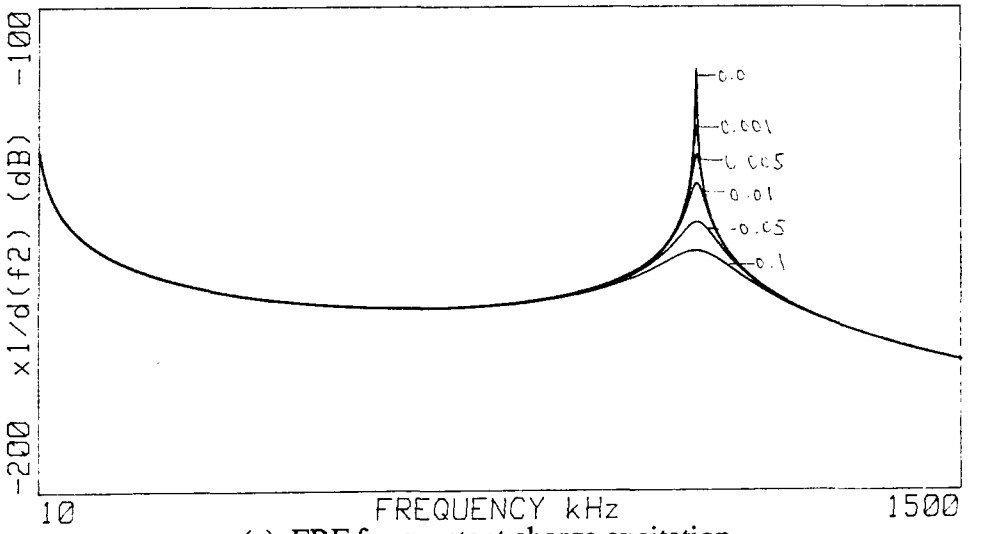

(c) FRF for constant charge excitation

Fig 2.11 The effects of the mechanical damping on the electrical impedance and frequency response functions of the piezoelectric disc

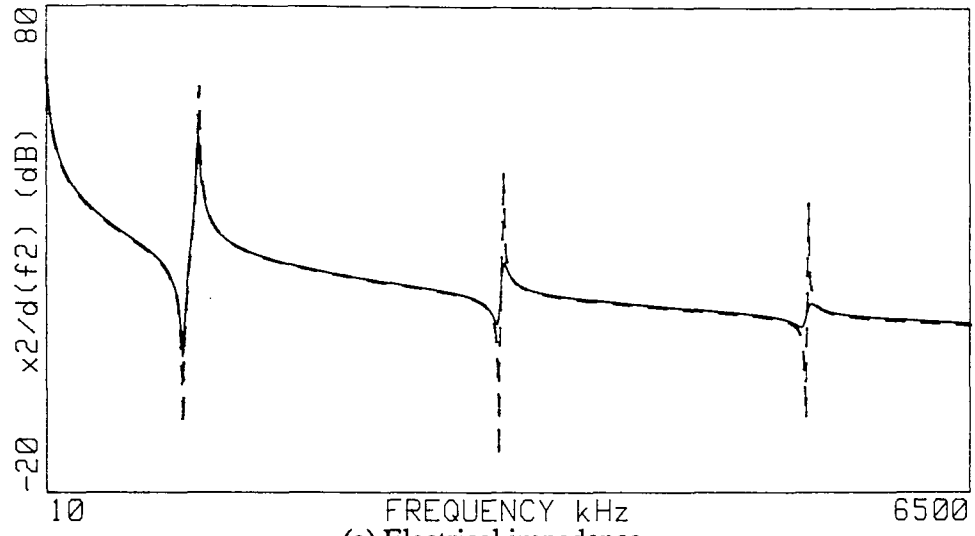

(a) Electrical impedance

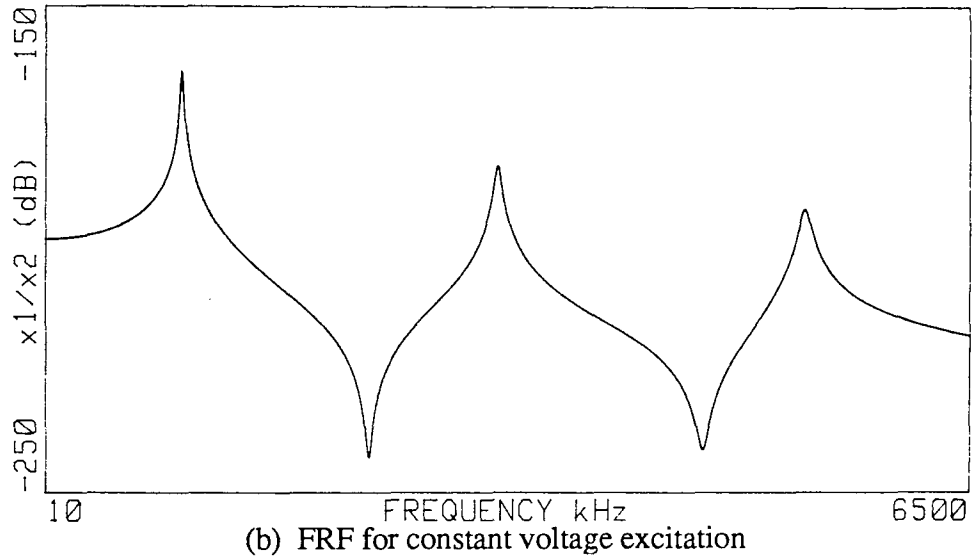

(b) FRF for constant voltage excitation

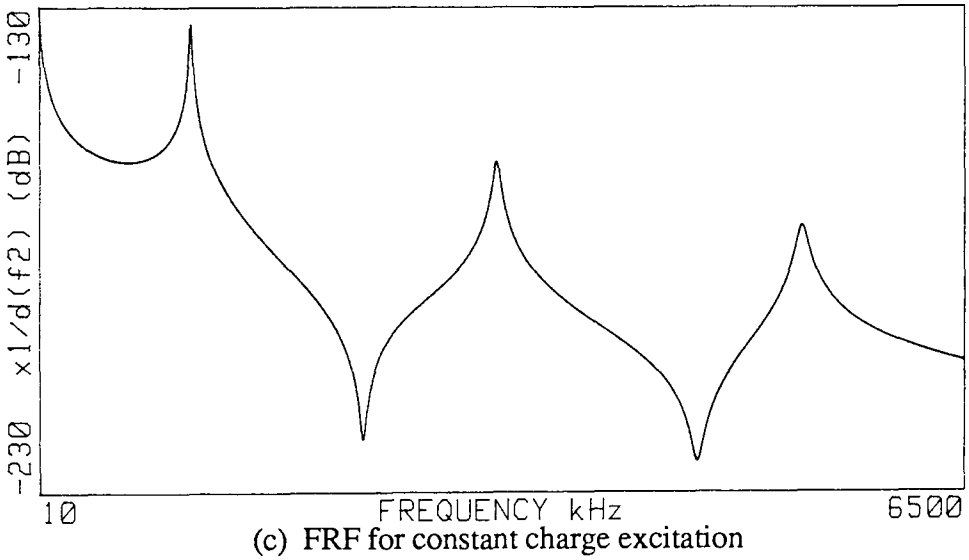

(c) FRF for constant charge excitation

Fig 2.12 The predicted electrical impedance response and frequency response functions of a piezoelectric disc with a D/T ratio of 20 in the frequency range 10 - 6500 kHz (broken line: predicted by the analytical method; solid line: predicted by the mechanical model)

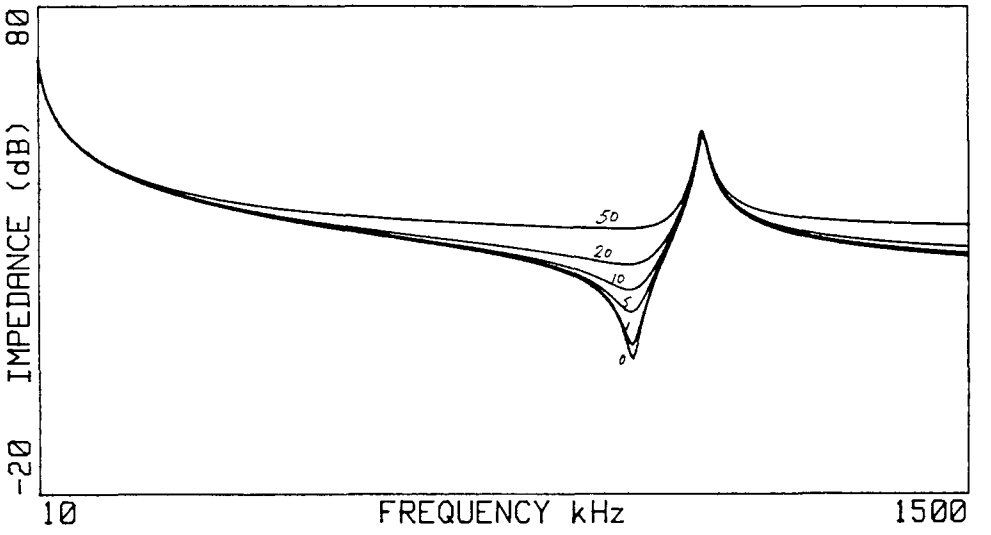

(a) in series with resistors (values in Ω)

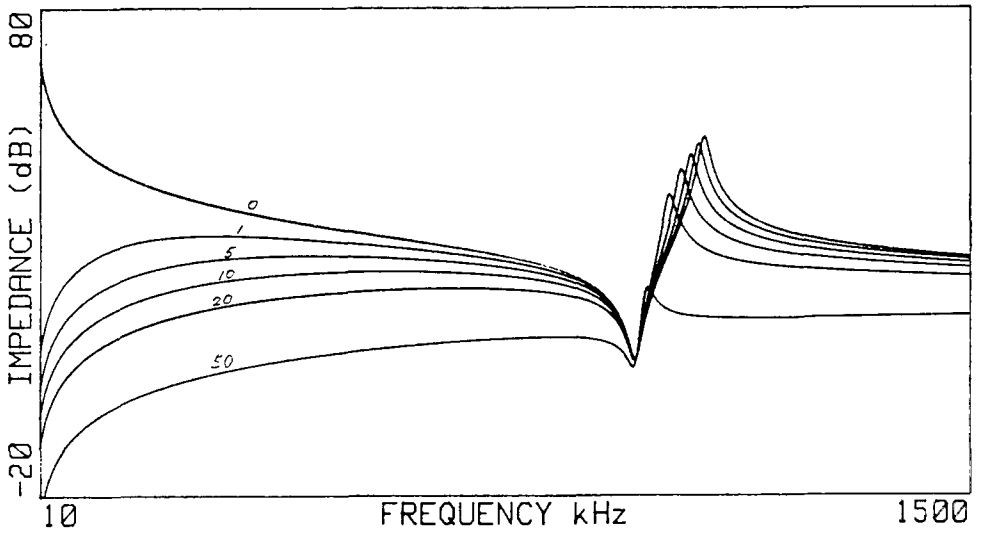

(b) in parallel with inductors (values in μH)

Fig 2.13 The predicted electrical impedances when the piezoelectric disc is in connection with electrical components

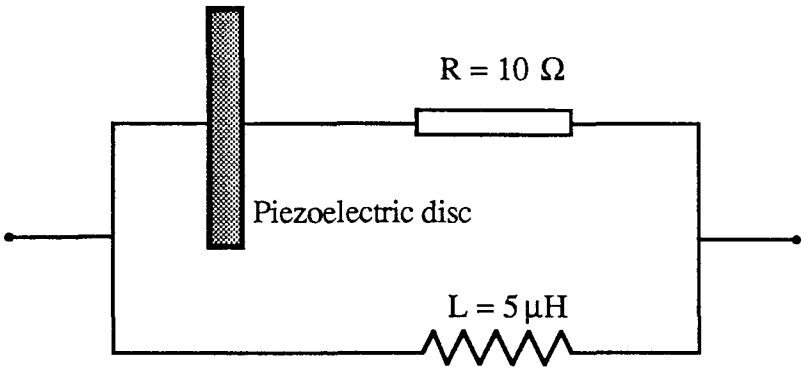

(a) The piezoelectric disc is in series with a resistor and then in parallel with an inductor

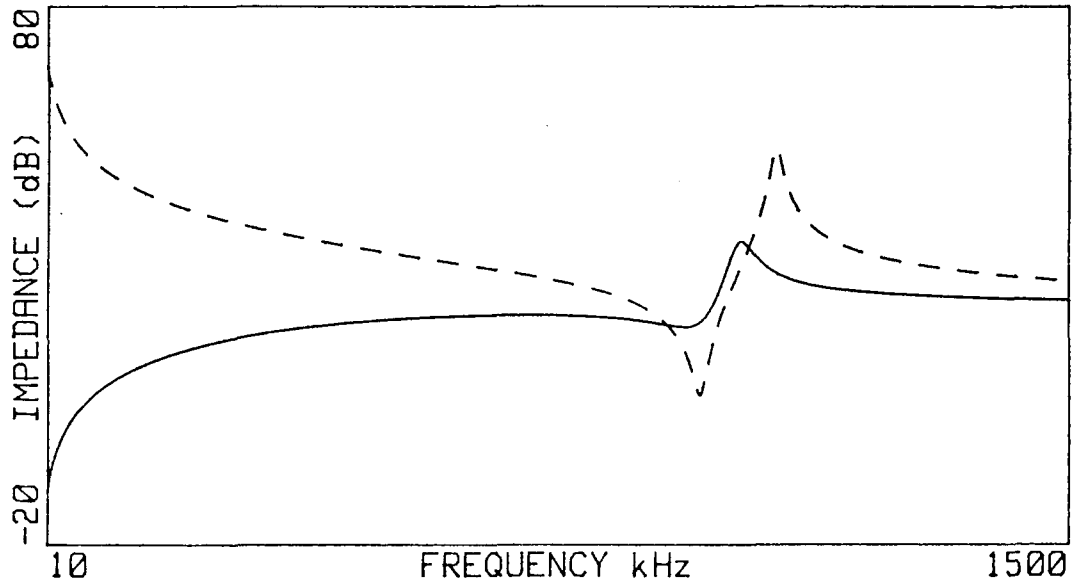

(b) The electrical impedance of the system shown in (a)

Fig 2.14 The electrical impedance of the piezoelectric disc in an electrical circuit (Broken line: for the disc alone; Solid line: for the circuit)

CHAPTER 3

THE FINITE ELEMENT ANALYSIS AND MODAL ANALYSIS OF PIEZOELECTRIC DISCS

3.1 Introduction

In this chapter, a finite element method for piezoelectric materials is formed in generalised variables and coordinates. The solution of eigenvalue problem is then discussed and the mechanical response function at constant voltage excitation and the electrical impedance characteristic functions are formed. This is followed by the estimation of the strength of excitation of the resonant modes of a piezoelectric disc and finally the transient mechanical response when a piezoelectric disc is subjected to a voltage pulse across its electrodes is obtained.

The general formulation of the finite element method for piezoelectric structures was first given by Allik and Hughes (1970). Here the formulation is obtained directly by the minimisation of the total potential energy of a piezoelectric structure. Most of the notation used in this chapter follows Zienkiewicz (1971) and Ewins (1984).

3.2 The formulation of the finite element method

3.2.1 The constitutive equations of piezoelectricity

The matrix form of the constitutive equation for linear piezoelectric materials is,

$$\{T\} = [c^E]\{S\} - [e]^T\{E\} \tag{3.1a}$$

$$\{D\} = [e]\{S\} + [\varepsilon^S]\{E\} \tag{3.1b}$$

where { } denotes a vector, [ ] denotes a matrix, and superscript T denotes a transposed vector or matrix. {S} and {T} are the mechanical strain and stress vectors; {E} and {D} are the electric field vector and the electric charge density vector; $[c^E]$, $[\varepsilon^S]$ and [e] are the elastic constant matrix, dielectric constant matrix at constant strain, and piezoelectric constant matrix.

The E and S superscripts on the constants refer to a particular choice of independent variables rather than particular boundary conditions. The material properties of a piezoelectric structure depend on [c], [ε] and [e] which couples the mechanical and electrical variables. An arbitrarily anisotropic (triclinic) material without a centre of

symmetry has 45 independent material constants (21 elastic constant, 18 piezoelectric constant and 6 dielectric constants) (Auld, 1973). However, for poled ferroelectric ceramics (with x_3 in the poling direction) which is of main interest here, they effectively have the symmetry of a hexagonal crystal, i.e, transversely isotropic. A material with this type of symmetry is described by 10 independent material constants (5 elastic constants, 3 piezoelectric constants and 2 dielectric constants). The elastic constants matrix [c], piezoelectric constants matrix [e] and dielectric matrix [ε], after dropping superscripts for convenience, are

$$[c] = \begin{bmatrix} c_{11} & c_{12} & c_{13} & 0 & 0 & 0 \\ c_{12} & c_{22} & c_{23} & 0 & 0 & 0 \\ c_{13} & c_{23} & c_{33} & 0 & 0 & 0 \\ 0 & 0 & 0 & c_{44} & 0 & 0 \\ 0 & 0 & 0 & 0 & c_{55} & 0 \\ 0 & 0 & 0 & 0 & 0 & c_{66} \end{bmatrix} \tag{3.2a}$$

$$c_{66} = \frac{1}{2}(c_{11} - c_{12})$$

$$[e]^T = \begin{bmatrix} 0 & 0 & 0 & 0 & e_{51} & 0 \\ 0 & 0 & 0 & e_{42} & 0 & 0 \\ e_{31} & e_{32} & e_{33} & 0 & 0 & \end{bmatrix} \tag{3.2b}$$

$$[\varepsilon] = \begin{bmatrix} -\varepsilon_{11} & 0 & 0 \\ 0 & -\varepsilon_{22} & 0 \\ 0 & 0 & -\varepsilon_{33} \end{bmatrix} \tag{3.2c}$$

The mechanical terms in equation (3.1) are related by Newton's second law,

$$\rho \frac{\partial^2 \{f\}}{\partial t^2} = -\{T\} \tag{3.3}$$

where $\{f\} = \{ u \; v \; w \}^T$ is the mechanical displacement vector along the x, y, z axes.

The strain vector $\{S\}$ is related to the mechanical displacement vector $\{f\}$ by

$$\{S\} = [B_f]\{f\} \tag{3.4}$$

where

$$[B_f] = \begin{bmatrix} \frac{\partial}{\partial x} & 0 & 0 \\ 0 & \frac{\partial}{\partial y} & 0 \\ 0 & 0 & \frac{\partial}{\partial z} \\ 0 & \frac{\partial}{\partial z} & \frac{\partial}{\partial y} \\ \frac{\partial}{\partial z} & 0 & \frac{\partial}{\partial x} \\ \frac{\partial}{\partial y} & \frac{\partial}{\partial x} & 0 \end{bmatrix} \tag{3.5}$$

The electrical terms in equation (3.1) are related by Gauss' law, assuming that the piezoelectric material is an insulating material, and no flow of charge occurs inside the transducer, which gives

$$\nabla\{D\} = 0 \tag{3.6}$$

The electric field is then related to the electrical potential ϕ by

$$\{E\} = -\{B_\phi\}\phi \tag{3.7}$$

where

$$\{B_\phi\} = \{ \frac{\partial}{\partial x} \quad \frac{\partial}{\partial y} \quad \frac{\partial}{\partial z} \}^T \tag{3.8}$$

A linear piezoelectric material may be completely modelled by equations (3.1) to (3.7). Any given problem can be solved by applying the associated boundary conditions. The electric field is the electrical analogue of mechanical strain so a generalised stress strain relationship may be written as

$$\{\sigma\} = [C]\,\varepsilon \tag{3.9}$$

where $\{\sigma\} = \{ T \quad D \}^T$ is the generalised stress vector and $\{\varepsilon\} = \{ S \quad -E \}^T$ is the generalised strain vector. The generalized elasticity matrix is therefore,

$$[C] = \begin{bmatrix} C^E & e \\ e^T & -\varepsilon^S \end{bmatrix} \tag{3.10}$$

The strain-displacement relationship is now,

$$\{\varepsilon\} = [B]\{f_G\} \tag{3.11}$$

where, $\{f_G\}$ is defined as the generalised displacement vector, and

$$\{f_G\} = \{f \quad \phi\}^T = \{ u \; v \; w \; \phi \}^T \tag{3.12}$$

The generalized B matrix is,

$$[B] = \begin{bmatrix} B_f & 0 \\ 0 & B_\phi \end{bmatrix} \tag{3.13}$$

The generalised coordinates and variables are used throughout in the formulation of the finite element method.

3.2.2 The FEM formulation of piezoelectric structuress

The finite element method may be developed from a displacement approach by minimising the total potential energy of the system (Zienkiewicz, 1971). If damping is not considered, the total potential energy of a structure may be written as

$$\chi = U + W \tag{3.14}$$

where, U is the strain energy of the structure, and W is the potential energy of the external loads, which may include the kinetic energy in dynamic analysis.

In a continuous structure the generalised displacement of any point within the structure, $\{f_G\}$, may be expressed approximately in terms of the displacement shape function [N], and vector $\{\delta\}$ containing a finite number of known nodal displacements:

$$\{f_G\} = [N]\{\delta\} \tag{3.15}$$

For a piezoelectric material, if the electrical effects must be considered, the electrical potential is then equivalent to the mechanical displacement. An extra degree of freedom, the electrical potential, ϕ, must therefore be considered for each node. For the present problem there are therefore four degrees of freedom at each node i. In a three dimensional Cartesian system of coordinate (x, y, z),

$$\begin{aligned} \{\delta_i\} &= \{ f_i \;\; \phi_i \}^T \\ &= \{ u_i \;\; v_i \;\; w_i \;\; \phi_i \}^T \end{aligned} \tag{3.16}$$

It should, however, be noted that the extra degree of freedom, the electrical potential, ϕ, has no mass associated with it in dynamic analysis.

For equilibrium, the total potential energy must be a minimum for admissible variations of displacement. Thus,

$$\frac{\partial \chi}{\partial \{\delta\}} = 0 \tag{3.17}$$

By applying equations (3.11) and (3.12), the strain energy of a piezoelectric structure is given as

$$U = \int_V \frac{1}{2}\{\varepsilon\}^T\{\sigma\}dV$$
$$= \int_V \frac{1}{2}\{\delta\}^T[B]^T[C][B]\{\delta\}dV \quad (3.18)$$

Since $\{\delta\}$, the vector of the nodal displacements is not a function of position, the strain energy U is given by

$$U = \frac{1}{2}\{\delta\}^T\left[\int_V [B]^T[C][B]dV\right]\{\delta\}$$

The stiffness matrix [K], is then defined as

$$[K] = \int_V [B]^T[C][B]dV \quad (3.19)$$

and

$$U = \frac{1}{2}\{\delta\}^T[K]\{\delta\} \quad (3.20)$$

If the external forces are a concentrated point force vector $\{R\}$, distributed forces $\{p\}$ and body forces $\{y\}$, then the potential energy of the external loads is equal to the work done by external loads but with opposite sign, i.e.

$$W = -\left[\{f_G\}^T\{R\} + \int_V \{f_G\}^T\{p\}dV + \int_V \{f_G\}^T\{y\}dV\right] \quad (3.21)$$

An extra term due to the inertia force must be included for the dynamic case,

$$W = \int_V \{f\}^T \rho \frac{\partial^2\{f\}}{\partial t^2} dV - \left[\{f_G\}^T\{R\} + \int_V \{f_G\}^T\{p\}dV + \int_V \{f_G\}^T\{y\}dV\right] \quad (3.22)$$

It should be noted here that the inertia term is only associated with the mechanical displacement f. Substituting the displacement expression (3.16) into the above equation gives

$$W = [\delta]^T \frac{\partial^2\{f\}}{\partial t^2} \int_V [N]^T\rho[N]dV - [\delta]^T\left[[N]^T\{R\} + \int_V [N]^T\{p\}dV + \int_V [N]^T\{y\}dV\right] \quad (3.23)$$

Applying equation (3.14), the final formulation is

$$[M]\frac{\partial^2\{\delta\}}{\partial t^2} + [K]\{\delta\} = \{R_B\} + \{R_S\} + \{R_p\} \tag{3.24}$$

where

$$[M] = \begin{bmatrix} m & 0 \\ 0 & 0 \end{bmatrix}$$

$$[m] = \int_V [N]^T \rho [N] dV$$

$$[K] = \int_V [B]^T [C][B] dV$$

$\{R_B\} = \int_V [N]^T \{y\} dV$ is the force vector due to the body force,

$\{R_A\} = \int_V [N]^T \{p\} dV$ is the force vector due to the distributed force,

$\{R_P\} = [N]^T \{R\}$ is the force vector due to the concentrated force.

The forces given above represent the generalised forces, which can be mechanical forces $\{F\}$ or electrical charges $\{Q\}$.

Equation (3.24) may be written separately in terms of mechanical and electrical variables, and if damping is added, it becomes,

$$\begin{bmatrix} M_{ff} & 0 \\ 0 & 0 \end{bmatrix}\begin{Bmatrix} \ddot{f} \\ \ddot{\phi} \end{Bmatrix} + \begin{bmatrix} G_f & 0 \\ 0 & G_\phi \end{bmatrix}\begin{Bmatrix} \dot{f} \\ \dot{\phi} \end{Bmatrix} + \begin{bmatrix} K_{ff} & K_{f\phi} \\ K_{f\phi}^T & K_{\phi\phi} \end{bmatrix}\begin{Bmatrix} f \\ \phi \end{Bmatrix} = \begin{Bmatrix} F \\ Q \end{Bmatrix} \tag{3.25a}$$

(3.25b)

where,

$$[M_{ff}] = \int_V [N]^T \rho [N] dV$$

$$[K_{ff}] = \int_V [B_f]^T [C^E][B_f] dV$$

$$[K_{f\phi}] = \int_V [B_f]^T [e][B_\phi] dV$$

$$[K_{\phi\phi}] = \int_V [B_\phi]^T [-\varepsilon^S][B_\phi] dV$$

In the finite element method, a structure is discretized into a finite number of elements in which all the expressions above are applicable to the individual elements (denoted by a superscript e). In addition, the compatibility condition between elements must be satisfied by means of continuity of nodal displacements across the boundary between elements, and the elements being conforming across their boundaries. The total strain energy of the system is then the sum of the strain energies of each element.

3.2.3 The axisymmetric piezoelectric element

The 'Serendipity' 8-node quadratic element described by Zienkiewicz (1971) is shown in Fig 3.1, having local coordinates ξ, η, with its edges being $\eta = \pm 1$ and $\xi = \pm 1$. The shape function for the corner nodes is

$$N_i = \frac{1}{4}(1 + \xi_0)(1 + \eta_0)(\xi_0 + \eta_0 - 1) \qquad i = 1, 3, 6, 8 \qquad (3.26a)$$

where $\eta_0 = \eta\eta_i$, $\xi_0 = \xi\xi_i$. For the midside nodes

$$N_i = \frac{1}{2}(1 - \xi^2)(1 + \eta_0) \qquad i = 2, 7 \qquad (3.26b)$$

$$N_i = \frac{1}{4}(1 + \xi_0)(1 - \eta^2) \qquad i = 4, 8 \qquad (3.26c)$$

These shape functions satisfy the condition that,

$$N_i = 1 \quad \text{if } i=j$$
$$N_i = 0 \quad \text{if } i \neq j \qquad (3.27)$$

In this case the generalized displacement at any point of the element is given by

$$\{f_G\} = [N]\{\delta\}^e \qquad (3.28)$$

where

$$\{\delta\}^e = \{\, \delta_1 \ \ldots\ldots \ \delta_8 \,\}^T$$
$$= \{\, u_1 \ v_1 \ w_1 \ \phi_1 \ \ldots\ldots \ u_8 \ v_8 \ w_8 \ \phi_8 \,\}^T \qquad (3.29)$$

Thus

$$u = N_1u_1 + N_2u_2 + \ldots\ldots + N_8u_8 = \Sigma N_iu_i$$
$$\ldots\ldots\ldots\ldots \qquad (3.30)$$
$$\phi = N_1\phi_1 + N_2\phi_2 + \ldots\ldots + N_8\phi_8 = \Sigma N_i\phi_i$$

By using the above shape functions, the stiffness and mass matrices can be constructed. To do this, however, the [B] matrix and the Jacobian matrix [J] must first be formed.

1 [B] matrix formulation

The general three dimensional expression for generalised strains in a piezoelectric material in Cartesian coordinates (x, y, z) is specified as follows,

$$\{\varepsilon\} = \begin{Bmatrix} \varepsilon_x \\ \varepsilon_y \\ \varepsilon_z \\ \gamma_{xy} \\ \gamma_{yz} \\ \gamma_{zx} \\ -E_x \\ -E_y \\ -E_z \end{Bmatrix} = \begin{bmatrix} \frac{\partial u}{\partial x} & 0 & 0 & 0 \\ 0 & \frac{\partial v}{\partial y} & 0 & 0 \\ 0 & 0 & \frac{\partial w}{\partial z} & 0 \\ \frac{\partial u}{\partial y} & \frac{\partial v}{\partial x} & 0 & 0 \\ 0 & \frac{\partial v}{\partial z} & \frac{\partial w}{\partial x} & 0 \\ \frac{\partial u}{\partial z} & 0 & \frac{\partial w}{\partial x} & 0 \\ 0 & 0 & 0 & \frac{\partial \phi}{\partial x} \\ 0 & 0 & 0 & \frac{\partial \phi}{\partial y} \\ 0 & 0 & 0 & \frac{\partial \phi}{\partial z} \end{bmatrix} \tag{3.31}$$

which can be transformed into cylindrical coordinates (r, z, θ) for the axisymmetric problem as,

$$\{\varepsilon\} = \begin{Bmatrix} \varepsilon_r \\ \varepsilon_z \\ \varepsilon_\theta \\ \gamma_{rz} \\ \gamma_{r\theta} \\ \gamma_{z\theta} \\ -E_r \\ -E_z \\ -E_\theta \end{Bmatrix} = \begin{bmatrix} \frac{\partial u}{\partial r} & 0 & 0 & 0 \\ 0 & \frac{\partial v}{\partial z} & 0 & 0 \\ \frac{u}{r} & 0 & \frac{1}{r}\frac{\partial w}{\partial \theta} & 0 \\ \frac{\partial u}{\partial z} & \frac{\partial v}{\partial r} & 0 & 0 \\ \frac{1}{r}\frac{\partial u}{\partial \theta} & 0 & \frac{\partial w}{\partial r} - \frac{w}{r} & 0 \\ 0 & \frac{1}{r}\frac{\partial v}{\partial \theta} & \frac{\partial w}{\partial z} & 0 \\ 0 & 0 & 0 & \frac{\partial \phi}{\partial r} \\ 0 & 0 & 0 & \frac{\partial \phi}{\partial z} \\ 0 & 0 & 0 & \frac{1}{r}\frac{\partial \phi}{\partial \theta} \end{bmatrix} \tag{3.32}$$

The expression above can take into account non-axisymmetric harmonic loadings, which can be represented as a superposition of Fourier components. For example, if the external nodal loading is symmetric about the z axis, it can be written as,

$$
\begin{aligned}
R &= \Sigma R^l \cos(l\theta) \\
Z &= \Sigma Z^l \cos(l\theta) \\
T &= \Sigma T^l \sin(l\theta) \\
Q &= \Sigma Q^l \cos(l\theta)
\end{aligned} \tag{3.33}
$$

where, R, Z, T are the nodal forces along the radial, axial and circumferential directions, Q is the electrical charge, l is the integer harmonic number. The response of an element subjected to this l'th loading is,

$$
\begin{aligned}
u^l &= N_i \cos(l\theta)\ \{u^l\}^e \\
v^l &= N_i \cos(l\theta)\ \{v^l\}^e \\
w^l &= N_i \sin(l\theta)\ \{w^l\}^e \\
\phi^l &= N_i \cos(l\theta)\ \{\phi^l\}^e
\end{aligned} \tag{3.34}
$$

where, $\{u^l\}^e$ is the nodal displacement due to the force of amplitude R^l, etc.

On substitution of the above expressions into (3.32), the [B] matrix for each harmonic, l, B^l_i, can be obtained as,

$$
B_i^l = \begin{bmatrix}
\frac{\partial N_i}{\partial r}\cos(l\theta) & 0 & 0 & 0 \\
0 & \frac{\partial N_i}{\partial z}\cos(l\theta) & 0 & 0 \\
\frac{N_i}{r}\cos(l\theta) & 0 & l\,\frac{N_i}{r}\cos(l\theta) & 0 \\
\frac{\partial N_i}{\partial z}\cos(l\theta) & \frac{\partial N_i}{\partial r}\cos(l\theta) & 0 & 0 \\
-l\,\frac{N_i}{r}\sin(l\theta) & 0 & (\frac{\partial N_i}{\partial r} - \frac{N_i}{r})\sin(l\theta) & 0 \\
0 & -l\,\frac{N_i}{r}\sin(l\theta) & \frac{\partial N_i}{\partial r}\cos(l\theta) & 0 \\
0 & 0 & 0 & \frac{\partial N_i}{\partial r}\cos(l\theta) \\
0 & 0 & 0 & \frac{\partial N_i}{\partial z}\cos(l\theta) \\
0 & 0 & 0 & -l\,\frac{N_i}{r}\sin(l\theta)
\end{bmatrix} \tag{3.35}
$$

Since the piezoelectric material is modelled by linear equations, all the element matrices, and hence the solution, can be evaluated separately for each harmonic case l. The total response is therefore the sum of the individual response of each harmonic component.

2 The elasticity matrix [C]

The generalised elasticity matrix for a piezoelectric material of class 6 is a 9x9 matrix and can be written in Cartesian coordinates as

$$[c] = \begin{bmatrix} c^E & e \\ e^T & -\varepsilon^S \end{bmatrix} \tag{3.36}$$

3 Jacobian matrix [J]

Since the shape functions are evaluated in the local coordinates, while the stiffness and other matrices are expressed in the global coordinates, the transformation matrix between local and global coordinates must be found. In the isoparametric element, the local coordinates are related to global coordinates by the same interpolation function N_i, which is used in the displacement function. Hence,

$$r = \sum N_i r_i$$

$$z = \sum N_i z_i \qquad \text{for} \quad i = 1, 2, ..., 8 \tag{3.37}$$

By the usual partial differentiation, the transformation between local (η, ξ) and global coordinates (r, z) is

$$\begin{Bmatrix} \frac{\partial N_i}{\partial \xi} \\ \frac{\partial N_i}{\partial \eta} \end{Bmatrix} = [J] \begin{Bmatrix} \frac{\partial N_i}{\partial r} \\ \frac{\partial N_i}{\partial z} \end{Bmatrix} \tag{3.38}$$

where [J] is the Jacobian matrix and is given by,

$$[J] = \begin{bmatrix} \frac{\partial r}{\partial \xi} & \frac{\partial z}{\partial \xi} \\ \frac{\partial r}{\partial \eta} & \frac{\partial z}{\partial \eta} \end{bmatrix} \tag{3.39}$$

On substitution of (3.37) the Jacobin matrix becomes,

$$[J] = \begin{bmatrix} \sum \frac{\partial N_i}{\partial \xi} r_i & \sum \frac{\partial N_i}{\partial \xi} z_i \\ \sum \frac{\partial N_i}{\partial \eta} r_i & \sum \frac{\partial N_i}{\partial \eta} z_i \end{bmatrix} \tag{3.40}$$

Substituting (3.40) into (3.38) gives the [B] matrix expressed as a function of the local coordinates ξ and η .

4 The stiffness matrix [K]

The stiffness matrix of an element may be calculated from (3.19) as

$$[K]^e = \int_S [B]^T[C][B]r \, dS$$

$$= \int_S [B]^T[C][B]r \det[J] \, d\xi d\eta$$

where dS is the area of the element, det[J] is the determinant of the Jacobian matrix given by (3.40), r is the coordinate in radial direction, [B] is a function of local coordinates ξ and η. Thus,

$$[K]^e = \int_{-1}^{+1} \int_{-1}^{+1} [B]^T[C][B]r \det[J] \, d\xi d\eta \tag{3.41}$$

This integral is evaluated using 3 point Gaussian integration, details of the appropriate abscissae and weighting coefficients may be found in (Zienkiewicz, 1971).

5 The mass matrix [M]

In a similar manner the mass matrix of an element can be calculated as,

$$[M]^e = \rho \int_{-1}^{+1} \int_{-1}^{+1} [N]^T[N]r \det[J] \, d\xi d\eta \tag{3.42}$$

where ρ is assumed to be constant within an element.

6 The damping matrix [G]

If damping is considered the damping matrix is then added as,

$$[G]^e = \int_{-1}^{+1}\int_{-1}^{+1} [B]^T[G][B]r\det[J]\, d\xi d\eta \tag{3.43}$$

In a practical piezoelectric transducer system, the piezoelectric disc is excited by a voltage from the generator through electrodes on its top and bottom surfaces. Damping in this system is from two sources. One is the mechanical damping inherent in the transducer structure, and the other is the energy dissipation in the circuit which can be modelled as a resistance R, so the damping matrix is

$$[G] = \begin{bmatrix} G_f & 0 \\ 0 & G_\phi \end{bmatrix} \tag{3.44}$$

where $[G_f]$, $[G_\phi]$ are the mechanical and electrical damping coefficient matrices respectively. However, in current analysis, the generalised damping has not been used, and the modal damping is used which is discussed in next section.

3.3 Modal analysis of piezoelectric discs

3.3.1 Dynamic equation and boundary conditions

The governing dynamic equation of piezoelectric materials obtained from the previous section may be written in matrix form as follows,

$$\begin{bmatrix} M_{ff} & 0 \\ 0 & 0 \end{bmatrix}\begin{Bmatrix} \ddot{f} \\ \ddot{\phi} \end{Bmatrix} + \begin{bmatrix} K_{ff} & K_{f\phi} \\ K_{f\phi}^T & K_{\phi\phi} \end{bmatrix}\begin{Bmatrix} f \\ \phi \end{Bmatrix} = \begin{Bmatrix} F \\ Q \end{Bmatrix} \tag{3.45a}$$

(3.45b)

where $\{f\} = \{\, u \;\; v \;\; w \,\}^T$ is the mechanical displacement vector, $\{\phi\}$ is the electrical potential vector, $[M_{ff}]$ is the mass matrix, $[K_{ff}]$, $[K_{f\phi}]$, and $[K_{\phi\phi}]$ are stiffness matrices, and $\{F\}$ and $\{Q\}$ are mechanical force vector and electrical charge vector.

Equation (3.45) in fact describes the dynamic behaviour of a raw piezoelectric material which is free from any boundary conditions. When a piezoelectric material is fabricated into piezoelectric devices, such as the piezoelectric discs used in ultrasonic transducers, the surface of the piezoelectric transducer usually consists of two areas, the electroded area and the non-electroded area as shown in Fig 3.2. The electroded area is usually covered by a thin layer of conducting material and is then connected to external electrical circuit. In practice, in the case of the piezoelectric disc, the top and bottom surfaces of the disc are usually uniformly electroded.

Each electroded area on the surface of a piezoelectric disc forms an equipotential surface. If the i'th electroded area has m finite element nodes on it, then the electrical potential and nodal charge on the i'th electrode surface have the following relationships,

$$\phi_1 = \phi_2 = \ldots\ldots = \phi_m = \varphi_i$$
$$Q_1 + Q_2 + \ldots\ldots + Q_m = Q_i \qquad (3.46)$$

where, φ_i and Q_i are the values of potential and total charge of the i'th electrode area.

A piezoelectric disc usually has only two electroded areas, such as the top and bottom surfaces of the disc, and is excited by an applied voltage across its two electrodes, and the important parameter is the potential difference between these two equipotential surfaces. Therefore the electrical boundary conditions are such that the electrical potential on one of the electrodes, for example, the one on the bottom surface, can be set to an arbitrary value as a reference. For convenience, this electrode is usually grounded, and the electrical degrees of freedom, ϕ_{pB}, at the nodes of bottom surface, are then all fixed to zero as

$$\varphi_B = 0 \quad \text{and}$$
$$Q_B = 0 \qquad (3.47)$$

Therefore the equation (3.46) can be written in a simple vector form for the only non-zero (top) electrode surface as,

$$\{\phi_p\} = \{I_p\}\varphi \quad \text{and}$$
$$Q = \{I_p\}^T Q_p \qquad (3.48)$$

where $\{I_p\}$ is a vector in which the components corresponding to the position of the finite element nodes on non-zero electrode surface are one and zero elsewhere.

Taken the above into consideration, equation (3.45) can be further partitioned for a piezoelectric disc having two different electroded areas, as

$$\begin{bmatrix} M_{ff} & 0 & 0 \\ 0 & 0 & 0 \\ 0 & 0 & 0 \end{bmatrix} \begin{Bmatrix} \ddot{f} \\ \ddot{\phi}_i \\ \ddot{\phi}_p \end{Bmatrix} + \begin{bmatrix} K_{ff} & K_{f\phi i} & K_{f\phi p} \\ K_{f\phi i}^T & K_{\phi i\phi i} & K_{\phi i\phi p} \\ K_{f\phi p}^T & K_{\phi i\phi p}^T & K_{\phi p\phi p} \end{bmatrix} \begin{Bmatrix} f \\ \phi_i \\ \phi_p \end{Bmatrix} = \begin{Bmatrix} F \\ 0 \\ Q_p \end{Bmatrix} \qquad (3.49a)$$
$$(3.49b)$$
$$(3.49c)$$

where the subscript i denotes the component corresponding to the electrical potential degree of freedom of the non-electroded nodes which include the internal nodes and the nodes on other non-electroded regions of the surface, while subscript p denotes the component corresponding to the electrical potential degree of freedom of the electroded

nodes. ϕ_i is the electrical potential vector corresponding to non-electroded nodes, and ϕ_p is the electrical potential vector corresponding to the nodes on the non-zero electrode surface since the equations corresponding to zero-electrode nodes can be deleted.

Appropriate excitation conditions or boundary conditions need to be considered before any computation can be carried out. For an ultrasonic transducer working in the transmitter mode, the mechanical boundary conditions can be assumed to be stress free. However, care must be taken with the electrical boundary conditions. The electrical boundary condition on the electrode of the top surface of the disc, φ_T, determines the vibration modes which a piezoelectric disc can possibly have. Two extreme cases, constant voltage excitation and constant charge (current) excitation, are considered below.

If the electrical potential of the electrode on the top surface of the disc is assigned to a known value, which sets the electrical potential difference between two electrodes to a constant or zero, the piezoelectric disc is then excited by constant voltage. The resonant frequencies calculated by applying this boundary condition correspond to the frequencies, denoted as f_{min}, at which the electrical impedance across the piezoelectric disc approaches zero. They are similar to the series resonant frequency f_s and the resonant frequency f_r discussed in the one dimensional model of Chapter 2.

With constant charge (current) excitation the resonant frequencies calculated by this condition correspond to the frequencies, termed as f_{max}, at which the electrical impedance across its two electrodes approaches a maximum. Sometimes they are also called as open circuit frequencies. They are similar to the parallel resonant frequencies f_p, and anti-resonant frequency f_a in the one dimensional model.

The eigenfrequencies of piezoelectric discs calculated by a three dimensional model will appear in pairs as constant voltage excitation resonant frequency and constant charge excitation resonant frequency at each mode. This is similar to the one dimensional case discussed in Chapter 2 where two sets of resonant frequencies (f_{min}, f_s, f_r) and (f_{max}, f_p, f_a) were identified. However, to find both f_{min}, and f_{max}, problems for constant voltage excitation and constant charge excitation have to be solved separately, alternatively as in this thesis, only the problem for f_{min} is solved, and f_{max} can be found through the maximum of the electrical impedance function if it is required.

3.3.2 Eigenvalue solution

The solution of equation (3.49) is usually obtained by using condensation techniques to eliminate the equations corresponding to the electrical potential degrees of freedom of the non-electroded nodes (Allik *et al.*, 1974; Naillon *et al.*, 1983), which may have the advantage of reducing the size of the problem for eigenvalue solution when the structure has a large proportion of non-electroded nodes. However, if any condensation process is used, the well-banded stiffness matrix is lost and it becomes fully populated. Hence, the solution for constant voltage excitation will be solved directly in this thesis, treating the electrical potential degrees of freedom exactly as mechanical degrees of freedom and preserving the well-banded stiffness matrix properties.

If F = 0, the first two equations of (3.49) can be written as,

$$\begin{bmatrix} M_{ff} & 0 \\ 0 & 0 \end{bmatrix} \begin{Bmatrix} \ddot{f} \\ \ddot{\phi}_i \end{Bmatrix} + \begin{bmatrix} K_{ff} & K_{f\phi i} \\ K_{f\phi i}{}^T & K_{\phi i\phi i} \end{bmatrix} \begin{Bmatrix} f \\ \phi_i \end{Bmatrix} = \begin{Bmatrix} -K_{f\phi_p}\phi_p \\ -K_{\phi i\phi_p}\phi_p \end{Bmatrix} \quad (3.50a)$$

(3.50b)

For voltage excitation the RHS of equation is a known force, and the eigenproblem (free vibration) is then,

$$\begin{bmatrix} M_{ff} & 0 \\ 0 & 0 \end{bmatrix} \begin{Bmatrix} \ddot{f} \\ \ddot{\phi}_i \end{Bmatrix} + \begin{bmatrix} K_{ff} & K_{f\phi i} \\ K_{f\phi i}{}^T & K_{\phi i\phi i} \end{bmatrix} \begin{Bmatrix} f \\ \phi_i \end{Bmatrix} = 0 \quad (3.51a)$$

(3.51b)

which is

$$[M]\frac{\partial^2\{\delta\}}{\partial t^2} + [K]\{\delta\} = 0 \quad (3.52)$$

Assuming the structure is vibrating harmonically in a form

$$\{\delta\} = \{\psi\} e^{i\omega t} \quad (3.53)$$

where $\{\psi_r\}$ is a time independent amplitude vector of order N, ω is the vibrating frequency. (3.53) can be written separately according the mechanical and electrical components as,

$$\begin{Bmatrix} f \\ \phi_i \end{Bmatrix} = \begin{Bmatrix} \psi_f \\ \psi_i \end{Bmatrix} e^{i\omega t} \quad (3.53a)$$

(3.53b)

Substituting (3.53) into (3.52) leads to,

$$[K]\{\psi\} = \omega^2[M]\{\psi\} \tag{3.54}$$

Equation (3.54) is a generalised eigenproblem, whose solution may be obtained by various eigenvalue solution schemes to give N pairs of eigenvalues and eigenvectors $(\omega_1^2, \{\psi\}_1)$, $(\omega_2^2, \{\psi\}_2)$, ..., $(\omega_r^2, \{\psi\}_r)$, ..., and $(\omega_N^2, \{\psi\}_N)$. The eigenvector $\{\psi\}_r$ is called the r'th mode shape vector and ω_r is the corresponding natural frequency of vibration.

For convenience, the eigenproblem solution solution can be expressed in matrix form as follows

$$[\Psi] = [\,\{\psi\}_1,\ \{\psi\}_2,\ ...,\ \{\psi\}_r,\ ...,\ \{\psi\}_N\,] \tag{3.55a}$$

$$[\Omega^2] = \begin{bmatrix} \omega_1^2 & & & & \\ & \omega_2^2 & & & \\ & & \cdots & & \\ & & & \omega_r^2 & \\ & & & & \cdots \\ & & & & & \omega_N^2 \end{bmatrix} \tag{3.55b}$$

where $[\Psi]$ is the matrix whose columns are the eigenvectors $\{\psi\}_r$ and $[\Omega^2]$ is the matrix which has the eigenvalues ω_r^2 on its leading diagonal, and all the off-diagonal terms are zero.

Since the stiffness matrix [K] given in equation (3.54) is non-positive definite, due to the negative dielectric terms in the elasticity [C] matrix (3.36), the particular numerical procedure to solve the above eigenproblem (3.54) has to be chosen so that it can accommodate a stiffness matrix with a negative determinant |K|. This problem can be avoided by static condensation to eliminate the second part of equation (3.50) (Allik and Hughes, 1974; Naillon *et al.*, 1983). However, as stated before, the resulting stiffness matrix is then fully populated, which reduces the solution efficiency. Alternatively, some matrix transformation must be carried out before the standard eigenproblem solution procedure in the finite element package is applied. Here a tridiagonalization of the matrices by the Lanczos method is adopted, see Appendix A. The general eigenproblem (3.54) is converted to a standard eigenproblem of the form

$$\frac{1}{\lambda}\{\psi^*\} = [T_n]\{\psi^*\} \tag{3.56}$$

where $\{\psi\} = [X][\{\psi^*\}$ and $[T_n]$ is a tridiagonal matrix.

Standard solution procedures, such as QR iteration (Bathe, 1982), are then applied to the new eigenproblem (3.56). The eigenvector $\{\psi^*\}$ in (3.56) can be related back to the original eigenvector $\{\psi\}$ in (3.54) by the transformation matrix [X] used in Lanczos method while the eigenvalues solved from (3.56) are identical to those from (3.54). The eigenvectors obtained from this procedure are mass-orthonormalized, which gives

$$[\Psi]^T[M][\Psi] = [I]$$
$$[\Psi]^T[K][\Psi] = [\Omega^2] \tag{3.57}$$

3.3.3 Steady state response functions

Having obtained the eigenvectors, the generalized nodal displacement vector, $\{\delta(t)\}$, can be expressed in (or transformed into) the generalized modal displacement vector $\{z(t)\}$

$$\{\delta(t)\} = [\Psi]\{z(t)\} \tag{3.58}$$

where $[\Psi]$ is the eigenvector matrix and $\{z(t)\}$ is the modal displacement vector or modal participation vector. (3.58) can be written in components as

$$\{\delta\} = \sum_{r=1}^{N} \{\psi_r\} z_r(t) \tag{3.59}$$

where $\{\psi_r\}$ and $z_r(t)$ correspond to the eigenvector and the modal displacement in mode r.

The forced response function can be obtained by pre-multiplying equation (3.50) by $[\Psi]^T$, and using equation (3.58).

$$-\omega^2[\Psi]^T\begin{bmatrix} M_{ff} & 0 \\ 0 & 0 \end{bmatrix}[\Psi]\{z\}+[\Psi]^T\begin{bmatrix} K_{ff} & K_{f\phi i} \\ K_{f\phi i}{}^T & K_{\phi i\phi i} \end{bmatrix}[\Psi]\{z\} = -[\Psi]^T\begin{Bmatrix} K_{f\phi_p\phi_p} \\ K_{\phi i\phi_p\phi_p} \end{Bmatrix} \tag{3.60}$$

By using the orthogonality (orthonomality) relations (3.57),

$$[\Psi]^T\begin{bmatrix} M_{ff} & 0 \\ 0 & 0 \end{bmatrix}[\Psi] = [I] \quad \text{and} \quad [\Psi]^T\begin{bmatrix} K_{ff} & K_{f\phi i} \\ K_{f\phi i}{}^T & K_{\phi i\phi i} \end{bmatrix}[\Psi] = [\Omega^2]$$

so

$$([\Omega^2] - [\omega^2])\{z\} = -[\Psi]^T\begin{Bmatrix} K_{f\phi_p\phi_p} \\ K_{\phi i\phi_p\phi_p} \end{Bmatrix} \tag{3.61}$$

Due to the orthogonality, the above equations are decoupled, and the modal displacement for mode r can be found as,

$$z_r = \frac{-\{\psi_r\}^T[K_{f\phi_p} K_{\phi i\phi_p}]^T\{\phi_p\}}{\omega_r^2 - \omega^2} \tag{3.62}$$

From (3.59) the generalized nodal displacement vector is therefore

$$\{\delta\} = \sum_{r=1}^{N} \frac{-\{\psi_r\}\{\psi_r\}^T[K_{f\phi_p} K_{\phi i\phi_p}]^T\{\phi_p\}}{\omega_r^2 - \omega^2} \tag{3.63}$$

Thus the mechanical part of the displacement vector is

$$\{f\} = \sum_{r=1}^{N} \frac{-\{\psi_{rf}\}\{\psi_r\}^T[K_{f\phi_p} K_{\phi i\phi_p}]^T\{\phi_p\}}{\omega_r^2 - \omega^2} \tag{3.64}$$

Similarly

$$\{\phi_i\} = \sum_{r=1}^{N} \frac{-\{\psi_{ri}\}\{\psi_r\}^T[K_{f\phi_p} K_{\phi i\phi_p}]^T\{\phi_p\}}{\omega_r^2 - \omega^2} \tag{3.65}$$

Substituting (3.64) into equation (3.49c) and taking $\{\phi_p\}$ outside of the bracket, gives

$$\Big[\sum_{r=1}^{N} \frac{-([K_{f\phi_p}]^T - [K_{\phi i\phi_p}]^T[K_{\phi i\phi_i}]^{-1}[K_{f\phi i}]^T)\{\psi_{rf}\}\{\psi_r\}^T[K_{f\phi_p} K_{\phi i\phi_p}]^T}{\omega_r^2 - \omega^2}$$
$$+ ([K_{\phi_p\phi_p}] - [K_{\phi i\phi_p}]^T[K_{\phi i\phi_i}]^{-1}[K_{\phi i\phi_p}])\Big]\{\phi_p\} = \{Q_p\} \tag{3.66}$$

Pre-multiplying equation (3.66) by $\{I_p\}^T$ and using the relation (3.48a)

$$\Big[\sum_{r=1}^{N} \frac{-\{I_p\}^T([K_{f\phi_p}]^T - [K_{\phi i\phi_p}]^T[K_{\phi i\phi_i}]^{-1}[K_{f\phi i}]^T)\{\psi_{rf}\}\{\psi_r\}^T[K_{f\phi_p} K_{\phi i\phi_p}]^T\{I_p\}}{\omega_r^2 - \omega^2}$$
$$+ \{I_p\}^T([K_{\phi_p\phi_p}] - [K_{\phi i\phi_p}]^T[K_{\phi i\phi_i}]^{-1}[K_{\phi i\phi_p}])\{I_p\}\Big]\varphi = Q$$

The electrical frequency response function can then be obtained as

$$\frac{Q}{\varphi} = \sum_{r=1}^{N} \frac{-r^A}{\omega_r^2 - \omega^2} + H_{\varphi\varphi} \tag{3.67}$$

where

$$r^A = \{I_p\}^T([K_{f\phi_p}]^T - [K_{\phi i\phi_p}]^T[K_{\phi i\phi_i}]^{-1}[K_{f\phi i}]^T)\{\psi_{rf}\}\{\psi_r\}^T[K_{f\phi_p} K_{\phi i\phi_p}]^T\{I_p\} \tag{3.68}$$

$$H_{\varphi\varphi} = \{I_p\}^T([K_{\phi_p\phi_p}] - [K_{\phi i\phi_p}]^T[K_{\phi i\phi_i}]^{-1}[K_{\phi i\phi_p}])\{I_p\} \tag{3.69}$$

r^A is defined as the modal constant of mode r in terms of frequency response function Q/φ (Ewins, 1984), which couples the external electrical force and the response of the systems, and $H_{\varphi\varphi}$ is the static capacitance of the piezoelectric structure. If mechanical damping, such as hysteretic (structural) damping is considered, it can be shown that the eigenvectors obtained for undamping case are also orthogonal with the damping matrix [G], the electrical FRF can be written as

$$\frac{Q}{\varphi} = \sum_{r=1}^{N} \frac{-r^A}{\omega_r^2 - \omega^2 + i\,\eta_r\omega_r^2} + H_{\varphi\varphi} \tag{3.70}$$

where η_r is the loss factor in mode r. In this thesis, η_r is assumed constant for all the modes.

It can readily be shown that

$$\{I_p\}^T([K_{f\phi_p}]^T - [K_{\phi i\phi_p}]^T[K_{\phi i\phi i}]^{-1}[K_{f\phi i}]^T)\{\psi_{rf}\} = \{\psi_r\}^T[K_{f\phi_p}\,K_{\phi i\phi_p}]^T\{I_p\} \tag{3.71}$$

and if we define the equivalent nodal force vector as

$$\{H_F\} = [K_{f\phi_p}\,K_{\phi i\phi_p}]^T\{I_p\} \tag{3.72}$$

and

$$H_r = \{\psi_r\}^T\{H_F\} \tag{3.73}$$

$$r^A = H_r^2 \tag{3.74}$$

The electrical impedance response function of the piezoelectric structure can then be obtained by differentiating the electrical charge as

$$Z(\omega) = \frac{\varphi}{i\omega Q} \tag{3.75}$$

The frequency response function for voltage excitation at the i'th degree of freedom can be obtained from equation (3.64). If $\psi_{rf}^{\,i}$ is the i'th component of eigenvector of mode r,

$$\begin{aligned} f_i &= \sum_{r=1}^{N} \psi_{rf}^{\,i}\, z_r \\ &= -\sum_{r=1}^{N} \frac{\psi_{rf}^{\,i}\{\psi_r\}^T[\,K_{f\phi_p}\,K_{\phi i\phi_p}\,]^T\{I_p\}\varphi}{\omega_r^2 - \omega^2} \end{aligned} \tag{3.76}$$

In terms of the frequency response function, then,

$$\frac{f_i}{\varphi} = -\sum_{r=1}^{N} \frac{\psi_{rf}{}^i \{\psi_r\}^T [\, K_{f\phi p}\, K_{\phi i\phi p}\,]^T \{I_p\}}{\omega_r{}^2 - \omega^2}$$

$$= -\sum_{r=1}^{N} \frac{\psi_{rf}{}^i H_r}{\omega_r{}^2 - \omega^2} \tag{3.77}$$

For hysteretic damping case, then

$$\frac{f_i}{\varphi} = -\sum_{r=1}^{N} \frac{\psi_{rf}{}^i H_r}{\omega_r{}^2 - \omega^2 + i\,\eta_r \omega_r{}^2} \tag{3.78}$$

To evaluate the strength of excitation of each mode (or the intensity of each mode), many forms piezoelectric coupling factors could be used as reviewed in Chapter 1. However, it has been found that it may not always be satisfactory to use piezoelectric coupling factors in the three dimensional analysis of piezoelectric discs since the modal density is very high. Locke *et al.* (1987) found that for some modes of the piezoelectric discs the anti-resonant frequency predicted by the finite element method f_a was smaller than their resonant frequency f_r, and it was also very difficult to identify f_a and f_r of the same mode without ambiguity.

It was therefore decided in this work to use the modal constant r^A defined in equation (3.74) to evaluate the strength of the excitation of each mode since it couples the external electrical force (voltage) to the response of the system.

3.3.4 Transient mechanical response when subjected to a voltage pulse

The transient mechanical response when a piezoelectric disc is excited by a voltage pulse can be obtained by using the mode superposition method (Zienkiewicz, 1979) as shown in equation (3.58)

$$\{\delta(t)\} = [\Psi]\{z(t)\}$$

With the eigenvectors being M-orthonormalized, the dynamic equation (3.50) becomes

$$\frac{\partial^2\{z\}}{\partial t^2} + [\Psi]^T[G][\Psi]\frac{\partial\{z\}}{\partial t} + [\Omega^2]\{z\} = [\Psi]^T\{R(t)\} \tag{3.79}$$

where $\{R(t)\}$, the forces vector when voltages are applied across the electrodes is given by

$$\begin{aligned}\{R(t)\} &= [\,K_{f\phi p}\;\; K_{\phi i\phi p}\,]^T\{\phi_p\}\\ &= [\,K_{f\phi p}\;\; K_{\phi i\phi p}\,]^T\{I_p\}\varphi(t)\\ &= \{H_F\}\varphi(t)\end{aligned} \tag{3.80}$$

and

$$\begin{aligned}[\Psi]^T\{R(t)\} &= [\Psi]^T\{H_F\}\varphi(t)\\ &= \{H_r\}\varphi(t)\end{aligned} \tag{3.81}$$

If damping is neglected, the above equation can be decoupled and

$$\frac{\partial^2 z_r}{\partial t^2} + \omega_r^2\, z_r = H_r\,\varphi(t) \qquad r = 1,2,\ldots,N\max \tag{3.82}$$

$\varphi(t)$ can be an arbitrary function of time, and by using the Duhamel integral, the solution of the above differential equation is

$$z_r(t) = \frac{1}{\omega_r}\int_0^t H_r\varphi(\tau)\sin[\omega_r(t-\tau)]d\tau + A_r\sin(\omega_r t) + B_r\cos(\omega_r t) \tag{3.83}$$

where A_r, B_r are determined from the initial conditions. If δ_0 and $\frac{\partial\delta_0}{\partial t}$ denote the displacement and velocity at $t = 0$, then,

$$\begin{aligned} z_r\,|_{t=0} &= \{\psi\}_r^T[M]\,\delta_0\\ \frac{\partial z_r}{\partial t}\,|_{t=0} &= \{\psi\}_r^T[M]\,\frac{\partial\delta_0}{\partial t}\end{aligned} \tag{3.84}$$

The Duhamel integral can be evaluated numerically, and an analytical solution can be obtained for some simple excitations.

To evaluate the overall response of the structure, the solution to all n equations of form (3.82) must be calculated. The nodal point displacements can then be obtained by superposition of the response in each mode from (3.59) as,

$$\{\delta(t)\} = \sum_{r=1}^{N}\{\psi\}_r\, z_r(t)$$

If the damping can be assumed to be proportional, in which case the eigenvectors are identical to undamped case,

$$\{\psi\}_r^T[G]\,\{\psi\}_j = 2\omega_r\xi_r\,\delta_{rj} \tag{3.85}$$

where, ξ_r is a modal damping parameter (viscous damping), and δ_{rj} is the Kronecker delta (δ_{rj} =1 for r = j, δ_{rj} = 0 for r ≠ j). Therefore, by using (3.85) the eigenvectors $\{\psi\}_r$ r = 1, 2, 3, ..., N_{max}, are also G-orthogonal and the equation (3.79) can still be decoupled into the form

$$\frac{\partial^2 z_r}{\partial t^2} + 2\omega_r \xi_r \frac{\partial z_r}{\partial t} + \omega_r^2 z_r = H_r \varphi(t) \qquad r = 1, 2, ..., N_{max} \tag{3.86}$$

In this case, the solution procedure of the dynamic response is the same as when damping is neglected except that the response of each mode is obtained by solving the above equation.

3.4 Conclusions

The formulation of the finite element analysis of piezoelectric materials has been carried out. The solution for the eigenproblem, and the formulation of various frequency response functions including the electrical impedance characteristic function have also been obtained.

Since the formulation and the solution of eigenvalue problem are carried out using generalised coordinates and variables, following the standard finite element analysis procedure, the analysis of the vibration characteristics of piezoelectric structures can be carried out with a standard finite element package, for example, FINEL, developed in Imperial College (Hitchings, 1984). The piezoelectric element is implemented simply by adding one extra degree of freedom to the corresponding elastic elements. The generalised material constants matrix which includes the elastic constants, the piezoelectric constants and dielectric constants must be input rather than just the elastic constants. The problem of the non-positive definite stiffness matrix which is caused by the dielectric constants, can be solved by transformation of the matrix. The resonant frequencies and the corresponding mode shapes of piezoelectric structures for constant voltage excitation can then be found by a standard eigenproblem solution scheme. By further manipulation to obtain modal constants and static capacitance of the piezoelectric disc, the frequency response functions and the transient response for constant voltage excitation can then be obtained by the modal analysis method.

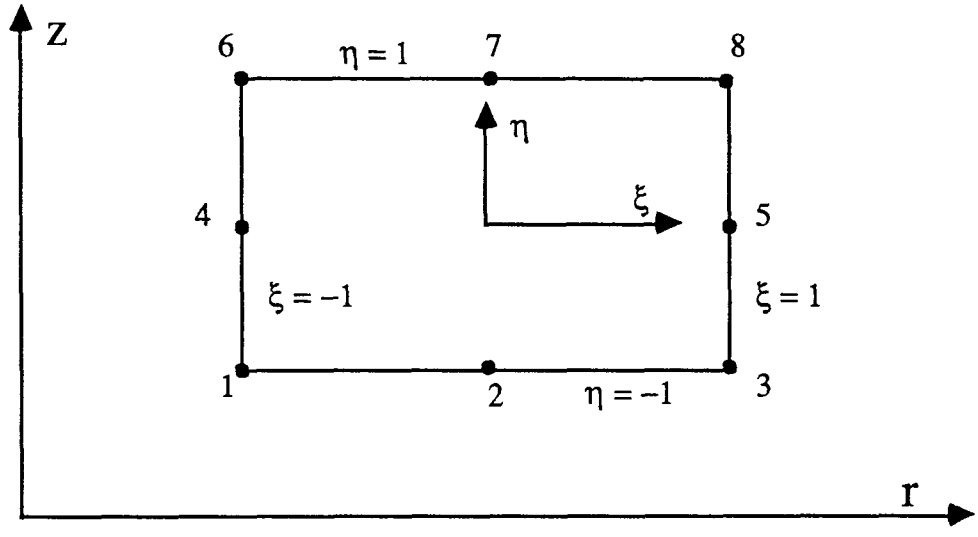

Fig 3.1 Global and local coordinate systems

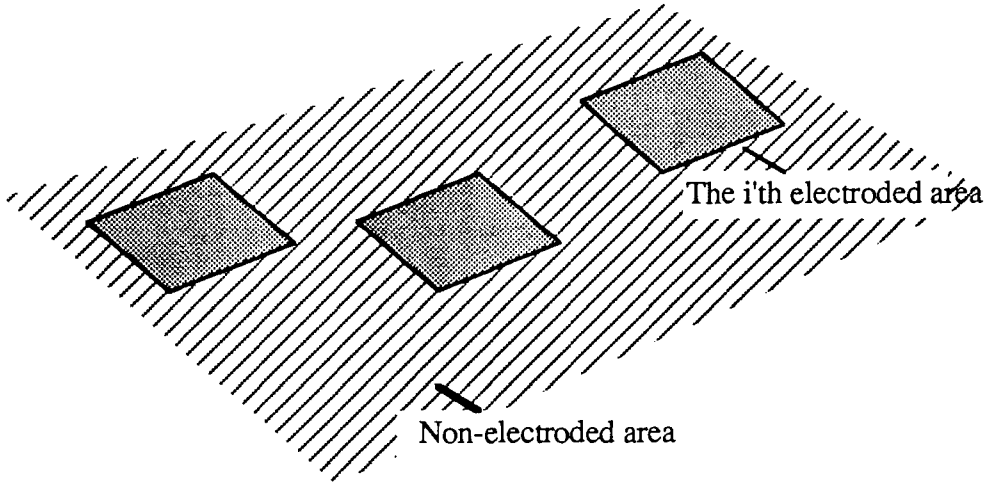

Fig 3.2 Electroded areas and non-electroded area over a surface of the piezoelectric material

CHAPTER 4

THREE DIMENSIONAL ANALYSIS OF VIBRATION CHARACTERISTICS OF PIEZOELECTRIC DISCS

4.1 Introduction

In Chapter 3 the formulation of the finite element analysis of piezoelectric structures has been presented. The various frequency response functions including the electrical impedance response and the mechanical frequency response function when the piezoelectric disc is subjected to a voltage excitation have been obtained.

In this chapter the vibration characteristics of piezoelectric discs are analysed by the three dimensional finite element model. To begin with, the possible types of resonant modes of piezoelectric discs in the frequency range of interest are discussed, and the natural frequencies, mode shapes and modal constants of piezoelectric discs with D/T ratios of 20, 10 and 0.5 are then predicted. The frequency response functions and the electrical impedance frequency responses of these discs are then calculated from these modal parameters.

Experimental results are then presented to verify the predictions from the theoretical model. The resonant frequencies and the electrical impedance frequency responses of a variety of discs have been measured and some mode shapes of the discs have been checked using laser interferometry.

4.2 Types of vibration modes predicted by the FE analysis

The resonant frequencies of piezoelectric discs are predicted for constant voltage excitation. These correspond to the short circuit resonant frequencies or the frequencies at which the electrical impedances of the disc are zero if energy dissipation is not considered, as discussed in Chapter 1. The mode shapes at these resonant frequencies are also computed. The disc analysed is assumed to be axisymmetric with full electrodes on the top and bottom surfaces, and the 8 node quadrilateral axisymmetric piezoelectric element developed in Chapter 3 is used. The harmonic number in equation (3.35) is set to zero since the forcing is axisymmetric. The FE eigenvalue solution predicted both the extensional modes and the flexural modes, however, only the extensional modes can be excited electrically in this manner and are presented.

Since the vibration characteristics of piezoelectric discs are most important around the frequency of the first through thickness mode of the piezoelectric disc defined by the one dimensional model, the frequency range of interest is in this range, and only the modes with frequencies up to approximately one and a half times the first through thickness frequency are predicted.

Good accuracy is ensured by both the eigenvalue solution routine itself and the finite element mesh used. The implemented eigenvalue routine in fact calculates about twice the number of modes required. This ensures that no mode in the frequency range of interest is missed, even though the modes do not always appear in strict rising frequency order.

The mesh density is usually so chosen that there are enough finite element nodes (5 to 7) per wavelength of the hightest mode required both in the radial and thickness direction. It is possible to maintain good accuracy for high order modes at the expense of the computing cost, but it is not necessary for the present work. Restrictions may arise from inadequate computing memory, such as that there may not be enough in core memory for the fast Lanczos transformation routine. The amount required depends upon the number of modes required.

It was found that there are a large number of modes predicted in the frequency range of interest for a piezoelectric disc, as discussed by previous experimental reports (Shaw, 1956; Ikegami *et al.*, 1974; Ueha, *et al.*, 1983), while no one of them has the piston-like motion of Fig 1.3(b) assumed by the one dimensional model. In many experimental reports, modes were classified by their characteristics in the measured frequency spectrum rather than their deformed pattern (Ikegami *et al.*, 1974). Here, the mode shapes predicted by the FE model are examined, and five groups of modes are classified according to their mode shapes, which are consistent with the previous reports. These are radial modes (R modes), edge modes (E modes), thickness shear modes (TS modes), thickness extensional modes (TE modes) and high frequency radial modes (A modes). Typical examples of these five types of mode shapes are shown in Fig 4.1(a) to 4.1(e) for a piezoelectric disc with a D/T ratio of 20. Since the disc is axisymmetrical, only the half of the cross section of the disc is plotted; the left edge is the central axis, and the right edge is the cylindrical surface. The broken line shows the finite element mesh itself, and the solid line represents the deformed shape of the disc at the resonant frequencies.

1. Radial modes (R)

The first group of the resonant modes predicted by the finite element analysis are the radial modes, with an example of the mode shapes shown in Fig 4.1(a). It can be seen that in radial modes the disc stretches in the radial direction and expands in the thickness direction due to the Poisson's ratio effects. The mode shapes of radial modes are characterised by large radial displacement at the cylindrical surface of the disc and nodal circles over the top and bottom surfaces of the disc at which the displacement in the axial direction is zero. The maximum axial displacement occurs at the centre of the surface and it approaches zero at the edge of the disc. The number of nodal circles increases as the order of the modes increases. Fig 4.1(a) shows a radial mode of 4 nodal circles.

Since the discs tend to have a large diameter compared with their thickness, the frequencies of the radial modes are rather lower than those of the other modes, and as the order of the radial modes increases, the frequencies are increased in a manner which are close to the roots of a Bessel function defined in equation (1.6) of Chapter 1.

2. Edge mode (E)

An edge mode is the mode in which the axial displacement at the edge of the surface of the disc is of the same order as that at the middle of the surface, for example, the mode shown in Fig 4.1(b). Apart from this difference, the edge mode has similar mode shape to the radial modes. It is also observed that the radial modes in the neighbourhood of the edge mode have fairly large axial displacement at the edge of the surface. However, only the mode which has the maximum axial displacement at the edge is defined as the edge mode.

3. Thickness shear modes (TS)

The third group of resonant modes are those having large radial deformation inside the disc which varies through the thickness but very little at the cylindrical surface as shown in Fig 4.1(c). They are characterised by nodal cylindrical rings inside the disc along the thickness direction at which the radial displacements are zero. As with the radial modes, the number of nodal rings increases with increasing order of the thickness shear modes. The mode shape shown in Fig 4.1(c) has 4 nodal rings (including one at the centre and one at the edge). The frequencies of the thickness shear modes are very close to the second through thickness shear mode defined by the one dimensional model.

4. Thickness extensional modes (TE)

The fourth group of resonant modes shown in Fig 4.1(d) are the thickness extensional modes, or the thickness modes in short. They lie in the frequency range of the first through thickness mode predicted by the one dimensional model, which is given by equation (1.2) with n = 1, and they may be the most interesting and important modes in piezoelectric discs. The axial displacement of the surface in the thickness extensional modes is similar to that in the radial modes in that it varies with radial position about a mean value. In the case of the radial modes, this mean value is zero and therefore the points at which the displacement has its mean value are the nodal circles. In the case of the TE modes, however, the mean value is non zero, so the axial displacement pattern is similar to that of the radial modes, but superimposed on a constant shift (or "dc" offset). This shift may be regarded as analogous to the piston-like motion shown in Fig 1.3(b) by the one dimensional analysis. The thickness extensional mode therefore has characteristics of the high order radial modes and one dimensional through thickness motion.

5. High frequency radial modes (A)

The last group of modes are the high frequency radial modes as shown in Fig 4.1(e). The axial surface displacement in the high frequency modes (A) is essentially a superposition of the displacement in the low order R-modes with that in the high order R-modes. This is shown schematically in Fig 4.2. The radial displacement at the cylindrical surface, however, is very small.

It can be seen that the thickness extensional modes predicted by the finite element analysis are much more complicated than expected from the one dimensional analysis; not only are the mode shapes complicated but also several similar modes in the frequency band around the through thickness frequency obtained from the one dimensional analysis are predicted. To decide which mode(s) can be strongly excited by an applied voltage, the excitation force pattern must be taken into consideration. In order to do this the modal constants of the resonant modes must be evaluated as described in chapter 3.

4.3 Vibration characteristics of a PZT5A disc with a D/T ratio of 20

In this section the vibration characteristics of a piezoelectric disc are analysed by the three dimensional finite element model. The material of the piezoelectric disc is PZT5A, which is a modified lead zirconate titanate ceramic. The material constants provided by

Vernitron Ltd. are listed in Table A.1. Like other piezoelectric ceramics PZT5A has a high charge sensitivity and also a relatively high loss factor with a mechanical Q factor of 75.

The disc analysed was 40.10 mm in diameter and 2.03 mm thick, the dimensions being chosen to correspond with one of the discs which was available for testing. This gives a diameter to thickness ratio of approximately 20, which is in the same order as the D/T ratio used in many NDT transducers. The disc was labelled P5A20 to denote PZT5A and the D/T ratio of 20. Since the disc is fairly thin with D/T of 20 the one dimensional analysis is also applicable, and comparison will be made between predictions from the three dimensional and one dimensional models.

The one dimensional theory predicts that the first through thickness mode of this disc had a frequency around 962 kHz, and the second through thickness shear mode had a frequency of 825 kHz. The frequency range of interest of this disc was therefore set from zero to 1500 kHz, and all the modes whose frequency was below 1500 kHz were required by the eigenvalue solution programme. A 2x48 mesh of the 8 node quadrilateral axisymmetric piezoelectric element described in Chapter 3 was used, which gave 5 nodes through the thickness and 97 nodes along a radius. Finer meshes were also used, and it was found that the accuracy was improved, but not significantly for those modes of interest, while the cost of computing increased drastically.

4.3.1 The natural frequencies and mode shapes

Within the frequency range 0 to 1500 kHz, a total of 130 modes were found by the eigenvalue prediction. Off these 66 modes were flexural (anti-symmetrical) modes which cannot be excited by a voltage applied to electrodes on the top and bottom surfaces of the disc, and so do not appear in the computed response functions. To save space only the frequencies of the first 48 extensional modes are listed in Table 4.1 which covers the frequency range of 0-1200 kHz. The corresponding mode shapes are shown in Fig 4.3. The modes listed in Table 4.1 were identified according to their mode shape characteristics and their mode types are given in the table.

It can be seen from Fig 4.3 a large proportion of the modes fall into radial mode group. The first 12 modes predicted are the lowest 12 radial modes with increasing numbers of nodal circles over the top and bottom surfaces of the disc. The maximum axial displacement over the surface occurs at the centre of the disc, and approaches zero at the edge of the disc. Their frequencies increase in a manner close the roots of Bessel function (Berlincourt *et al.*, 1963), which shows that the radial modes are nearly evenly

distributed. Mode 13 at a frequency of 657.7 kHz is the edge mode with very pronounced axial displacement at the edge of the surface. Modes 12 and 14 also have a fair amount of axial displacement at the edge of the disc, though they are regarded as radial modes. Modes 15 to 21 are higher order radial modes.

Five consecutive modes between 22 and 26 are thickness shear modes; they have very close frequencies, 873.2, 876.4, 880.0, 887.0 and 893.2 kHz and have similar mode shape characteristics with very strong radial deformation inside the disc along the thickness direction. They have very little deformation at the edge of the disc in both thickness and radial directions, and the radial deformation on the cylindrical surface approaches zero. The number of nodal rings increases with increasing frequency. However, the first thickness shear mode predicted at 873.20 kHz has two nodal rings, which is not the simplest mode shape of this sort . The mode 27 - 29 are high order radial modes.

Modes 30 to 34 are the thickness extensional modes, or the thickness modes. Their axial surface displacement varies along the radial direction but with a non zero mean value. In particular mode 32 at frequency of 964.9 kHz has a very large mean value. This makes mode 32 similar to the first through thickness mode assumed by the one dimensional model. It was subsequently found that this similarity was not so clear for piezoelectric discs with lower D/T ratios.

For the modes above this range, the mode shapes are more and more complicated. Some of them are high order R modes, while some are A modes, for example, modes 34, 37 and 40. It can be seen that A modes have frequencies above those of the thickness extensional modes, as reported by Ikegami *et al.* (1974), and the mode shapes are close to those shown in Fig 1.15(c) which were obtained analytically by applying the zero radial displacement boundary condition (Aggarwal, 1952b).

It is evident that the thin piezoelectric disc with a D/T of 20 has many more resonant modes than predicted by the one dimensional model, and no one of them has the piston-like mode shape shown in Fig 1.3(b). For this particular piezoelectric disc with a D/T of 20, one of the thickness extensional modes, whose frequency predicted at 964.94 kHz is very close to the first through thickness frequency at 962 kHz predicted by the one dimensional model (less than 0.3% difference), has a very large mean value of the axial displacement over the surface of the disc. This mode shape has considerable similarities with the through thickness mode assumed by the one dimensional theory.

4.3.2 The modal constants

To evaluate the strength of each mode, the modal constant defined in (3.74) was calculated using the equivalent force vector given by (3.72) and the eigenvector (mode shapes) obtained in the eigenvalue routine for all the modes predicted (including both symmetrical and anti-symmetrical modes). The equivalent nodal force in the axial direction on the surface due to the applied voltage is plotted in Fig 4.4 as a function of normalised radial position. It can be seen that the equivalent nodal force increases with a zig-zag form along the radius. The zig-zag variation between the middle-element nodes and the inter-element nodes results from the axisymmetric element used and the nature of discretisation of the finite element method. It can be reduced by increasing the finite element mesh density, however, this is not necessary for the present work.

The calculated modal constants of the first 48 modes in the frequency range of 0 to 1200 kHz are listed in Table 4.1, and the values normalised to the maximum modal constant are plotted in Fig 4.5. It can be seen that the modes around the frequency range 900 to 1000 kHz have very large modal constants, mode 32 having the maximum value of 26010; modes 30, 31 and 34 also have very large values, which indicates that these thickness extensional modes can be strongly excited. The low frequency radial modes in general have relatively small modal constants though the first mode has a slightly higher value than the others while the modes around the edge mode have larger modal constants, which suggests that they are more strongly excited than the adjacent radial modes. The radial modes above the edge mode and the thickness shear modes have very small modal constants, therefore they can only be weakly excited by an applied voltage. The modes above the frequency range of the thickness extensional modes, such as high order R modes and high frequency A modes have small modal constants, and therefore can be only weakly excited.

The modal constants may be interpreted by considering the equivalent nodal force over the surface of the disc and the mode shape of the modes. Since the equivalent nodal forces are nearly in linear relationship with the radial position, as shown in Fig 4.4, if the movement over the surface of the disc has a non-zero mean value as in the case of the TE modes, the terms in equation (3.74) are additive, giving a large sum for the modal constant, while if the movement changes sign over the surface of the disc as is the case in radial modes, different terms in (3.74) tend to cancel. In the first radial mode, the axial displacement is in the same direction over the whole surface of the disc (same sign), giving a high modal constant. The value, however, is lower than in the the TE modes since the absolute value of the displacement is small compared with the radial displacement. This is the reason

why the modal constant of the first radial mode is slightly bigger than the others. The modes around the edge mode have very large displacement at the edge of the disc and the nodal force at edge of the disc reaches maximum, so this term contributes significantly to the modal constants, resulting in the small peak in Fig 4.5. The thickness modes have large modal constants since they have non zero mean value of the axial displacement, this is particularly obvious for mode 32 at a predicted frequency of 964.94 kHz, in which the mean value is so large that the displacements over the surface mostly have almost the same sign, which results in the largest modal constant of all the modes of the disc. The high frequency A-modes have very small modal constants due to the changing sign of the motion over the surface of the disc, which is similar to the case in the low order R modes.

The modal constant can also be used to explain why the flexural modes (anti-symmetrical modes) cannot be excited by the voltage applied to the electrodes of the disc, since all the modal constants calculated for the flexural modes are almost zero (calculated values 10^{20} less than those of the extensional modes). This is because the dot product of the symmetric force vector with the anti-symmetric mode shape vector is zero.

4.3.3 The frequency response functions and electrical impedance response

The electrical impedance characteristics and the mechanical frequency response function may easily be obtained by using equations (3.75) and (3.77). The electrical impedance response of the PZT5A disc with D/T of 20 is shown in Fig 4.6(a) in which all 130 modes predicted were included in the calculation, while Fig 4.6(b) shows the corresponding mechanical FRF in which the response is the axial mechanical displacement at the central point of the disc and the force is the voltage applied across the disc.

As discussed in Chapter 1, the electrical impedance of the disc is given by the static capacitance of the disc in parallel with the effective impedance given by the mechanical properties coupled with the piezoelectric coupling factor. At low frequency the characteristic is dominated by the effective impedance, which is capacitive. Above the resonant frequency, the effective impedance becomes inductive and above the anti-resonant frequency the effective impedance is dominated by the static capacitance of the disc. In one dimensional analyses, each resonant mode is followed by a corresponding anti-resonant mode at a higher frequency in the electrical impedance response. However, this may not be true for the resonant modes whose frequencies are very close to each other, for example, around the frequency range of thickness modes in Fig 4.6(a).

At the resonant frequencies the electrical impedance should drop to zero while at the anti-resonant frequencies the electrical impedance should reach infinity if damping is not considered. However, in practice finite values are seen due to the finite frequency step used in the analysis. For the response shown in Fig 4.6 where damping was not included and with a frequency resolution of 1 kHz, very sharp troughs appear at the resonant frequencies, and spikes at the anti-resonant frequencies. All the 64 extensional modes predicted in the frequency range from 0 to 1500 kHz are present in the plot, though some of them are too weak to be seen.

Structural damping, which is proportional to the stiffness, was introduced in both the electrical impedance and the mechanical frequency response function in equations (3.70) and (3.78). Fig 4.7 shows the same response as Fig 4.6 but with a structural damping factor of 0.013 according to the mechanical Q factor listed in Table A.2. It is evident that damping smooths the overall response and gives finite amplitude of response at the resonant frequencies and the anti-resonant frequencies.

It can be seen from Fig 4.7 that the electrical impedance response of this disc is dominated by a single mode, mode 32, at a frequency of 964.9 kHz, and it has been already shown in Fig 4.5 that mode 32 has the largest modal constant, with a very large mean value of the axial displacement over the surface of the disc. This suggests that when the piezoelectric disc has a large D/T ratio, or is very thin, the three dimensional prediction may give similar results to those given by the one dimensional analysis.

The mechanical frequency response functions in the axial direction of the centre of the surface when voltage excitation is applied shown in Fig 4.6(b) and Fig 4.7(b) have amplitude peaks at the resonant frequencies.

To verify the three dimensional analysis of the piezoelectric disc by the finite element model, experiments were made to measure the electrical impedance response and the resonant frequencies of the modes for the P5A20 disc.

4.3.4 Set up for measurement of electrical impedance response

Sine wave excitation, which is widely used to measure the frequency response function in standard modal testing analysis (Ewins, 1984), was used to measure the electrical impedance characteristics of piezoelectric discs. The configuration of the equipment is shown in Fig 4.8. The piezoelectric disc was in series with a reference resistor with resistance of 100 Ω which was used to measure the current through the circuit, and

excitation was provided by the function generator in a Solartron 1255 two channel frequency response analyser (FRA). The voltages across the electrodes of the piezoelectric disc and the resistor were measured simultaneously by the FRA, which can analyse signals up to a frequency of 20 MHz. The system was controlled by a micro-computer to make a sweep measurement in the frequency range of interest by varying the frequency of the output voltage from the generator in the FRA. The electrical impedance frequency function can then be obtained directly from the FRA output as

$$Z(\omega) = R\frac{V_1}{V_2} \tag{4.2}$$

where $Z(\omega)$ is the measured electrical impedance of the piezoelectric disc, R is the resistance of the reference resistor, and V_1 and V_2 are the voltages across the piezoelectric disc and the resistor respectively.

Since the piezoelectric disc shows inductive characteristics above each resonant frequency, care must be taken to avoid effects from the external electrical circuit, such as the length of the leads. Problems may also be encountered from the shunt capacitance in the FRA, which may seriously distort the measured electrical impedance response when the static capacitance of the piezoelectric disc is very small or comparable to the shunt capacitance in the circuit.

4.3.5 Experimental results

The measured electrical impedance response is shown in Fig 4.9 for P5A20, a PZT5A disc with D/T ratio of 20, together with the predicted response with structural damping factor of 0.013, by the three dimensional model and the one predicted by the one dimensional model as given in equation (1.5). Since the electrical impedance of a piezoelectric disc drops to zero when it vibrates at a resonant frequency for the undamped case, the resonant frequencies may be found by locating the frequencies at which the electrical impedance is a minimum. The anti-resonant frequencies can be found in a similar way by locating the maxima in the electrical impedance. The smaller the impedance at the resonant frequency, the more strongly the disc can be excited at that mode. The measured resonant frequencies from the impedance curve are listed in Table 4.1.

The modal constants may be derived from the experimental data by standard modal testing techniques (Ewins, 1984) using MODENT, a software package developed in Imperial College. The measured electrical impedance response must first be converted into the form of equation (3.70), which can be regard as a receptance FRF, then the various modal analysis techniques may be applied. Here a single degree of freedom technique

called the Bendent extraction method (Dobson, 1985), see details in Appendix C, was used to find the modal parameters. The Bendent method is available in MODENT, a software package developed in Imperial College, and has been modified to accommodate the electrical impedance.The measured modal constants at resonant modes of this PZT5A disc are listed in Table 4.1. Their normalised values to the maximum modal constant are plotted in Fig 4.10 as a function of frequency.

It can be seen from Fig 4.9 that there is excellent agreement between the measured and the predicted electrical impedance responses, and several modes can clearly be identified. Since the damping of PZT5A is relatively high, a large number of modes which can only be weakly excited were not seen, and it was very difficult to correlate all the predicted modes with the measured ones. Emphasis was therefore placed on the modes which were well separated and those having very distinct features, such as the low frequency radial modes, the edge mode, and the thickness extensional modes.

In the low frequency radial modes range, the resonant modes are well separated from each other with resonances followed by their corresponding anti-resonances. Both the predicted and measured response curves show an increase in strength of excitation in the edge mode range. However, some shifts occur in the values of resonant frequency of high order radial modes. The gradually increasing discrepancy with the order of radial modes between the predicted and measured values in resonant frequencies may result from several sources. The material constants used in prediction, such as, the elastic constants in radial direction, may not be accurate enough, which may affect the accuracy of the predicted high order radial resonant frequencies, and may shift the order of the modes. Also, the accuracy of the finite element model decreases as the mode order increases.

The predicted electrical impedance response in the thickness frequency range agrees well with the measured response both in the amplitude of response and in the values of resonant frequencies. The frequencies of the major modes in this range show a difference between prediction and experiment of less than 1.5%. The measured resonant mode at frequency of 951 kHz, which corresponds to mode 32 predicted at 964.9 kHz, is the most strongly excited mode for this disc. It has such a large modal constant that the response is dominated by this single mode as expected from the one dimensional model. The measured response over the thickness shear modes range and the frequency range above the thickness modes shows very small resonant ripples, and the corresponding modal constants were too small to be derived from the experimental data, which confirms the predicted result that these two types of modes can only be excited very weakly. The

measured modal constants of the modes are somewhat different from the predicted ones, but the normalised values shown in Fig 4.5 and 4.9 have good agreement in form.

4.4 Vibration characteristics of piezoelectric discs with D/T of 10 and 0.5

4.4.1 A PZT5A disc with D/T of 10

In this section a piezoelectric disc of PZT5A which has a diameter of 19.96 mm and thickness of 2.01 mm is considered theoretically and experimentally. The disc, labelled P5A10, has a diameter to thickness ratio around 10, and is not as thin as the disc with D/T of 20 though the diameter of the disc is still considerably larger than the thickness.

A 2x32 finite element mesh was used for this disc. The predicted and measured electrical impedance responses are shown in Fig 4.11. The measured resonant frequencies of the modes and their modal constants are listed in Table 4.2 together with the values from the analysis.

It was anticipated that there would be some discrepancy between the predicted and measured resonant frequencies, which may come from a number of sources, such as variation in the measurement of dimensions of disc, imperfections of the disc during the manufacture (lack of flatness, out of round, etc.), inaccuracy in the material constants used in prediction, and the finite element discretisation. However, the discrepancy over the thickness frequency modes range was considerablely larger in this disc than in the disc with D/T ratio of 20, and varying the FE mesh (a 4x32 mesh) has not improved the results, which indicated that the material constants in the thickness direction used in prediction were far from accurate. It was therefore decided to check the the longitudinal velocity in the thickness direction of the piezoelectric disc by using the ultrasonic spectroscopy technique (Pialucha *et al.*, 1989). The longitudinal velocity listed in Table A.1 is 4350 m/s, which is taken from handbook provided by the manufacturer (Vernitron, 1976). It was found that the measured longitudinal velocity in the disc with D/T ratio of 20 is 4303 m/s which is only 1.1% smaller than the book value, while the measured velocity in the PZT5A disc with D/T of 10 is 4190 m/s which is 4% smaller than the book parameter. This is not surprising since the piezoelectric material varies from batch to batch so that it is not uncommon that the discrepancy between the measured material constants and the book parameters can be as great as 20% in supposedly similar types of piezoelectric materials (Smith, 1973). Since it was difficult to measure all the material constants of the piezoelectric material used in the prediction, and the main interest was in the trend of vibration characteristics of the piezoelectric disc rather than the accuracy of

particular resonant frequencies of the disc, no further study of the cause of the discrepancy has been undertaken.

Apart from these shifts in frequencies, good agreement is shown between the electrical impedance characteristics predicted by the FE model and the measurement. It can be seen that the overall response is no longer dominated by a single mode, which is the case for the disc P5A20. Two strongly excited thickness extensional modes at measured frequencies of 895.9 kHz and 933.7 kHz are also seen in the predicted curve at 964.7 kHz and 988.0 kHz (957.5 kHz and 989.6 kHz obtained for 4x32 mesh). The predicted mode shapes of these two modes have very large mean values of axial movement over the surface of the disc, as shown in mode shape plot in Fig 4.12, but neither of the modes is similar to mode 32 of the disc P5A20. The modal constants of these two modes have similar values: one is 3072, the other is 3684, which are much greater than those of all other modes, as listed in Table 4.2. Another mode at 915.1 kHz which also has a relatively large mean value of motion over the surface is also strongly excited. The predicted thickness shear mode at 880.6 kHz has one "nodal ring" only. This simple shear mode was not seen in the disc studied previously (P5A20) in which the first shear mode predicted has two "nodal rings".

4.4.2 A PZT5A disc with D/T of 0.5

In this section a piezoelectric disc with D/T ratio of 0.5, labelled P5A005, was studied; the disc was 10.07 mm long and 5.00 mm in diameter with the top and bottom end surfaces being electroded. Since the disc was essentially a cylinder, an 8x4 element mesh was used in the prediction, which gave 17 element nodes in the thickness direction and 9 along the radial direction.

There were six modes predicted over the frequency range of 0 to 600 kHz; the frequencies of the modes are listed in Table 4.3, while the mode shapes are shown in Fig 4.13. It can be seen that mode 1 at a frequency of 133.45 kHz is an extensional mode which has a half wavelength through the thickness and is similar to the first longitudinal mode in a long bar, the displacements are a maximum over the top and bottom surfaces and are almost uniform, and this uniform displacement may also be observed at other cross sections. Since the disc still has a finite diameter, some small radial displacement is observed at the cylindrical surface. Mode 2 at a frequency of 353.49 kHz has a similar mode shape in the axial direction to that in mode 1, but the axial motion varies with the radius, and changes sign, giving one nodal circle on the surface of the disc. Mode 3 has one and a half wavelengths through the thickness, and the axial motion varies slightly along the radius

with a nodal circle near the edge. Modes 2 and mode 3 may therefore be regarded as overtones of the mode 1 in the radial and thickness directions respectively, and the motions in the axial and thickness directions are coupled with each other since the disc has comparable thickness and diameter. Other modes which have more complicated mode shape are higher order modes in the radial or thickness direction, and are not discussed any further.

Mode 1 has the largest modal constant of all the modes as shown in Table 4.3, and is the most strongly excited mode by voltage excitation. The predicted electrical impedance response is shown in Fig 4.14, together with the one predicted by a one dimensional long rod model. Although the one dimensional long rod model is usually only considered to be applicable to a piezoelectric disc with D/T ratio less than 0.1, it shows similar electrical impedance characteristics to the three dimensional analysis with the first longitudinal mode at a frequency of 137 kHz for a disc of thickness of 10.07 mm.

Since the static capacitance of the disc was only 13 pF as predicted both by the FE analysis and the 1D model, which was much smaller than the shunt capacitance in the frequency response analyser (< 330 pF, given in Solartron 1255 Manual) and the electrical circuit, the measured electrical impedance of this disc was incorrect, as shown in Fig 4.14. Although the resonant frequencies were not affected, the anti-resonant frequencies were significantly reduced, and the amplitude of the response was reduced from its true value, which also smeared out the weakly excited modes. To verify the FE model, an estimated shunt capacitance of 250 pF was added to the static capacitance of the disc. The calculated electrical impedance was shown in Fig 4.15, which in fact represents the response of the piezoelectric disc in parallel with the shunt capacitance. It can be seen that there is good agreement between the measurement and the prediction using the modified model.

The measured resonant frequencies and modal constants are listed in Table 4.3 together with the predicted values. It can be seen that mode 4 has a large difference in values of the predicted and measured modal constants. The reason for this is not clear. Apart from this, good agreement is obtained in both the frequencies of resonant modes and their modal constants, particularly for the first mode.

4.5 Measurement of mode shapes by laser interferometry

It has been demonstrated in the previous sections that the finite element analysis of piezoelectric discs gives excellent agreement with the measured electrical impedance

response and the frequencies of resonant modes. However, the predicted mode shapes of the resonances have so far not been verified experimentally, which is necessary to fully validate the finite element model. Extensive experimental results are available for the mode shapes of piezoelectric disc in the D/T range of 1 to 12 (Shaw, 1954; Ueha *et al.*, 1983). Shaw (1954) measured the surface displacement of a piezoelectric disc of $BaTiO_3$ disc in the D/T range 1.14 to 6.63 by an optical fringe system. In his report the edge mode was confirmed experimentally with a large displacement at the edge of the surface and some modes in the frequency range of the first through thickness mode were observed with large axial displacement similar to those in the thickness extensional modes predicted by the finite element model. Ueha *et al.* (1983) has measured the vibration velocity distributions over the surface of piezoelectric disc of $Pb(Zr.Ti)O_3$ in the D/T range from 2 to 12 by an optical heterodyne technique where the radial modes and the high frequency radial modes were extensively measured.

Although the experimental mode shapes of the piezoelectric disc have been available, it is very difficult to correlate them in detail to the predicted mode shapes by the finite element model because different material were used. Moreover, no experiment has been reported for a piezoelectric disc with a D/T ratio as large as 20. It was decide to measure the mode shapes of some important modes, such as the mode shapes of some radial modes, the edge mode, and the thickness extensional modes.

In this section the predicted mode shapes of the resonant modes are checked by laser interferometry. The measurements were initially done using a laser interferometer loaned to Imperial College for a short time by Ometron Ltd. This laser interferometer was unable to work at frequencies higher than 200 kHz, so a phase lock laser interferometer developed at AERE, Harwell was then hired for one day to measure the mode shapes of some high frequency modes.

4.5.1 Measurement configuration

The configuration of the measurement is shown in Fig 4.16, where the piezoelectric disc (target) is excited by a frequency generator set to the frequency of interest; the laser interferometer system emits an optical beam and receives the reflections from the vibrating target. Detailed descriptions of the operation of the interferometers can be found from Moss (1980).

The vibration laser interferometer, Spate, which is a commercial instrument from Ometron Ltd., was designed to measure low frequency vibration in large dynamic structures. Since

the system was unable to work at frequencies higher than 200 kHz, experiments with this system were restricted to the largest disc available, which is 10 mm thick and has a diameter of 50 mm.

The optical "phase locked" interferometer developed at AERE, Harwell, was able to work at higher frequencies. However, problems were encountered in using the system during the course of the experiments. First of all, this laser interferometer was unable to measure the phase of the surface movement, therefore the in-phase and out-phase motion were shown in the same direction in the plot (rectified). Secondly the system was very sensitive to extraneous noise which seriously interfered with the small vibration signal from the displacement of the target, the surface of the disc. This noise generated random spikes in the measured displacement pattern. Furthermore, the frequency generator used to excite the disc was not sufficiently stable, so the frequency tended to drift during the experiments.

4.5.2 Mode shapes of a piezoelectric disc with D/T of 5

Due to the frequency limitation of the vibration laser interferometer, Spate, the largest piezoelectric disc available with a diameter of 50 mm and thickness of 10 mm was chosen, giving a D/T ratio of 5. The disc was made of PZT5H, a modified lead zirconate titanate ceramic with the material constants listed in Table A.1.

Fig 4.17 shows the predicted and measured electrical impedance response over the frequency range from 0 to 300 kHz. The predicted and measured resonant frequencies are listed in Table 4.4 with the thickness extensional modes lying around frequency range from 190 to 220 kHz. It can be seen that there is good agreement between predictions and measurements apart from some variation in the frequency range of the edge mode.

Since the instrument was unable to work in the frequency range beyond 200 kHz, measurements were only made on the low frequency radial modes. The first seven measured mode shapes (axial surface displacement) are shown in Fig 4.18 in 3D plots. The scanning mesh of the laser beam chosen depended on the particular mode of interest (finer meshes were used with more complex mode shapes). For the discs, a square mesh was used, which means that the number of measurement points in each row is the same as the number of rows. The surface displacements of the disc are shown in Fig 4.18, in which the measured displacement at each point is plotted, and points on each row are jointed by straight lines.

Fig 4.19 shows the measured surface displacement along a diameter (i.e., along the middle row) and the corresponding prediction by the finite element analysis. Arbitrary amplitude scales are used in these plots, and mode shapes are shown in the order of their frequencies. It can be seen that there is excellent agreement between the predicted and measured mode shapes for the first and second modes which have simple mode shapes. Mode 1, predicted at 37.7 kHz and measured at 38.5 kHz, shows that the displacement reaches a maximum at the centre of the surface, and then gradually reduces to zero at the edge of the disc. There is an apparent small shift to the right in the measured plot since the measurement at the beginning was slightly off centre, which is also seen in Fig 4.18. Mode 2 measured at 91.0 kHz has two nodal circles (including one at the edge), which is perfectly matched to the predicted mode at 90.4 kHz.

However, there is a large discrepancy between measurement and prediction for modes 3 and 4. The measured mode shape for mode 3 at 120.5 kHz is the edge mode with two nodal circles and large displacement at the edge (the spikes in the response are due to noise), and mode 4 at 155.5 kHz is a radial mode with 4 nodal circles (including the edge). However, the predicted mode 3 at 121.6 kHz is a radial mode with 2 nodal circles and mode 4 at 132.8 kHz is the edge mode with 3 nodal circles. It seems that the predicted modes 3 and 4 are in reverse order compared with the experiments. This may again be due to the inaccurate material constants used in prediction.

The measured modes at 162.5 kHz and 180.0 kHz show the radial mode shapes corresponding to the predicted mode 5 at 150.0 kHz and mode 6 at 173.2 kHz respectively, and good agreement between the measurements and predictions has been obtained. The predicted mode 7 is a thickness shear mode, which has a very small modal constant, and was not excited experimentally.

The most interesting result in the measurement may be the last mode measured at 197.5 kHz. The measured surface displacement of this mode has a non-zero mean value of the axial displacement over the surface of the disc. This agrees with the predicted mode 8 at 195.1 kHz and indicates that the predicted characteristics of the thickness extensional modes are correct.

Since the equipment had a maximum operating frequency of 200 kHz, it was not possible to verify another thickness extensional mode which was predicted at 211.3 kHz and measured at 202.5 kHz by the electrical impedance response. Nevertheless, the mode shapes which have been measured show good agreement in form with those predicted by the finite element analysis.

4.5.3 Mode shapes of piezoelectric discs with large D/T ratios

In last section it has been shown that there is a good agreement between measured and predicted mode shapes. The disc used had a diameter to thickness ratio of 5.0, and in one thickness extensional mode of the disc, the surface displacements showed a non-zero mean value along the radius in both measurement and prediction. However, since the "dc component" of displacement in this disc is smaller than that predicted for the thickness extensional modes in a disc with a D/T ratio of 20, it was decided to measure the mode shapes in a disc with a large D/T ratio using the Harwell phase lock interferometer.

In this case the laser beam was only scanning along a diameter, and the displacement over the diameter was recorded. Fig 4.20(a) shows the measured surface displacement of the PZT5A disc with a D/T of 20 at a frequency of 50 kHz, and the predicted surface displacement of the first radial mode at 49.47 kHz. The predicted surface displacement is plotted in a rectified form in order to compare with the measured one which is in the absolute value. It can be seen that the measurement shows the same pattern as the prediction for this simple mode shape; however, the spikes in the surface displacement may cause interpretation difficulties if more complicated modes are considered.

Apart from the first radial mode, the mode shapes of other modes of the PZT5A disc were found to be difficult to measure since PZT5A has a relatively large structure damping factor of 0.013, and the displacements which could be excited were too small to be distinguished from the noise spikes. Two PZT4 discs which have structural damping factors of only 0.002 (mechanical Q factor of 500) were therefore used in these tests, one had a D/T ratio of 8.0 (disc P4_08) and the other a D/T ratio of 20 (disc P4_20). The material constants of PZT4 can be found from Table A.1.

Measured surface displacements of the disc by this laser interferometer in the edge mode, the fourth radial mode and a thickness extensional mode are shown in Fig 4.20(b) to 4.20(d). The plots on the left hand side of Fig 4.20 are the measured mode shapes while the predicted mode shapes are shown on the right hand side.

Fig 4.20(b) shows the measured and predicted edge modes of a PZT4 disc with a D/T ratio of 8 (disc P4_08), measured at 224.3 kHz and predicted at 227.94 kHz, and it can be seen that 9 displacement maxima appear in the measured plot and there is a large displacement at the edge. Therefore, 4 nodal circles can be recognised if the rectification

effect is taken into consideration. This agrees well with the predicted plot which is also shown in the rectified form in Fig 4.20(b).

The measured and predicted mode shapes of the fourth radial mode of P4_20, a PZT4 disc with a large D/T ratio of 20, are shown in Fig 4.20(c). It is believed that this shows good agreement between the measurement and prediction. Since the fourth order radial mode predicted at 316.90 kHz has four nodal circles (including one at the edge), the movement over the surface should have 7 peaks if the absolute displacements are plotted along a diameter. This is confirmed by the measured displacements at a frequency of 315 kHz plotted in the left hand side of Fig 4.20(c), though the disc was not exactly centred during the measurements and several noise spikes are seen.

Fig 4.20(d) shows the measured surface displacement of this large D/T disc at 1.033 MHz, together with the predicted surface motion at 983.49 kHz which is in the thickness modes range of this disc. It can be seen that both measurement and prediction show large deformation at centre and agree with each other qualitatively. However, the spikes present in the experiment curve make it difficult to clarify clearly.

Although the mode shape measurement by using the high frequency laser interferometry were not completely satisfactory due to the difficulties encountered in using the equipment, the mode shapes obtained were still representative and agreed qualitatively with the predicted ones. The tests verified the theoretical prediction that in the thickness extensional modes of the piezoelectric discs with large D/T ratios the surface movement is far from uniform as expected from the one dimensional model, but it does have a large mean value of the axial displacement.

4.6 Conclusions

The vibration characteristics of piezoelectric discs with different diameter to thickness ratios have been studied by the finite element analysis and experimental measurement.

It has been shown that the resonant frequencies and their corresponding mode shapes of piezoelectric discs are very complicated. There are a large number of resonant modes in the frequency range of interest, which have been classified into five groups according to their mode shapes: the radial modes (R), the edge mode (E), the thickness shear modes (TS), the thickness extensional modes (TE) and the high frequency radial modes (A). No mode has been found having piston-like motion assumed by the one dimensional theory.

However, the thickness extensional modes do have non zero mean value of the axial displacement over the surface of the piezoelectric disc. The number of thickness extensional modes varies with the D/T ratio of the piezoelectric disc. However, when the D/T ratio of the piezoelectric disc is around 20 there is a thickness extensional mode in which the mean value is so large that it may be analogous to the first through thickness mode by the one dimensional model.

The modal constant has been successfully used to evaluate how strongly the mode can be excited by an external electrical force. For a piezoelectric disc excited by applying a voltage across electrodes over the top and bottom surfaces of the disc, many modes can be excited. It has been shown that the modes which have large modal constants can be strongly excited, and the modes having small modal constants can be weakly excited, while the modes with null modal constant cannot be excited at all. The thickness extensional modes, which have large modal constants, can be very strongly excited. The edge mode and low frequency radial modes which have relatively small modal constants can be fairly strongly excited. The thickness shear modes and the modes above the thickness modes range have very small modal constants, and they can only be weakly excited. The flexural modes (anti-symmetrical) have zero modal constants, hence they can hardly be excited.

Since the modal constant depends upon the electrical force pattern and the mode shape of the mode, it is suggested that the modal constant can be a very useful parameter in the design and analysis of piezoelectric transducers. By changing the modal constant, which can be achieved by, for example, varying the pattern of the electrodes on the disc, the modes can be selected according to the application requirement. Since the conventional methods are often broken down for the case of piezoelectric discs, in which the modal density in the thickness extensional modes range is so high that it is not possible to pair the resonant frequencies and their corresponding anti-resonant frequencies, it is therefore believed that the modal constant offers considerable advantage over the conventional methods in both the experiment and prediction to determine the excitation strength of each resonance.

Extensive experiments have been made to verify the predicted vibration characteristics of the piezoelectric disc in respect of resonant frequencies, mode shapes, modal constants of the modes and the electrical impedance response of the disc. Generally speaking, there is very good agreement between the measured results and the finite element predictions, particularly in the electrical impedance characteristics.

Some discrepancy has been found in the values of resonant frequencies, and sometimes in the order of the modes. This is probably mainly because the material constants used in prediction are not accurate enough, and the material properties can vary even from disc to disc of the same nominal material type.

	Prediction			Measurement	
Mode No.	Frequency (kHz)	Modal constant (F/s^2)	Mode type	Frequency (kHz)	Modal constant (F/s^2)
1	49.56	260.3	R	50.20	212.6
2	128.1	215.5	R	129.9	177.0
3	201.6	214.1	R	204.8	182.2
4	272.1	215.9	R	276.7	183.2
5	338.5	217.8	R	344.6	189.0
6	399.9	218.1	R	407.4	192.6
7	455.2	215.9	R	463.7	191.6
8	503.8	212.1	R	512.8	193.8
9	545.9	211.3	R	555.5	197.4
10	582.3	225.2	R	592.8	237.3
11	614.0	288.7	R	623.2	588.6
12	640.6	539.6	R	639.2	319.0
13	657.7	465.4	E		
14	677.6	18.86	R		
15	703.1	4.825	R		
16	729.5	22.07	R		
17	756.3	40.27	R		
18	783.5	63.86	R		
19	811.3	102.5	R		
20	839.4	179.0	R		
21	867.7	360.4	R		
22	873.2	8.618	TS		
23	876.4	6.261	TS		
24	880.0	55.66	TS		
25	887.0	39.52	TS		
26	893.2	410.9	TS		
27	896.6	798.5	R	893.5	616.6
28	914.1	1188	TS		
29	924.8	1480	R		
30	943.5	4189	TE	936.5	7065
31	955.9	2368	TE		
32	**964.9**	**26010**	**TE**	**951.1**	**17350**
33	975.5	26.25	R		
34	991.8	2455	TE	972.1	1218
35	995.2	324.0	TS		
36	1010	49.44	R		
37	1026	635.1	A	1003	589.1
38	1040	84.07	R		
39	1051	37.04	R		
40	1064	265.0	A	1041	125.9
41	1081	53.92	R		
42	1102	4.601	R		
43	1108	108.2	TS	1080	41.13
44	1122	67.16	R	1123	46.98
45	1145	3.729	A		
46	1166	84.82	R		
47	1167	.004	TS		
48	1187	2.36	A	1170	

Table 4.1 The predicted and measured resonant frequencies and their modal constants of the first 48 extensional modes of the PZT5A disc with a D/T ratio of 20 (Blank: values are too small to be measured)

	Prediction			Measurement	
Mode No.	Frequency (kHz)	Modal constant (F/s^2)	Mode type	Frequency (kHz)	Modal constant (F/s^2)
1	99.21	262.4	R	98.01	200.8
2	252.4	221.1	R	250.0	189.0
3	384.8	220.9	R	382.3	193.2
4	493.2	214.9	R	490.4	193.0
5	572.2	219.2	R	572.5	205.0
6	634.9	370.9	R	625.1	350.3
7	663.3	252.1	E		
8	703.4	2.108	R		
9	755.9	34.77	R		
10	810.2	88.74	R		
11	864.8	277.1	R	827.1	396.8
12	880.6	3.293	TS		
13	891.9	198.4	TS		
14	915.1	1308	R	849.9	308.8
15	938.8	533.0	TS		
16	**964.7**	**3072**	**TE**	**895.9**	**1663**
17	**988.0**	**3684**	**TE**	**933.7**	**5933**
18	1014	64.39	A	969.3	374.6
19	1042	84.39	TS		
20	1057	376.5	A	1004	563.1
21	1092	25.24	A	1054	538.8
22	1136	31.82	R	1088	112.8
23	1157	49.82	TS	1181	422.0
24	1174	31.62	A		

Table 4.2 The predicted and measured resonant frequencies and their modal constants of the first 24 extensional modes of the PZT5A disc with a D/T ratio of 10 (Blank: values are too small to be measured)

	Prediction			Measurement	
Mode No.	Frequency (kHz)	Modal constant (F/s^2)	Mode type	Frequency (kHz)	Modal constant (F/s^2)
1	**133.4**	**9.393**	**TE1**	**134.0**	**9.229**
2	353.5	.4498	R		
3	389.3	2.099	TE2	405.0	3.210
4	486.7	3.399		478.6	.7603
5	535.2	3.217		547.1	3.306
6	583.9	.3355		590.4	1.418

Table 4.3 The predicted and measured resonant frequencies and their modal constants of the first 6 extensional modes of the PZT5A disc with a D/T ratio of 0.5 (Blank: values are too small to be measured)

	Prediction		Measurement	
Mode No.	Frequencies (kHz)	Mode type	Frequencies (kHz)	Mode type
1	37.7	R	38.5	R
2	90.4	R	91.0	R
3	121.6	R	120.5	E
4	132.8	E	155.5	R
5	150.0	R	162.5	R
6	173.2	R	179.5	R
7	183.1	TS		
8	**195.1**	**TE**	**197.5**	**TE**
9	**211.3**	**TE**	**202.0**	**-**
10	219.2	TS		-
11	227.4	R	233.5	-
12	248.1	A		-

Table 4.4 Resonant frequencies and their corresponding mode shapes of the first 12 extensional modes of the PZT5H disc with a D/T ratio of 5 predicted by the FE model and measured by the laser interferometer.
(Blank: too weak to be measured; - : not measured due to restriction of equipment)

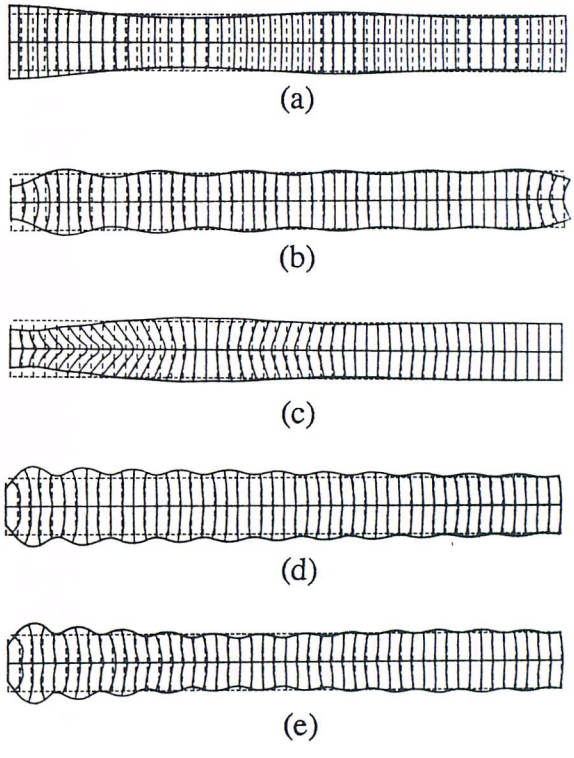

Fig 4.1 The five types of mode shapes of a piezoelectric disc with a D/T ratio of 20 predicted by the finite element analysis
(a) radial mode (mode 4, 272 kHz)
(b) edge mode (mode 13, 658 kHz)
(c) thickness shear mode (mode 22, 873 kHz)
(d) thickness extensional mode (mode 32, 965 kHz)
(e) high frequency radial mode (mode 37, 1026 kHz)

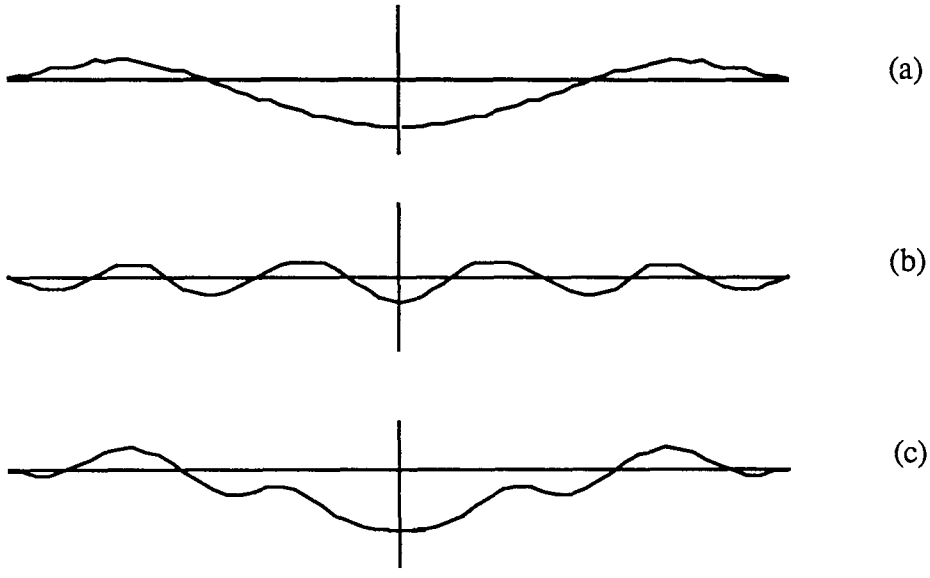

Fig 4.2 Schematic representation of the high frequency radial modes (A-modes) (The mode shape in the A modes, (c), is a superposition of the motion in the low order radial modes (a) and the higher order radial modes (b))

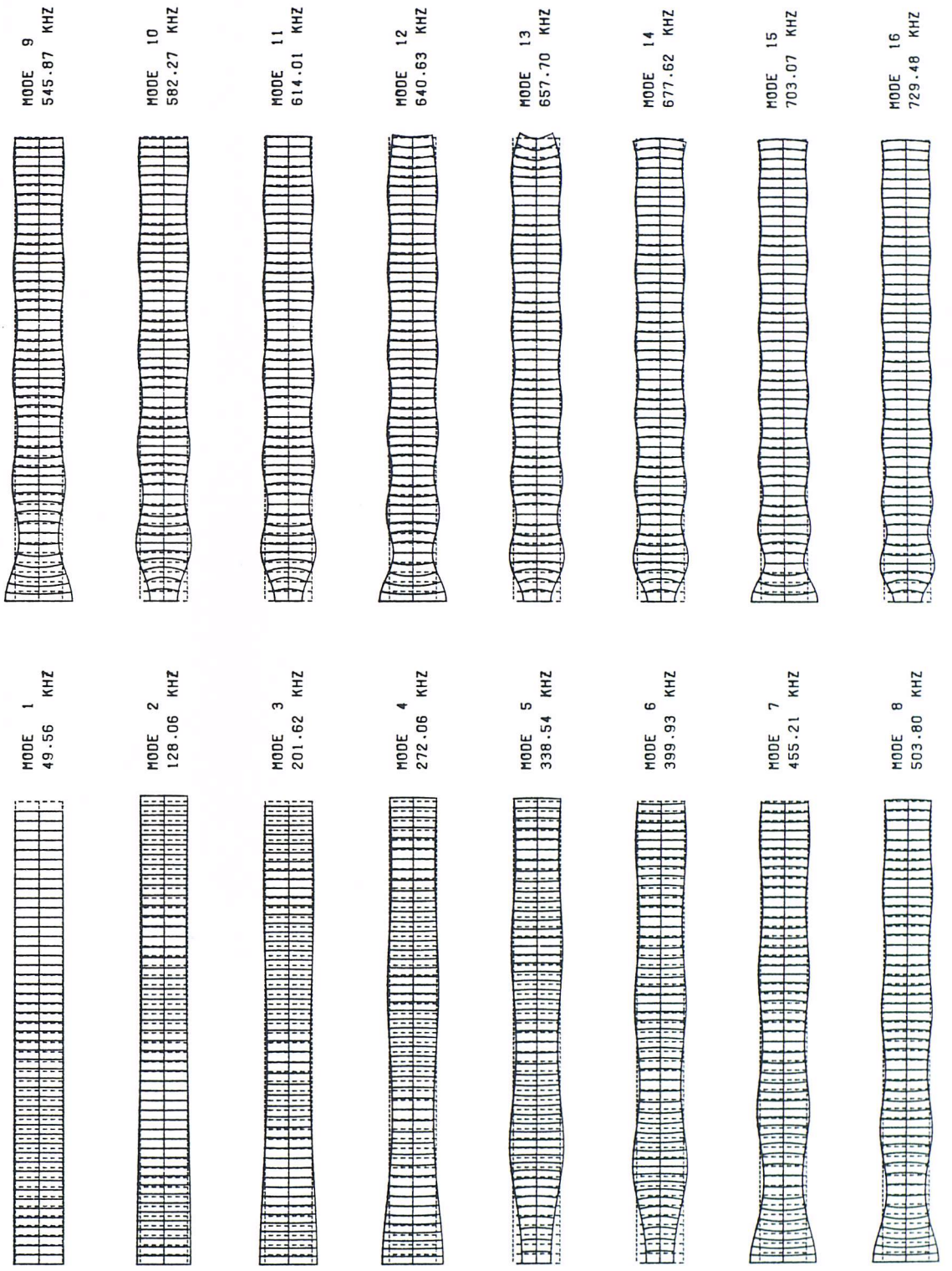

Fig 4.3 The predicted mode shapes of the first 48 extensional modes of the PZT5A disc with a D/T ratio of 20

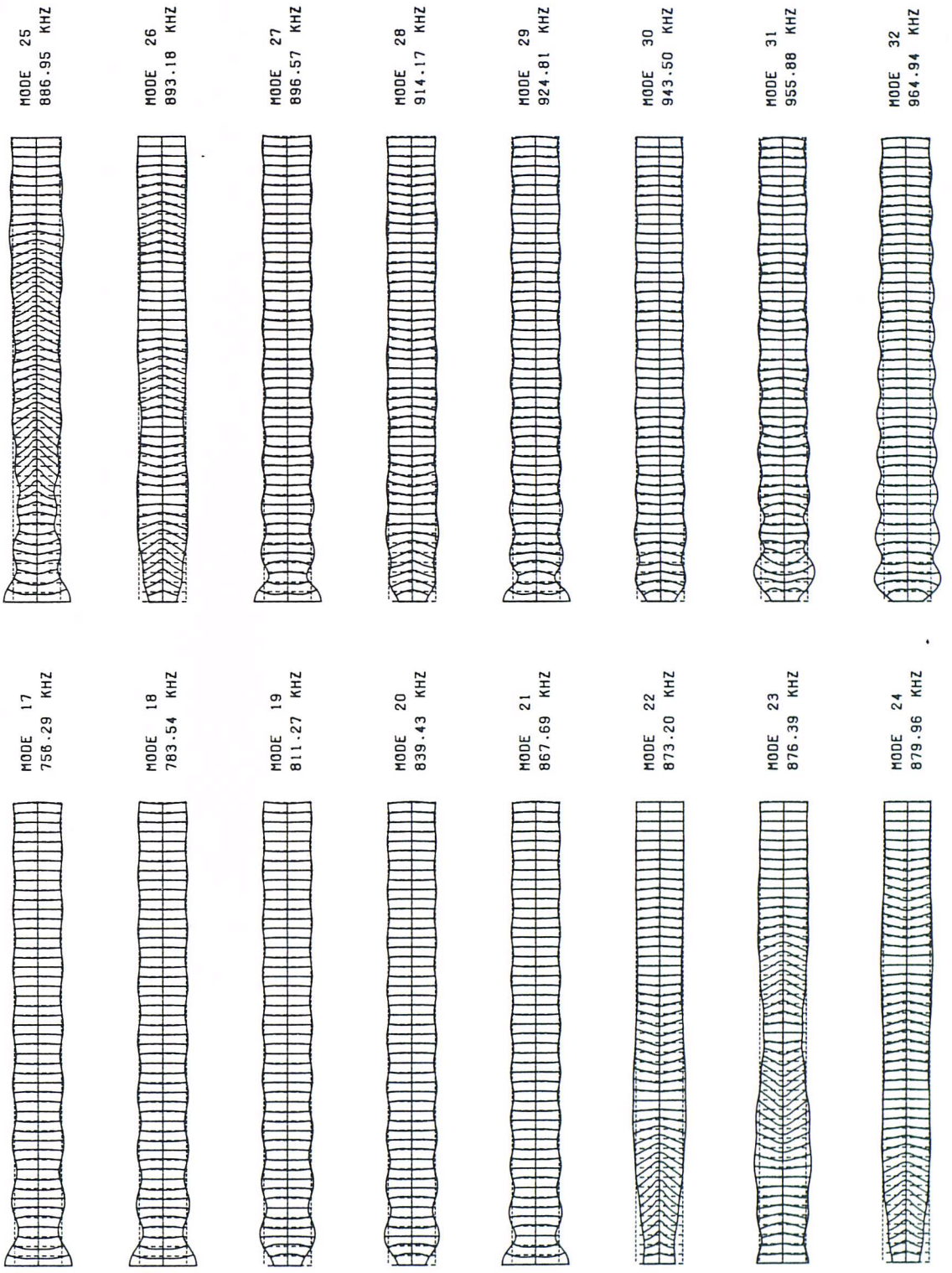

Fig 4.3 Continued (modes 17 to 32)

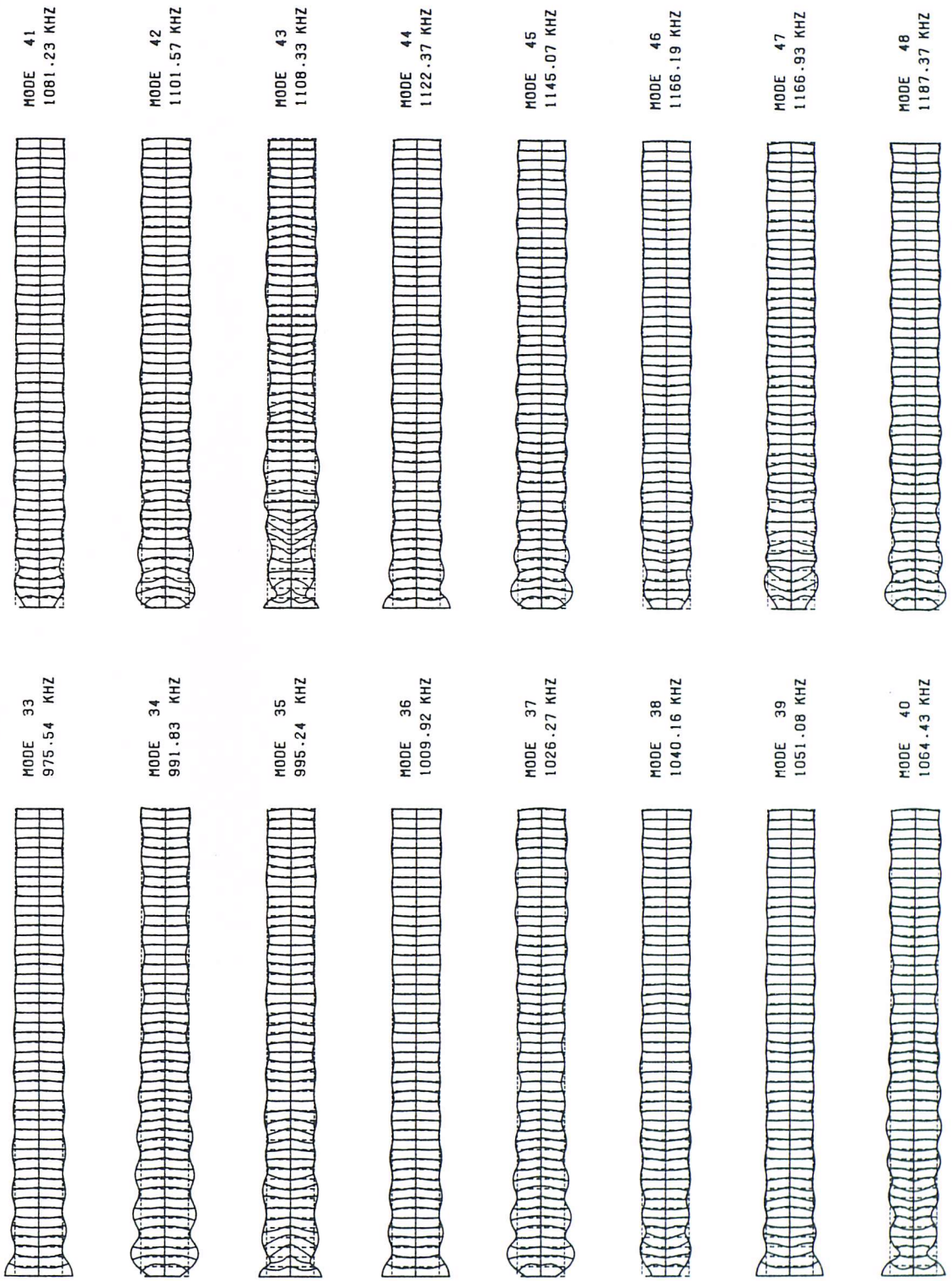

Fig 4.3 Continued (modes 33 to 48)

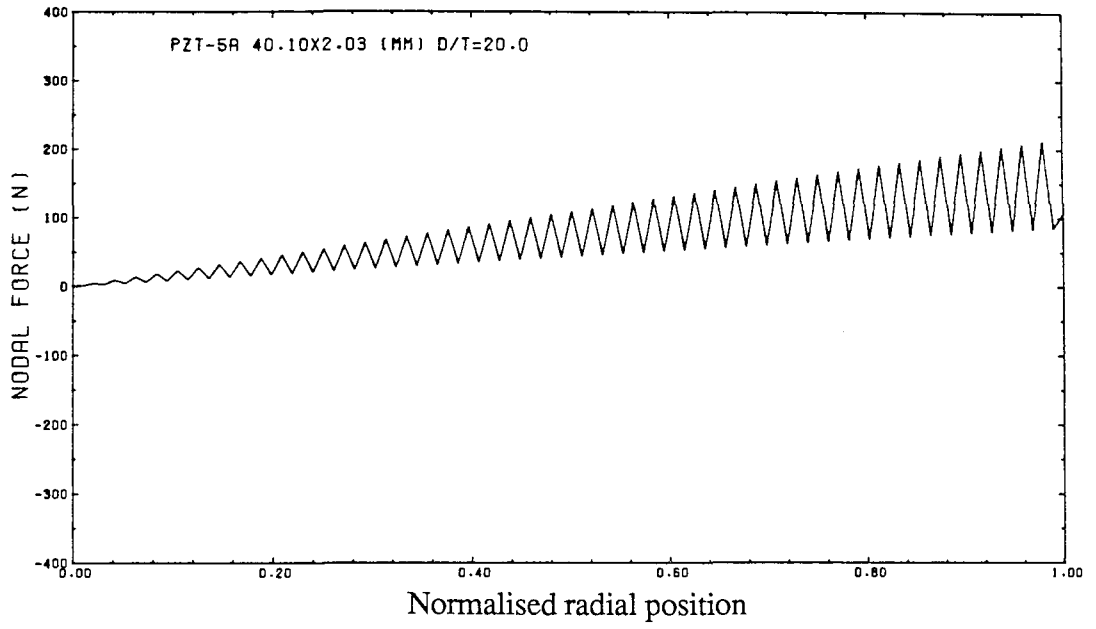

Fig 4.4 The axial equivalent nodal forces over the surface of the PZT5A disc with a D/T ratio of 20 as a function of radius

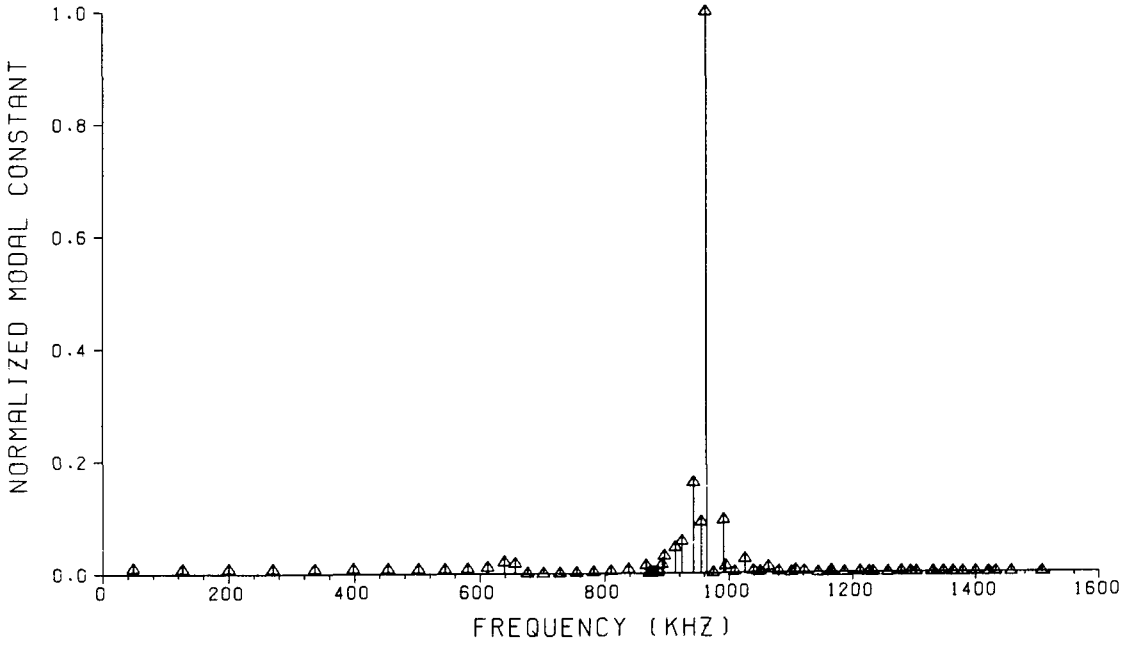

Fig 4.5 The predicted normalised modal constants of the PZT5A disc with a D/T ratio of 20 as a function of frequency

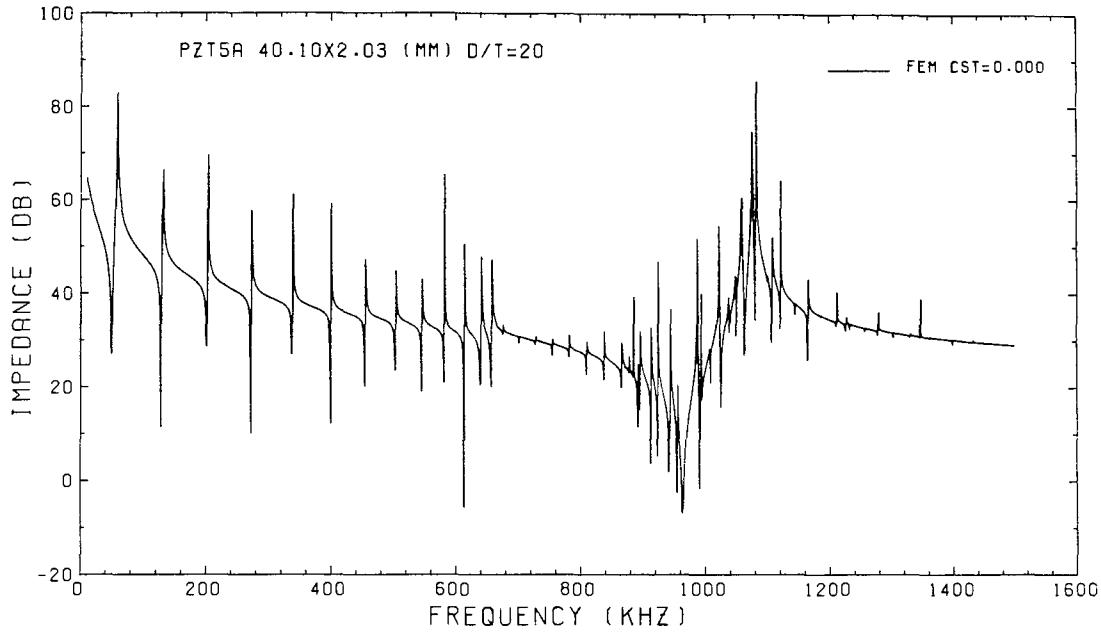

(a) the electrical impedance function

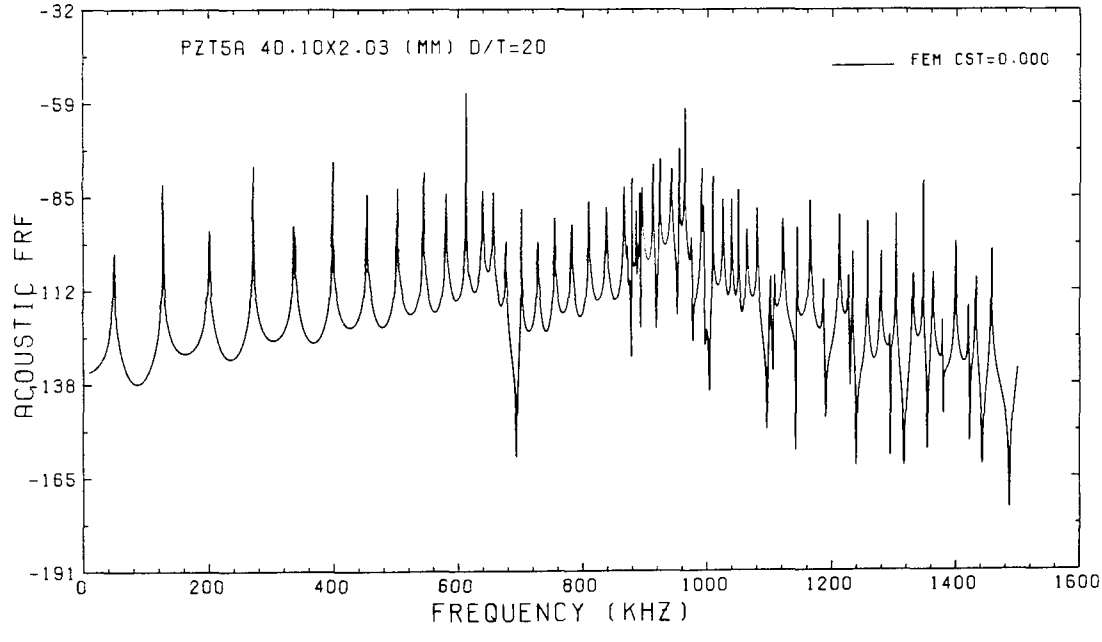

(b) axial mechanical frequency response function at the central point of the surface

Fig 4.6 The responses of the PZT5A disc with a D/T ratio of 20 without considering damping

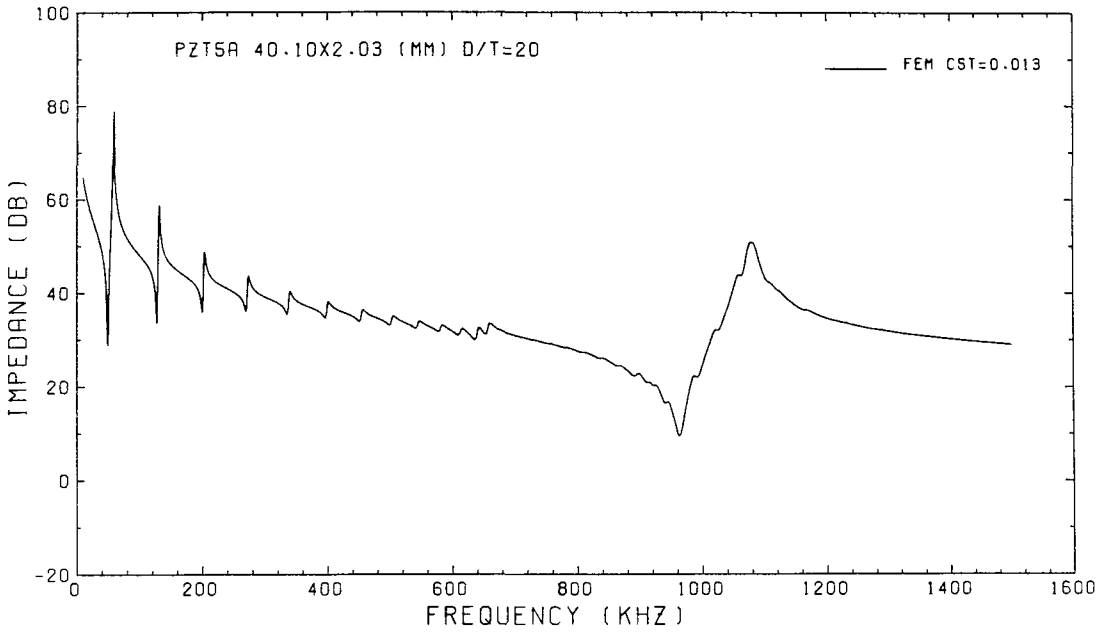

(a) electrical impedance function

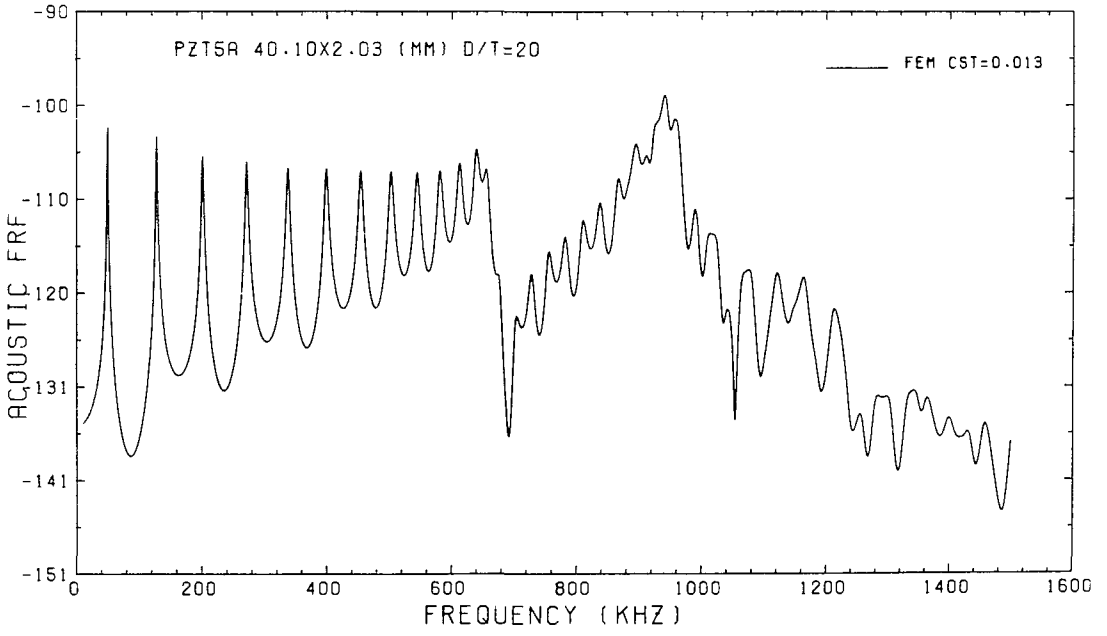

(b) axial mechanical frequency response function at the central point of the surface

Fig 4.7 The predicted responses of the PZT5A disc with a D/T ratio of 20 with a structural damping factor of 0.013

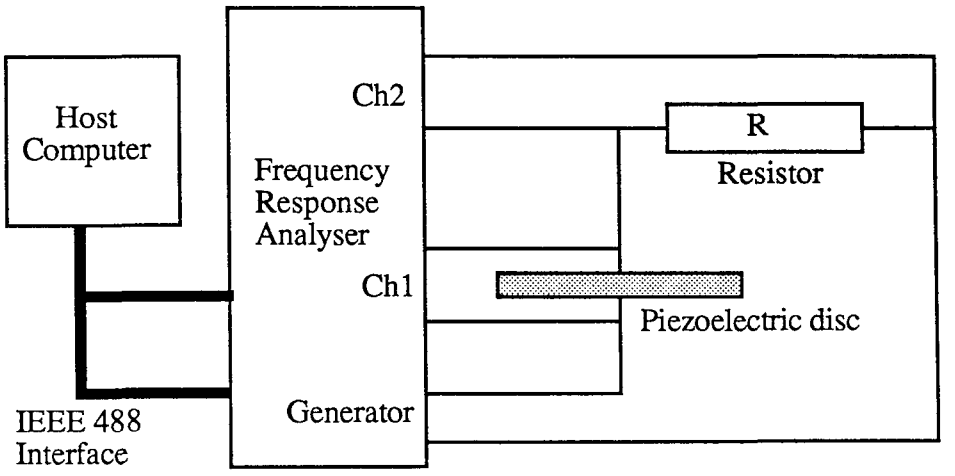

Fig 4.8 Apparatus used for measurement of the electrical impedance response of piezoelectric discs

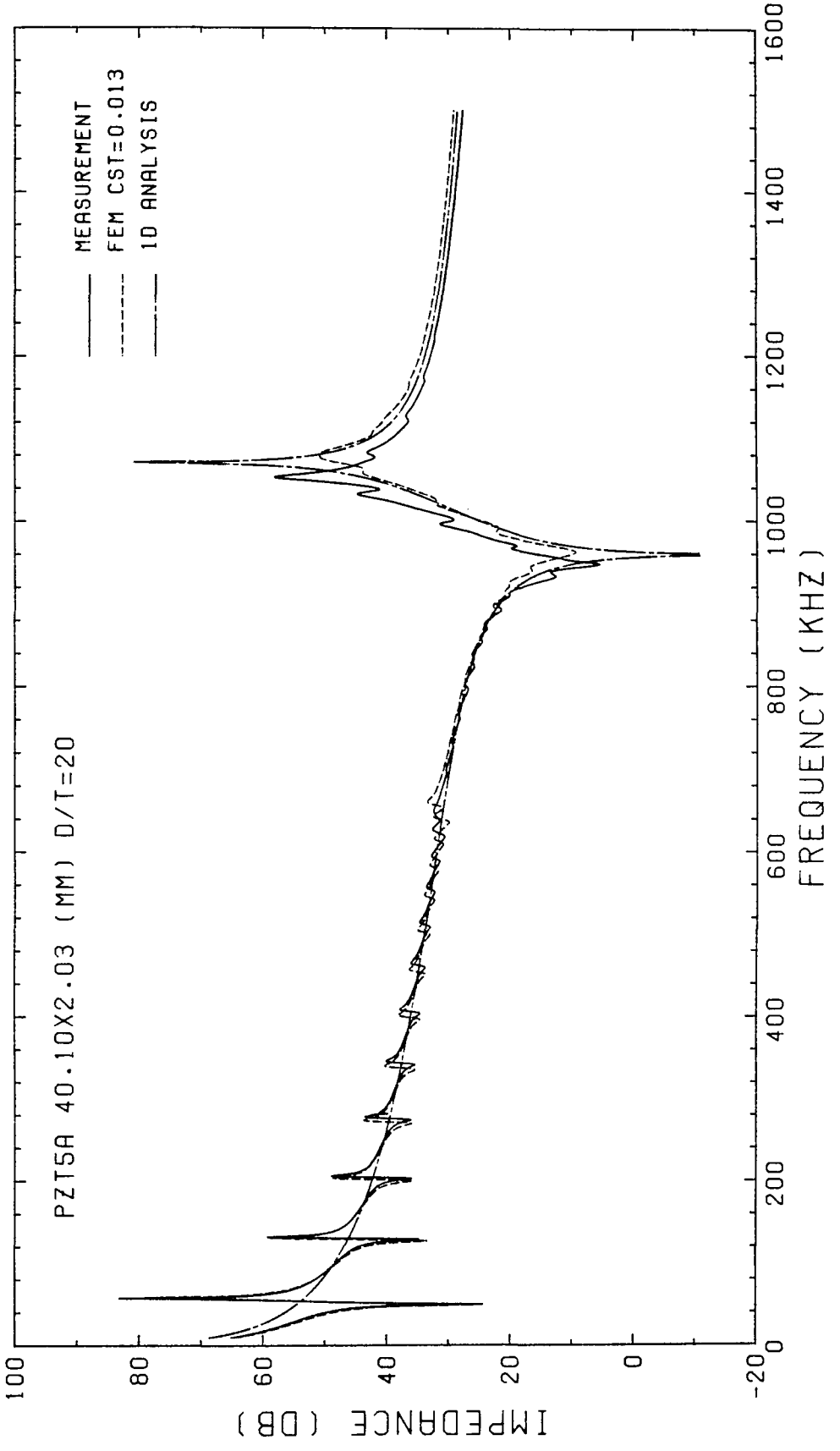

Fig 4.9 The measured and predicted electrical impedance responses of the PZT5A disc with a D/T ratio of 20 by both three dimensional and one dimensional models

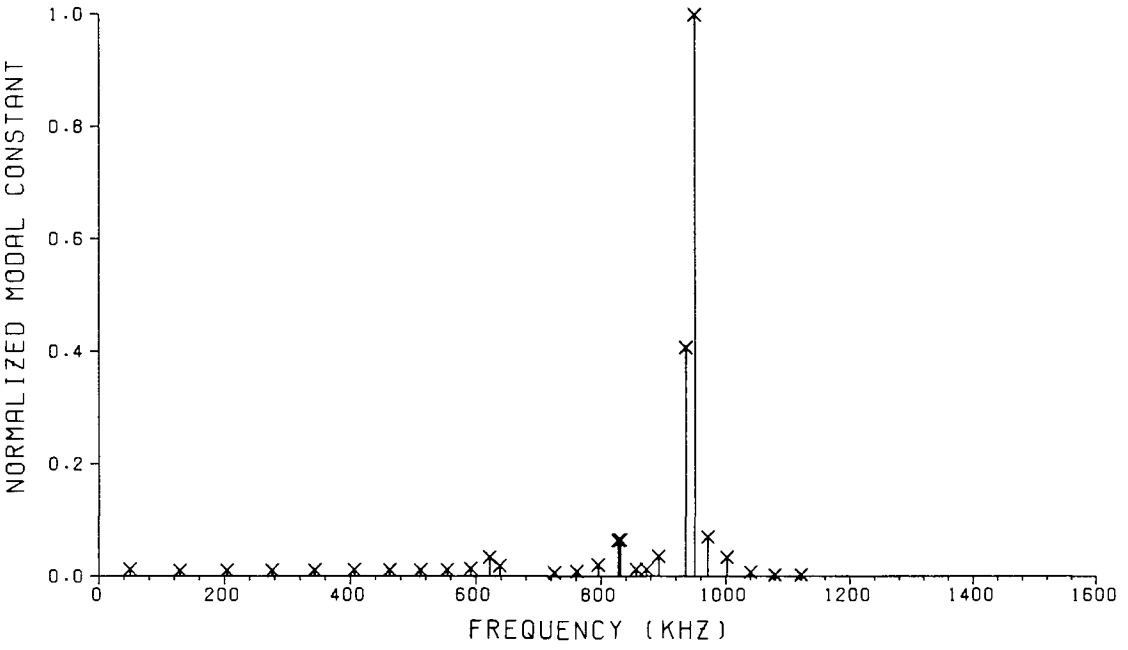

Fig 4.10 The measured normalised modal constants of the PZT5A disc with D/T ratio of 20 as a function of resonant frequencies

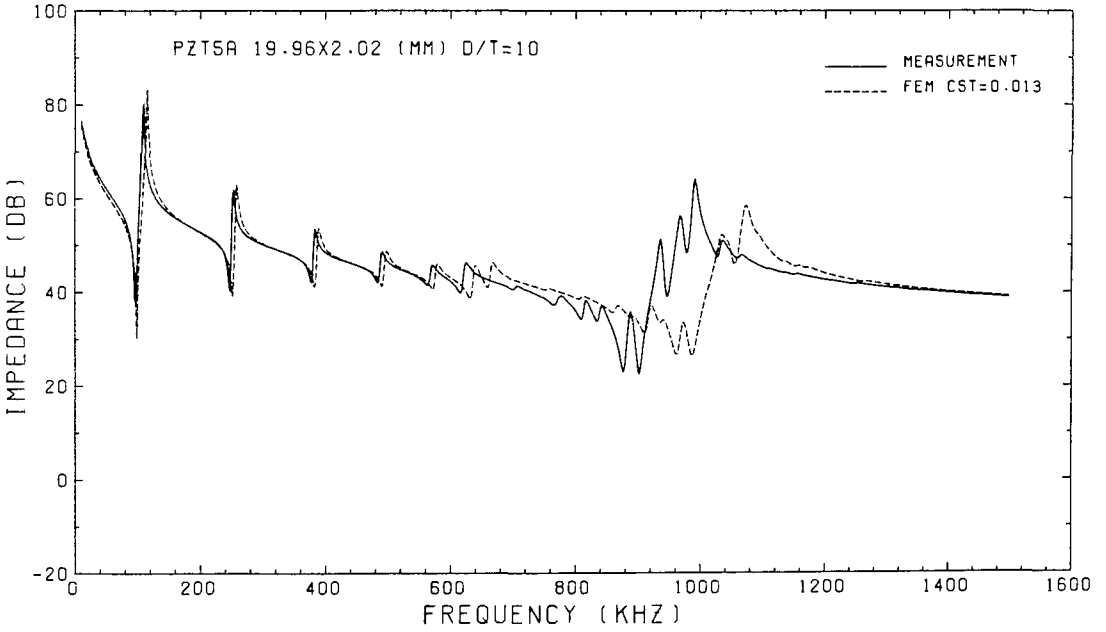

Fig 4.11 The measured and predicted electrical impedance responses of the PZT5A disc with a D/T ratio of 10 (_____ measurement; _ _ _ _ prediction with a structural damping factor of 0.013)

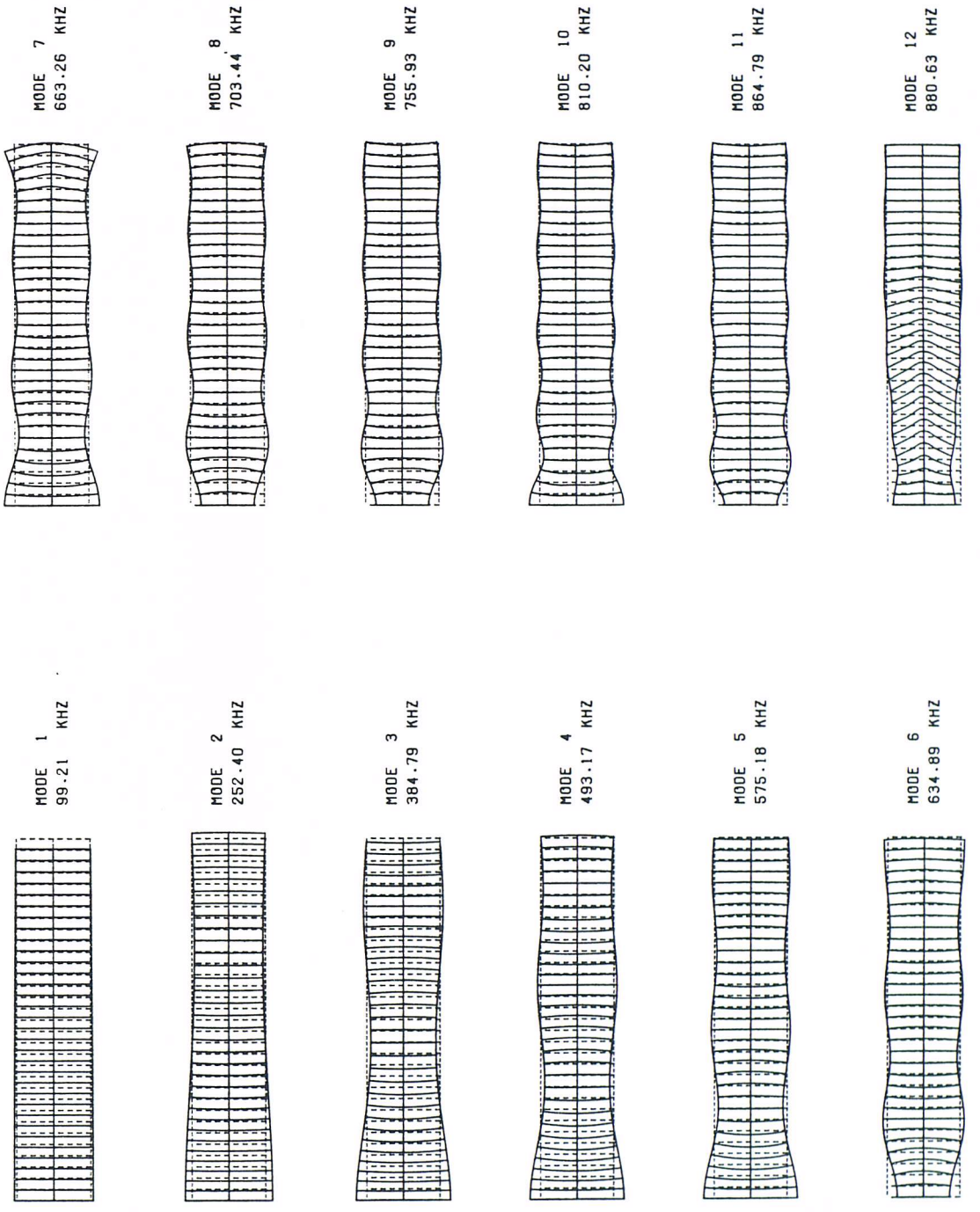

Fig 4.12 The predicted mode shapes of the first 24 modes of the PZT5A disc with a D/T ratio of 10

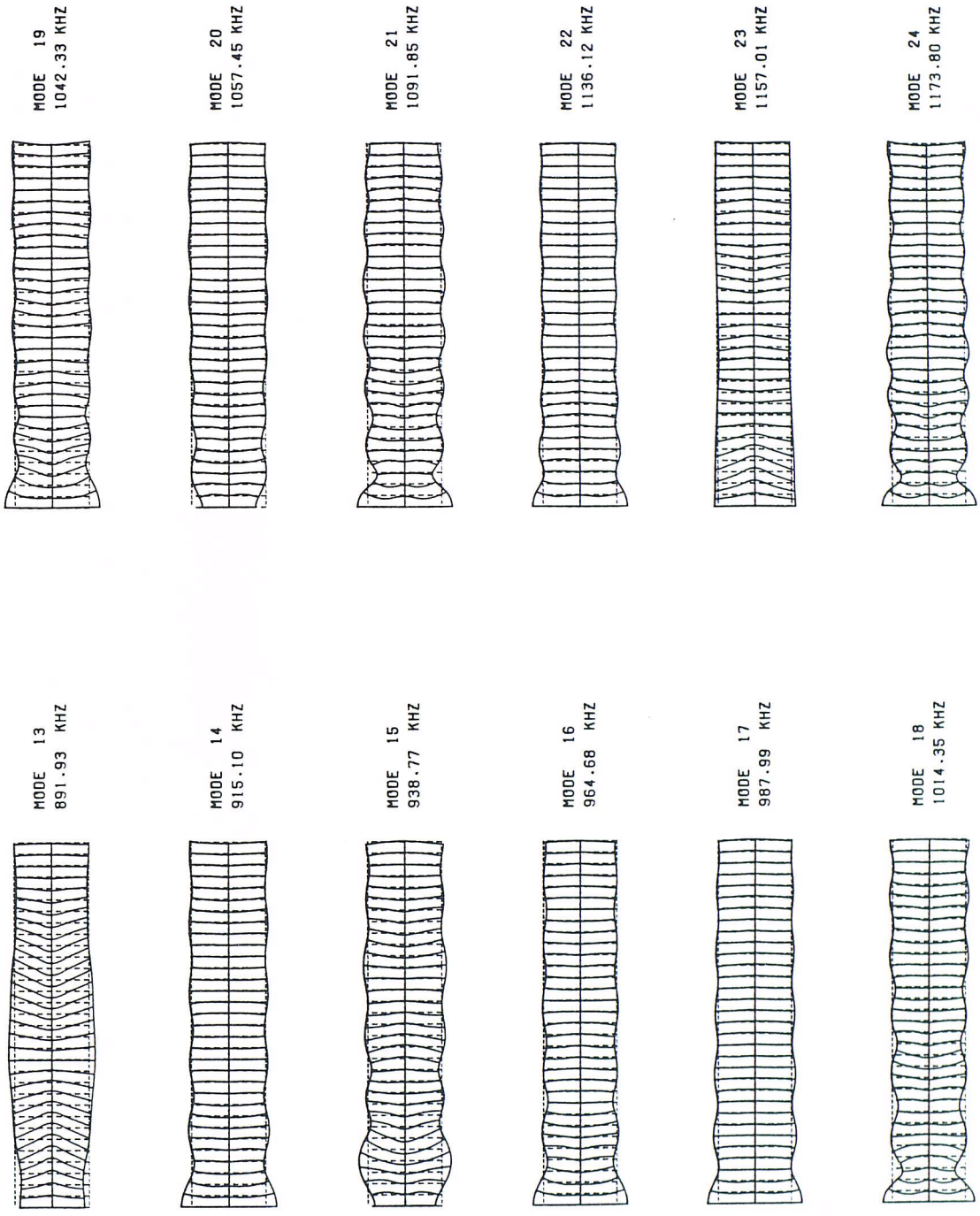

Fig 4.12 Continued (modes 13 to 24)

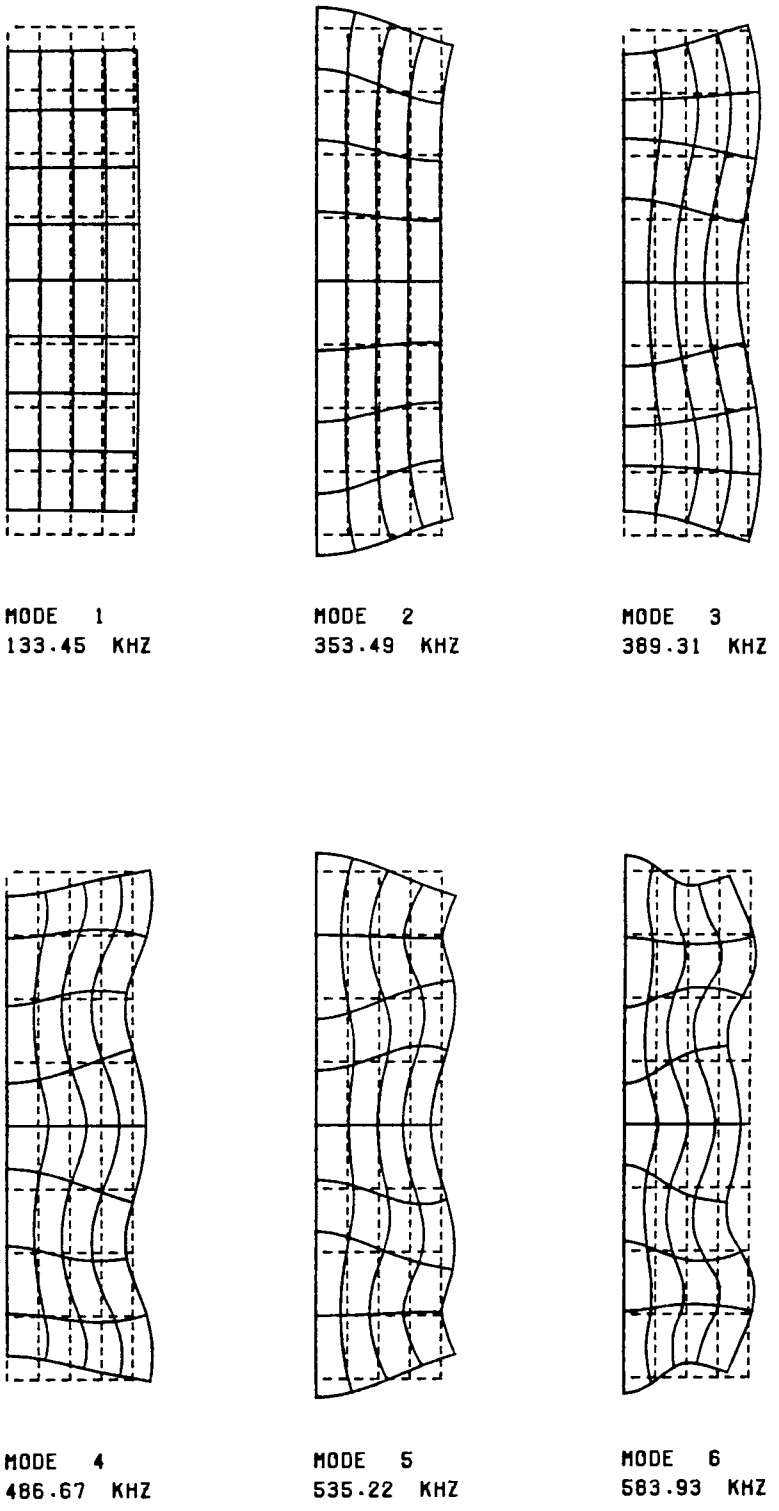

Fig 4.13 The predicted mode shapes of the PZT5A disc with a D/T ratio of 0.5

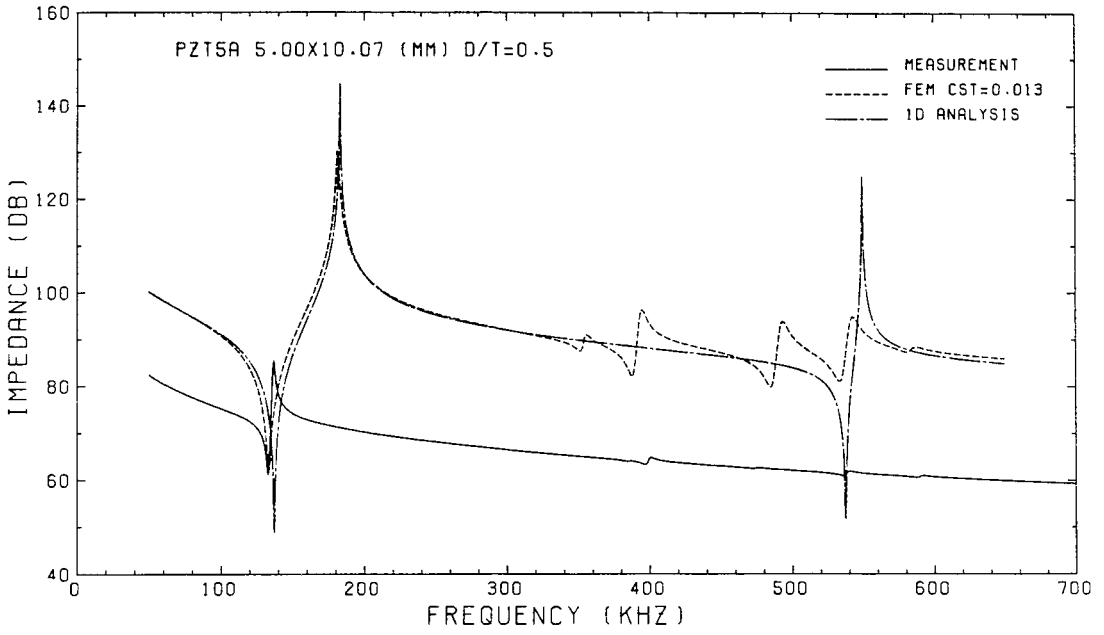

Fig 4.14 The measured and predicted responses of the PZT5A disc with a D/T ratio of 0.5 by the three dimensional and one dimensional bar models

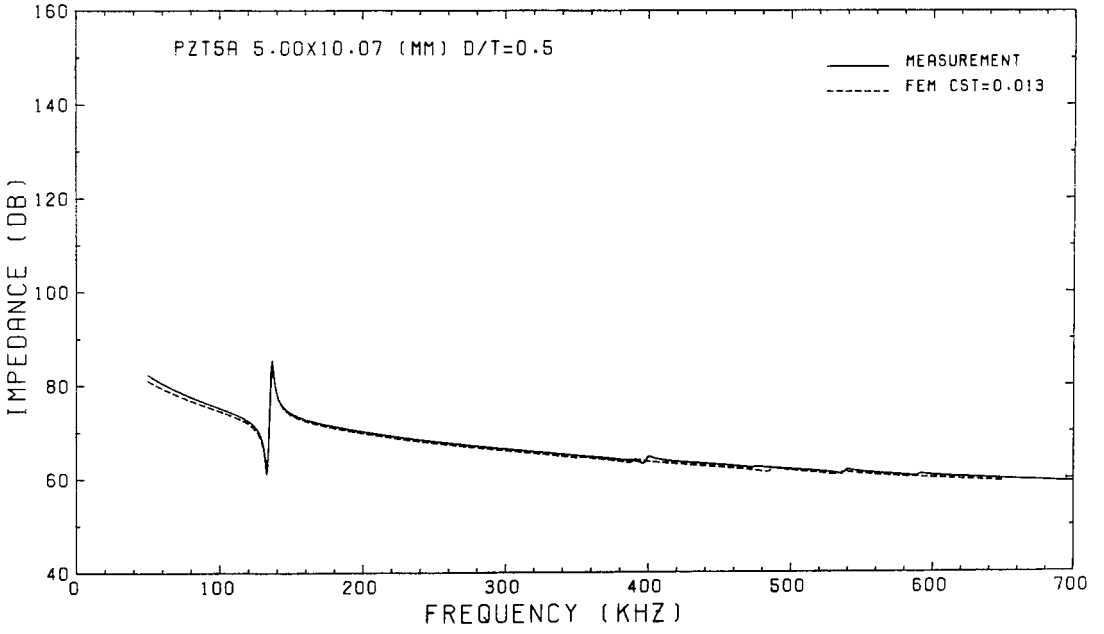

Fig 4.15 The measured and modified predicted impedance responses of the PZT5A disc with a D/T ratio of 0.5

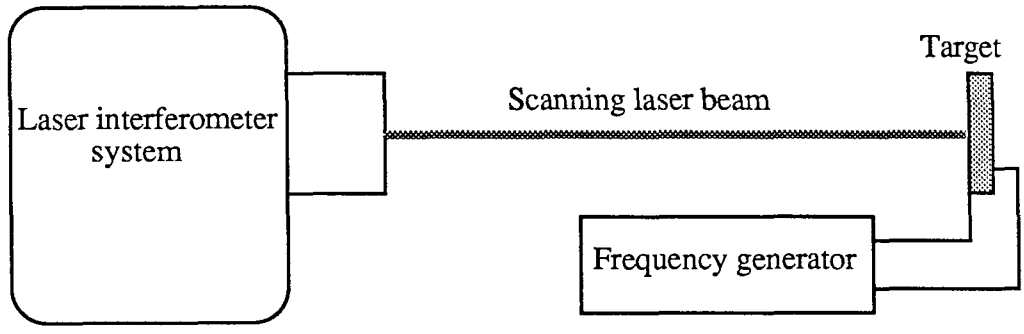

Fig 4.16 Schematic representation of apparatus used to measure the surface displacement of the piezoelectric discs by laser interferometry

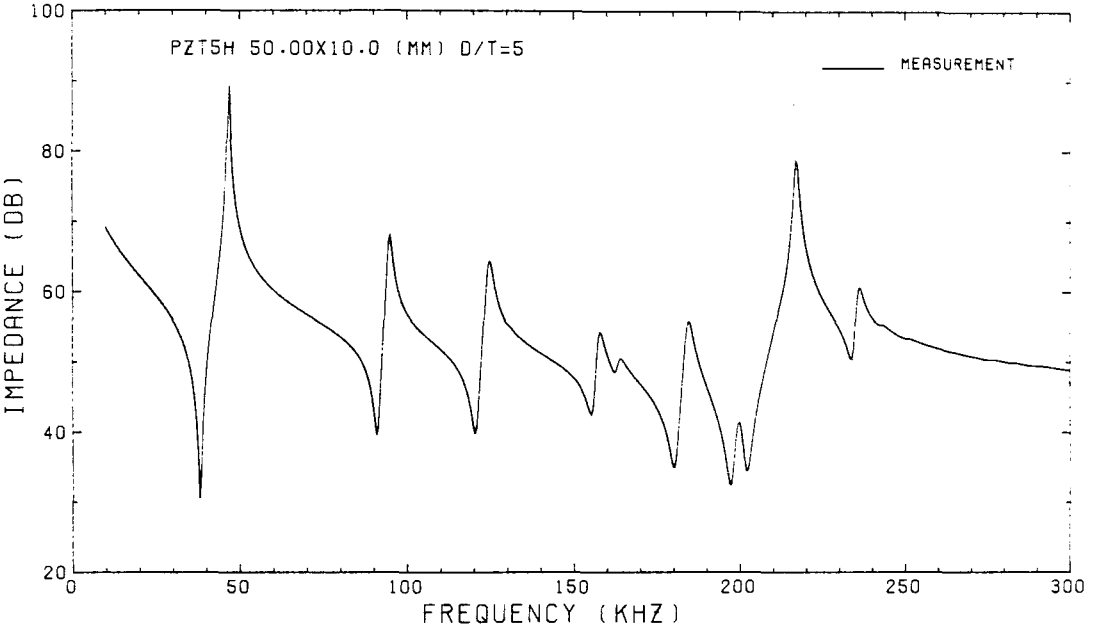

(a) measurement

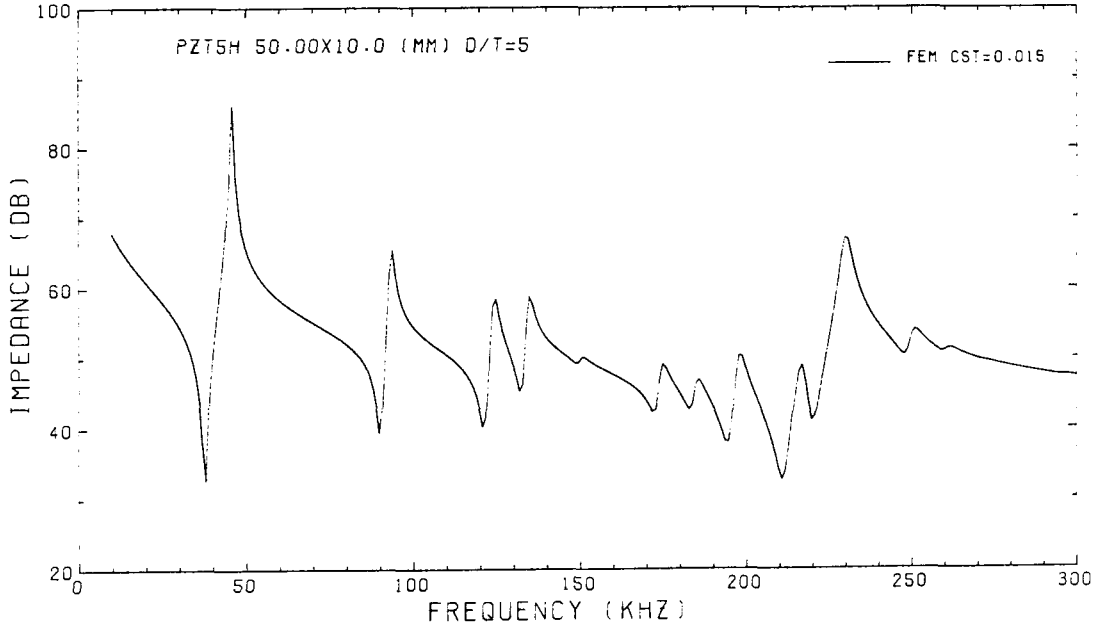

(b) prediction with a structural damping factor of 0.015

Fig 4.17 The measured and predicted electrical impedance responses of the PZT5H disc with a D/T ratio of 5

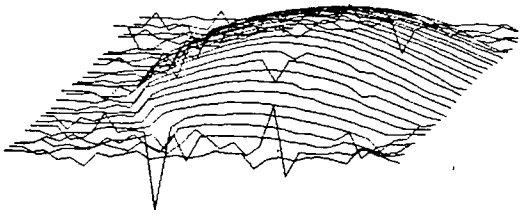

mode 1 38.5 kHz

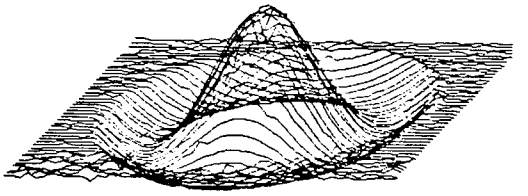

mode 2 91.0 kHz

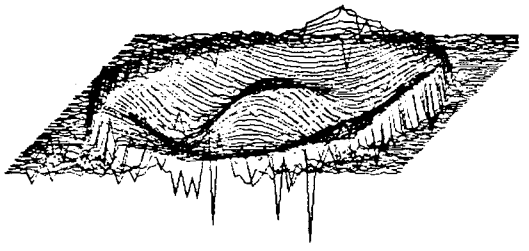

mode 3 120.5 kHz

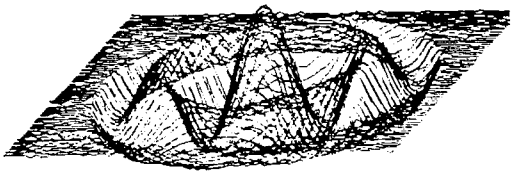

mode 4 155.5 kHz

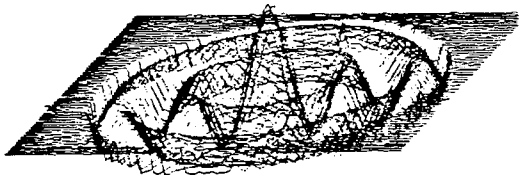

mode 5 162.5 kHz

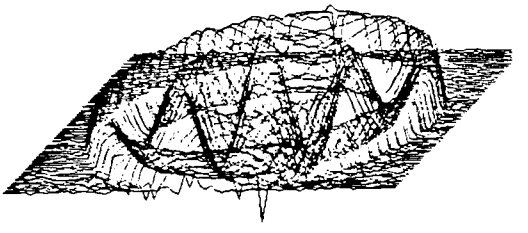

mode 6 180.0 kHz

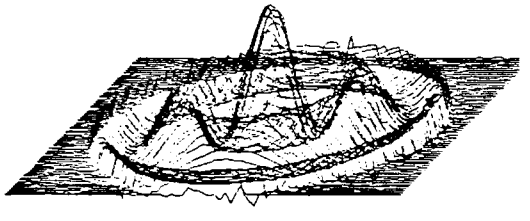

mode 7 197.5 kHz

Fig 4.18 The measure mode shapes of the PZT5H disc with a D/T ratio of 5 in 3D view

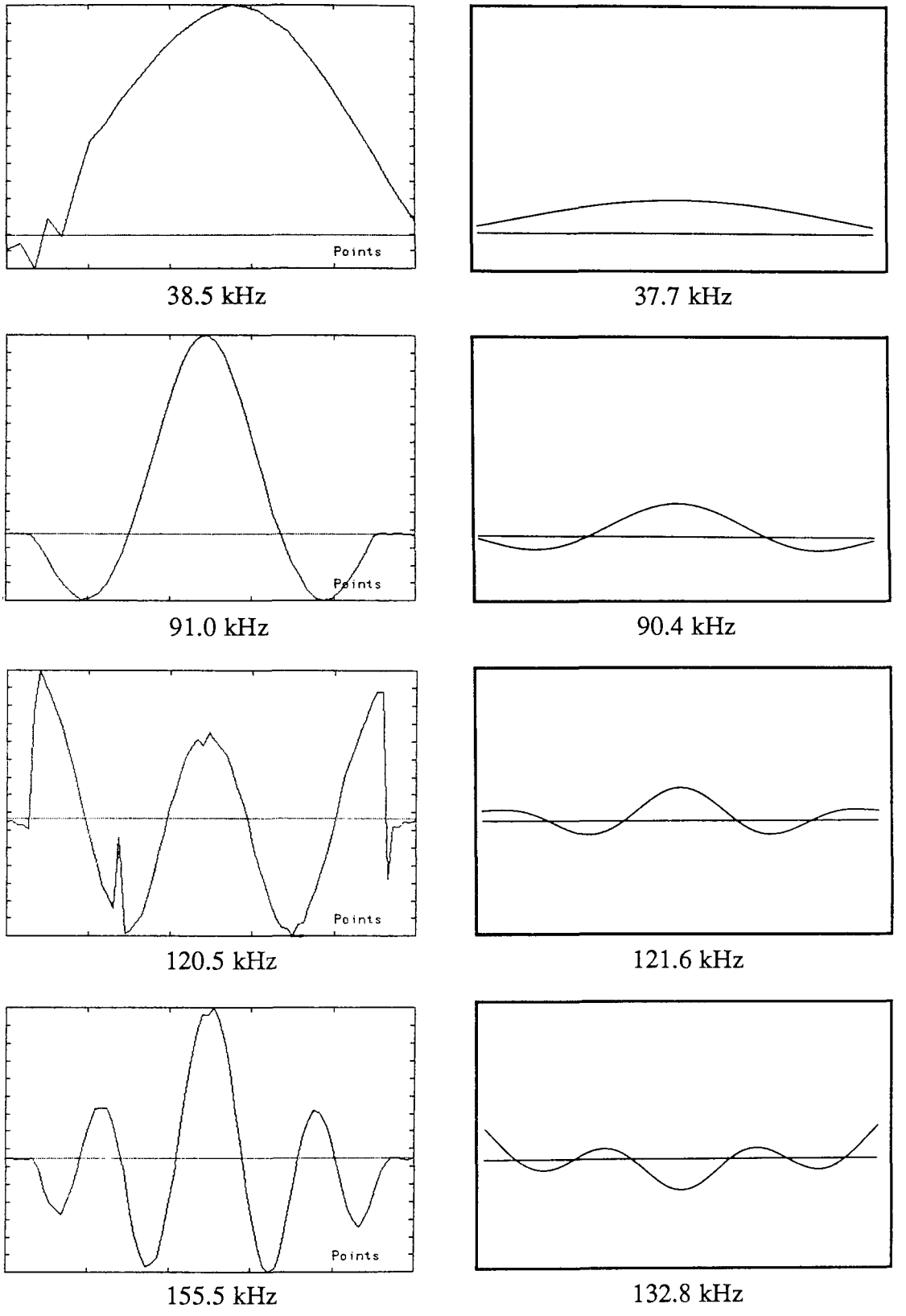

Fig 4.19 The measure and predicted surface displacement of the PZT5H disc with a D/T ratio of 5 (arbitrary amplitudes. left side: measurement; right side: prediction)

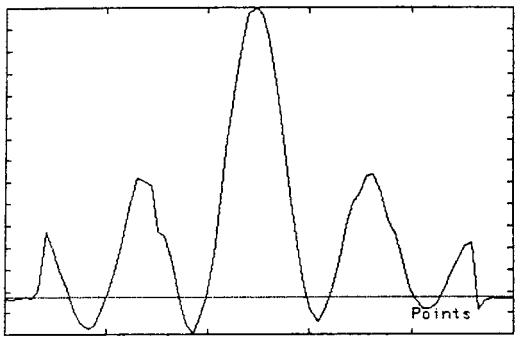

162.5 kHz

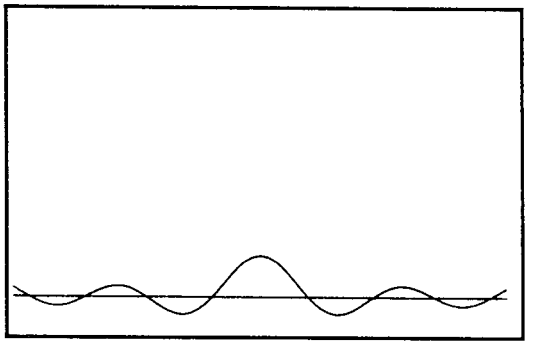

150.0 kHz

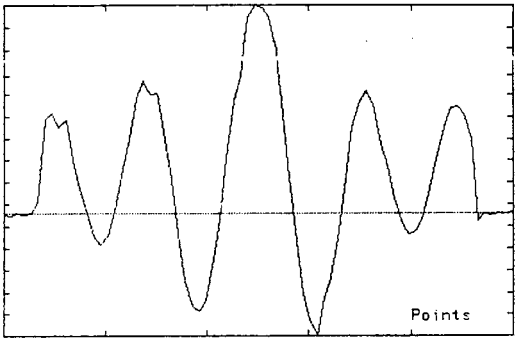

180.0 kHz

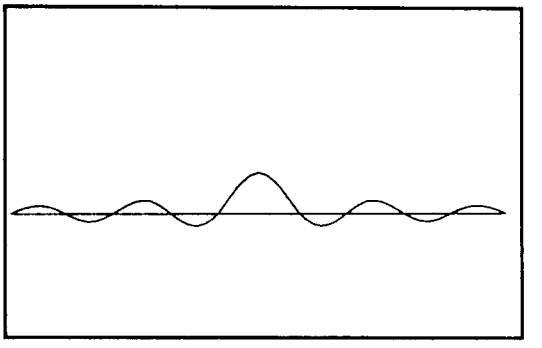

173.2 kHz

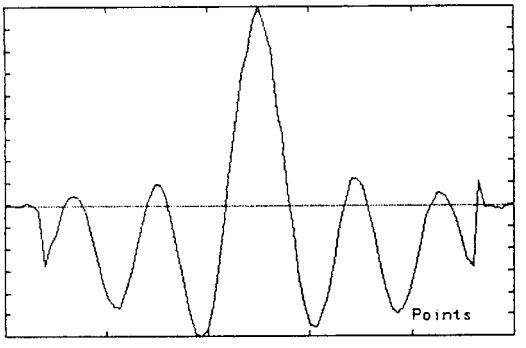

197.5 kHz

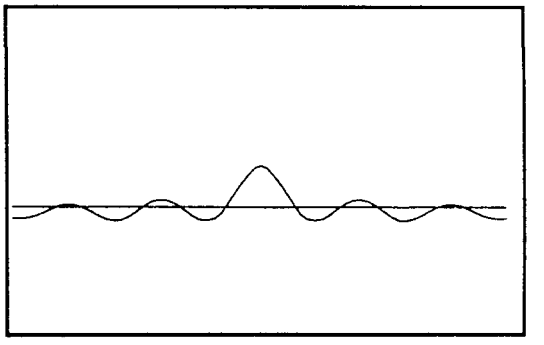

195.1 kHz

202 kHz (NA)

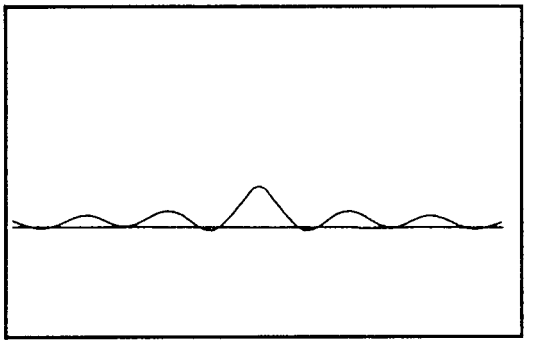

211.3 kHz

Fig 4.19 Continued

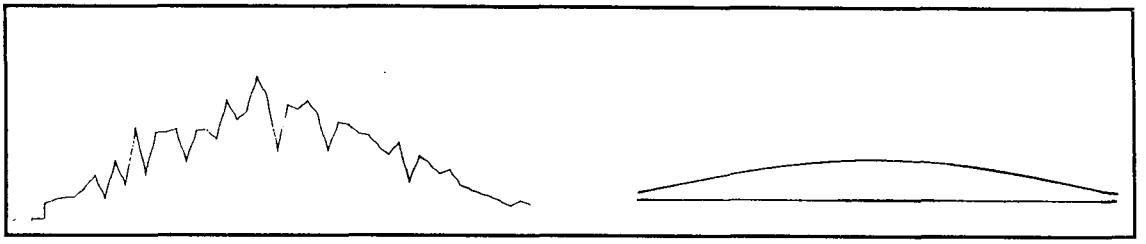

50.5 kHz 50.0 kHz

(a) the first radial mode of the PZT5A disc with a D/T ratio of 20

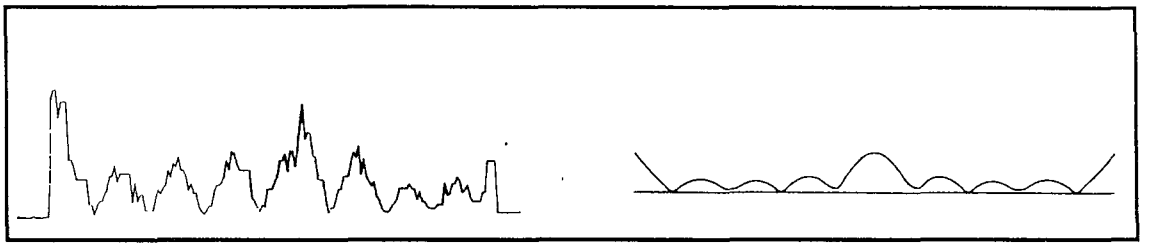

224 kHz 228 kHz

(b) the edge mode of the PZT4 disc with a D/T ratio of 8

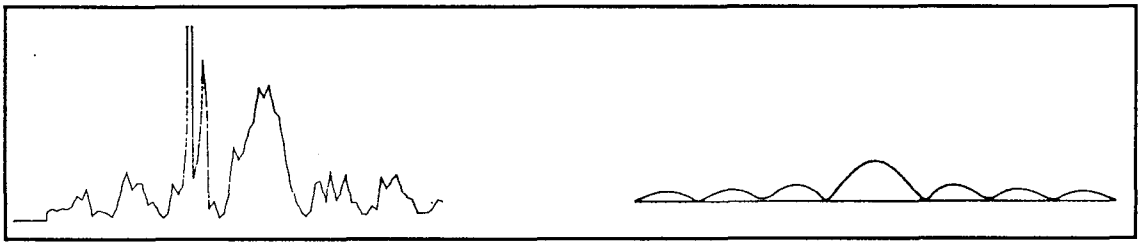

315 kHz 317 kHz

(c) the fourth radial mode of the PZT4 disc with a D/T ratio of 20

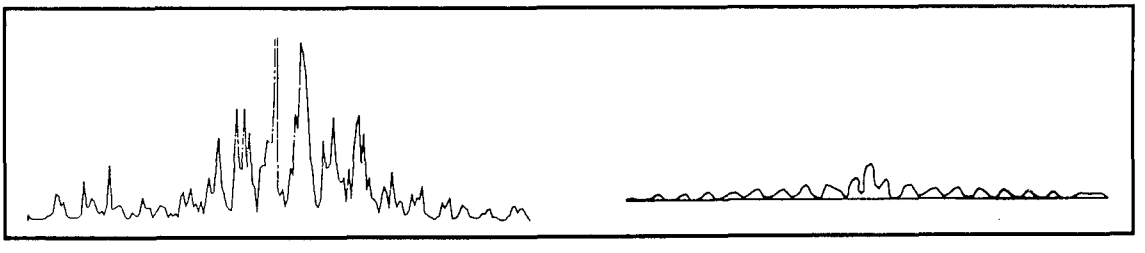

1033 kHz 983 kHz

(d) a thickness extensional mode of the PZT4 disc with a D/T ratio of 20

Fig 4.20 The measured and predicted surface displacements of piezoelectric discs with large D/T ratios in rectified form (Left side: measurement; Right side: Prediction)

CHAPTER 5

THE FREQUENCY SPECTRUM OF PIEZOELECTRIC DISCS

5.1 Introduction

In Chapter 4 the vibration characteristics of piezoelectric discs have been thoroughly analysed by finite element predictions and experiments. It has been shown that the vibration modes of piezoelectric discs are very complicated, and discs with different diameter to thickness ratios can present markedly different characteristics.

The dependence of the vibration characteristics on the geometry of the piezoelectric disc, namely the D/T ratio, is studied by the finite element model in terms of the frequency spectrum. The frequency spectrum, which is quite different from the usual definition in vibration signal analysis, is defined as the relationship between the product of resonant frequencies and the thickness of the piezoelectric disc (fT) and the diameter to thickness ratio (D/T). Since the frequency spectrum correlates the vibration characteristics with the geometrical properties of the piezoelectric disc, it can be a very important factor in the analysis and design of piezoelectric transducers. It has been evident from the review in Chapter 1 that the frequency spectrum has been studied extensively by a number of authors as a means of studying how three dimensional effects influence on the vibration characteristics of piezoelectric discs, both in experiments (Shaw, 1956; Ikegami *et al.*, 1974; Ueha *et al.*, 1983) and theoretical studies (Mindlin and Medick, 1959; Ikegami *et al.*, 1976; Locke *et al.*, 1987).

The radial modes were well classified by the analytical approximate solution and the plate theory, and the experiments have shown good agreement with the predictions; however, the edge mode and the thickness modes were less well defined. Furthermore, the parameters used to determine the intensity of the resonance are coupling factors, which required the resonant frequency and corresponding anti-resonant frequency of the mode to be identified. This was not practical and often gave rise to ambiguity since the modal density was high in the frequency range of interest.

In this chapter the frequency spectrum of piezoelectric discs is predicted by the finite element model in the D/T ratio range from 0.1 to 20. The modal constant at each resonance, which has been successfully used in last chapter, is incorporated to obtain the strength of each resonance in the frequency spectrum. Since the modal constant is only

involved with the resonant frequencies, the difficulties encountered by the previous authors can be removed. The form of the frequency spectrum is then discussed in terms of the variation in the mode shapes with D/T ratio. Experimental results are then presented from a few piezoelectric discs to verify the predictions. Finally the piezoelectric effect is discussed by comparing the frequency spectra predicted with and without electrical effects.

5.2 Frequency spectrum of piezoelectric discs

5.2.1 Predicted frequency spectrum by the finite element method

The eigenvalue solution programme was used again to predict the resonant frequencies and corresponding mode shapes of piezoelectric discs in which the top and bottom surfaces were fully electroded, and the modal constant of each mode was computed by using the predicted mode shape and the equivalent nodal forces. The piezoelectric material was PZT5A, which was used in the last chapter, and the material constants listed in Appendix A were used in the prediction.

The D/T ratio was varied from 0.1 to 20 with a step of 0.5 (step of 0.1 from 0.1 to 0.5), which is the range over which the piezoelectric discs are often used. The lower end of the D/T range was chosen as 0.1 since a disc with this ratio is essentially a long cylinder, and the one dimensional model (the length expander model) could be used to analyse the vibration characteristics and to compare with the finite element prediction, while the upper-limit of D/T ratio was taken as 20 since piezoelectric discs with about this ratio are often used in ultrasonic transducers in NDT, and the one dimensional through thickness model is also applicable.

The vertical coordinate of the frequency spectrum is the product of resonant frequencies and the thickness of the piezoelectric disc, fT, in kHz.mm, which is same as those in Fig 1.4 by Ikegami *et al.* (1974) and in Fig 1.5 by Shaw (1956). They were plotted in this form because the vibration characteristics are a function of frequency thickness product rather than frequency alone, so the spectrum was obtained in discs with different thickness and diameter. Since the frequency range around the first through thickness mode defined by the one dimensional model is most interesting and most important, the frequency range chosen was from zero to 1.5 times the first through thickness frequency. For instance, in PZT5A, the first through thickness mode (frequency thickness product) is around 1950 kHz.mm; therefore, only the modes from 0 to 3000 kHz.mm were predicted and plotted. Although it is possible to predict the modes beyond 3000 kHz.mm

by the same technique, the accuracy of the high order modes would be reduced or the mesh would have to be refined and the computing cost would increase significantly.

An alternative vertical coordinate of the frequency spectrum, Ω, has sometimes been used as shown in Fig 1.6 (Ueha *et al.*, 1983; Locke *et al.*, 1987). This is the ratio of the frequency of the resonant mode to the frequency of the second through thickness shear mode (or the first symmetrical thickness shear mode) defined by the one dimensional model. The frequency thickness product of the second through thickness shear mode for PZT5A material is 1650 kHz.mm. In this thesis the frequency thickness product, fT, is used, though the transformation from one to the other could readily be made.

Since the frequency spectrum covered a large range of D/T ratios and the frequencies of the modes were within the range 0 - 3000 kHz.mm, the finite element meshes used for discs with different D/T ratios had to be varied. For the present study the 8-node quadrilateral axisymmetrical piezoelectric element defined in Chapter 3 was used throughout. An 8x4 mesh, i.e., 8 elements in thickness and 4 elements in radius, was used for the cylindrical types of disc while a 2x48 mesh was used for discs with large D/T ratios, which gave 2 elements in the thickness and 48 elements along the radius. Some other meshes, such as 2x32, and 4x8 were also employed for discs with medium D/T ratios, as shown in Table 5.1. In general, the mesh for each disc was chosen to ensure that there were sufficient (5 to 7) finite element nodes per wavelength for all the modes of interest.

The predicted frequency spectrum is plotted in Fig 5.1. The predicted modal constant of each mode was normalised to the largest one for that disc, and each mode is indicated with a circle centred on the appropriate fT value whose diameter is proportional to the normalised modal constant value. The normalised modal constants of many modes are too small to appear larger than dots in the plot. The centres of the circles corresponding to modes of the same order at different D/T ratios are joined in the plot.

The overall pattern of the predicted frequency spectrum is similar to the measured frequency spectra produced previously by other authors. Several features are clearly seen in the frequency spectrum as shown in Fig 5.1. Three "terraces" are seen across the whole frequency spectrum. The first 'terrace' in the low frequency range is the edge mode terrace and appears around fT = 1350 kHz.mm; the second 'terrace' is the thickness shear modes terrace band around 1770 to 1820 kHz.mm, and with increasing of D/T ratio the number of modes on this terrace band is increased and the frequencies of the modes gradually converge; the third 'terrace' is the thickness extensional modes terrace around

1960 kHz.mm in which all the modes have very large modal constants. At low D/T ratios the modes with large modal constants spread over a significant fT range. As the D/T ratio is increased, this range reduces and one mode tends to dominate. However, the thickness extensional modes terrace is only seen clearly because of the large values of modal constant of the modes in this region, characterised by the large "modal constant" circles in Fig 5.1. If the frequency spectrum is plotted without drawing the "modal constant" circles as shown in Fig 5.2, the thickness extensional modes terrace tends to be less pronounced than that in Fig 5.1.

As the D/T ratio approaches 0.1, the first mode of the disc approaches a constant frequency thickness product of 1375 kHz.mm; this is almost identical to the first longitudinal mode predicted by the one dimensional piezoelectric rod model at 1380 kHz.mm. In fact the second and third extensional modes (symmetrical) of this cylindrical type of disc predicted by the three dimensional model are also very close to the third and fifth modes of the piezoelectric rod given by the one dimensional model as shown in Table 5.2 (the predicted flexural modes (anti-symmetrical) which cannot be excited correspond to the even numbered modes predicted by the one dimensional model). The mode shapes of the first three symmetric modes predicted by the FE model are shown in Fig 5.3, which are very close to those shown in Fig 1.3(a) assumed by the one dimensional model, though some small displacements in the radial direction are observed in the higher order modes. It is therefore evident that there is excellent agreement between the three dimensional prediction by the finite element model and the analytical solution by the one dimensional model, and the one dimensional piezoelectric rod model is therefore fairly accurate for the disc with a D/T ratio around 0.1.

At high D/T ratios, the vibration modes of the disc with D/T ratio of 20 are much more complicated as discussed in detail in the previous chapter. The first mode of the disc is the fundamental radial planar mode, which has maximum radial displacement at the edge of the disc, and smooth displacement over the disc surfaces with null axial displacement at the edge. The frequencies of the higher radial modes increase in an inharmonic manner which are given by a Bessel function as discussed in Chapter 1. The mode shapes of those radial modes shown in Fig 1.16 by the approximate analytical solution are similar to the predictions by the FE analysis. It can be seen that the smooth variation of the frequency thickness product of the radial mode with the D/T ratio is distorted to form the edge mode terrace around 1350 kHz.mm. This is also seen in the results of Ueha *et al.* (1983) shown in Fig 1.6.

As the D/T ratio of piezoelectric discs changes from 0.1 to 20, the geometry of the disc changes drastically, and the effective boundary conditions of the free disc change from plane stress to plane strain; the first order mode of the disc which is the first longitudinal mode at D/T = 0.1 becomes the fundamental planar radial mode at D/T = 20 and the thickness extensional and shear modes which do not exist in the low range of D/T ratio come into play.

The radial modes (R-modes), edge mode (E-mode), thickness shear modes (TS-modes), thickness extensional modes (TE-modes) are easily distinguished in the predicted frequency spectrum. The high frequency radial modes (A-modes) discussed in the previous chapter also exist, but are mixed together with radial modes in the region above 2000 kHz.mm.

5.2.2 Discussion of form of frequency spectrum

Lamb wave modes in a plate may be used to help the understanding of the vibration modes of piezoelectric discs (Furgason and Newhouse, 1973). The symmetric modes of the Lamb wave equation in an isotropic plate can be written as (Auld, 1973),

$$\frac{\mathrm{Tan}\left(\kappa T\sqrt{1-\left(\frac{c_2}{c}\right)^2}\right)}{\mathrm{Tan}\left(\kappa T\sqrt{\left(\frac{c_2}{c_1}\right)^2-\left(\frac{c_2}{c}\right)^2}\right)} = -\frac{4\left(\frac{c_2}{c}\right)^2\sqrt{1-\left(\frac{c_2}{c}\right)^2}\sqrt{\left(\frac{c_2}{c_1}\right)^2-\left(\frac{c_2}{c}\right)^2}}{\left[2\left(\frac{c_2}{c}\right)^2-1\right]^2} \tag{5.1}$$

where c is the phase velocity of the Lamb wave modes, c_1 and c_2 are the longitudinal and shear wave velocity respectively, and κ is the wavenumber.

The roots of the above transcendental frequency equation may be plotted as dispersion curves. Each root of the equation forms a dispersion branch, which represents a certain group of modes in the plate. Since piezoelectric ceramics are orthotropic materials, the above equation do not apply exactly, but can be used to analyse roughly the Lamb wave characteristics in piezoelectric plates. The dispersion curves can be plotted in terms of the Lamb wavenumbers (k) or phase velocity (c) as a function of the frequency thickness product (fT). For PZT5A with c_1 = 3784.4 m/s and c_2 = 1650.0 m/s, the dispersion curves in both forms are plotted in Fig 5.4.

Strictly speaking the dispersion curves are only valid for infinite plates. However, when a disc has a large diameter, they can be used to analyse the vibration modes, and the different groups of vibration modes in the frequency spectrum of the disc can be assigned

to each branch of the dispersion curve shown in Fig 5.4. For example, within the frequency range of interest (below 3000 kHz.mm), S_0, gives the R-mode series; S_1, which has a cutoff frequency at the second thickness shear mode by the one dimensional model (1650 kHz.mm), represents the thickness shear modes group (TS), and S_2, which has a cutoff frequency at the first through thickness mode (1892.2 kHz.mm), gives the thickness extensional modes and high frequency radial A modes. Since the disc has finite thickness and diameter, the different modes can be coupled, which has been shown in the mode shapes discussed in the previous chapter, such as Fig 4.3.

The T-modes series in Fig 1.4 defined by Ikegami *et al.* (1974) may in fact correspond to the thickness shear modes (TS-modes) in the frequency spectrum as shown in Fig 5.1. Although Ikegami *et al.* (1974) measured the frequency spectrum of discs with D/T ratios up to 28, no mode shape was provided to clarify the nature of the vibration modes. Nevertheless he assigned the measured T modes to the theoretical shear modes predicted by the plate theory though they were not in very good agreement.

Unlike other modes, the edge mode cannot be simply explained by the dispersion curves shown in Fig 5.4. Gazis and Mindlin (1960) used the second order plate theory and suggested that edge modes may be associated with the complex wavenumbers in the low frequency range. They may come from the radial modes at the particular frequency reflected on the free edge boundary. However, the predicted frequency values of the edge modes by the second order plate theory were always much lower than the measured ones (Gazis and Mindlin, 1960; Ikegami *et al.*, 1974).

The edge mode may in fact be characteristic of the finite disc with free boundary conditions on the cylindrical surface. It can be seen from the frequency spectrum shown in Fig 5.1 that the frequency thickness products of edge modes are independent of the D/T ratio with fT around 1350 kHz.mm, which indicates that the edge modes depend on the thickness of the disc only. This frequency thickness product roughly coincides with the first longitudinal mode of the rod by the one dimensional theory at 1375 kHz.mm

Fig 5.5 shows the axial surface displacements of the edge mode and some adjacent modes at D/T ratios from 2 to 20, together with the first mode of discs with D/T ratios of 0.1 and 0.5. It can be seen that in the edge mode the displacements at the edge and at the centre of the discs are comparable, but that the phase of the edge displacement relative to that of the centre varies as the D/T ratio is increased. The edge mode may be associated with the first longitudinal mode of the rod, they both have similar mode shapes, and have approximately same frequency thickness products.

The thickness extensional modes, however, are quite remarkable as shown in both Fig 5.1 and Fig 5.2. In the frequency spectrum with "modal constant" circles shown in Fig 5.1, the thickness extensional modes "terrace" is broad around a D/T ratio of 5 and then gradually converges to a single mode when the D/T ratio approaches 20. However, the "terrace" for the values of the frequency thickness product shown in Fig 5.2 is not so obvious, and the frequency spectrum in the range of thickness modes becomes reasonably flat only when the D/T ratio exceeds 12. This agrees in form with the prediction by the second order plate theory for a material with Poisson's ratio larger than 1/3 (Ikegami *et al.*, 1976).

5.2.3 Measurements of the frequency spectrum

Measurements of the frequency spectrum shown in Fig 5.1 would be very tedious if piezoelectric discs with all the D/T ratios were tested. Since extensive experimental measurements on the frequency spectrum of piezoelectric discs have been reported in the literature for various piezoelectric materials: $BaTiO_3$ (Shaw, 1954), $PbTiO_3$ (Ikegami *et al.*, 1974), and $Pb(Zr.Ti)O_3$ (Ueha *et al.*, 1983) and these spectra show qualitative agreement with the FE predictions made here, only 8 PZT5A discs were used to verify the predicted frequency spectrum. The discs tested have D/T ratio of 20, 10, 5.0, 3.0, 2.5, 2.0, 1.0, 0.5, which covers most of the D/T range of the predictions; since the frequency spectrum is plotted as fT vs D/T, some discs with different thickness could be used. The experimental procedure was the same as in Section 4.2.3. The electrical impedance response functions of these piezoelectric discs were first measured, and then they were used to find the resonant frequencies and the modal constants of each mode by the modal analysis technique.

The measured frequency spectrum for these discs is shown in Fig 5.6, together with the predicted form shown in Fig 5.2. The measured modal constant of each mode is normalised to the largest one of that disc, and then plotted as a circle; the circle diameter is proportional to the normalised value of the measured modal constant, but many of them can not be seen since their values are too small. It can been seen that good agreement is obtained between the experiments and the predictions.

The measured radial modes and thickness modes are generally in good agreement with the predictions as expected. From the frequency spectrum shown in Fig 5.6 and the detailed study in the previous chapter, it seems that a good correlation between the measured frequency of the edge mode and the predicted one by the FE model is obtained, which

was not the case by using the plate theory. This can be understood since the numerical prediction by FE analysis satisfies all the boundary conditions of a free disc explicitly while the plate theory or other approximate analytically solution always have certain implicit assumptions.

5.3 The influence of piezoelectric effects on the spectrum

Piezoelectric materials exhibit coupling between the elastic and the electric (dielectric) properties. The piezoelectric coupling has a stiffening effect on the elastic properties of the material. However, sometimes the resonant frequencies and mode shapes of a piezoelectric disc can be obtained fairly accurately even when the piezoelectric effect is ignored (Guyott *et al.*, 1986). EerNisse (1967b) compared the frequency spectra of $BaTiO_3$ in the D/T ratio range 1 to 6 both neglecting the piezoelectric properties and taking them into account. He found that the resonant frequencies with piezoelectric properties were in general higher than those neglecting the piezoelectric effects.

In the present study the frequency spectrum of PZT5A discs was predicted in the D/T range of 0.1 to 20 by the finite element method without considering the electrical effect. The computation procedure and the finite element mesh used in the previous section were used except that an 8-node elastic axisymmetric element was used instead of the corresponding piezoelectric element.

The predicted frequency spectrum without considering the piezoelectric effect (or electrical properties) is shown in Fig 5.7. It has not been overlaid on the piezoelectric frequency spectrum shown in Fig 5.2 to avoid complication. It can be seen that the overall patterns of these two frequency spectra are similar. As expected, the values of the frequency thickness product of each mode for a purely elastic material are smaller than those for a piezoelectric material, which is due to the piezoelectric stiffening effect. However, this stiffening effect varies for discs with different D/T ratios and for different modes of the same disc.

Generally the piezoelectric effect produces more difference in frequency values for discs with lower D/T ratios. This can be demonstrated by the comparison of the first mode frequency between piezoelectric discs and elastic discs as a function of D/T ratio as shown in Fig 5.8. The difference caused by the piezoelectric effect is largest at small D/T ratios, and then gradually decreases as the D/T ratio is increased. Above a D/T ratio of 6, the difference can hardly be seen.

Fig 5.9 compares the predicted resonant frequencies of a disc with and without piezoelectric properties. The disc has the properties of P5A20, which is the PZT5A disc with a D/T of 20 studied in detail in the previous chapter. It can be seen from the plot that the piezoelectric property has little effect on the frequencies of the first few modes, and the frequency difference gradually increases with the order of the modes. However the frequency difference reaches a maximum in the frequency range of the thickness extensional modes and remains approximately constant after this.

The above phenomena may be interpreted by considering the electrical properties of the piezoelectric disc. From the equations discussed in Chapter 3 the stiffening effect actually comes from the non-electroded regions in the piezoelectric structure, so the mechanical displacement here is more important if the piezoelectric coupling effect is taken into consideration. Since piezoelectric discs are usually poled in the thickness direction, the piezoelectric property has a much more pronounced effect in the vibration modes having strong deformation in the thickness direction than in the modes having large radial deformation. If the D/T ratio of the disc is very small, such as 0.1, the disc is essentially cylindrical and very large deformation in the thickness direction occurs for the first mode of the disc. The piezoelectric stiffening effect is therefore very significant and large differences in the frequency values result as shown in Fig 5.8. As the D/T ratio increases, the first mode of the disc gradually has less deformation in the thickness direction and more radial deformation, the piezoelectric effect is then reduced and the frequency difference is reduced. When it finally approaches the fundamental planar mode, in which deformation in the radial direction dominates, the piezoelectric effect therefore has very little influence on the value of the resonant frequency. Similarly, for different modes of the same disc as shown in Fig 5.9, the first few modes are lower order radial modes which have relatively small deformation in the thickness direction, so the piezoelectric properties have little effect. With increasing mode order the deformation in the thickness direction increases, the stiffening effect is therefore more important, and relatively large differences in frequency result, particularly in the frequency range of the thickness modes.

The mode shapes predicted are very similar for both the piezoelectric and elastic cases. This is why the elastic theory developed in 1950s was often used to analyse the measured vibration characteristics of piezoelectric discs, and the theoretical analysis on elastic discs was verified by experiments on piezoelectric discs.

5.4 Conclusions

The geometrical dependence of the vibration characteristics of piezoelectric discs has been studied by means of the frequency spectrum in the diameter to thickness ratio 0.1 to 20. It has been found that the vibration characteristics of the piezoelectric disc change drastically with D/T ratio.

It has been shown that the modal constants of the thickness extensional modes of the piezoelectric discs are the largest of all the modes, and with increasing D/T ratio, the thickness extensional modes which have the largest modal constants converge to a single mode. This suggests that the modal constant can be a very useful parameter in analysis and design of piezoelectric transducers since it is also directly related to the excitation force and the vibration pattern.

The predicted frequency spectrum has been verified by measurement on a limited number of discs, and good agreement has been obtained. The predicted frequency thickness products of edge modes show similar values to that of the first longitudinal mode of a piezoelectric rod, and the edge mode shows similar mode shape characteristics to that of the first longitudinal mode. This suggests that the edge mode, in which the displacement is maximum at the free boundary may be associated with the longitudinal mode of a rod.

D/T ratios	No. of elements in thickness	No. of elements in radius
0.1 - 1.0	8	4
1.0 - 2.5	4	4
2.5 - 5.0	4	8
5.0 - 10.0	4	16
10.0 - 15.0	2	32
15.0 - 20.0	2	48

Table 5.1 The finite element mesh used for piezoelectric discs with different D/T ratios

Mode No.	Predicted by the FE model (kHz)	Predicted by the 1D model (kHz)
1	136.57	137.29
2	534.99	537.76
3	907.30	909.55

Table 5.2 The resonant frequencies of the first three modes of a PZT5A disc with a D/T ratio of 0.1 (D = 1 mm, T = 10.07 mm)

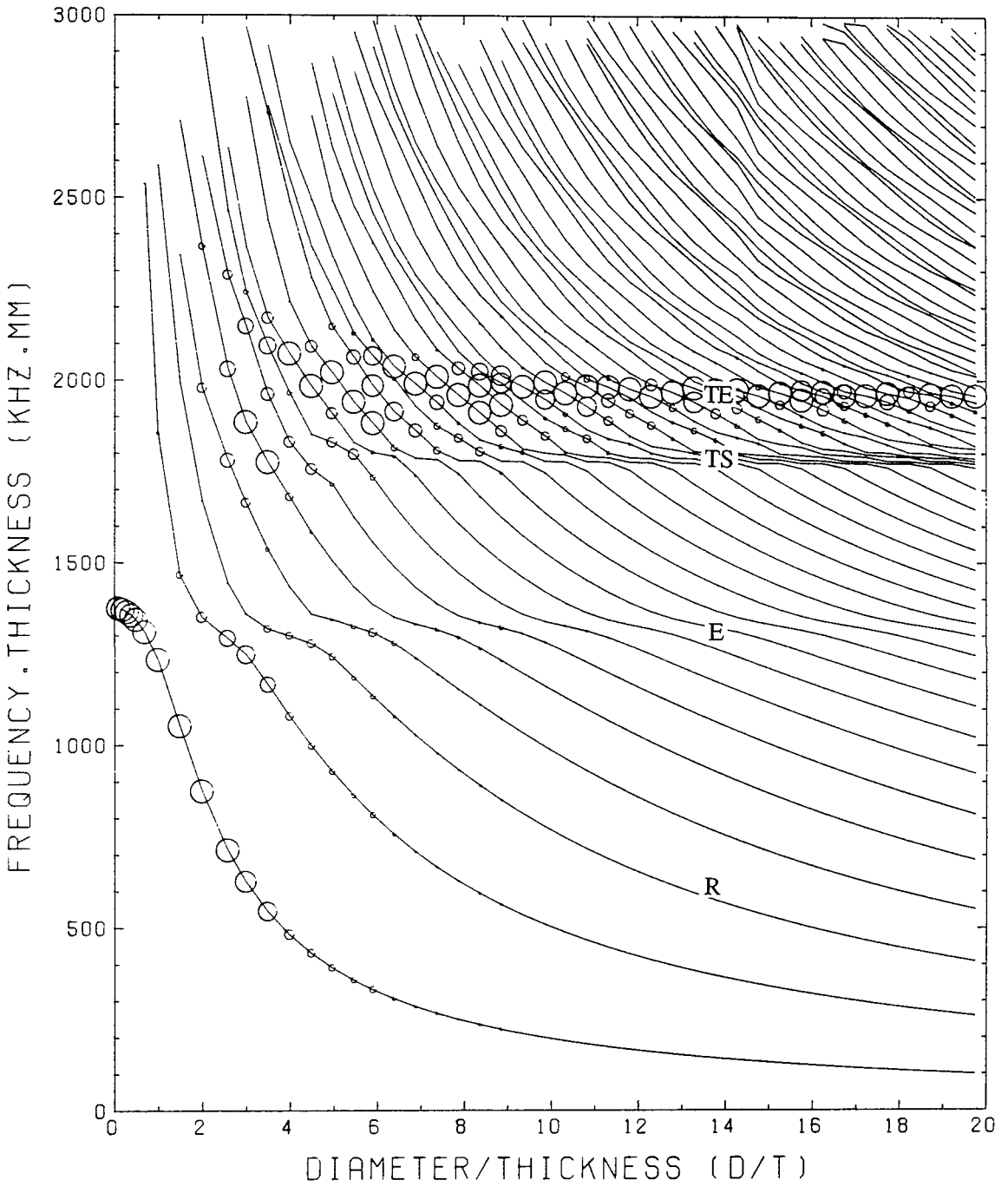

Fig 5.1 The predicted frequency spectrum of PZT5A discs with modal constants (Circle diameters proportional to the normalised modal constants, some are too small to be seen)

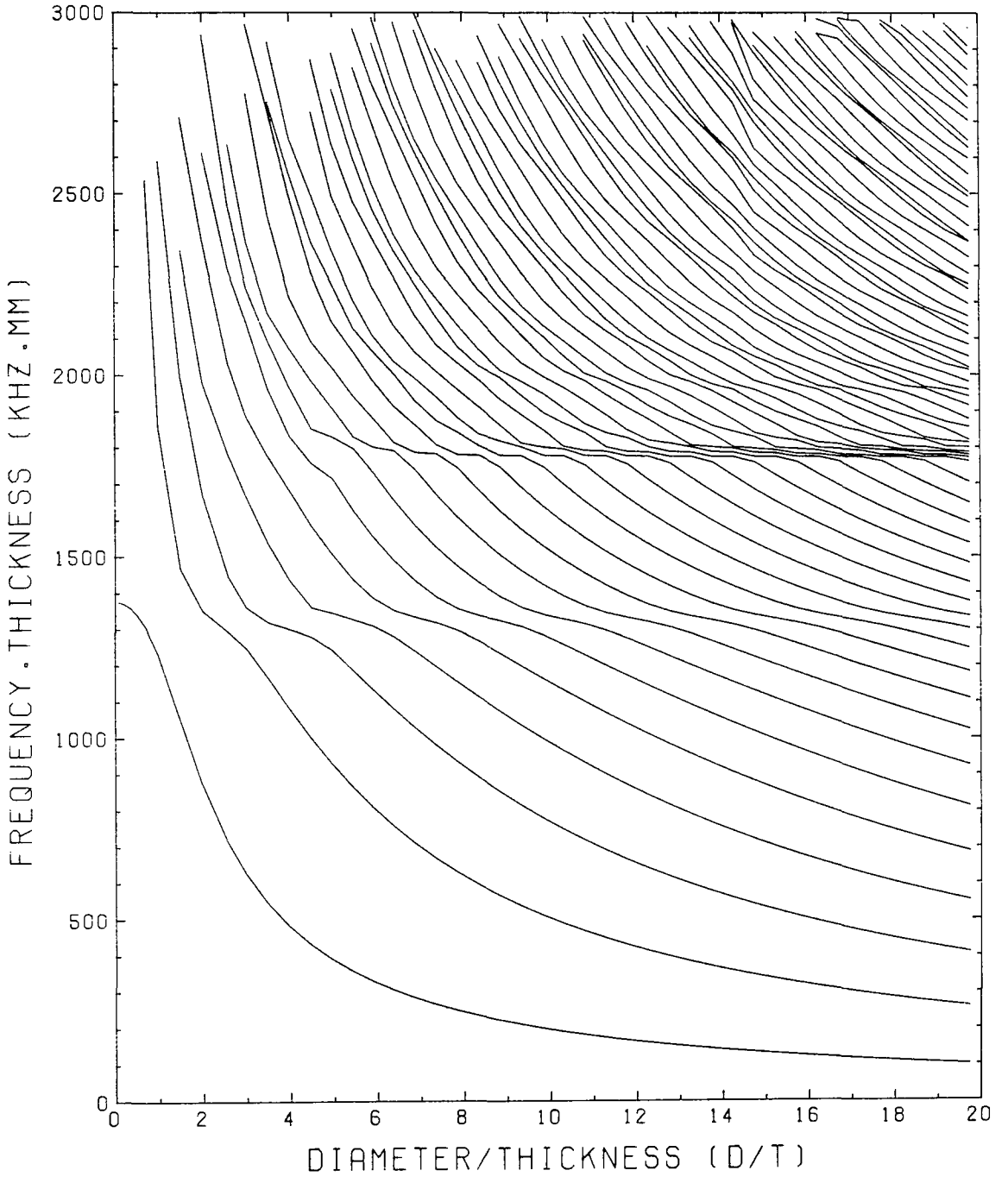

Fig 5.2 The predicted frequency spectrum of PZT5A discs

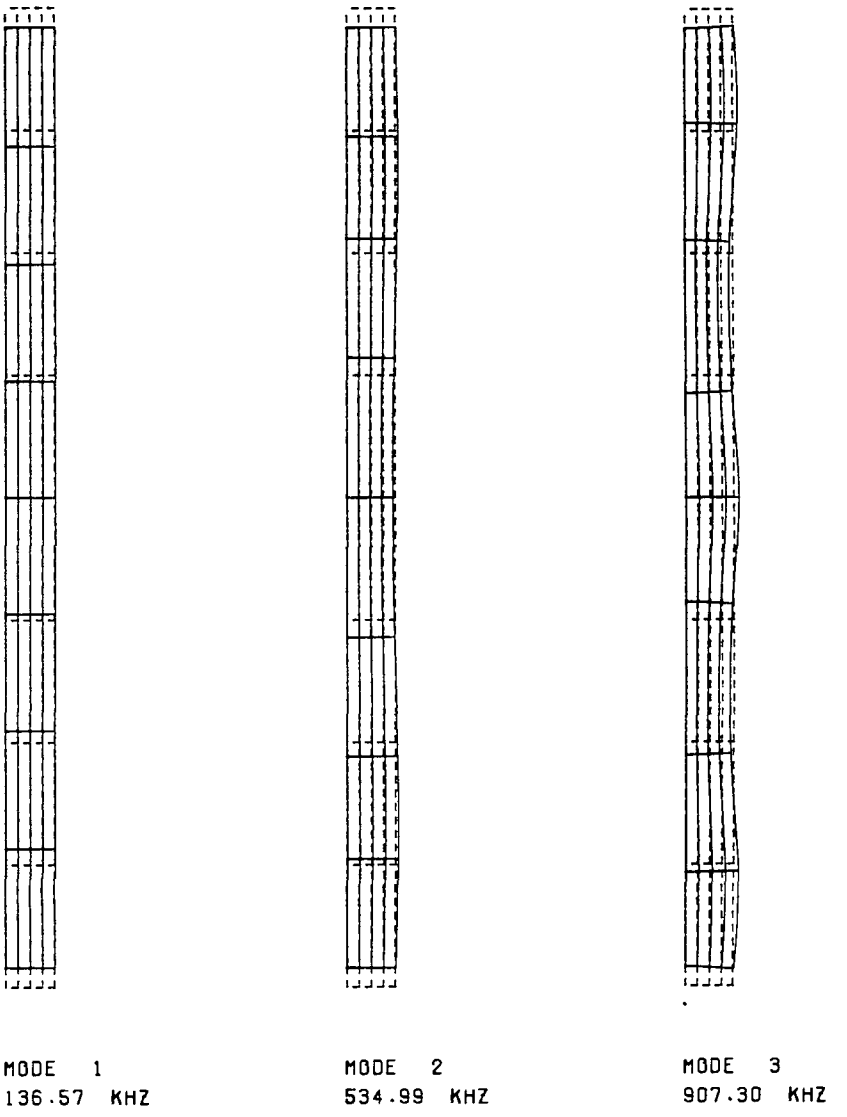

Fig 5.3 Mode shapes of the first three extensional modes of a piezoelectric disc with a D/T ratio of 0.1 (D = 1.00 mm, T = 10.07 mm)

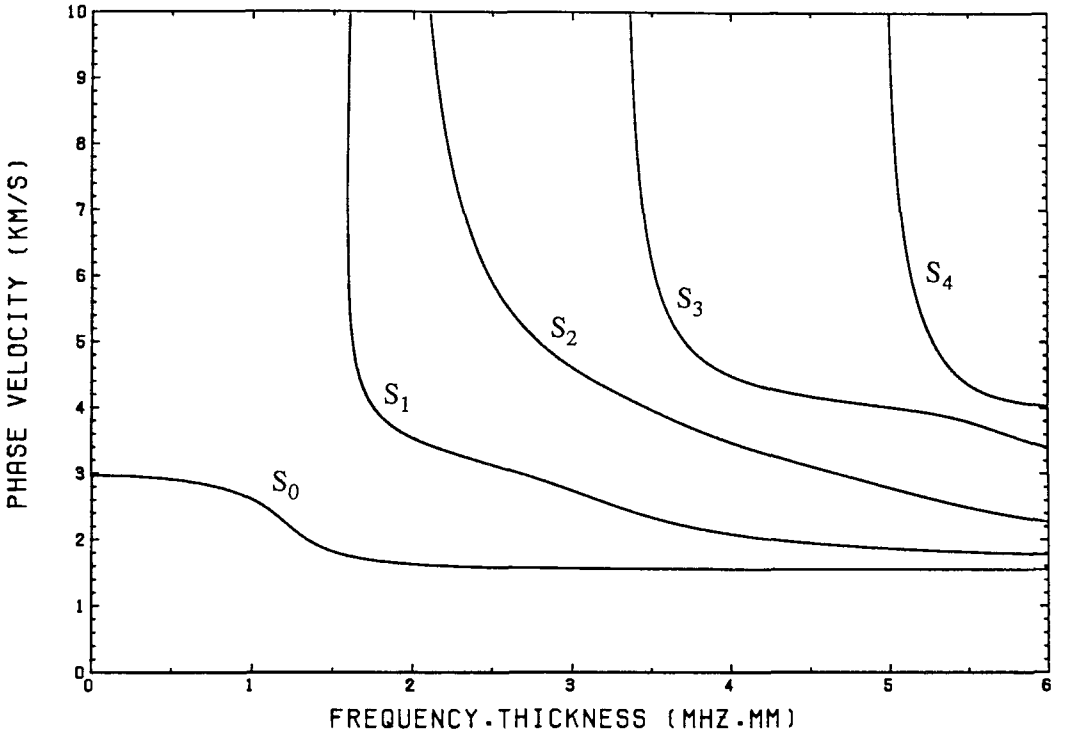

(a)

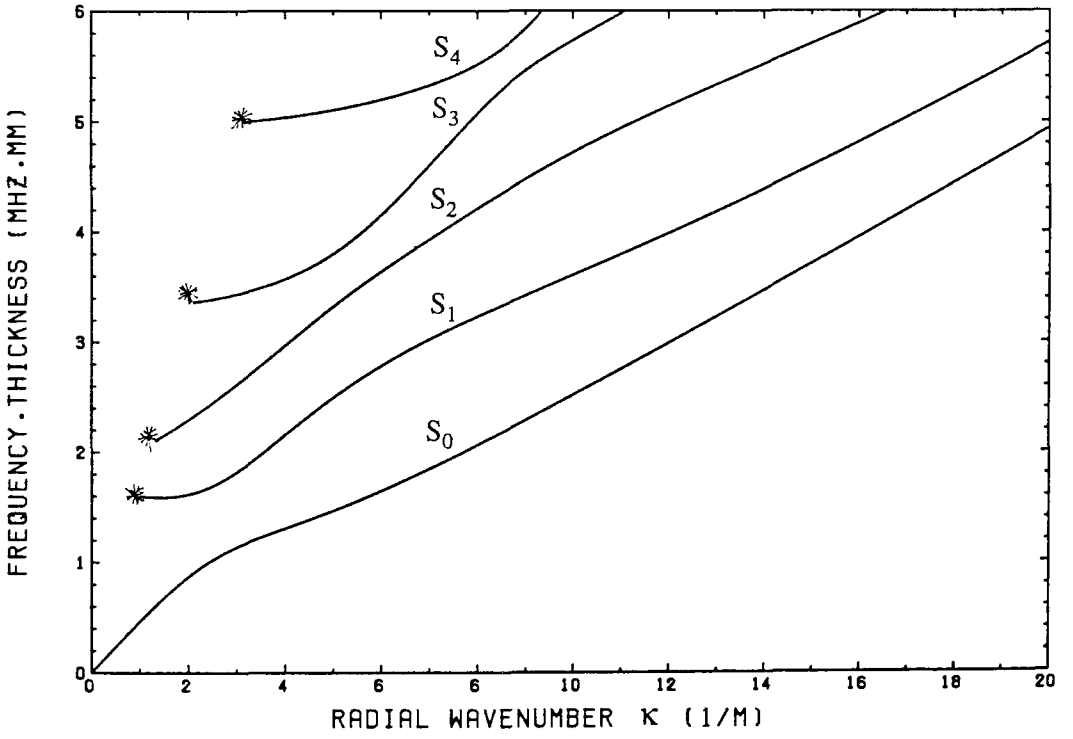

(b)

Fig 5.4 Dispersion curves of the symmetrical modes of Lamb wave (c_1 = 3784.4 m/s, c_2 = 1650 m/s)
(The curves marked * do not extend to zero wavenumber and the cut-off frequency because they were derived from Fig 5.4(a) in which the dispersion curves are only calculated up to phase velocity of 10 km/s)

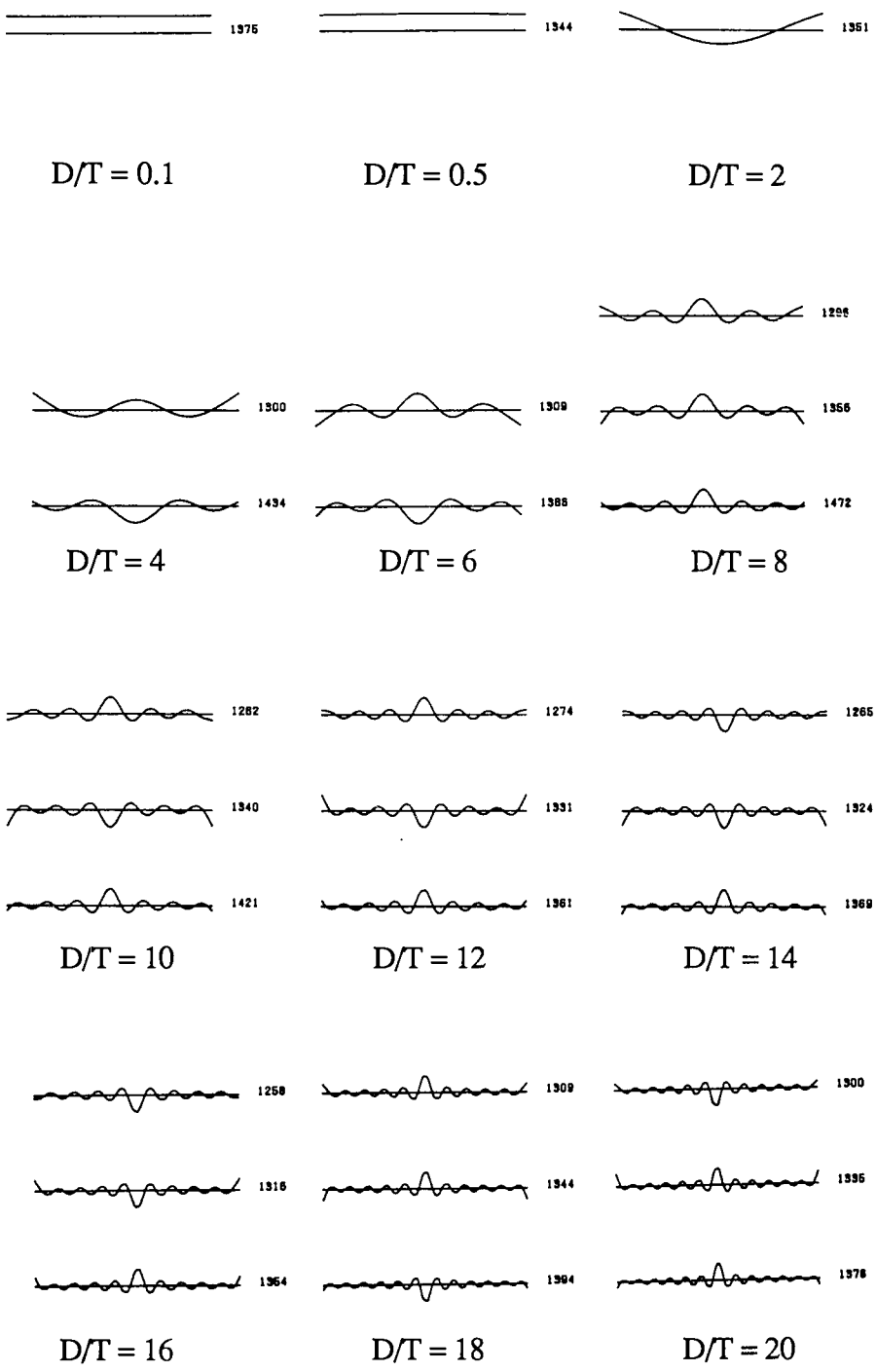

Fig 5.5 The axial surface displacement of the edge modes and their adjacent modes as a function of D/T ratios
(Values corresponding to fT values in the frequency spectrum)

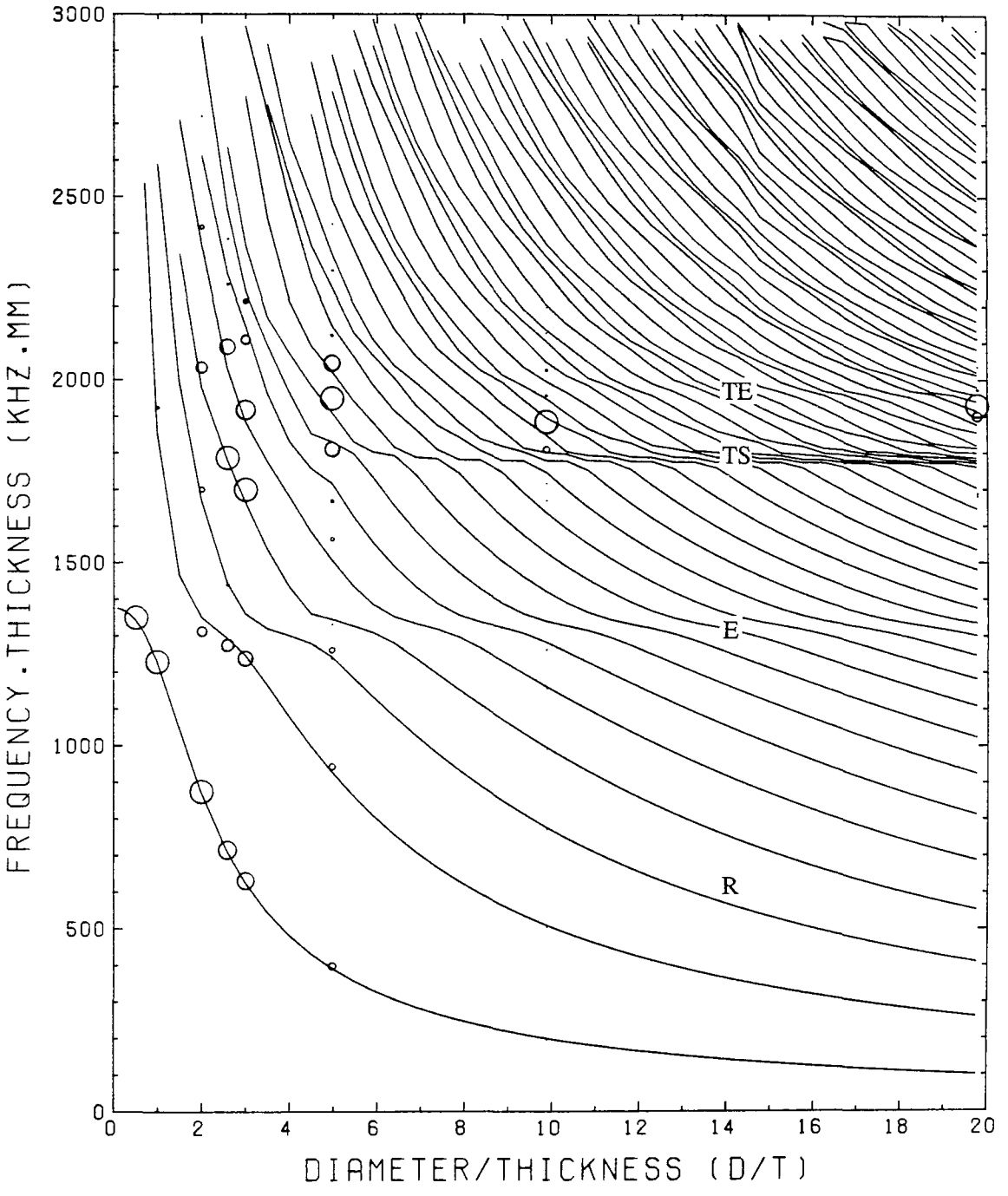

Fig 5.6 The measured and predicted frequency spectra of PZT5A discs with measured modal constants (circle diameters proportional to the measured normalised modal constants, some are too small to be seen)

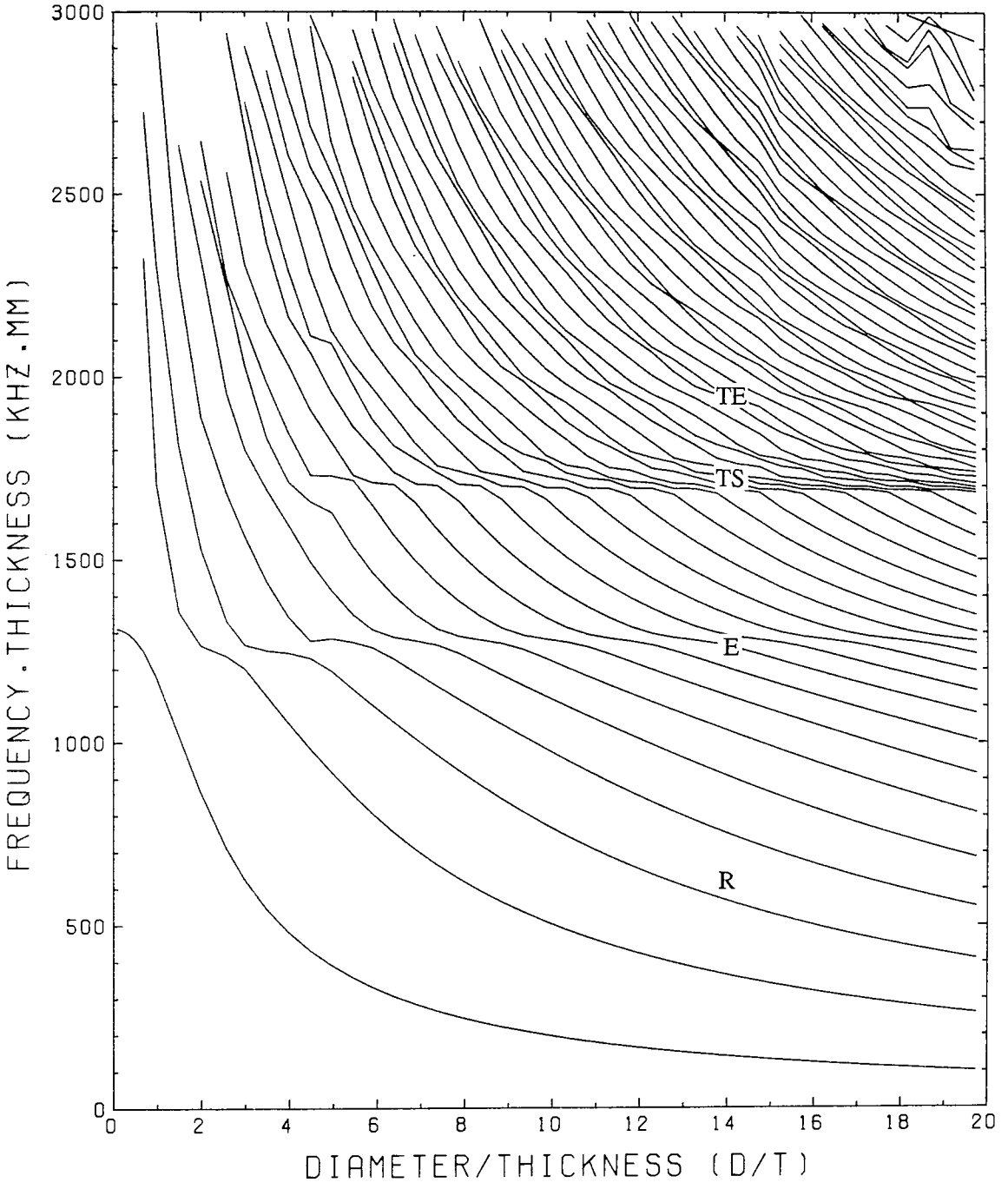

Fig 5.7 The frequency spectrum of PZT5A discs predicted without considering electrical properties

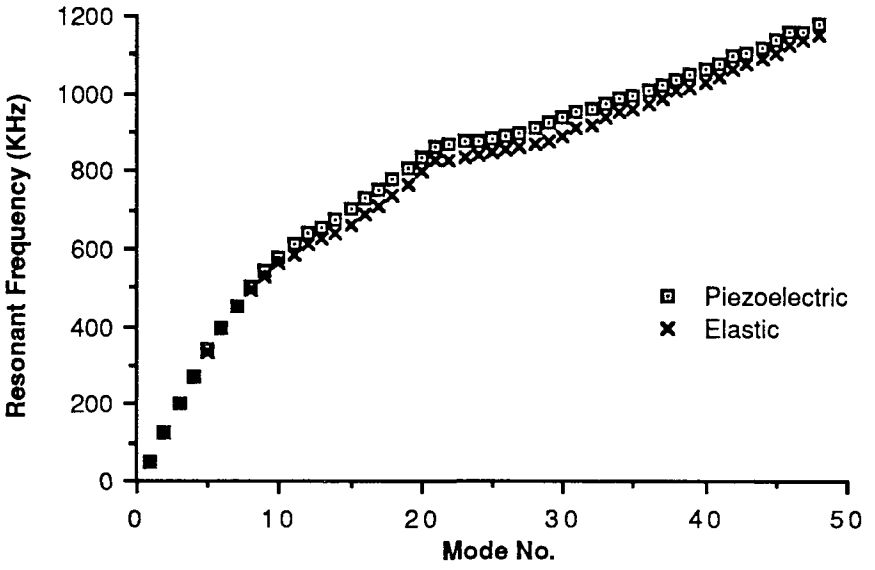

Fig 5.8* The first mode of PZT5A discs as a function of D/T ratios predicted with and without electrical properties

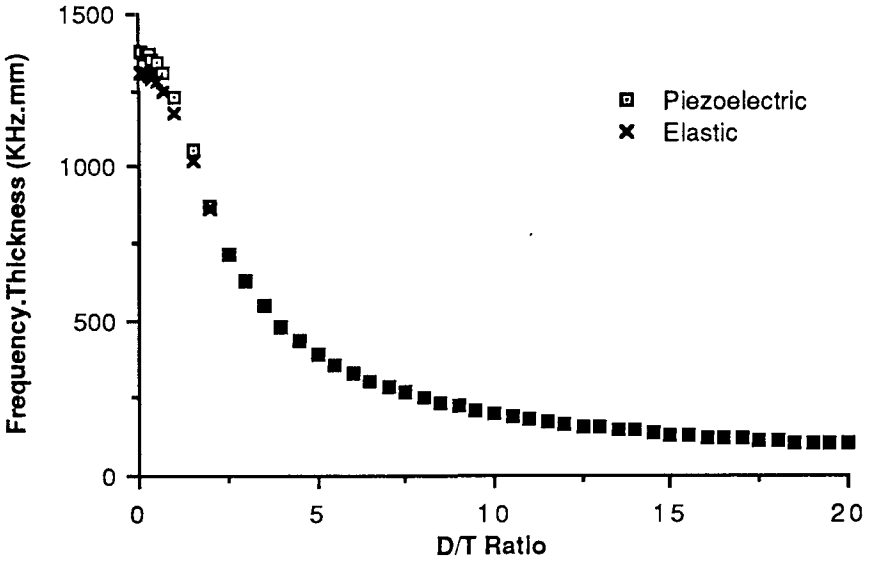

Fig 5.9* The first 48 modes of the PZT5A disc with a D/T ratio of 20 predicted with and without electrical properties (D = 40.10 mm, T = 2.03 mm)

* ERRATUM: Figures in Fig 5.8 and Fig 5.9 should be swapped.

CHAPTER 6

THE TRANSIENT RESPONSE OF THE PIEZOELECTRIC DISCS

6.1 Introduction

The steady state responses of piezoelectric discs, including the electrical impedance function and the mechanical response function when the disc is subjected to voltage excitation across the electrodes of the discs, have been studied in detail in the previous chapters. It has been shown that the piezoelectric discs have many vibration modes in the frequency range of interest and none of these modes has the mode shape assumed by the one dimensional theory.

However, in the analysis of the performance of the transducers the transient response is also very important. The transient response can be solved in two ways by the finite element analysis (Bathe, 1982). One solution is to integrate the dynamic differential equation in Chapter 3 directly for each time step, the advantage of this method is that it is efficient when the structure is very large and the response at a limited number of time steps is required. The alternative is to use modal analysis techniques (or mode superposition), which require the modal parameters, including the resonant frequencies and corresponding mode shapes and modal constants to be found and then to superimpose the contribution from all the modes in the frequency range of interest; the advantage of this method is that little extra work is required if the eigenproblem has already been solved. However, the method is very costly at the eigenvalue solution stage if the structure to be analysed has many modes in the frequency range of the excitation.

In this chapter the mechanical transient response function of the piezoelectric disc is studied by the modal analysis technique. Since all the necessary modal parameters have already been found in the eigenvalue solution routine, the mechanical transient response at any degree of freedom can be obtained easily.

6.2 Axial surface displacement of a piezoelectric disc when the disc is excited by various voltage pulses

6.2.1 A PZT5A disc with a D/T ratio of 20

The PZT5A disc analysed is the same as the one in Chapter 4 with a D/T ratio of 20; it is assumed to be excited by voltage pulses across the electrodes on the top and bottom

surfaces of the disc. Since the normal displacement over the surfaces of the disc is of most interest, the axial displacement at each nodal point over the surface of the disc can be computed as a function of time. The formulation for the transient mechanical response of the disc in the axial direction at any nodal point has already been found by using the Duhamel integral as equation (3.83) in Chapter 3,

$$z_r(t) = \frac{1}{\omega_r}\int_0^t H_r\varphi(\tau)\sin[\omega_r(\tau - t)]\,d\tau + A_r\sin(\omega_r t) + B_r\cos(\omega_r t) \qquad (6.1)$$

where A_r, B_r are determined from the initial conditions, r denotes modal parameters at mode r, H_r is a function of equivalent nodal force and the mode shape of mode r; $\varphi(\tau)$ is the applied voltage, which can be an arbitrary function of time. The Duhamel integral can be evaluated numerically, but some simple inputs are used here in which an analytical solution can be obtained. The displacement can then be obtained by superimposing the above expression over all the modes which have been predicted.

The modal solution includes all the modes up to 1500 kHz for this disc. This is well beyond the first through thickness mode at 962 kHz predicted by the one dimensional model which is of most interest. The simple analytical inputs used here (Dirac, rectangular pulses and single cycle sine wave) do have some energy above 1500 kHz. However, the response of the disc to this energy is not included in the modal solution. This is not a significant problem since in practical excitation pulses applied to discs with a 1.0 MHz thickness frequency also have only very limited energy above around 1.5 MHz.

In modal solutions the time step taken in the transient analysis depends only on the highest frequency of the mode predicted, i.e., 1500 kHz here, and the problems which may be encountered in the direct time integration scheme, such as aliasing and instability, are therefore removed. A time step of 0.1 μs is used here, which is believed to be sufficient.

Following are responses corresponding to three simple forms voltage excitation pulses: the Dirac pulse, rectangular pulse, and one single cycle sine wave.

1. Dirac pulse

Since only the modes up to 1500 kHz are considered, the spectrum of the Dirac pulse has a cut-off frequency at 1500 kHz. Fig 6.1 shows the transient axial mechanical displacement response at the central point of the surface of the piezoelectric disc when the

disc is excited by a Dirac voltage pulse. The transient response is plotted in the range 0-20 μs and 0-200 μs separately in Fig 6.1(a) and (b) in order to obtain a clear view of the crucial initial portion of the response, and linear amplitudes normalised to a maximum value of unity are used in these and the following figures. Since the structural damping model, which assumes harmonic motion, is invalid for the modelling of transient responses, the modal damping included in the transient analysis is viscous damping, with a damping coefficient ξ of 0.007, which corresponds to a Q factor of 75 for PZT5A ($\xi = \frac{1}{2Q}$), and the decaying response is seen in Fig 6.1(b).

It can be seen from Fig 6.1 (a) that although the response at the beginning shows the presence of more than one mode, the dominant period of the oscillation is about 1 μs. This is believed to be due to mode 32 predicted at 965 kHz which is the most strongly excited mode for this disc. However, the response becomes complicated after 10 μs, and many modes including the low frequency radial modes appear in the response.

Fig 6.1(b), which records the response over a larger range of time from 0 to 200 μs, shows that the general response is very complicated since all 64 modes predicted in the frequency range of interest are superimposed in the response. The high frequency modes are damped out quickly with time, and the response in the time range around 200 μs is dominated by the low order radial modes, and it can be observed that the oscillation has a period of about 20 μs, which corresponds to the first radial mode with a resonant frequency predicted at 50 kHz.

In order to see clearly how the piezoelectric disc responds with time when the voltage pulse is applied, the surface axial displacement of the disc, i.e., the axial displacements at all surface nodes, are calculated as a function of time. These "snap shots" of the surface of the disc are then plotted for selected time instants.

Fig 6.2 shows snap shots of the surface of the disc, from 0.1 to 4 μs in steps of 0.1 μs. It is very interesting and surprising that the displacement response over the surface of the disc shows remarkable flatness within the first 2 μs since it has been shown in Chapter 4 that there is no mode having a mode shape close to the piston-like motion suggested by the one dimensional model. Since the first through thickness frequency assumed by the one dimensional theory is 962 kHz, and the most strongly excited mode predicted by the three dimensional FE model is 965 kHz, the period of the one dimensional through thickness mode and that of the most strongly excited mode is about 1 μs.

The piston-like motion of the disc predicted for the first few microseconds after the excitation is applied is due to the superposition of contributions from all the modes of the disc. In particular, there are many modes in the thickness frequency range which have some "dc" component of displacement over the surface of the disc as well as a component which varies along a diameter. When the contribution from the different modes are added together, the "dc" components tend to add while the varying components tend to cancel, giving a roughly constant displacement over the surface, other than close to the edge.

To verify the above explanation, the transient surface displacement responses due to the contribution from different mode components are calculated in time from 0.1 to 2.0 μs and are shown in Fig 6.3. Fig 6.3(a) shows the surface response due to a single mode (mode 32) at 965 kHz, which is in fact identical to the mode shape shown in Fig 4.3; Fig 6.3(b) shows the response including mode 32 and the first five radial modes from 0.1 to 2.0 μs; and Fig 6.3(c) shows the response including mode 32 and the other high frequency thickness extensional modes from 880 kHz to 1080 kHz. It can be seen that the contribution of radial modes shown in Fig 6.3(b) is not responsible for the piston-like motion, while the result shown in Fig 6.3(c) is close to that of Fig 6.2 in which the disc has a relatively uniform surface motion.

Fig 6.4 shows the surface deformation of the disc in the time range 10-12 μs. Since the high frequency thickness extensional modes become weaker due to the damping effect and the contribution from the radial modes is increased in the response, the surface motion becomes more and more complicated.

Fig 6.5 shows the axial surface displacement of the disc in the time range 200-240 μs. It can be seen that the high frequency modes are almost damped out, the low frequency radial modes dominate the transient response. Mode 1 at 50 kHz and mode 2 at 110 kHz are both seen in the response at 200 μs, while it can be shown that only the first radial mode at 50 kHz (period 20 μs) remains at around 300 μs.

It is evident that the transient surface displacement of this PZT5A disc with a D/T ratio of 20 has three different phases when it is excited by voltage pulses. At the initial stage, the disc vibrates at a frequency close to the most strongly excited mode at 965 kHz, but exhibits almost piston-like motion due to mode coupling with other adjacent high frequency modes. At the second stage, the disc vibrates in a very complicated manner since all the modes including radial modes contribute to the response. The third stage is that the high frequency modes are damped out, only the low order radial modes are still in the response, and the first radial mode is the last mode in the response to die away.

2. Rectangular pulse

Similar computations were made for the response to a rectangular voltage pulse excitation, since it is easily generated in experimental studies. The pulse was assumed to have a duration of 0.2 μs. Since the pulse is relatively short, the frequency content is believed similar to that of Dirac pulse in the frequency range from 0 to 1500 kHz.

The transient axial mechanical response at the central point of the surface of the disc is shown in Fig 6.6 over the periods 0 to 20 μs and 0 to 200 μs. It can be seen that the response is very similar to that for the dirac pulse shown in Fig 6.1.

Snap shots of the surface movement of the disc within the first 2 μs are shown in Fig 6.7. Again the results are similar to those obtained with Dirac pulse excitation.

3. One cycle sine wave

The transient response was also calculated for a one cycle sine voltage wave excitation applied to the piezoelectric disc. This is of interest since many practical excitation pulses have an approximately zero mean value. Therefore, the response to a single cycle sine wave will have features seen with these practical pulses.

Fig 6.8 shows the transient response of the disc at the central point of the surface to a single cycle of 1 MHz sine wave voltage. It can be seen that the high frequency components, in particular, mode 32 at 965 kHz, clearly dominates the response at the initial stage of the response. This is then followed by the low frequency radial modes. The snap shots of the surface movements of the disc, shown in Fig 6.9 for this case from 0 to 2 μs, also exhibit the piston-like features seen with the previous pulses.

The above results, particularly the transient surface movement of the disc in the first phase, may be significant. It indicates that the disc initially (over about 2 periods of the through thickness resonance by the 1D theory) is able to vibrate in a form close to the piston-like motion due to mode superposition of the thickness extensional modes when the disc is excited by voltage pulses. Since the transient response may be damped out after the first few periods of the through thickness resonance by other damping sources, such as the backing of the transducers, this result can be very encouraging. It explains that although there are many modes in the piezoelectric disc, and the mode shape of any one thickness extensional mode is quite different from the piston-like motion assumed by the

one dimensional theory, the superposition of the contributions from these many thickness extensional modes does produce motion close to a piston-like pattern in the transient response over the first few periods of the through thickness resonance.

6.2.2 A PZT5A disc with a D/T ratio of 10

It has been shown in Chapter 4 that the PZT5A disc with a D/T ratio of 10 has two equally strongly excited modes, one at 965 kHz and the other at 988 kHz. It is therefore of interest to see whether the piston-like motion obtained for the previous disc with a D/T ratio of 20 which had a single dominant mode is also seen with this disc.

The axial mechanical response at the central point of the disc is shown in Fig 6.10 from 0 to 20, and from 0 to 200 μs. The corresponding surface displacement from 0.1 to 4 microseconds are plotted in Fig 6.11. It can be seen that from these "snap shots" that the piston-like motion is also seen at the start of the response. However, the motion is much less well defined than that in the previous case shown in Fig 6.2, particularly after 1.5 μs.

6.2.3 A PZT5A disc with a D/T ratio of 0.5

The PZT5A disc with a D/T ratio of 0.5, which has been analysed in the previous chapters, is now discussed. Although the disc has six modes in the frequency range from 0 to 600 kHz, it has been shown in Chapter 4 that only the first mode at 133 kHz can be strongly excited by the voltage excitation since it has a much larger modal constant than those of the other modes.

Fig 6.12 shows the transient response by using the modal analysis technique, all six modes obtained in the eigenvalue solution being included in the calculation. It can be seen that the transient response shows almost purely sine oscillation though slight distortion is observed due to the effects of other modes. This demonstrates the dominance of a single mode in the response of the disc.

6.3 The measured transient voltage response of piezoelectric discs when various voltage pulses are applied

6.3.1 The measurement set up

Since it is very difficult to measure the transient surface displacement of piezoelectric discs when a voltage pulse is applied across the electrodes on the top and bottom surfaces of the disc by conventional techniques, and the advance measurement techniques, such as

laser interferometry (Krammer, 1989), were not always available, a direct comparison with the computed mechanical response of the disc is not sought at moment. It was decided to measure the induced voltage response of the piezoelectric disc when the disc is excited by a voltage pulse (Ying *et al.*, 1979), and to analyse the frequency content of the response by ultrasonic spectroscopy (Pialucha *et al.*, 1989).

Fig 6.13 shows the measurement set up, which is slightly different from the one used to measure the electrical impedance as shown in Fig 4.8. A pulse generator (4001, Global Specialties Corporation) having an output impedance of 50 Ω, which is capable of generating a rectangular pulse with a duration as short as 0.1 μs and a single cycle sine wave up to a frequency of 20 MHz, is used to excite the piezoelectric disc. When a voltage pulse is applied to the disc the transient voltage response induced across the disc is picked up and recorded by a digital oscilloscope (LeCroy 9400). This voltage signal is then sent to a FFT analyzer (B&K 2033) to obtain the frequency spectrum of the response. The peaks in the spectrum correspond to the resonant frequencies of the vibration present in the response.

6.3.2 The experimental results

1. A PZT5A disc with a D/T ratio of 20

Fig 6.14 shows the excitation and the transient response of the PZT5A disc with a D/T ratio of 20, in which Fig 6.14(a) is the induced transient voltage response across the disc, and the voltage excitation pulse of duration 0.1 μs is also shown in the top of the right hand side of Fig 6.14(a). The sampling frequency used is 25 MHz, which is sufficiently high to avoid aliasing (Randall, 1977). Before the response in Fig 6.14(a) was sent to the FFT analyzer the excitation pulse shown in the response trace was gated out and then a Hanning window was applied to the response to avoid leakage (Randall, 1977); the corresponding spectrum of the voltage response was then obtained and is shown in Fig 6.14(b).

The spectrum shows the vibration modes which have been excited by the voltage pulse. Each peak in the spectrum represents a mode in the response, and the value of frequency corresponds to the resonant frequency of the mode. Table 6.1 lists the measured resonant frequencies by locating the peaks in the FFT spectrum of the transient response and those measured by the minimum of the electrical impedance in Chapter 4. It can be seen that there are a large number of modes which have been excited by the pulse. This verifies the result obtained in the previous chapters.

If the pulse generator has a very small output impedance, the electrical boundary conditions of the disc can be assumed to be short circuit after the disc is excited by the applied voltage pulse, and the peaks in the FFT spectrum should correspond to the resonant frequencies of the modes (or the frequencies at constant voltage). However, the pulse generator used here has a finite output impedance of 50 Ω, which violates the ideal electrical boundary conditions. Some discrepancy between the values of resonant frequencies measured by the electrical impedance and those measured by the FFT spectrum are therefore expected, particularly in the frequency range of the thickness extensional modes. This explains why the resonant frequencies measured by the transient method shown in Table 6.1 are all higher than those measured from the impedance plot.

Similar results have been obtained for a single cycle sine voltage of 1.0 MHz which was applied to a PZT4 disc with a D/T ratio of 20 (PZT4 has a Q factor of 500). The transient response from 0 to 200 μs is shown in Fig 6.15(a), and corresponding spectrum is shown in Fig 6.15(b). It can be seen that in this case the radial modes in the low frequency range are much less strongly excited than with the previous rectangular pulse due to the different frequency content of the pulse.

2. A PZT5A disc with a D/T ratio of 0.5

It has been shown in Chapter 4 that the first mode of the PZT5A disc with a D/T ratio of 0.5 can be excited much strongly. This can also be shown by the pulse excitation of the disc.

Fig 6.16(a) shows the transient voltage response across the disc when a rectangular pulse with a duration of 3.5 μs shown on the top of the right hand side of the figure is applied to the disc. The small distortion which occurs in the first few cycles and disappears soon afterwards indicates that there are some very weak high frequency components in the response. The response then essentially becomes a decaying sine wave. The form of the oscillation and the small distortion are very similar to the computed mechanical response shown in Fig 6.12. The FFT spectrum of the response is shown in Fig 6.16(b), the peak frequencies of the spectrum correspond to the resonant frequencies of the modes of the disc, and the first peak frequency in the spectrum is 134 kHz which is very close to the one measured by the impedance method at 133 kHz.

6.4 Conclusions

The transient mechanical response of piezoelectric disc when it is excited by a voltage pulse has been studied by the modal analysis technique.

It is evident from Chapter 4 (both prediction and measurement of frequency response functions and mode shapes) that the piezoelectric disc cannot vibrate in the piston-like motion suggested by the one dimensional theory at any single frequency. However, the transient study in this chapter has shown that it is possible for piezoelectric discs to vibrate in a form close to piston-like motion due to high modal density and mode superposition effects. The mechanism producing this simple motion has been explained.

The induced transient voltage response across piezoelectric discs when a voltage pulse is applied to the discs has been measured, and its corresponding spectrum has been computed. It has been shown that the measured resonant frequencies have close correlation with those measured by the steady state excitation (electrical impedance response). However, it would be very interesting to be able to measure the transient surface motion of the disc when it is excited by voltage pulses.

F1 (kHz)	F1 (kHz)	F1 (kHz)	F2 (kHz)
50	51	826	829
130	131	836	841
204	206	856	860
275	278	872	875
343	346	895	899
405	408		
461	464		
510	514	936	942
552	557	951	972
590	594	972	1000
620	626	1004	1041
698	700	1041	1082
730	733	1080	1126
764	768		
798	803		

Table 6.1 The measured resonant frequencies of the PZT5A disc with a D/T ratio of 20 by sweep sine and transient tests
F1: measured at the minimum electrical impedance in sweep sine test
F2: measured at the maximum of FFT spectrum in transient test.
(Blanks: modes in these ranges are too weak to be excited)

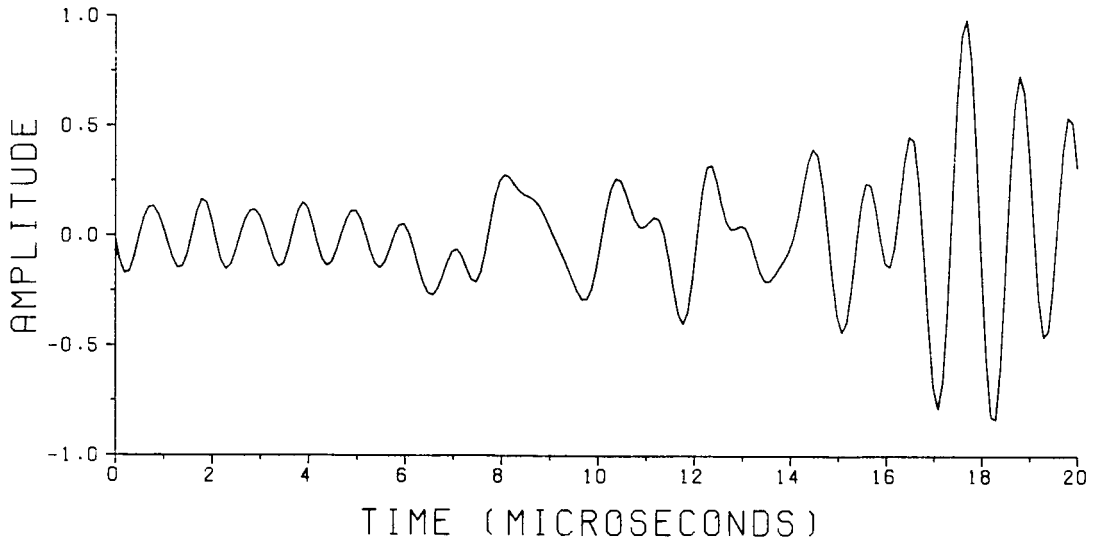

(a) 0 to 20 μs

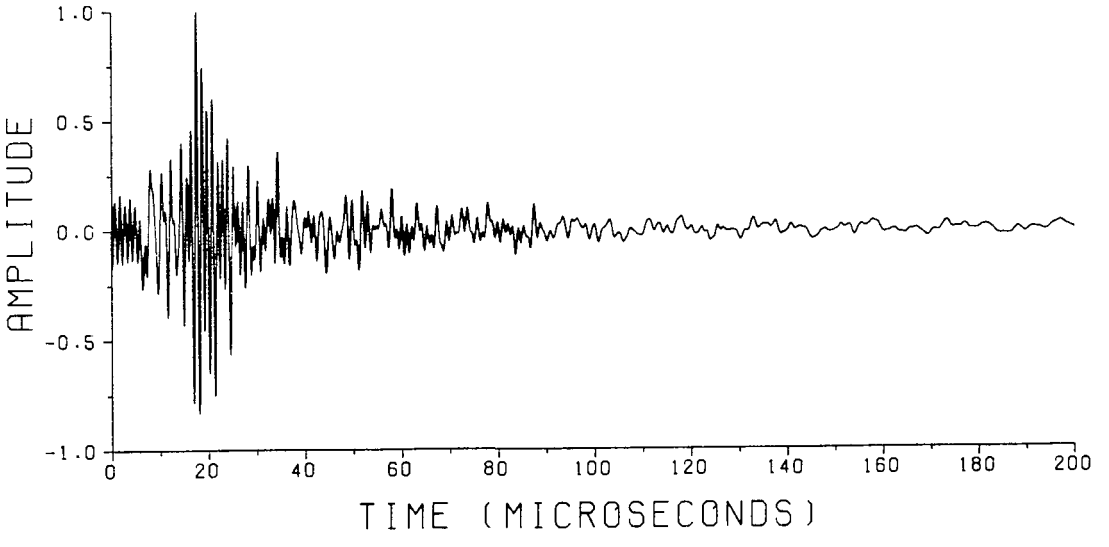

(b) 0 to 200 μs

Fig 6.1 The predicted transient axial displacement at the central point of the surface of the PZT5A disc with a D/T ratio of 20 when the disc is excited by a Dirac voltage pulse

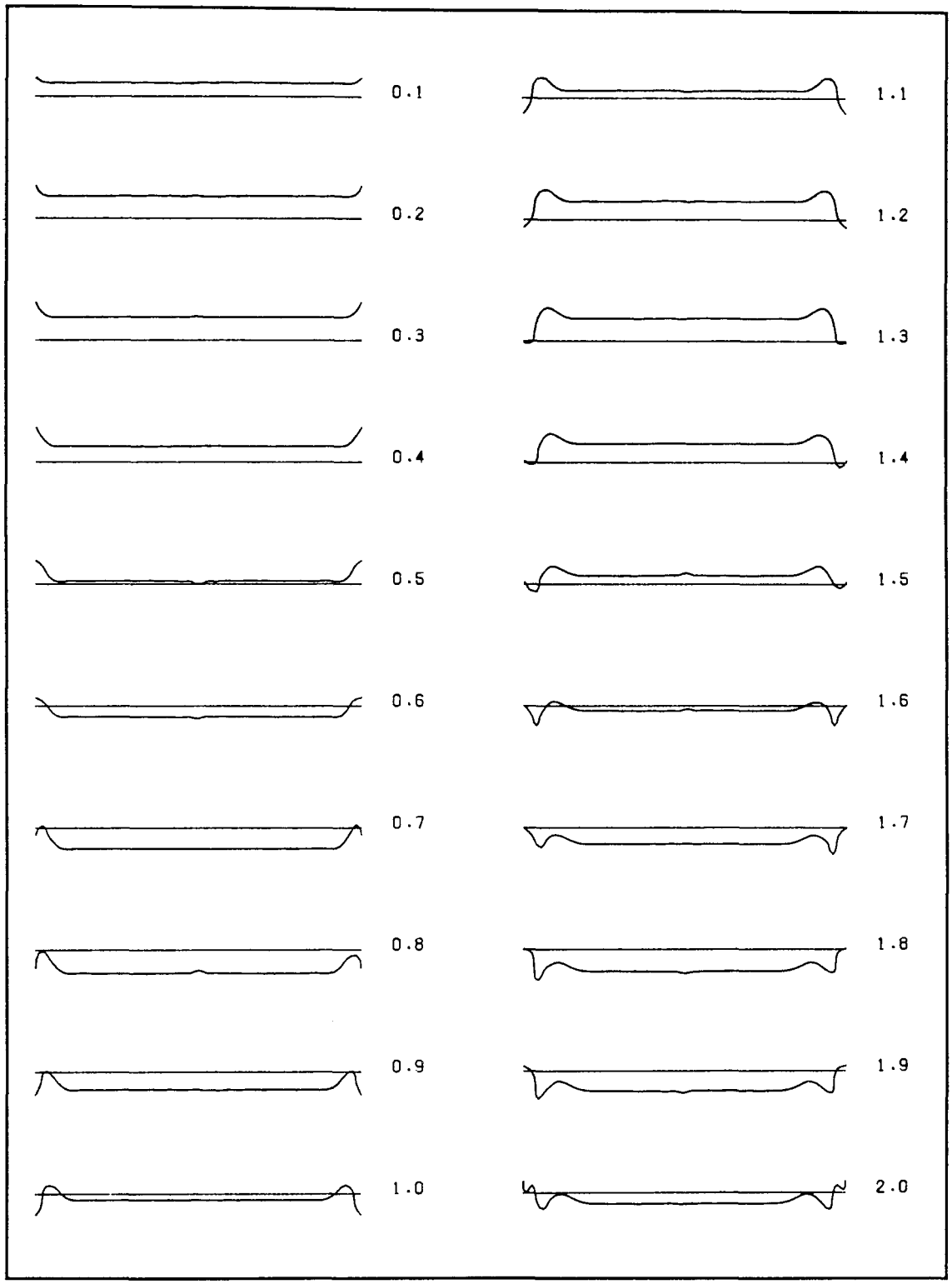

Fig 6.2 The predicted axial surface displacement of the PZT5A disc with a D/T ratio of 20 when the disc is excited by a Dirac voltage pulse (0.1 to 4.0 μs)

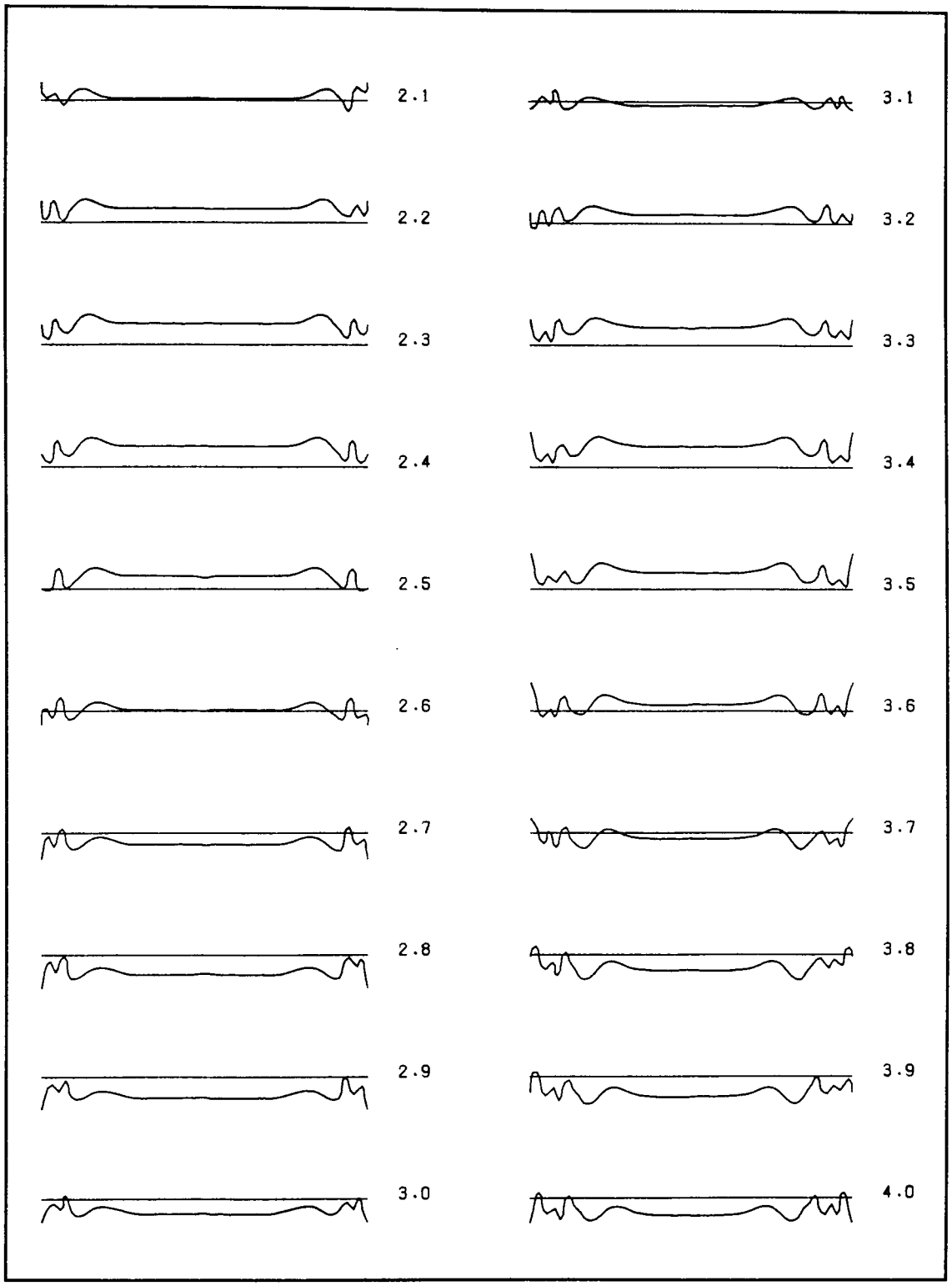

Fig 6.2 Continued (2.1 to 4.0 μs)

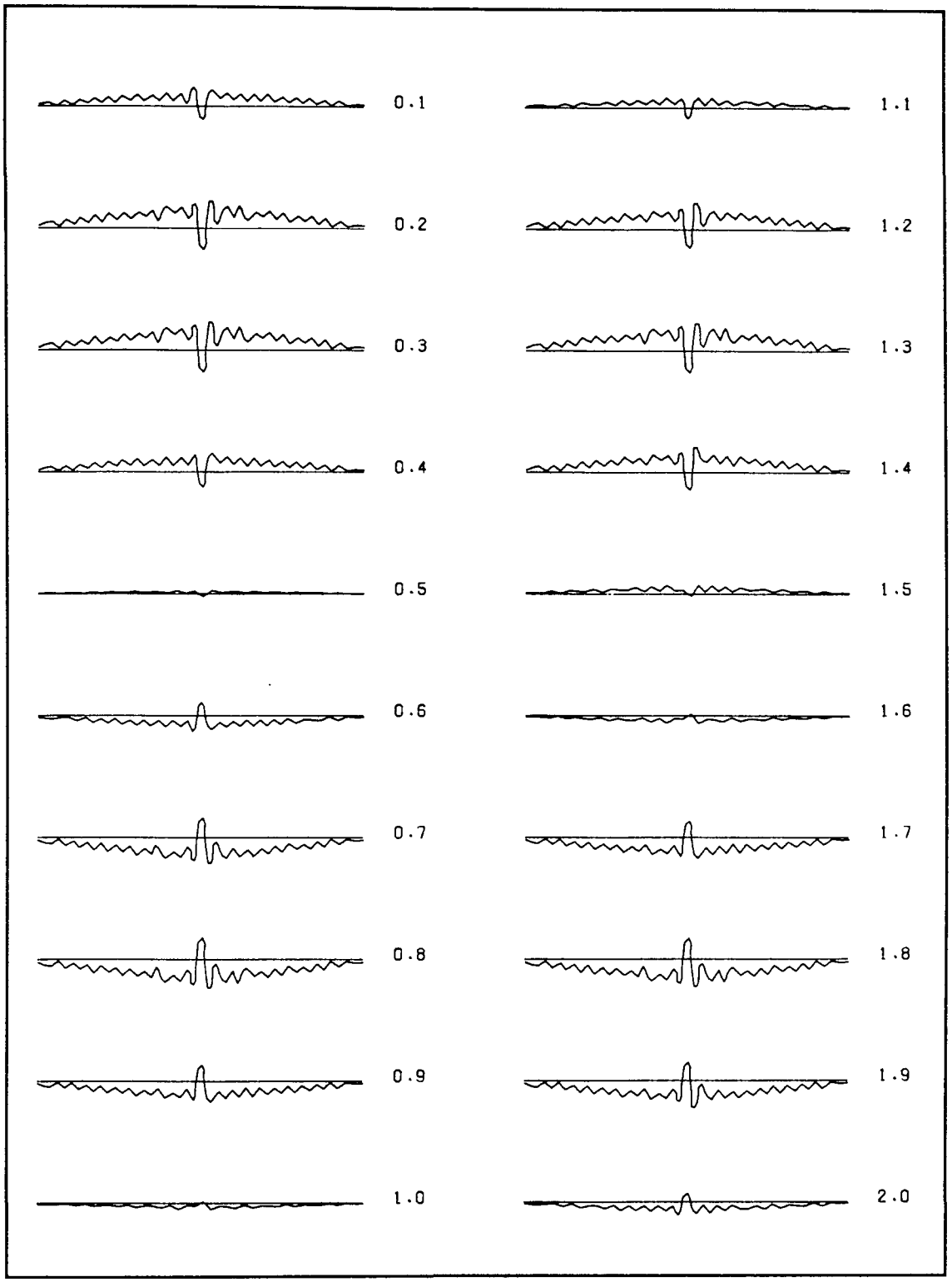

(a) Mode 32 at 965 kHz only

Fig 6.3 The predicted axial surface displacement of the PZT5A disc due to different mode components from 0.1 to 2.0 μs

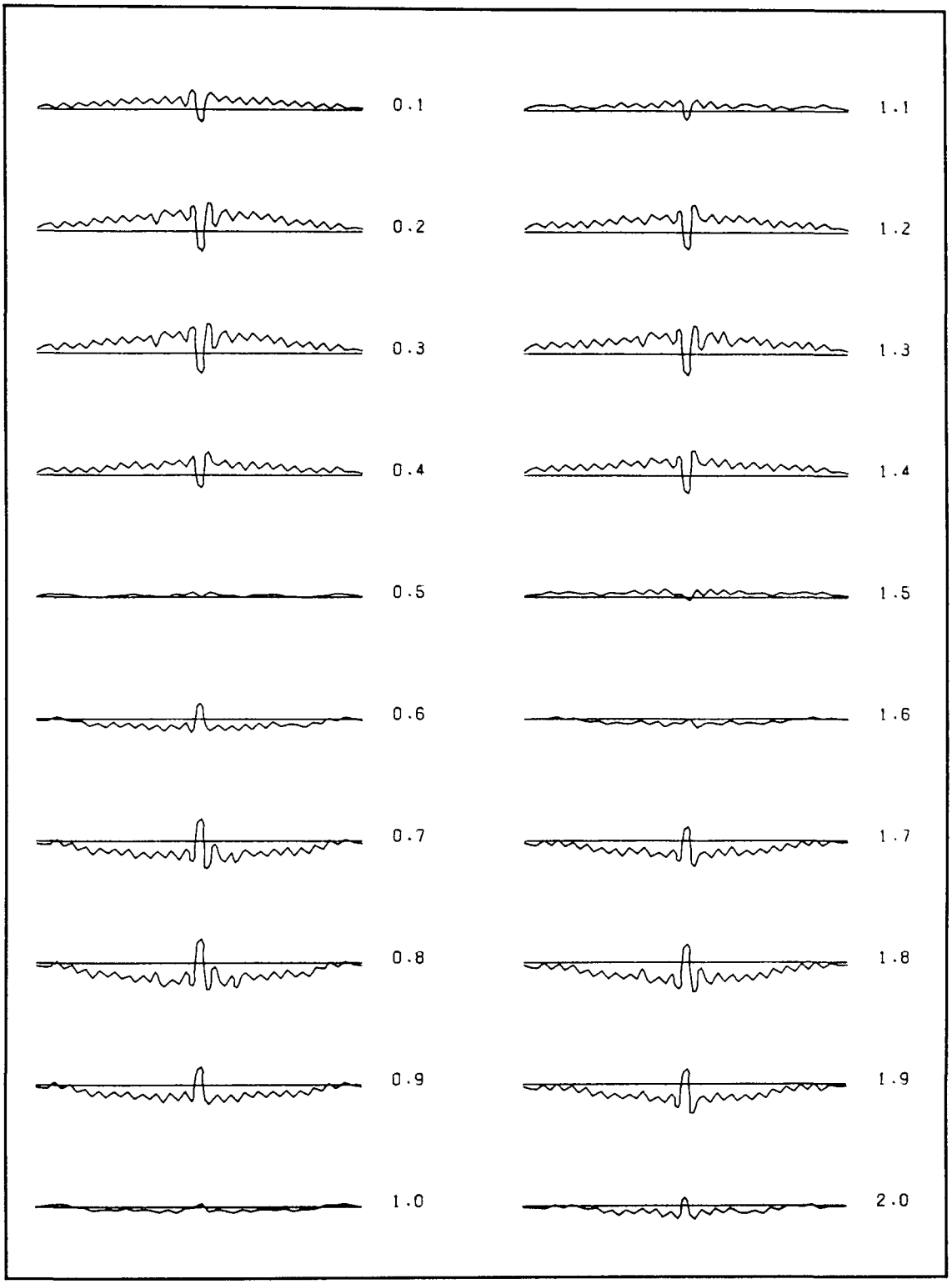

(b) Mode 32 + The first 5 radial modes

Fig 6.3 Continued

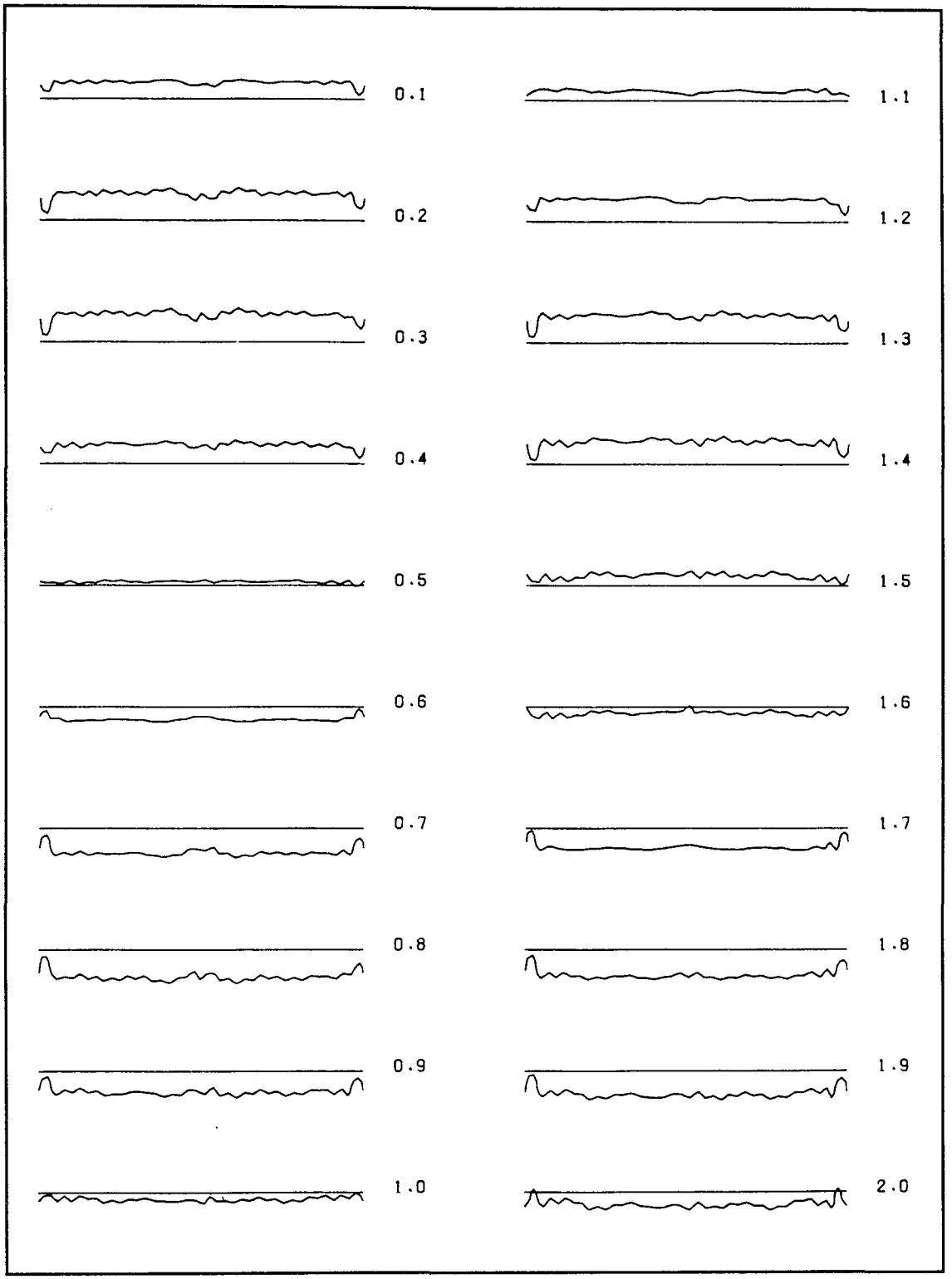

(c) Mode 32 + High frequency modes from 880 to 1080 kHz

Fig 6.3 Continued

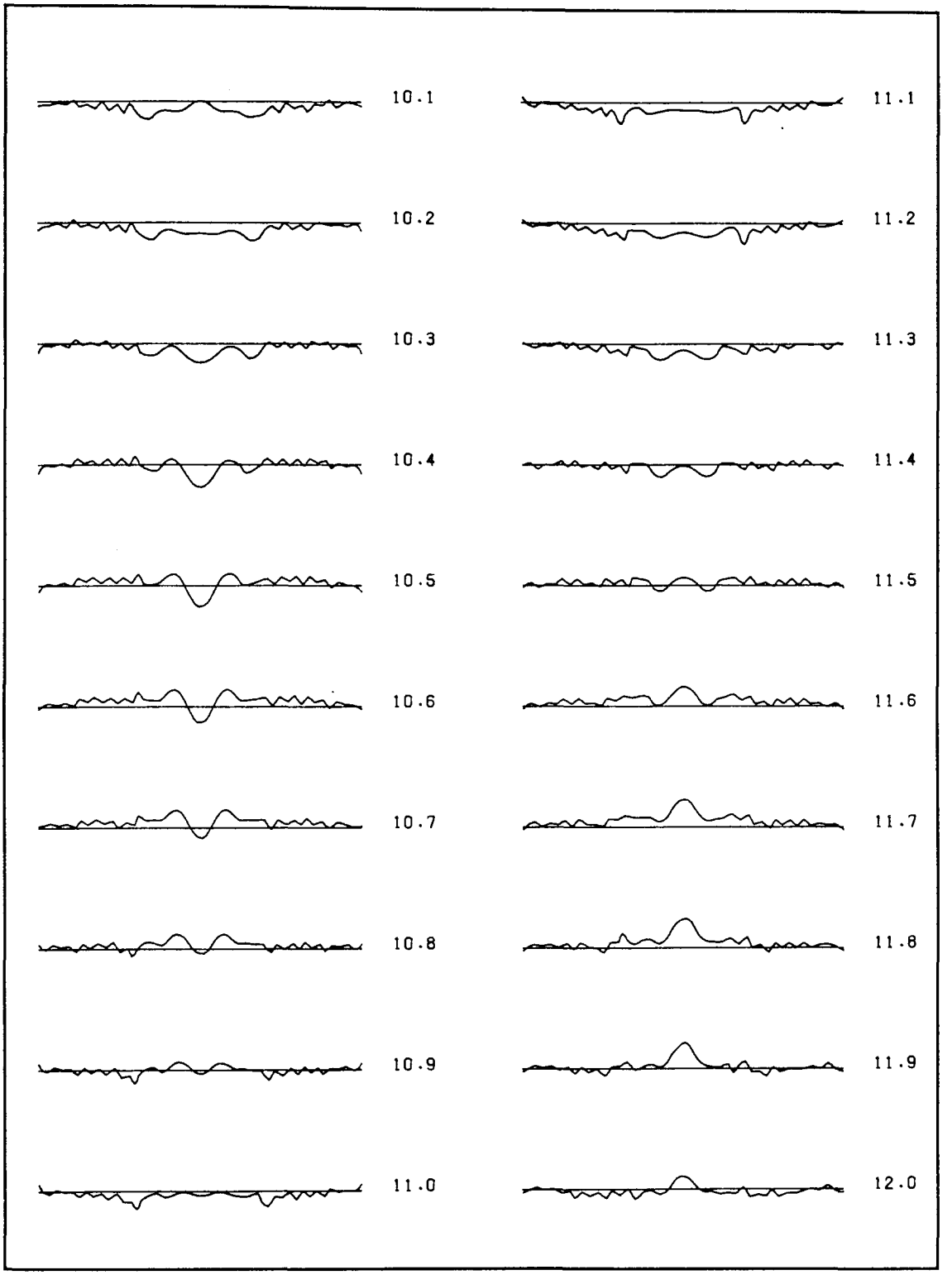

Fig 6.4 The predicted axial surface displacement of the PZT5A disc with a D/T ratio of 20 when the disc is excited by a Dirac voltage pulse (10.1 to 12.0 μs)

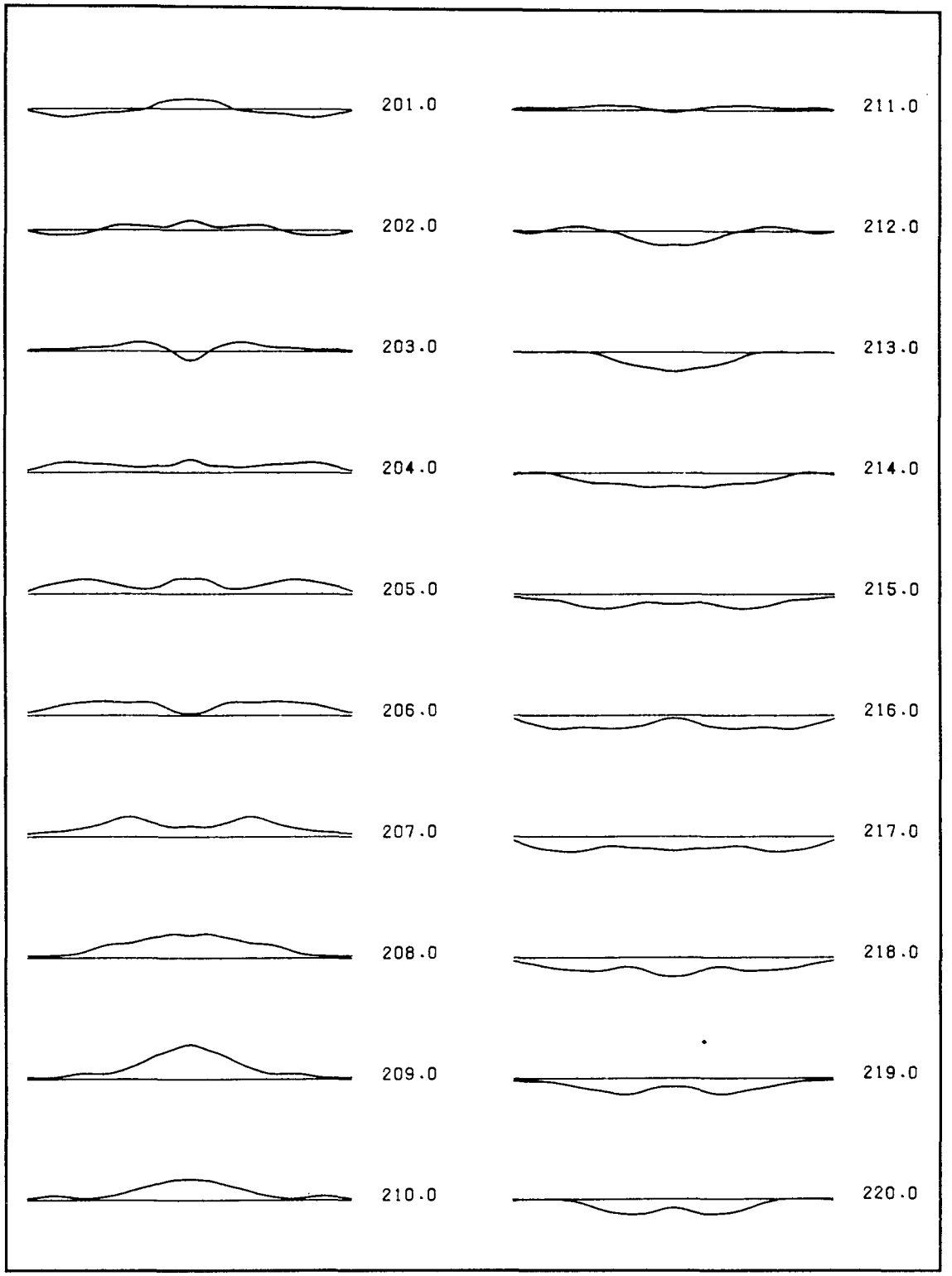

Fig 6.5 The predicted axial surface displacement of the PZT5A disc with a D/T ratio of 20 when the disc is excited by a Dirac voltage pulse (201 to 240 μs)

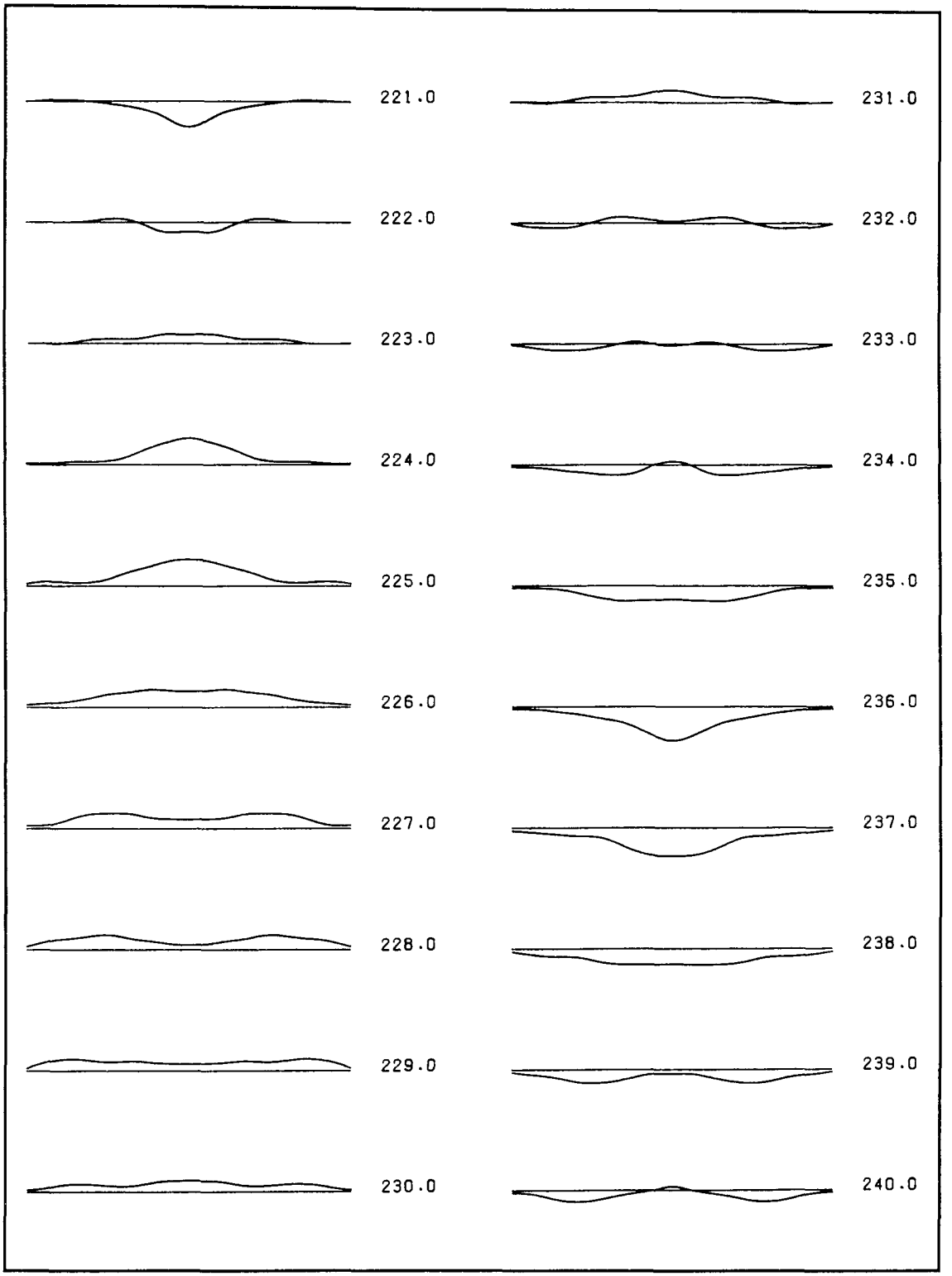

Fig 6.5 Continued (221 to 240 μs)

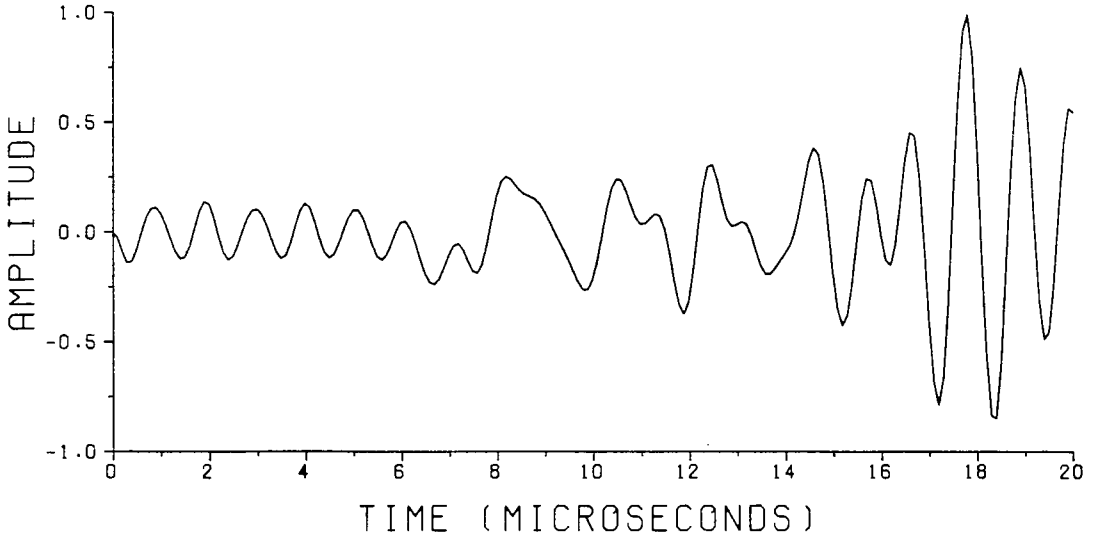

(a) 0 to 20 μs

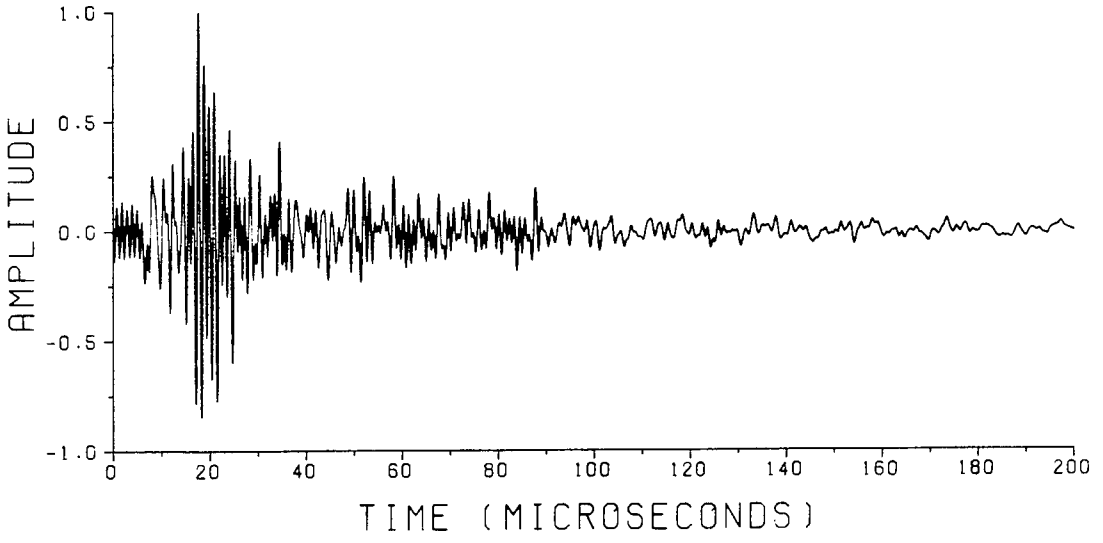

(b) 0 to 200 μs

Fig 6.6 The predicted transient axial displacement at the central point of the surface of the PZT5A disc with a D/T ratio of 20 when the disc is excited by a rectangular voltage pulse of 0.2 μs

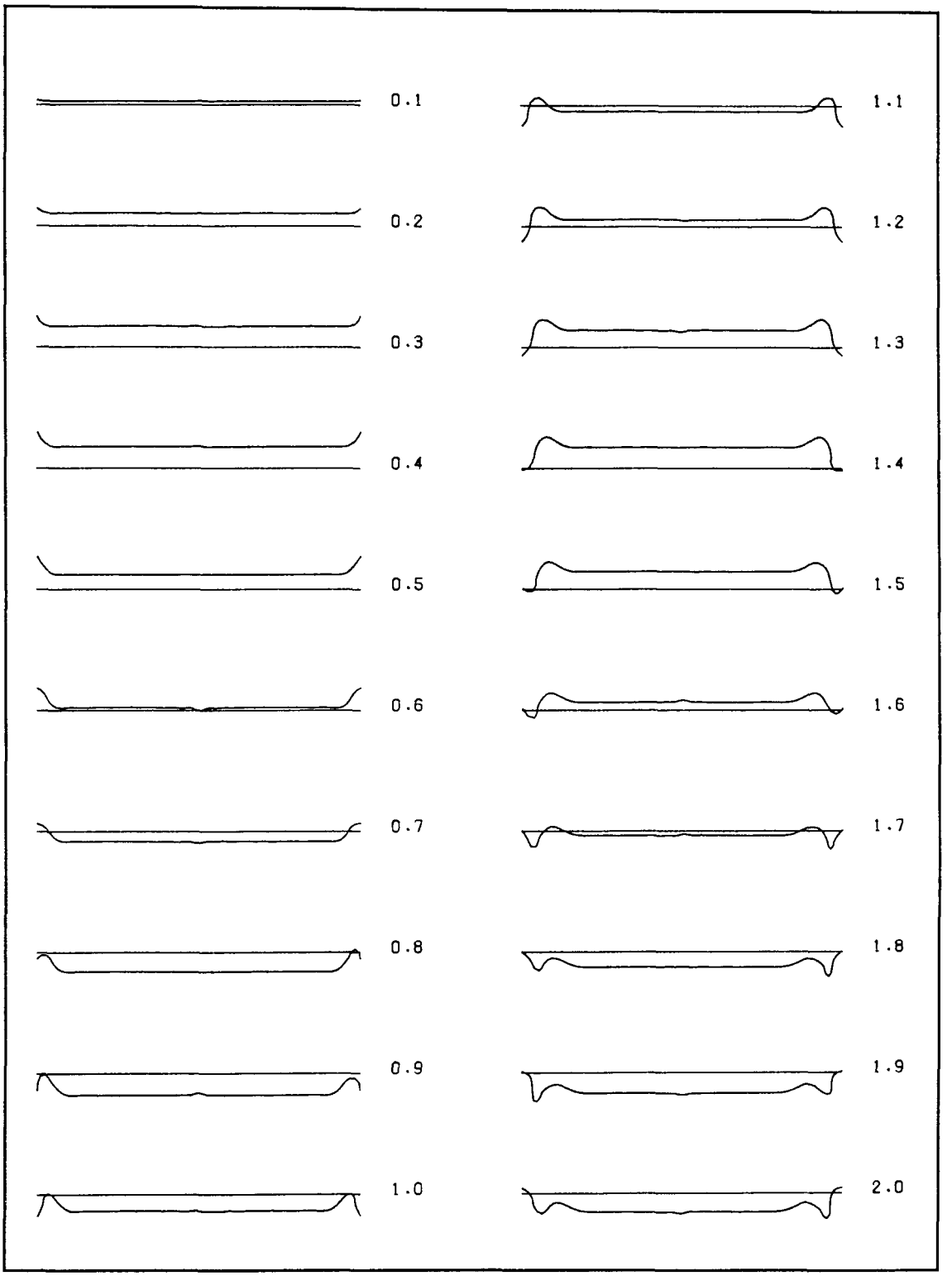

Fig 6.7 The predicted axial surface displacement of the PZT5A disc with a D/T ratio of 20 when the disc is excited by a rectangular voltage pulse of 0.2 μs (0.1 to 2.0 μs)

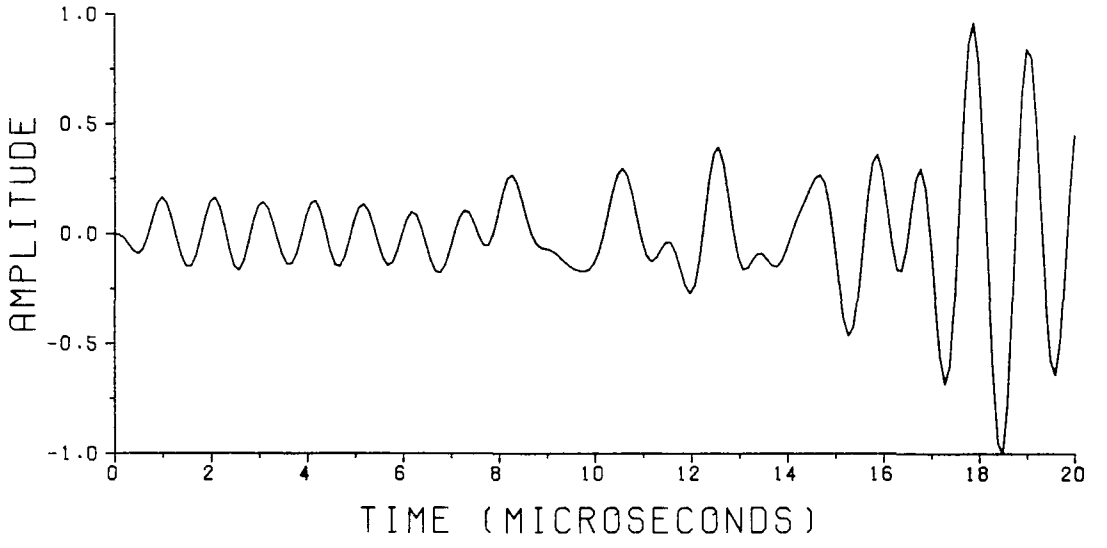

(a) 0 to 20 μs

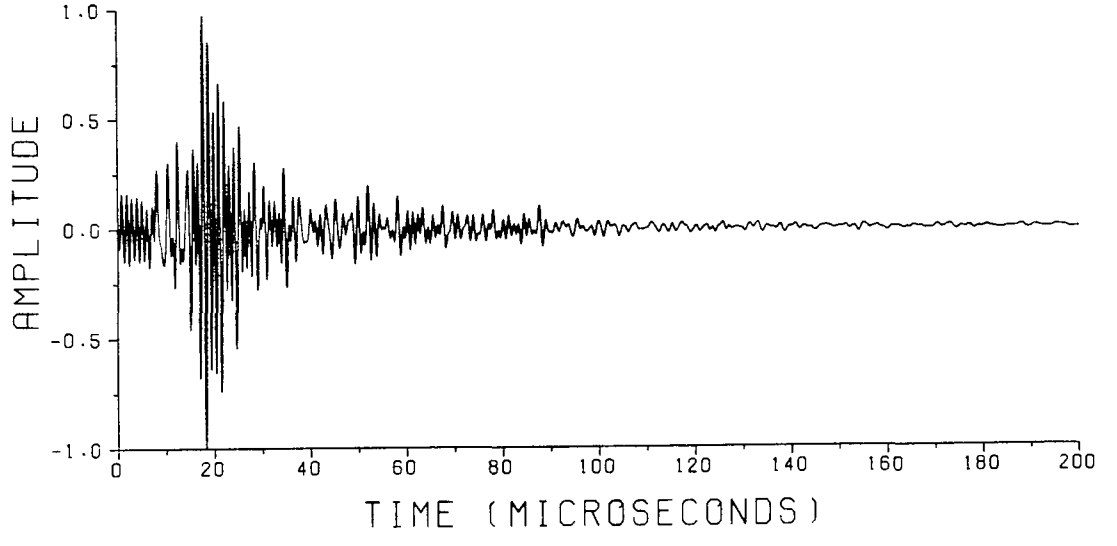

(b) 0 to 200 μs

Fig 6.8 The predicted transient axial displacement at the central point of the surface of the PZT5A disc with a D/T ratio of 20 when the disc is excited by a single cycle 1 MHz sine wave voltage

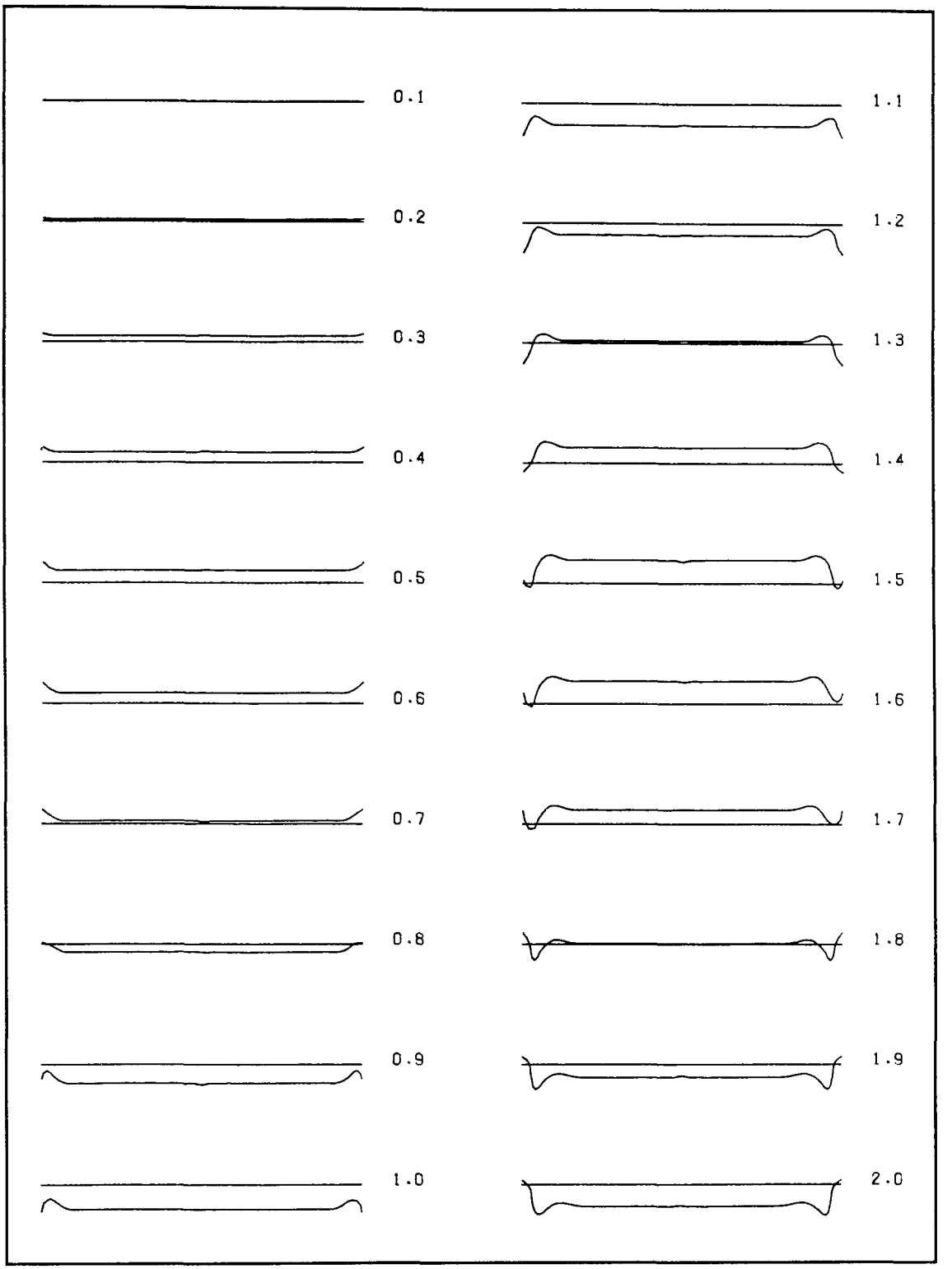

Fig 6.9 The predicted axial surface displacement of the PZT5A disc with a D/T ratio of 20 when the disc is excited by a single cycle 1 MHz sine wave voltage (0.1 to 2.0 μs)

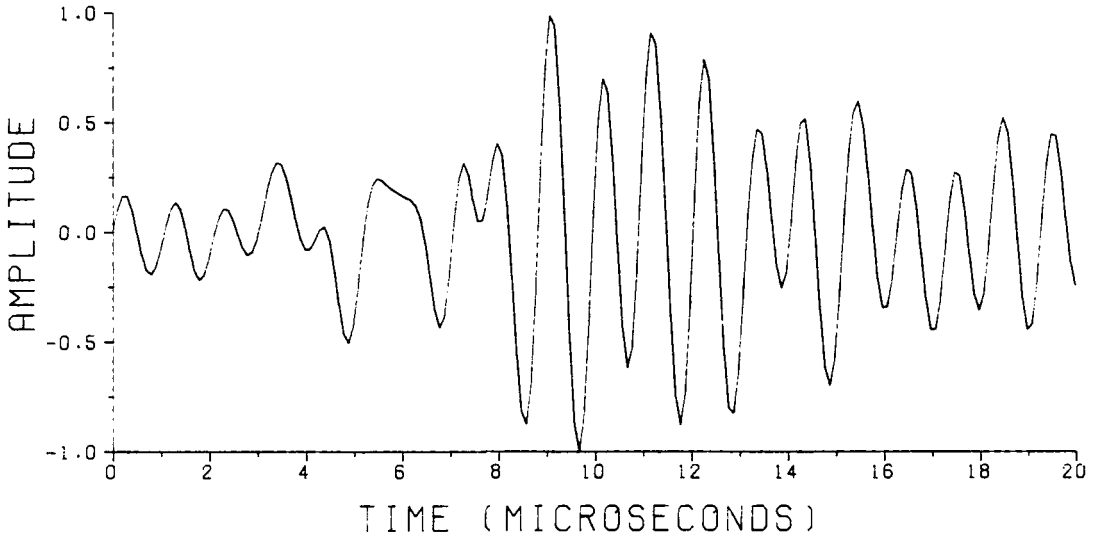

(a) 0 to 20 μs

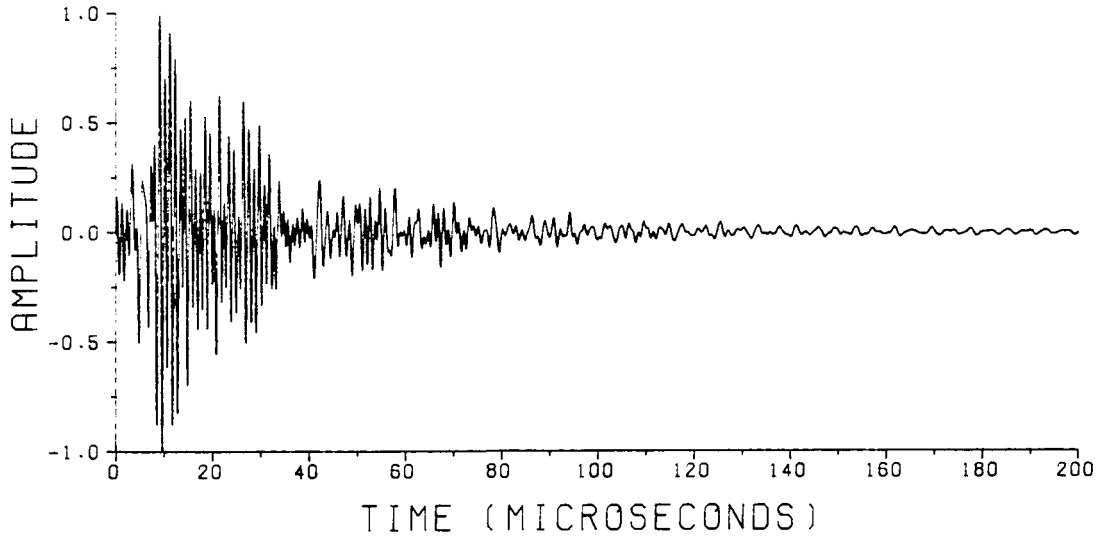

(b) 0 to 200 μs

Fig 6.10 The predicted transient axial displacement at the central point of the surface of the PZT5A disc with a D/T ratio of 10 when the disc is excited by a Dirac voltage pulse

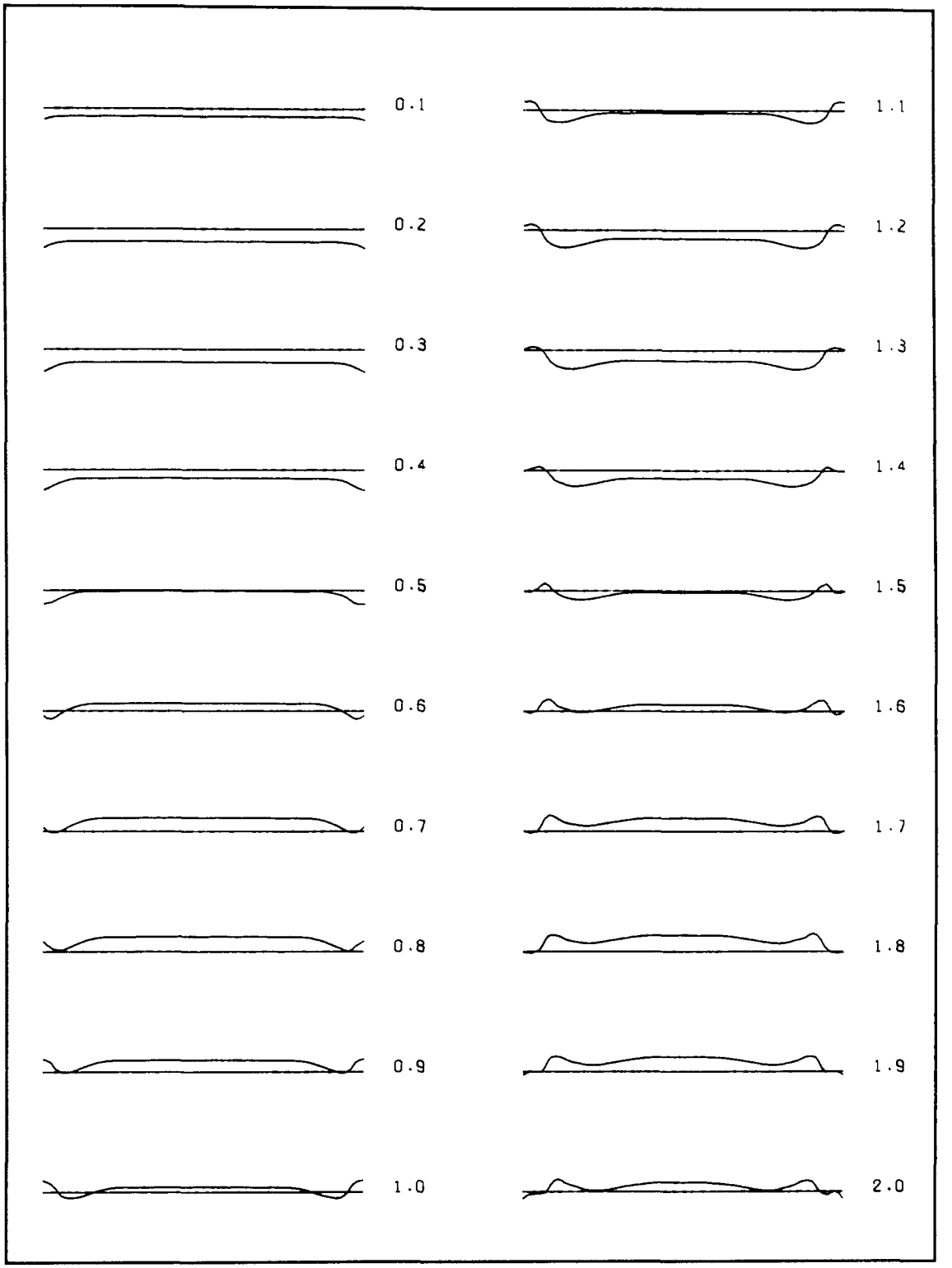

Fig 6.11 The predicted axial surface displacement of the PZT5A disc with a D/T ratio of 10 when the disc is excited by a Dirac voltage pulse (0.1 to 4.0 μs)

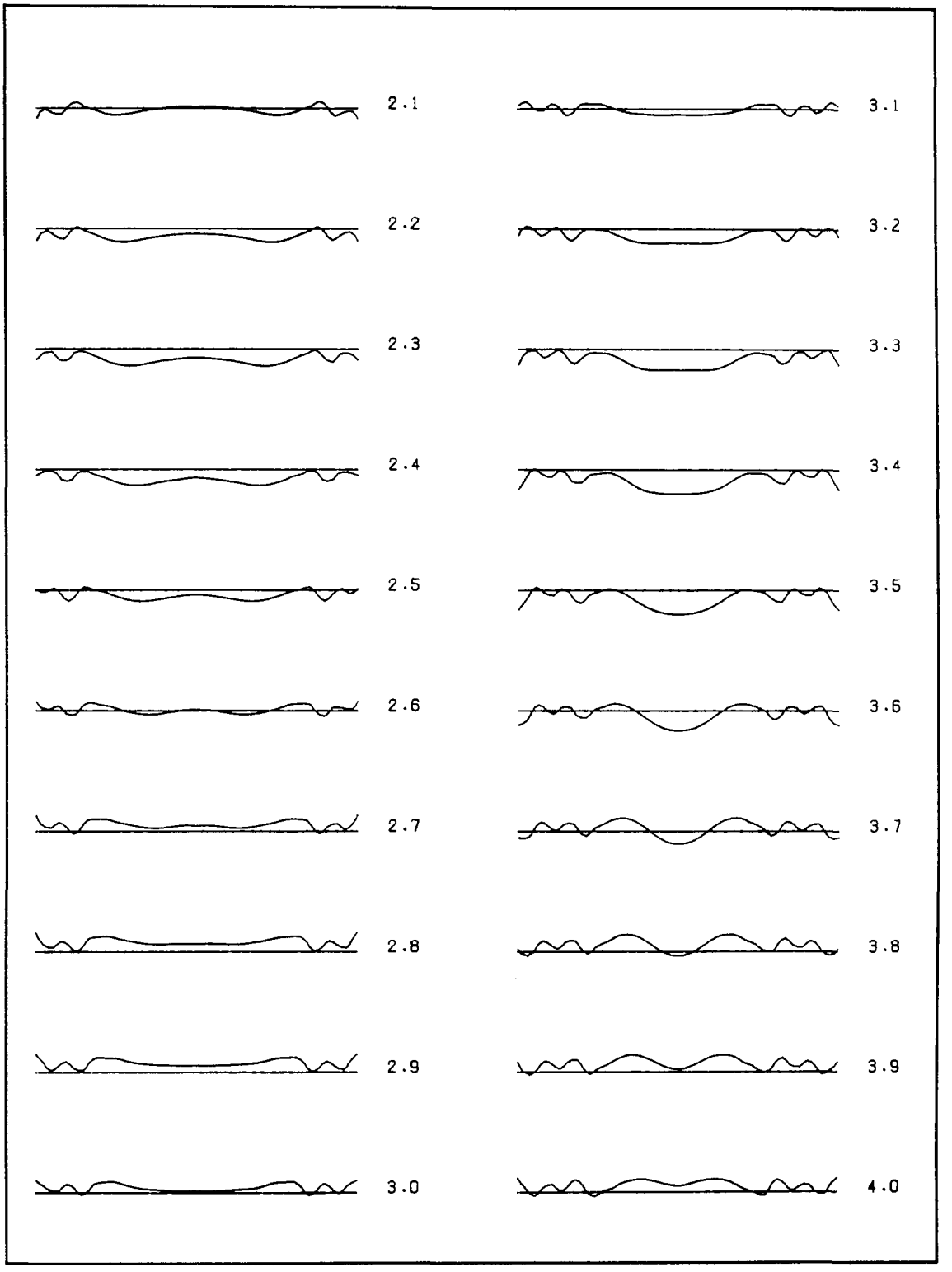

Fig 6.11 Continued (2.1 to 4.0 μs)

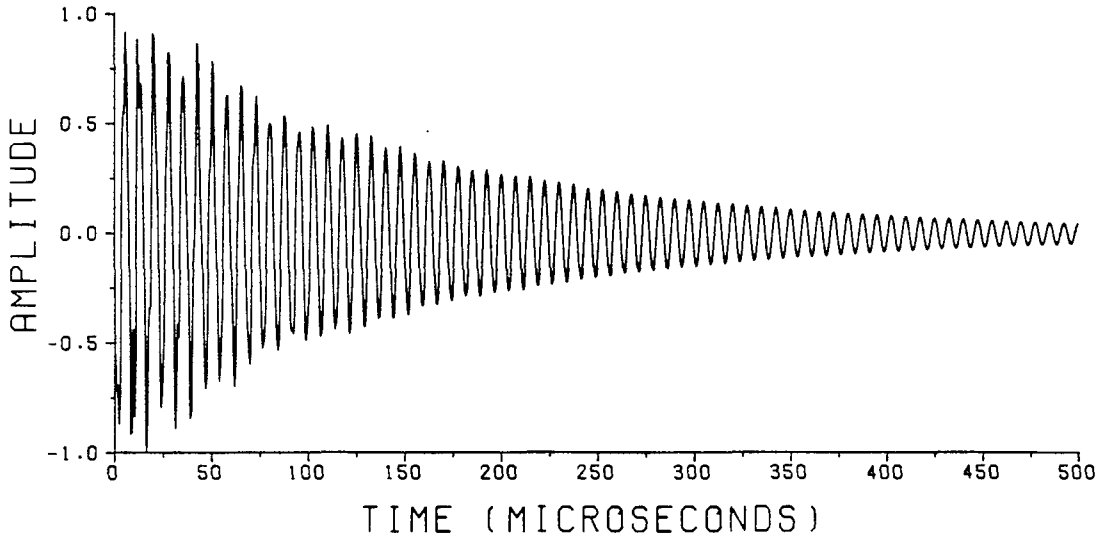

Fig 6.12 The predicted transient axial displacement at the central point of the surface of the PZT5A disc with a D/T ratio of 0.5 when the disc is excited by a Dirac voltage pulse

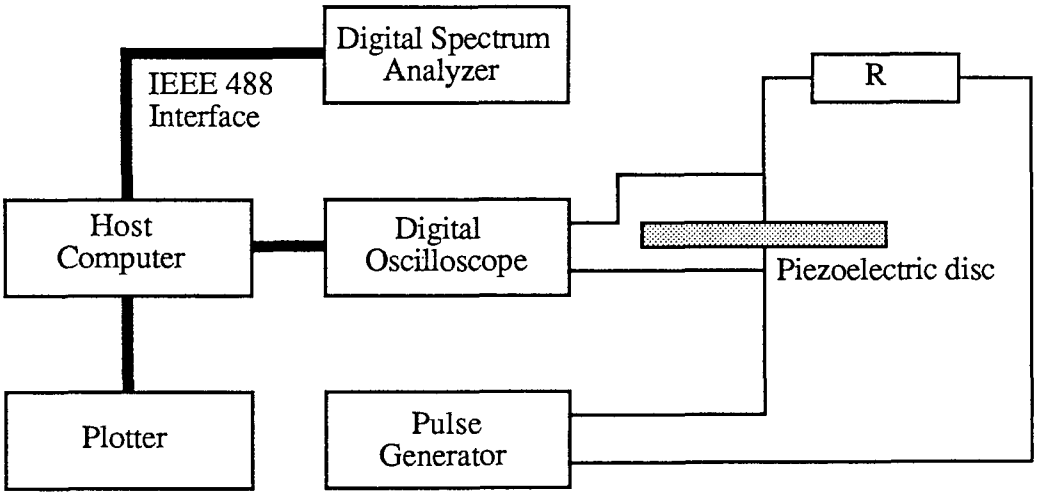

Fig 6.13 Configuration of the apparatus used in pulse excitation

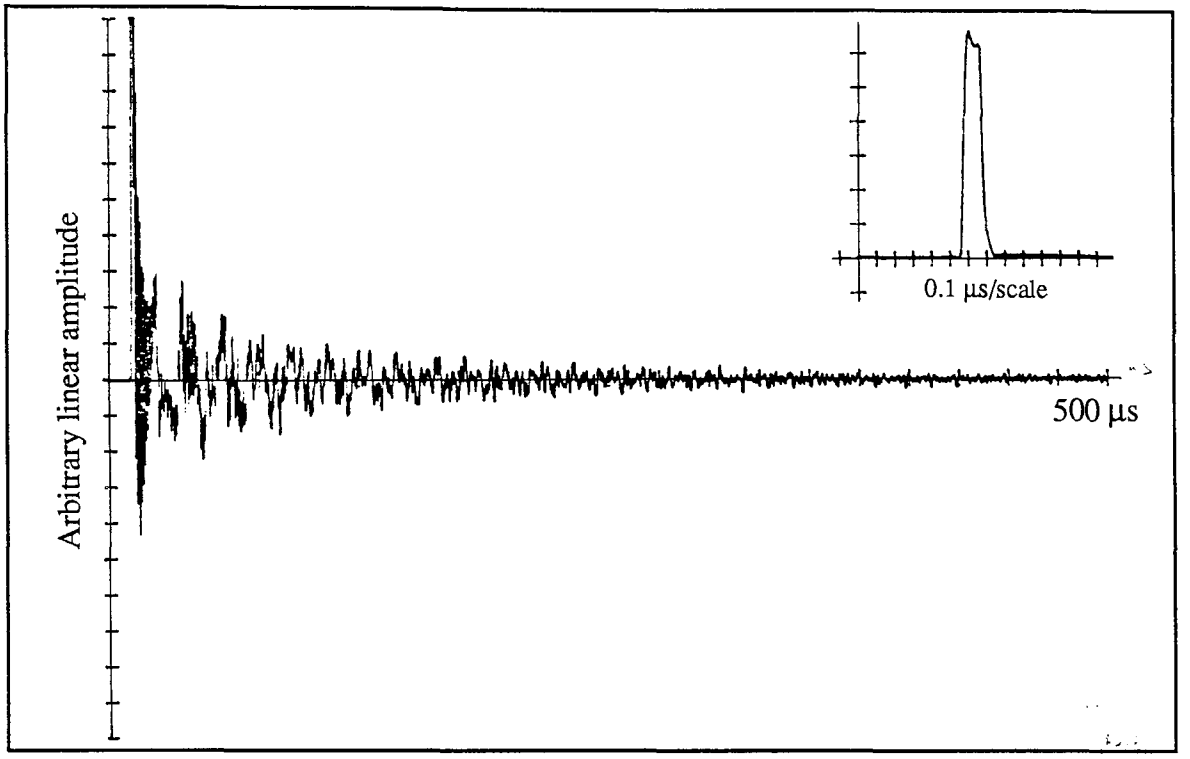

(a) the induced transient voltage response across the disc

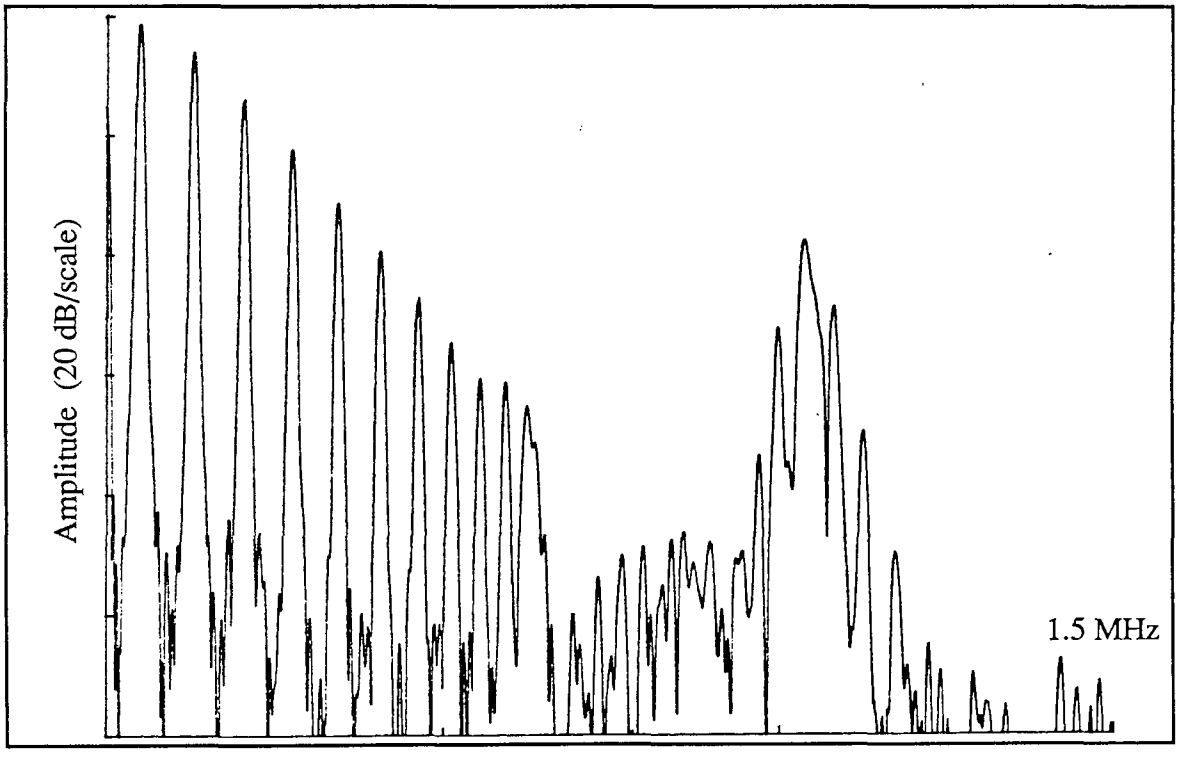

(b) the spectrum

Fig 6.14 The transient response of the PZT5A disc with a D/T ratio of 20 to a rectangular pulse with duration 0.1 μs

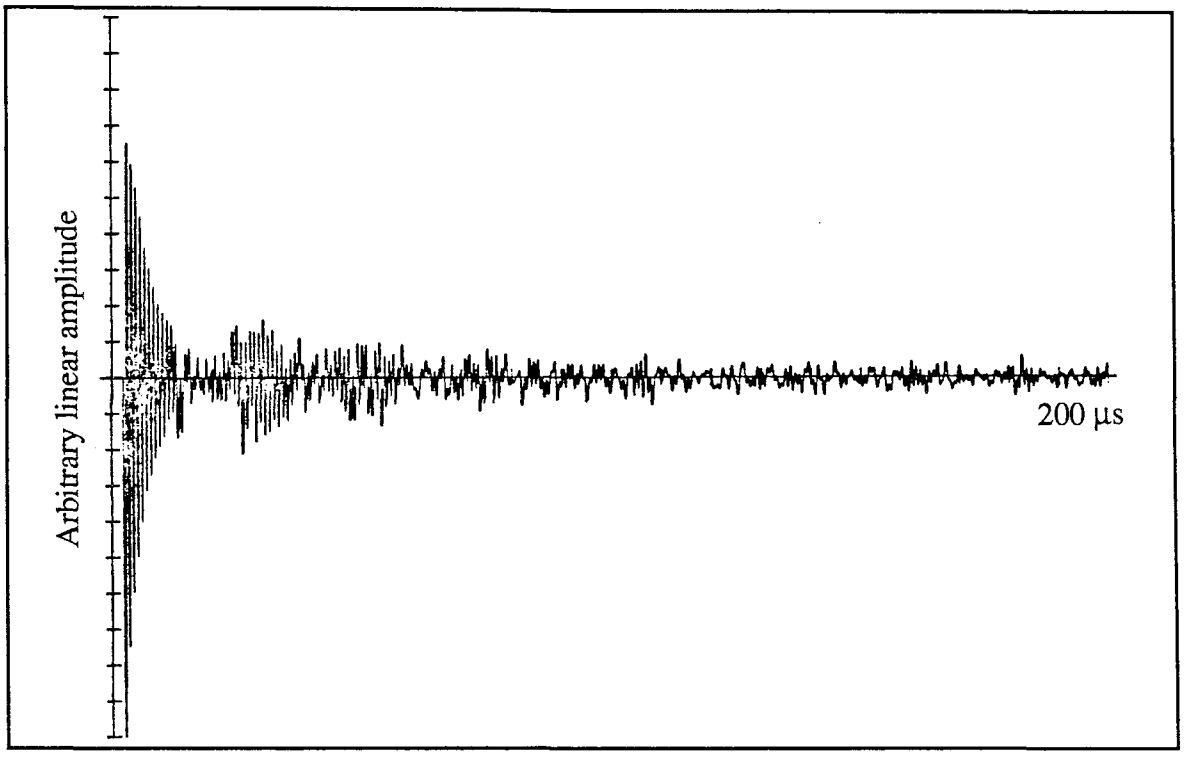

(a) the induced transient voltage response across the disc

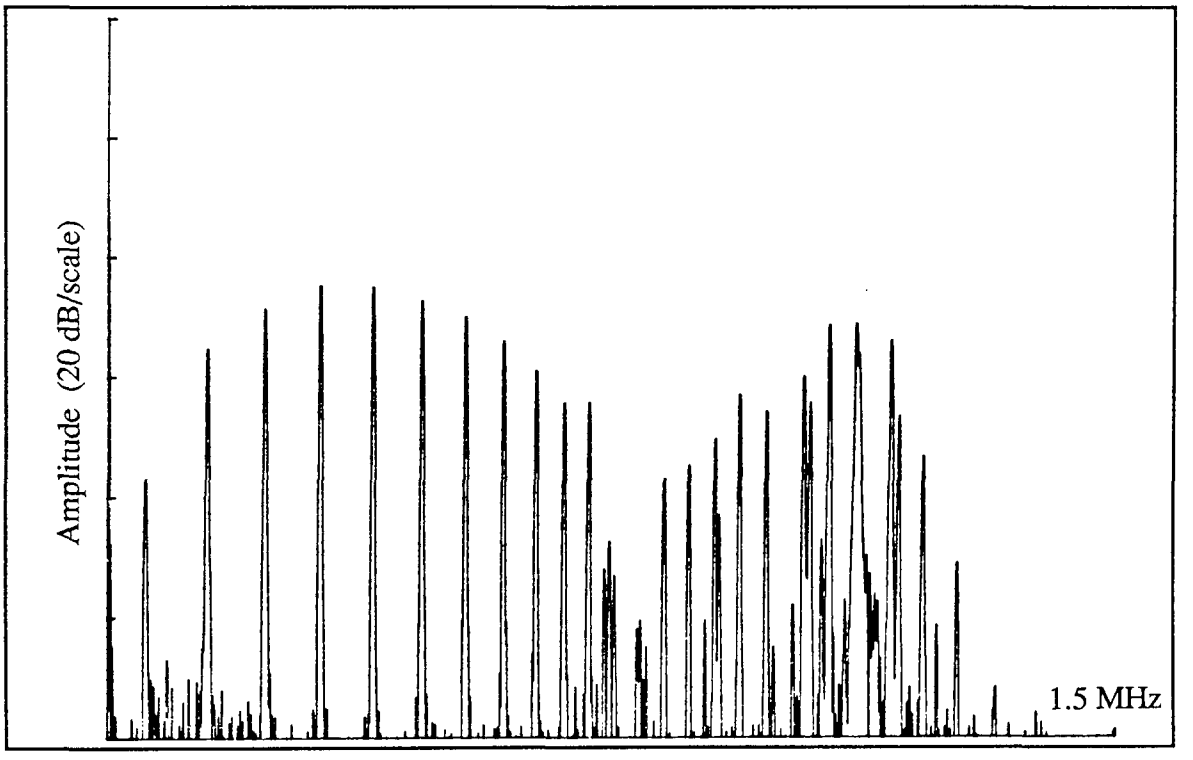

(b) the spectrum

Fig 6.15 The transient response of the PZT4 disc with a D/T ratio of 20 to a single cycle 1.0 MHz sine voltage

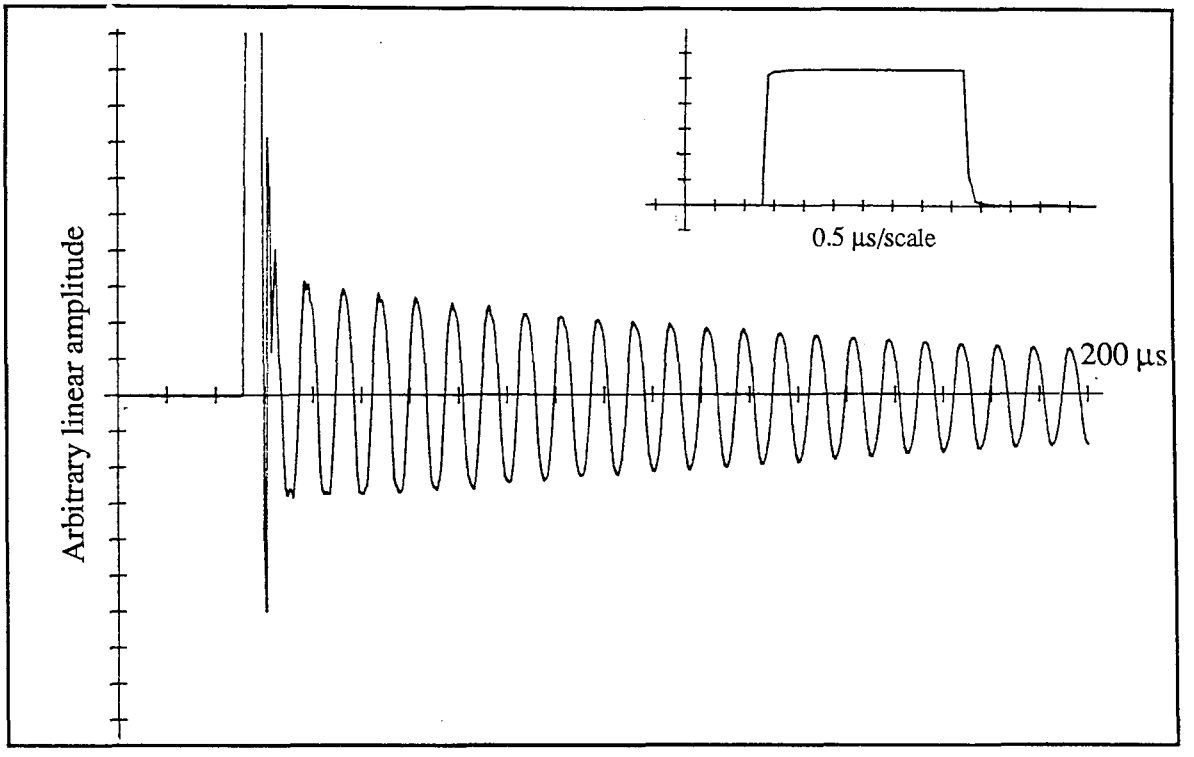

(a) the induced transient voltage response across the disc

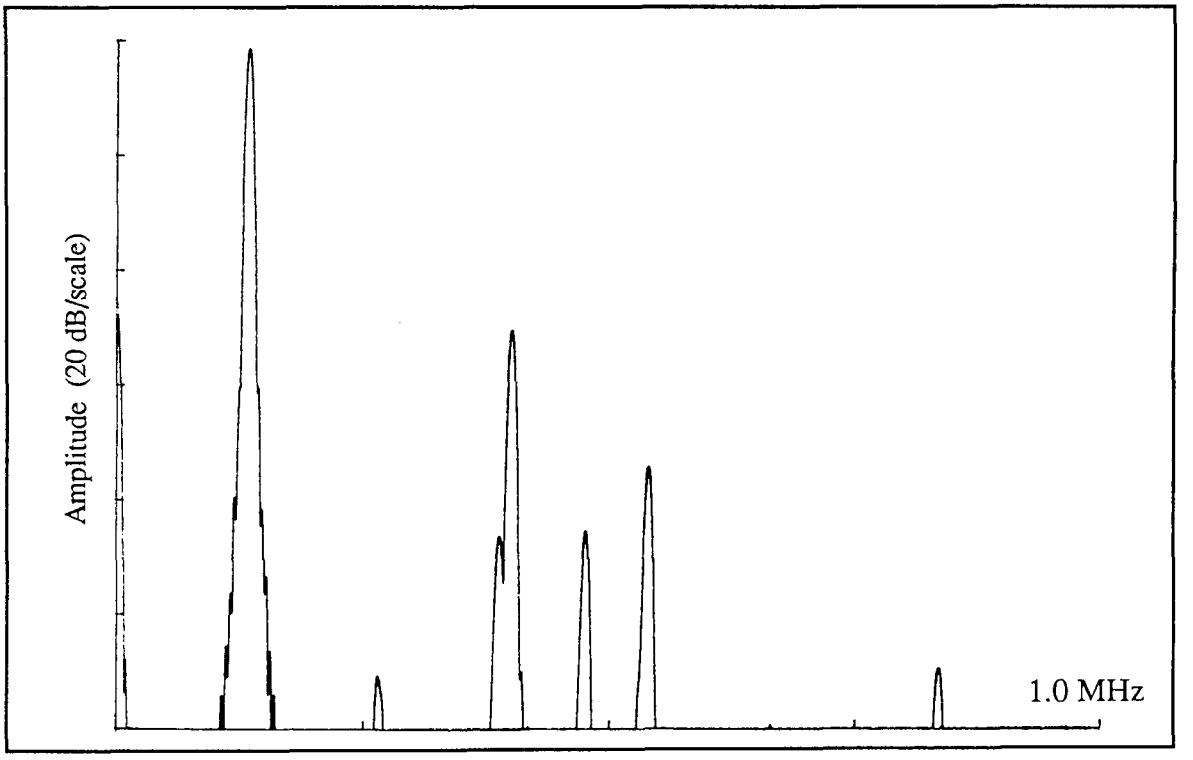

(b) the spectrum

Fig 6.16 The transient response of the PZT5A disc with a D/T ratio of 0.5 to a rectangular pulse with duration 3.5 μs

CHAPTER 7

THE APPLICATION OF THE THREE DIMENSIONAL MODEL TO OTHER PIEZOELECTRIC DISCS

7.1 Introduction

The vibration characteristics of piezoelectric discs have been studied in the previous chapters. The natural frequencies and mode shapes of the vibration modes have been predicted by the eigenvalue solution, the frequency response function and the electrical impedance of the disc have been calculated by the modal analysis techniques, and the transient mechanical response of the disc when a voltage pulse is applied across the disc has been calculated.

In this chapter the analyses are extended to some other aspects of the piezoelectric disc. The damping sources of a piezoelectric transducer which include mechanical damping and electrical loss are discussed first. Piezoelectric discs with an elastic addition are then studied in order to see the effects of the addition on the vibration characteristics of the disc, which may help the understanding and modelling of the backing of piezoelectric transducers. Furthermore, the three dimensional model is applied to predict the vibration characteristics of some other piezoelectric discs, such as the discs which are partially electroded on the top and bottom surfaces.

7.2 Analysis of damping sources in piezoelectric transducers

The damping effect is very important in the performance of ultrasonic transducers. In linear vibration theory it is often modeled in idealised forms, such as viscous damping and structural or hysteretic damping. The damping in piezoelectric transducers is very complicated since there are many damping sources in the transducers. Generally they can be classified as mechanical damping and electrical damping.

7.2.1 Mechanical damping

One source of mechanical damping in transducers is material damping in the piezoelectric elements, which has already been modeled successfully as proportional damping in the previous chapters, i.e., in terms of structural damping factors in steady state analyses and in terms of viscous damping in transient analyses. The other sources of mechanical

damping include loss in the bonding layers between the piezoelectric element and backing, and between the element and matching layer, etc. However, if the bonding layer can be assumed to be perfect and negligibly thin, the effects of these damping sources are not very significant (Silk, 1983).

The main damping source in ultrasonic transducers is the backing of the transducers, which is designed to remove reflections from the back face of the disc, or to reduce vibration of the disc to such extent that the oscillation of the piezoelectric disc only lasts a very few cycles.

A backing block which has the same acoustic impedance as that of the piezoelectric disc is called matched backing, and it usually has a very high loss factor. From the wave transmission point of view, when an elastic wave reaches the boundary between the disc and a matched backing, the wave is completely transmitted into the backing part from the piezoelectric disc due to the matched impedance, and the transmitted wave is then heavily absorbed when it propagates through the backing due to the high loss nature of the backing material, which results in very little energy coming back to the piezoelectric disc. From the vibration point of view, it is known that the high lossy extra mass can damp out the vibration level of the disc and shift the resonant frequencies of the original structure; however, it is not very clear how exactly this backing affects the vibration characteristics of the disc, such as the resonant frequencies, mode shapes and corresponding modal constants of the different types of vibration modes.

Backing was not intended to be analysed in this thesis; however, in Section 7.3 some brief studies are carried out to investigate the effect of an elastic addition on the vibration characteristic of piezoelectric discs, which may assist the understanding and further modelling of transducers.

Apart from the damping inside the ultrasonic transducers, there are other sorts of mechanical damping, such as the loss from interaction with surrounding fluids when the transducers are operated in immersion mode, or the damping from the contact gel when it is operated in contact with specimens.

7.2.2 Electrical damping

Another source of damping in piezoelectric transducers is electrical losses. The electrical loss may come from the internal dielectric loss of the piezoelectric material, i.e., the

tangential loss (Hilke, 1973). This part is usually very small and negligible for most of materials, and can be modeled as the imaginary part of the material constants.

The electrical damping may be increased by an electrical resistor in the electric circuit (O'Donnell *et al.*, 1981). In real transducers there are frequently electrical components inside transducer housing, such as resistors in series with the piezoelectric disc and inductors in parallel with the piezoelectric disc which form a matching network between transducers and generators. The series resistor is designed to increase the minimum impedance of the transducers and to match to the output impedance of the electrical sources, the bandwidth of the vibration modes is therefore increased significantly.

Fig 7.1(a) illustrates the predicted electrical impedance of the PZT5A disc with a D/T ratio of 20 in series with resistors as the value of the resistor varies from 0 to 5, 20 and 50 Ω. Fig 7.1(b) shows the corresponding measured impedances of such a system. It can be seen from both the measurements and the predictions that the minimum values of the impedance of the piezoelectric discs have been increased significantly around the resonances, and the corresponding bandwidths are increased.

The actual effect of the electrical damping due to the series resistor is that the real part of the impedance of the piezoelectric disc is increased. Fig 7.2(a) and (b) show the predicted real and imaginary parts of the impedance of a piezoelectric disc alone with a D/T ratio of 20 respectively. The added series resistors increase the real part of the impedance shown in Fig 7.2(a) and the overall impedances are changed.

However, in all case, the damping improves the bandwidth of the transducers at the expense of the sensitivity of the response.

7.3 Analyses of vibration characteristics of piezoelectric discs with an addition

In this section piezoelectric discs with an elastic addition are studied by the finite element model and the modal analysis method.

Two types of material were used as the addition of the piezoelectric disc, one is perspex, which has a very small mass density, Young's modulus, and small loss factor. The other addition is epoxy with titanium filler, which has a large mass density, and has a large loss factor. The material of all the additions is assumed to be isotropic. The material properties of the PZT5A, perspex and epoxy with titanium filler are listed in Table 7.1. The loss factors of the two additions were obtained from ultrasonic measurements (Ugayr, 1979).

The acoustic impedances of the above materials were calculated and are also listed in Table 7.1, which are defined as

$$Z = \rho c$$

where ρ is the mass density of the material and c is the longitudinal velocity in the material. For PZT5A, the acoustic impedance is very high, 33.7 $x10^6$ kg/m^2s. The perspex has a relatively small acoustic impedance compared to that of the PZT5A, only 3.22 $x10^6$ kg/m^2s, while the epoxy has a comparable acoustic impedance of 9.91 $x10^6$ kg/m^2s due to the dense titanium filler, and a high loss factor of 0.38. This was intended to simulate the sort of material which is likely to be used as the backing of the piezoelectric transducers. The bonding line between the disc and addition is assumed to be perfect and infinitely thin, and the mechanical effect of the bond layer is negligible.

It can be seen from Table 7.1 that the damping factors for piezoelectric disc and elastic additions are different, particularly between PZT5A and epoxy addition. Since non-uniform damping is not considered in the eigenvalue routine programme, and uniform damping is assumed when the frequency response functions and the electrical impedance are calculated by the modal analysis method, some discrepancy is expected. The damping factor used in the modal solution calculations is a compromise taking into account the damping factors of the disc and the addition (in between these two values), and was tuned to obtained the best agreement with the experimental measurements. The structural damping factors used in calculating the electrical impedances are 0.01 for the disc with perspex addition, and 0.035 for the disc with epoxy addition.

Due to the added mass of the elastic addition to the piezoelectric disc, the number of vibration modes which need to be computed in the eigenvalue routine is increased drastically if the frequency range of interest in the composite structure is still from 0 to one and a half times the through thickness frequency of the piezoelectric disc itself. This may be restricted by the computer core size and by the cost. In order to limit the mesh size required, a small disc 10 mm in diameter and 2.01 mm thick giving a D/T ratio of 5 was used in these tests.

The numerical and experimental studies were carried out on the PZT5A discs with two different elastic additions. Both additions had the same diameter as the piezoelectric disc but with a length of 6 mm for the perspex and a length of 10.54 mm for the epoxy, as listed in Table 7.2. The specimens were prepared by bonding the piezoelectric discs and additions together, and the two leads contacting the top and bottom surfaces of the disc are connected with the voltage source as illustrated in Fig 7.3.

Fig 7.4(a) to (c) show respectively the predicted electrical impedances for the PZT5A disc alone with a D/T ratio of 5, the disc with the perspex addition and the disc with the epoxy addition. The normalised modal constants, which evaluate the strength of excitation at resonances, are plotted in Fig 7.5(a) to (c) for each case.

As has been shown by the predicted frequency spectrum in Fig 5.2 of Chapter 5, there can be more than one mode which is strongly excited by voltage excitation of a piezoelectric disc with a small D/T ratio. Among 16 modes predicted for the PZT5A disc with a D/T ratio of 5 in the frequency range of interest from 0 to 1500 kHz, two thickness extensional modes at 956.9 kHz (mode 8) and 1018 kHz (mode 9) are most strongly excited and have almost equal strength of excitation, together with the first radial mode at 195.2 kHz which is relatively strongly excited. The axial surface displacements of these three modes are plotted in Fig 7.6(a), and the predicted electrical impedance of the disc is shown in Fig 7.4(a).

For the disc with an addition as light as the perspex the general form of the electrical impedance response shown in Fig 7.4(b) remains more or less similar to the response for the single disc in Fig 7.4(a) though there are many more modes predicted in the frequency range of interest. The two modes which are most strongly excited in this composite structure are modes at 958.6 kHz and 1029.2 kHz. Their surface displacement patterns shown in Fig 7.6(b) are similar to those of modes 8 and 9 of the disc alone shown in Fig 7.6(a). The first radial mode at 195.2 kHz for disc alone shown in Fig 7.6(a) is now predicted at 199.2 kHz with a similar surface displacement pattern. It is therefore evident that for the disc with a perspex addition, the deformed shape of the free surface for the most strongly excited modes have not been changed too much, while their corresponding resonant frequencies are increased slightly, indicating that the perspex is contributing more stiffness than mass in these modes.

For the disc with an addition of large mass density, Young's modulus and loss factor, such as the epoxy addition with titanium filler, the predicted impedance response shown in Fig 7.4(c) is extremely complicated not only because of the large number of the resonant modes predicted in the frequency range of interest but also because no single mode has a much larger modal constant than the others. Therefore no single mode dominates the frequency response. The discussion below concentrates on the frequency region of the first radial mode of the disc and the frequency range around the thickness frequency of the disc.

In the frequency range from 150 to 250 kHz, there are 9 modes predicted for the disc with the epoxy addition, and they all have approximately the same modal constants, however, the mode having maximum modal constant among them is at frequency of 186.1 kHz, which has same type of surface motion shown in Fig 7.6(c) as the first radial mode of the disc alone, though its frequency is lower than the 195.2 kHz for the disc alone and 199.2 kHz for the disc with a perspex addition.

In the frequency range of 948 to 977 kHz, there are 4 modes which are strongly excited. The mode at 967.5 kHz has the largest modal constant among all modes of the composite structure, and the mode at 948.2 kHz has the second largest modal constant. Their surface displacements are shown in Fig 7.6(c), and it can be seen that the both modes have a similar pattern to mode 9 at 1019 kHz of the disc alone shown in Fig 7.6(a). The mode at 967.5 kHz has a particularly large "dc" component of displacement across the surface of the disc.

Another mode at 1039 kHz has a relatively large modal constant, and its surface displacement is shown in Fig 7.6(c). It seems that the surface displacement of this mode is similar to mode 9 of the disc alone, but the "dc" component of the surface displacement is lower.

It is therefore clear that for the titanium addition, many more modes are predicted and their corresponding resonant frequencies are reduced for the modes which have similar surface displacement patterns to those of the disc alone. This is because the addition has such a high mass density.

Fig 7.7(a) to (c) show the corresponding measured electrical impedances for the piezoelectric disc alone, the disc with a perspex addition and the disc with an epoxy addition. In general it can be seen that the predictions and measurements for the additions agree qualitatively well with each other; in particular there is very good correlation between the prediction and measurement for the disc with the perspex addition. The prediction and measurement for disc with the epoxy addition show good agreement in the low frequency range, and agree reasonably well in the form of the response throughout, but significant discrepancy occurs in the first through thickness frequency range. This may be because the titanium loaded epoxy has much higher damping than the disc itself so the damping in the system is highly non-uniformly distributed where the modal analysis assumes uniformly distributed damping.

It is evident that additions have significant effects on the vibration characteristics of piezoelectric discs and changes depend on the material properties of the addition, such as mass density, Young's modulus and and the loss factor. The effect on the vibration characteristics of the disc is rather small for a disc with an addition which has small mass density and acoustic impedance; although many extra modes arise in the impedance response, their strength of excitation is very small, and the modes which can be most strongly excited have similar surface displacement patterns to those modes which are strongly excited for the piezoelectric disc alone. However, the effect is quite severe for the addition of a high mass density; a large number of modes are predicted, but no single mode dominates the response, and many modes which have similar strength of excitation cluster in the same frequency range and are coupled with each other.

The high loss factor of the addition reduces the amplitudes of the response at resonant frequencies and couples modes with each other. The increased modal density and mode coupling effect due to the addition with high loss factors may spread the energy over a larger frequency range, and the frequency bandwidth is therefore increased.

The current modelling for the elastic addition to the piezoelectric discs seems rather crude for accurate analyses of transducers with backing, which inherently has a loss factor much different from that of the disc. More accurate results would be obtained if the finite element analysis had accommodated non-uniform damping.

7.4 Application of the FE model to piezoelectric discs with varying pattern of electrodes

The finite element analysis and modal analysis techniques may be particularly useful and flexible for the analysis of the vibration characteristics of piezoelectric structures with complicated geometries and boundary conditions, such as piezoelectric discs with curved surfaces (Vopilkin, 1987), discs of non-uniform thickness (Hutchins *et al.*, 1987), tapered transducers (Barthe and Benkeser, 1987), piezoelectric structures with an inhomogeneous electric field (Kazhis and Lukoshevichyus, 1976; Brittain and Weight, 1987) and discs with irregular distribution of electrodes. These advanced transducers which were previously studied by experimental methods and simple analyses can now be possibly analysed much more accurately.

In this section the vibration characteristics of partially electroded discs are studied as an example of the application of the three dimensional model. The two discs analysed have identical geometries to the fully electroded disc studied in Chapter 4. They are PZT5A

discs with D/T ratio of 20, having diameters of 40.10 mm and thickness of 2.03 mm. One disc has electrode layers only on the outer half of the top and bottom surfaces and the other has the inner half of the surfaces electroded. They are illustrated in Fig 7.8. The finite element analysis of these two discs was carried out using the method described in Chapter 4 apart from a slight change in the electrical boundary conditions.

Table 7.3 lists the predicted first 48 resonant frequencies of the discs with inner and outer half electroded surfaces together with the result previously obtained for the fully electroded disc. Since the static capacitances of these discs are quite different, the corresponding modal constants of these modes are normalised to the maximum of the disc and are also listed in Table 7.3. It can be seen that the predicted resonant frequencies of the partially electroded discs are higher than those of the fully electroded disc due to the increased piezoelectric stiffening effect from the extra non-electroded area.

With partial electrodes on the top and bottom surfaces, the piezoelectric discs are only excited by the electrical voltage on the electroded area. The equivalent mechanical forces on the surface of the discs for both inner and outer half electroded discs are therefore different from that of the fully electroded disc. The equivalent nodal force is only applied in the electroded area, while the non-electroded area is in free boundary condition. The static capacitance of the piezoelectric disc is also reduced due to the reduction of the electroded area.

Due to the change of electrode pattern, the strength of excitation of each mode, i.e., the modal constant of each mode is also changed. The modal constant normalised to the maximum for any mode in each disc is therefore used to compare modes for the different discs. It can be seen from Table 7.3 that the most strongly excited mode for the inner half electroded disc is mode 32 at 976.8 kHz, and for the fully electroded disc the most strongly excited mode is mode 32 at 965 kHz; however, there are differences in their corresponding mode shapes.

The mode shapes of mode 32 and other modes of the inner half electroded disc which can be relatively strongly excited are shown in Fig 7.9. It can be seen that mode 32 is markedly different from those modes described in the fully electroded disc. The inner third of the disc has a very large and almost uniform axial displacement over the surfaces; in the middle third of the surface, the axial displacement decreases linearly along the radial direction accompanied by considerable radial deformation; while in the outer third of the disc, there is almost no radial or axial motion at all. The other two modes, which are also excited relatively strongly, are mode 24 at 888 kHz and mode 36 at 1029 kHz. They have

a similar type of deformation pattern to mode 32, with large displacement both in the axial and radial directions in the inner part of the disc and almost no deformation in the outer part of the disc. This sort of mode has not been found before for the fully electroded discs and has not been reported elsewhere.

There is no single dominant mode for the outer half electroded disc. Mode 32 at 974.1 kHz and mode 33 at 990.3 kHz of the outer half electroded disc are the modes which are most strongly excited, and several other modes at frequencies of 917.1, 928.4, 945.5, and 958.0 kHz are also excited relatively strongly. The mode shapes of these modes are shown in Fig 7.10, and they are similar to the modes described in Chapter 4.

One PZT5A disc with D/T ratio of 20 which was originally fully electroded was used to measure the electrical impedance of the inner half electroded disc. The outer half of the electroded surfaces were removed by rubbing with an abrasive cloth and the electrical impedance was obtained using the procedure described in Chapter 4.

Fig 7.11 shows the predicted and measured electrical impedance of the inner half electroded disc. It can be seen that there is generally good agreement between the measurement and prediction, particularly in the low frequency range where mode 4 in both the prediction and measurement is excited very weakly and mode 6 is not excited at all in comparison to the result shown in Fig 4.9 for the fully electroded disc. And in the frequency range of the first through thickness mode, i.e., around 970 kHz, both the prediction and the measurement show single mode domination, and agree very well apart from a slight shift in the values of the resonant frequencies.

However, some discrepancy is observed over the frequency range of the thickness shear modes, i.e., between 870 kHz to 910 kHz in Fig 7.11. The only major difference between the predictions and the measurements is that mode 24 at 888.2 kHz which was predicted to be excited relatively strongly, does not appear in the measured impedance curve. The reason for this is not clear.

Fig 7.12 shows the predicted electrical impedance of the outer half electroded disc. It can be seen that unlike the single mode domination in the fully electroded disc shown in Fig 4.9 and the inner half electroded disc shown in Fig 7.11, the response has two modes which are excited roughly equally strongly at 974.1 kHz and 990.3 kHz.

7.5 Conclusions

The sources of mechanical damping and electrical loss in piezoelectric transducers have been discussed in this chapter, together with analyses of piezoelectric discs with an addition and discs with partial electrodes on the top and bottom surfaces.

The brief study on the addition to the piezoelectric discs shows some useful features for the understanding the mechanism of the backing on the transducer. It is believed that the addition of backing increases the modal density, and also the extent of mode coupling due to the high loss factor, so the frequency bandwidth of the transducer is increased. For the more accurate modelling of backing, however, the non-uniform damping should be taken into account in the finite element analysis.

The three dimensional model has been further applied to analyse the vibration characteristics of partially electroded piezoelectric discs. The impedance measurement of the inner electroded disc has shown good agreement with the prediction from the FE analysis. It has been shown that the electrode pattern has a significant effect on the vibration characteristics of the piezoelectric discs. By changing the electrode pattern, the natural frequencies and mode shapes of the disc can be changed together with the strength of the excitation at different modes. This has demonstrated the flexibility of the finite element method and modal analysis techniques in analysis of piezoelectric discs with complicated boundary conditions.

	Mass density (kg/m^3)	Young's modulus (GN/m^2)	Acoustic Impedance (10^6 kg/m^2s)	Loss factor
PZT5A(appx.)	7.750	111.0	33.7	0.0133
Perspex	1.180	6.324	3.22	0.008*
Epoxy(+titanium)	6.064*	16.21*	9.91*	0.380*

Table 7.1 The material properties of perspex and epoxy with titanium filler. (*by measurement, others are book values)

	Diameter (mm)	Thickness (mm)
The PZT5A disc	10.0	2.01
The perspex addition	10.0	6.00
The epoxy addition	10.0	10.54

Table 7.2 The geometries of the piezoelectric discs and their elastic additions.

	Fully electroded disc		Inner half electroded disc		Outer half electroded disc	
Mode	Freq(kHz)	RA	Freq(kHz)	RA	Freq(kHz)	RA
1	49.56	.010	53.74	.0070	54.87	.015
2	128.1	.0083	140.6	.0061	138.5	.062
3	201.6	.0082	215.8	.0085	216.9	.023
4	272.1	.0083	295.5	.0019	295.0	.0030
5	338.5	.0084	364.5	.012	363.4	.042
6	399.9	.0084	431.6	0.	433.0	.052
7	455.2	.0083	491.2	.010	488.2	.0057
8	503.8	.0082	539.6	.0027	541.2	.020
9	545.9	.0081	585.4	.0034	583.2	.056
10	582.3	.0087	618.7	0.	617.5	.0029
11	614.0	.011	651.0	.0035	645.4	.042
12	540.6	.021	675.8	.0035	660.3	.052
13	657.7	.018	700.1	0.	680.5	0.
14	677.6	0.	718.8	0.	702.8	.0044
15	703.1	0.	728.8	0.	725.0	.0023
16	729.5	0.	748.2	0.	747.0	0.
17	756.3	.0015	770.9	0.	770.8	.0027
18	783.5	.0025	795.9	0.	794.8	.011
19	811.3	.0039	821.5	0.	820.5	.015
20	839.4	.0069	848.4	0.	846.7	.017
21	867.7	.014	874.4	.012	873.3	.0130
22	873.2	0.	876.1	0.	879.8	.055
23	876.4	0.	881.4	.0020	883.3	.047
24	880.0	.0021	888.2	.15	893.7	.11
25	887.0	.0015	894.9	.0020	894.3	.016
26	893.2	.016	899.8	0.	899.7	.027
27	896.6	.031	904.8	0.	901.9	.046
28	914.2	.046	918.1	.0013	917.1	.084
29	924.8	.057	934.0	0.	928.4	.16
30	943.5	.16	948.7	0.	945.5	.22
31	955.9	.091	964.2	.0010	958.0	.18
32	**964.9**	**1.0**	**976.8**	**1.0**	**974.1**	**1.0**
33	975.5	.0010	987.6	0.	**990.3**	**.94**
34	991.8	.094	997.8	0.	996.4	.011
35	995.2	.012	1022	0.	1014	.015
36	1010	.0019	1029	.081	1035	.0087
37	1026	.024	1043	0.	1047	.018
38	1040	.0032	1057	0.	1057	.0013
39	1051	.0014	1078	0.	1077	.0010
40	1064	.010	1084	0.	1085	0.
41	1081	.021	1101	.0024	1103	.0092
42	1102	0.	1110	.0013	1109	.0056
43	1108	.0042	1120	.0026	1121	0.
44	1122	.0026	1139	.0055	1139	.022
45	1145	0.	1155	.0022	1154	.0049
46	1166	.0033	1175	0.	1175	0.
47	1167	0.	1182	0.	1183	.0088
48	1187	0.	1196	0.	1196	.0087

Table 7.3 The resonant frequencies of the vibration modes and corresponding normalised modal constants of piezoelectric discs with fully and partially electrodes (RA: normalised modal constants).

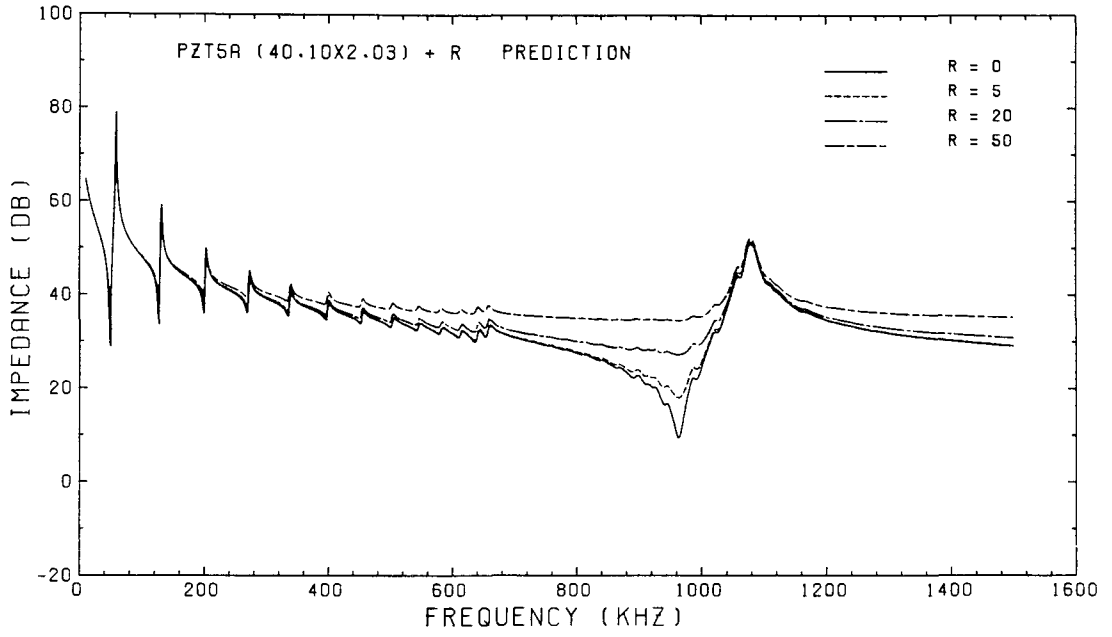

(a) predictions

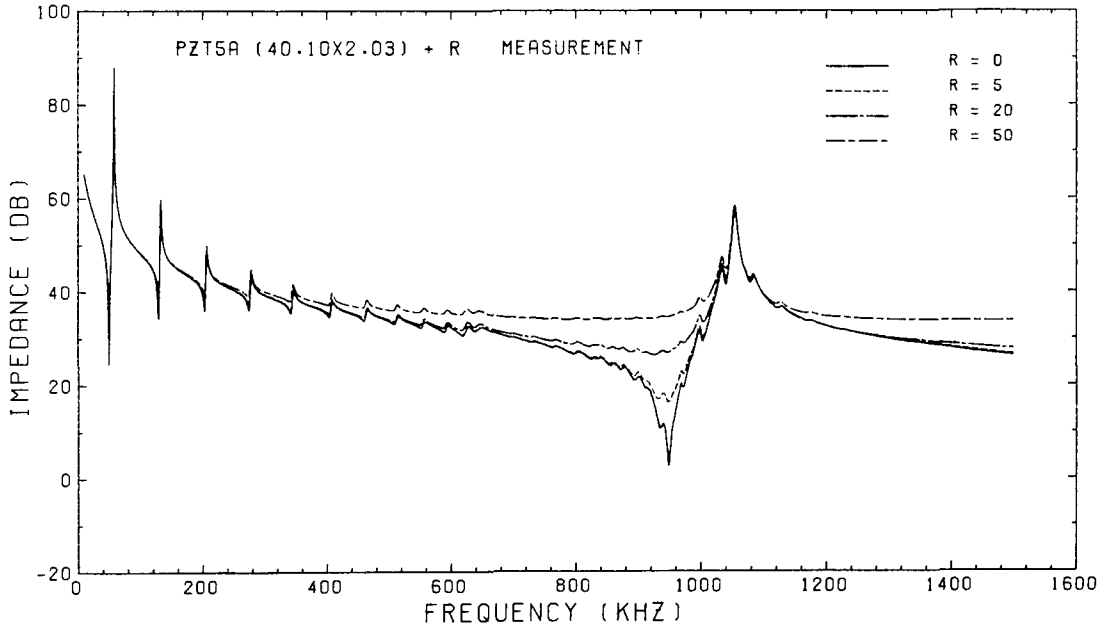

(b) measurements

Fig 7.1 The predicted and measured electrical impedance responses of a piezoelectric disc in series with resistors

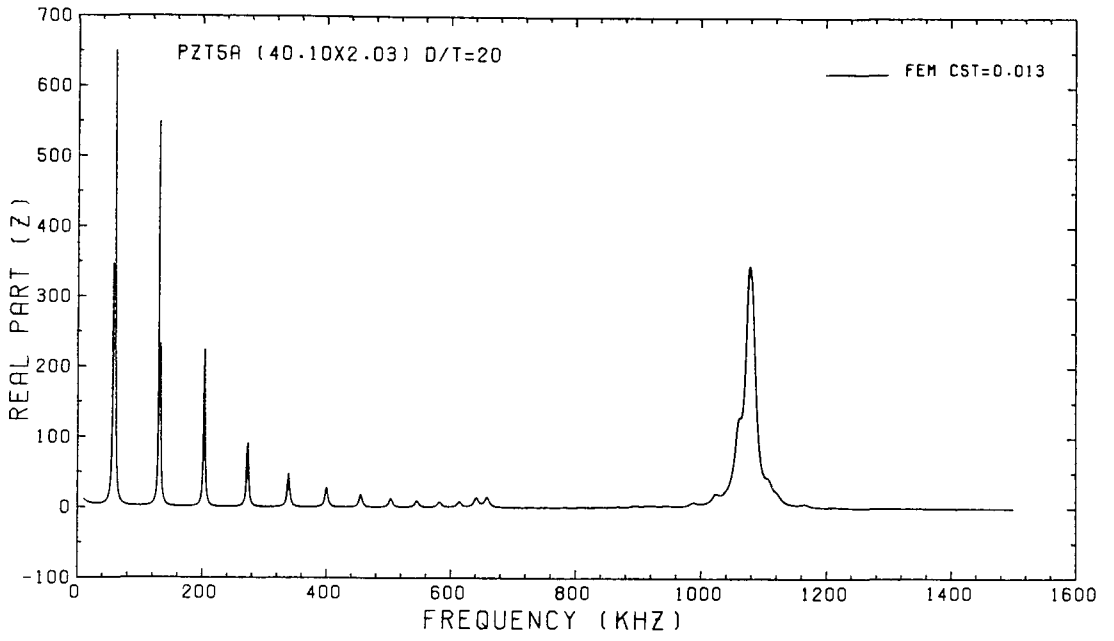

(a) real part

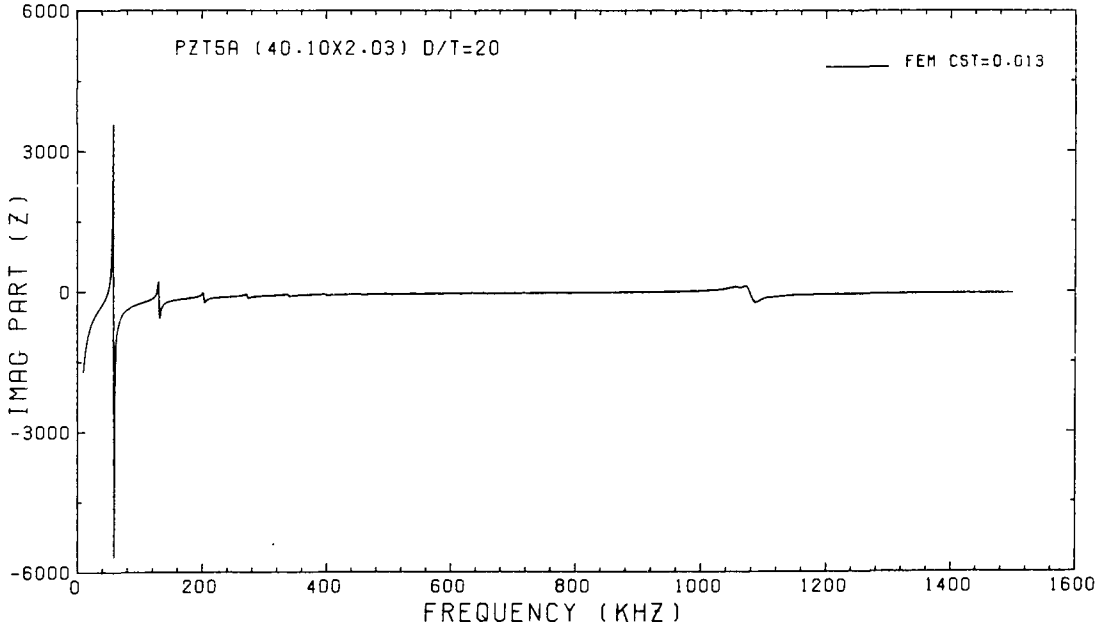

(b) imaginary part

Fig 7.2 The predicted real and imaginary parts of the electrical impedance responses of a PZT5A with a D/T ratio of 20

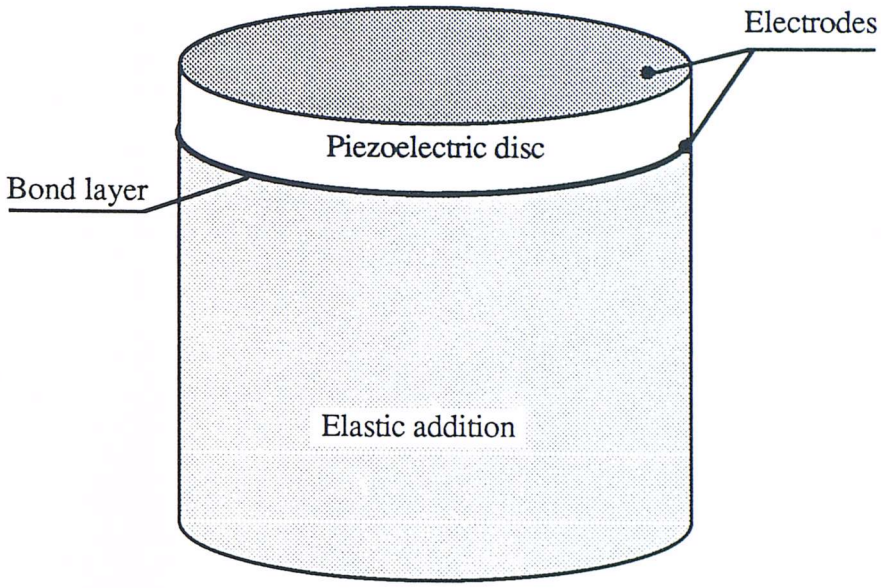

Fig 7.3 The configuration of the piezoelectric disc with an elastic addition

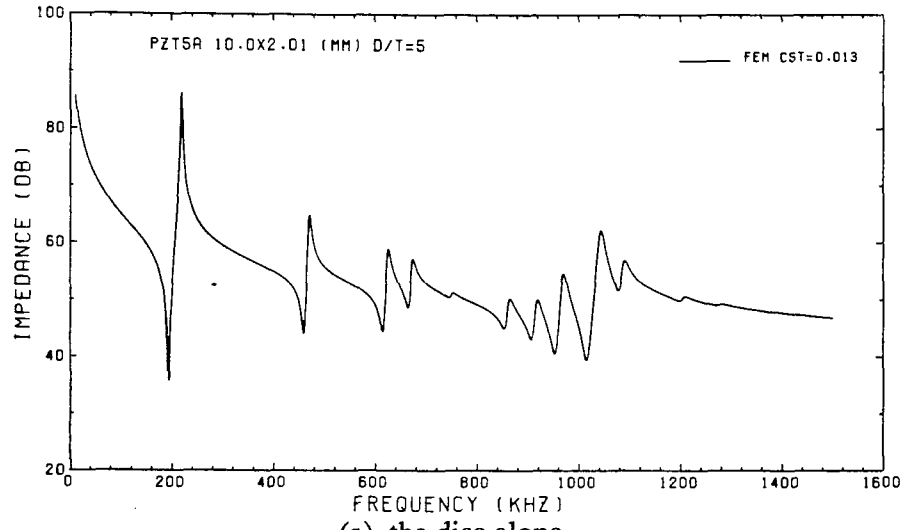

(a) the disc alone

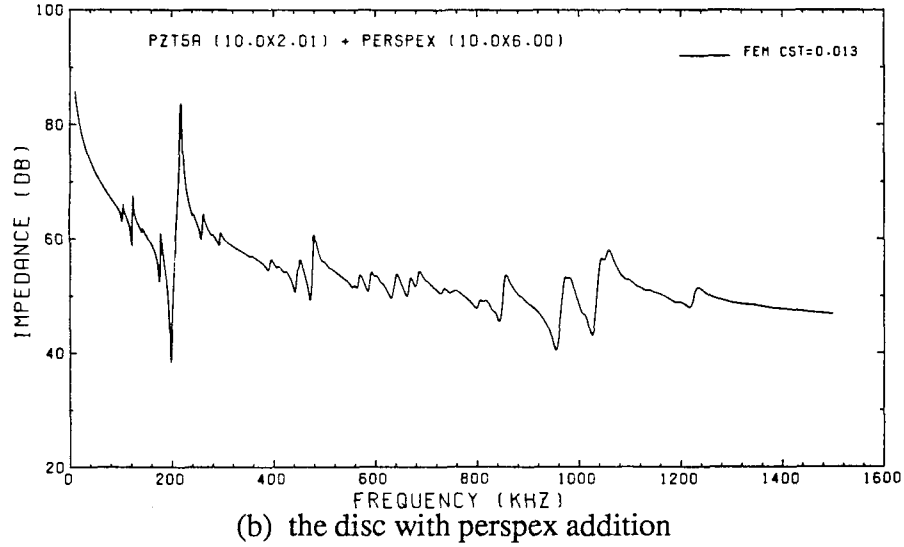

(b) the disc with perspex addition

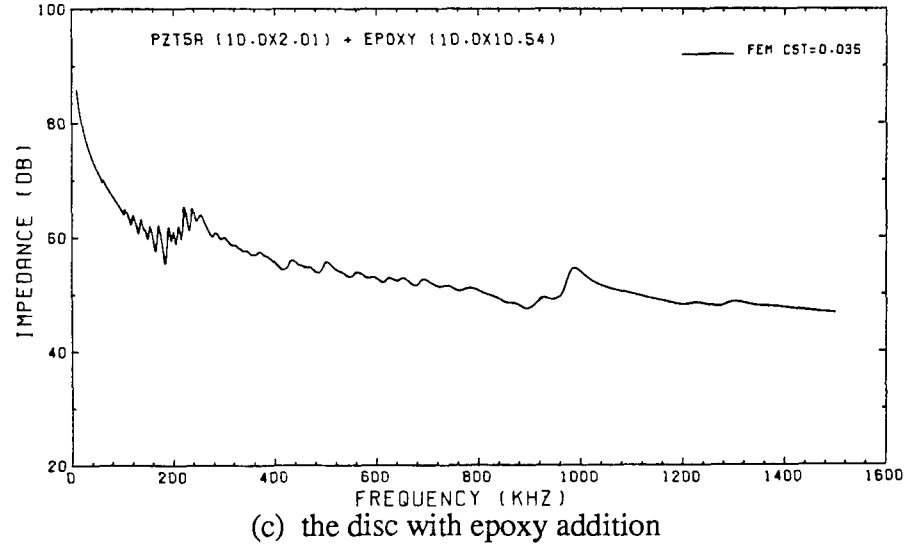

(c) the disc with epoxy addition

Fig 7.4 The predicted electrical impedance response of a PZT5A disc with a D/T ratio of 5, the disc with perspex addition and the disc with epoxy addition

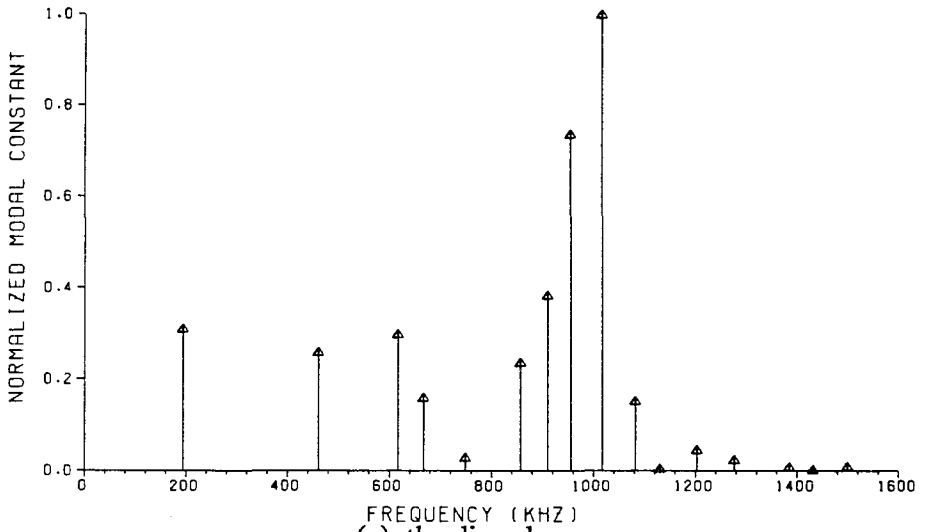

(a) the disc alone

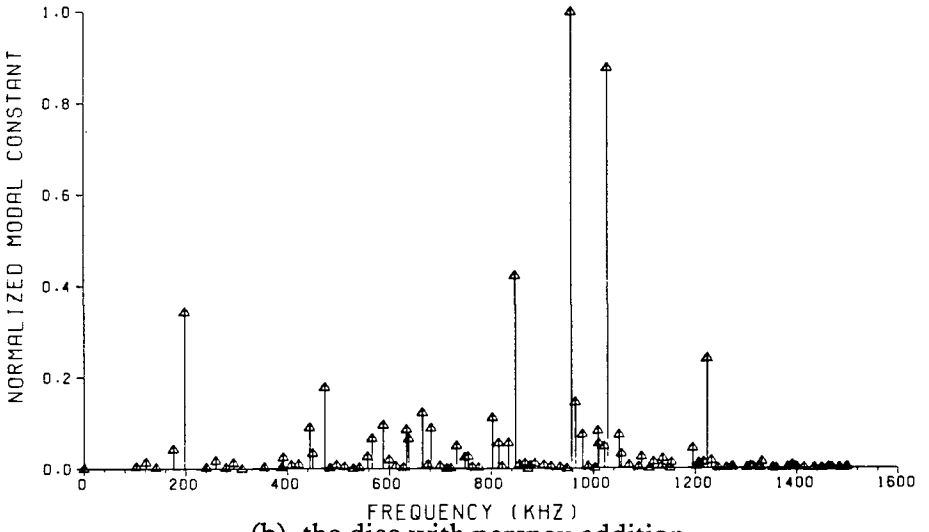

(b) the disc with perspex addition

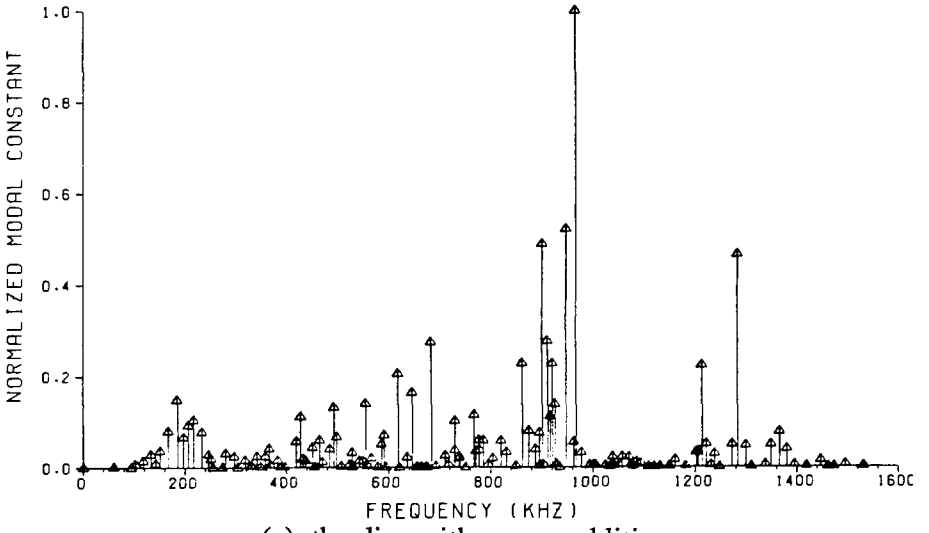

(c) the disc with epoxy addition

Fig 7.5 The normalised modal constants of vibration modes of a PZT5A disc with a D/T ratio of 5, the discs with perspex addition and the disc with epoxy addition

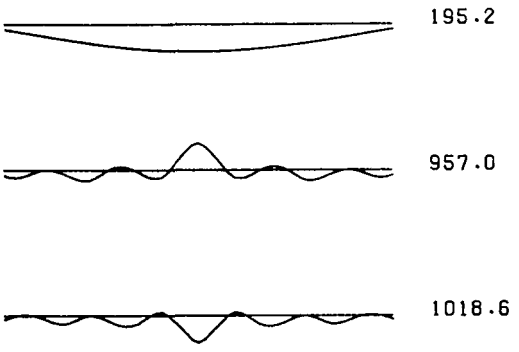

(a) the disc alone

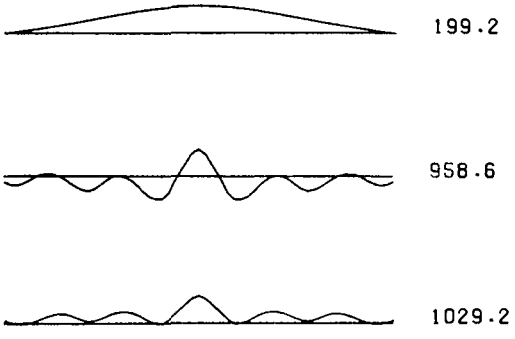

(b) the disc with perspex addition

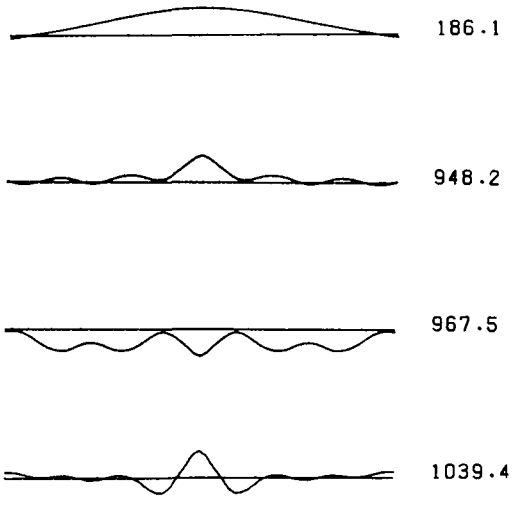

(c) the disc with epoxy addition

Fig 7.6 The axial surface displacements at some resonant frequencies of the PZT5A disc with a D/T ratio of 5, and the discs with elastic additions

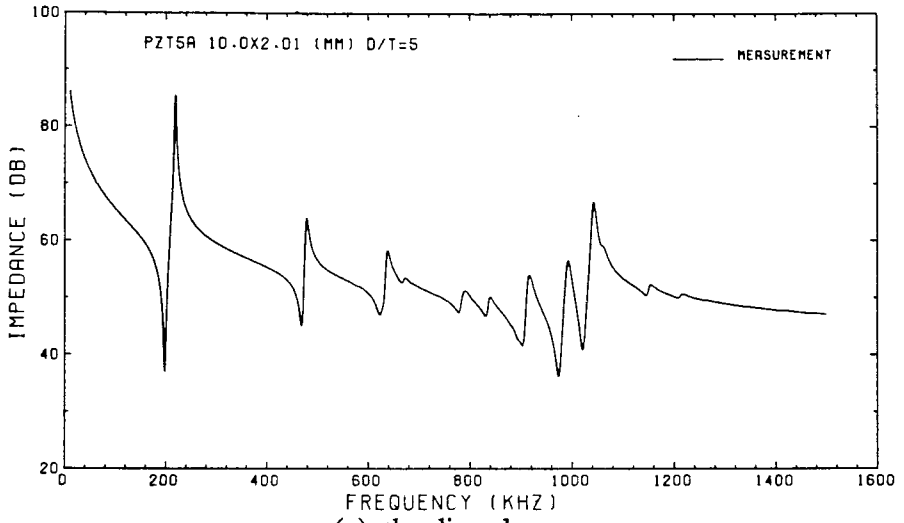

(a) the disc alone

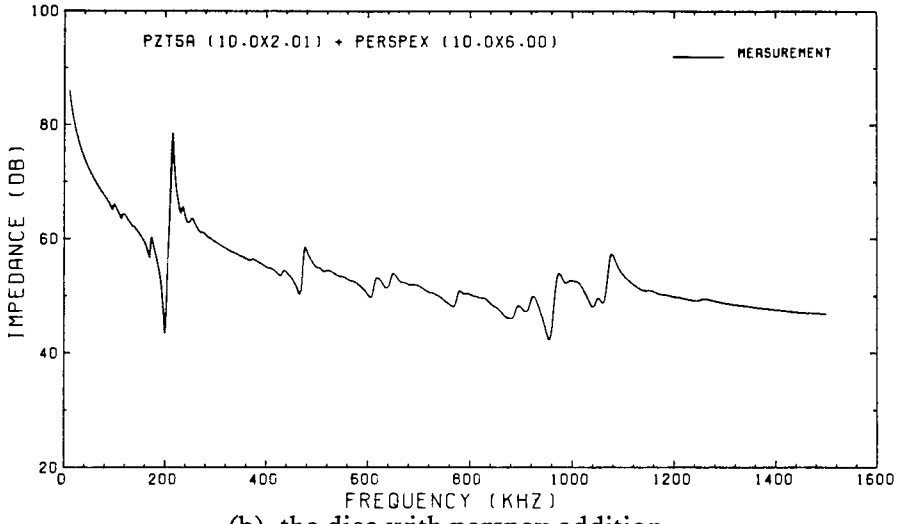

(b) the disc with perspex addition

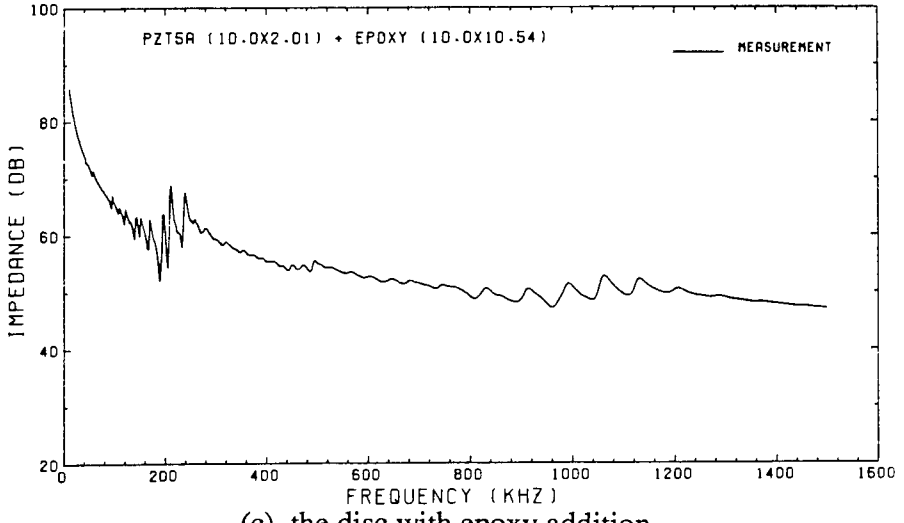

(c) the disc with epoxy addition

Fig 7.7 The measured electrical impedance response of a PZT5A disc with a D/T ratio of 5, the disc with perspex addition and the disc with epoxy addition

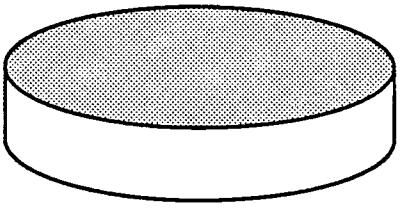

(a) fully electroded disc

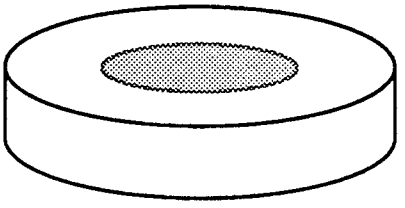

(b) inner half electroded disc

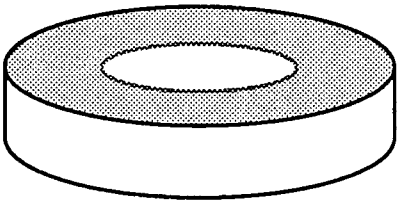

(c) outer half electroded disc

Fig 7.8 Configuration of piezoelectric discs with fully and partially electroded surfaces

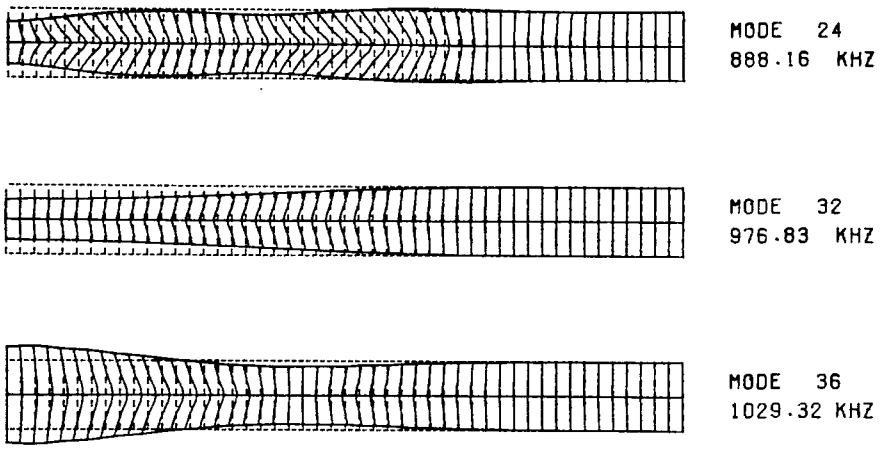

Fig 7.9 The mode shapes of some modes of the inner half electroded disc

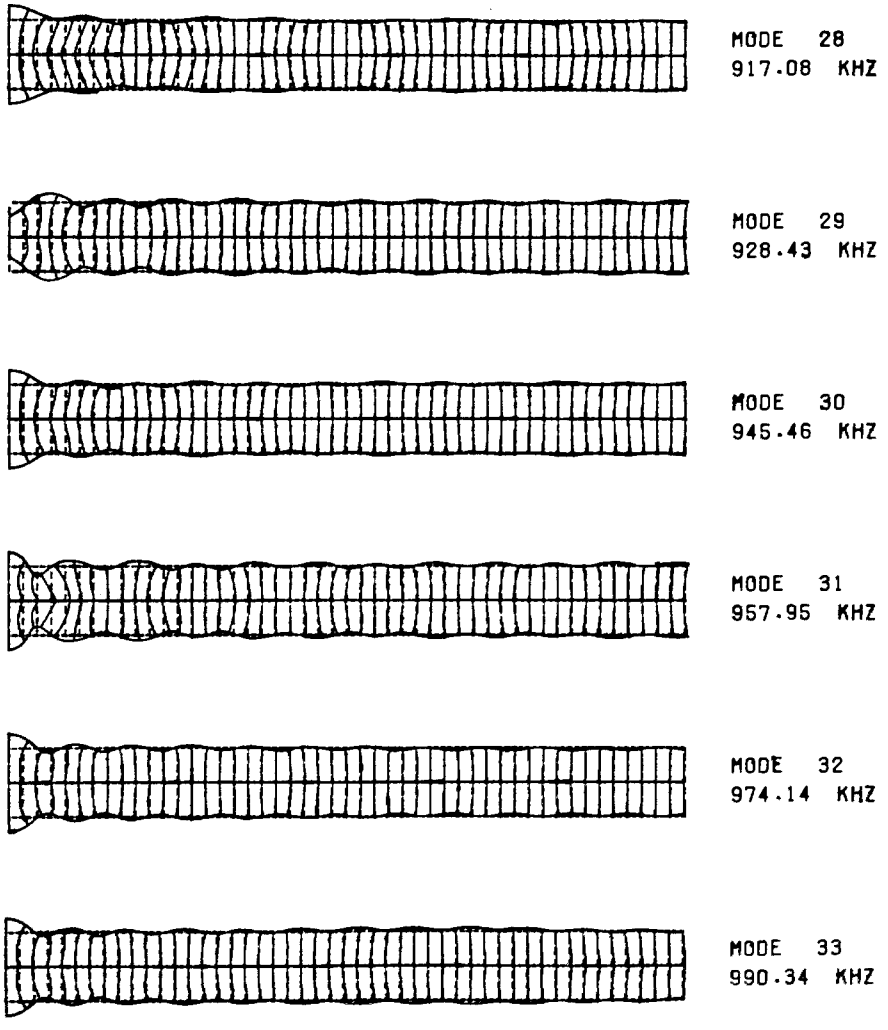

Fig 7.10 The mode shapes of some modes of the outer half electroded disc

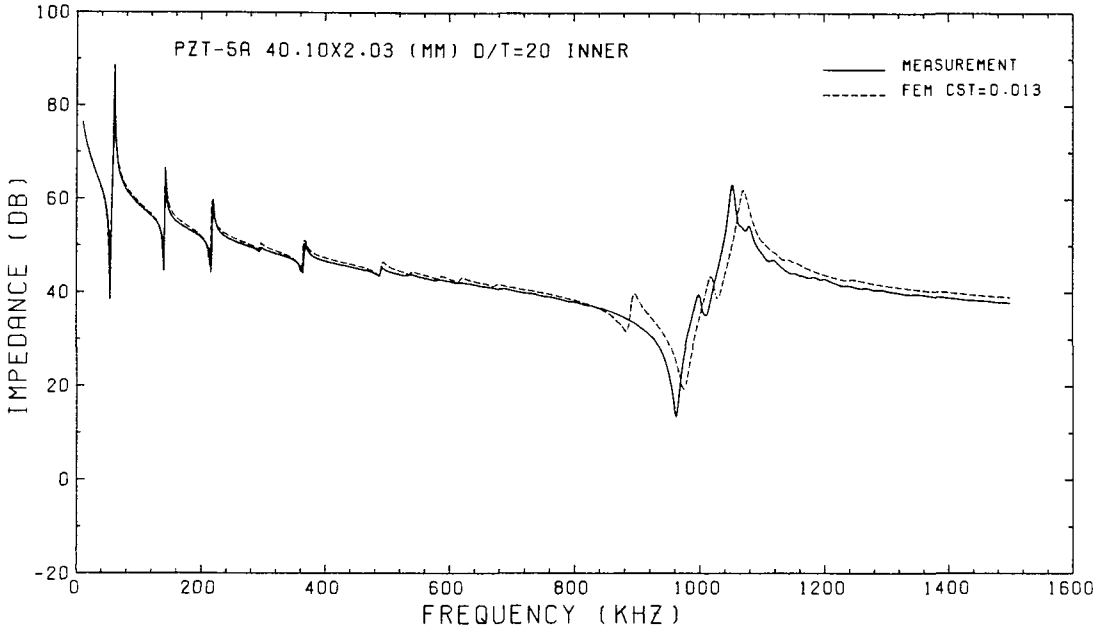

Fig 7.11 The predicted and measured electrical impedance responses of the inner half electroded disc

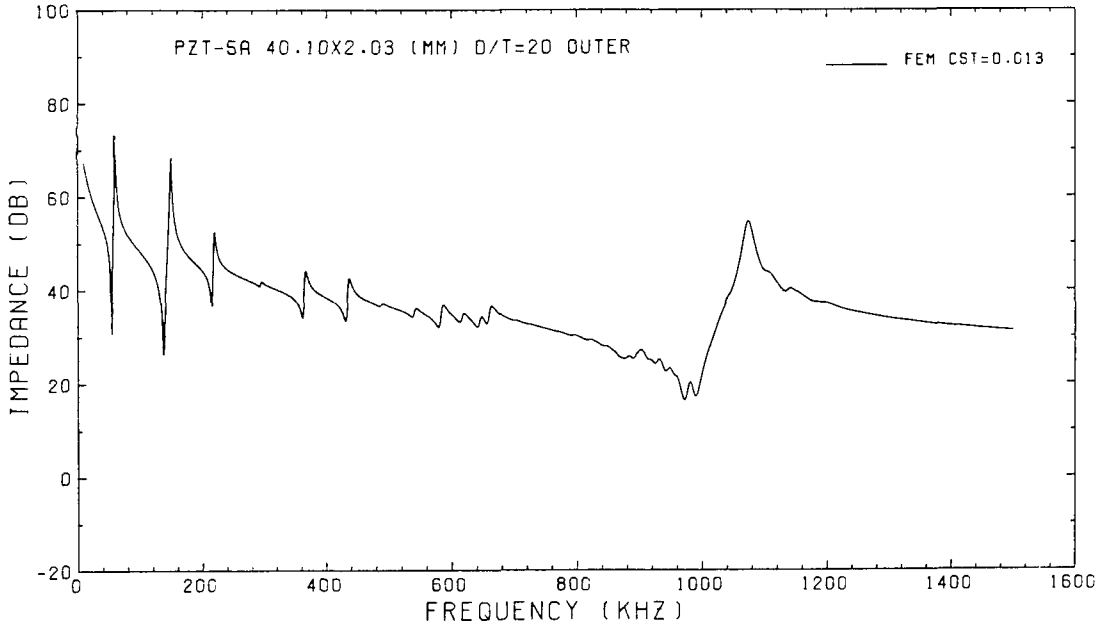

Fig 7.12 The predicted electrical impedance response of the outer half electroded disc

CHAPTER 8

CONCLUSIONS AND FURTHER WORK RECOMMENDED

8.1 Conclusions

The vibration characteristics of piezoelctric discs have been studied thoroughly in this thesis. It includes a review of available techniques to analyse the performance of transducers and previous studies of piezoelectric discs. This has been followed by a brief study on the transient responses of piezoelectric transducers by a one dimensional analytical method and detailed study of vibration characteristics of piezoelectric discs by a model using finite element analysis and modal analysis. Finally, the model has been applied to analyse discs with an addition and discs with partial electrodes.

The review has shown that there are many techniques used in modelling piezoelectric transducers, and most of them are one dimensional. However, two and three dimensional techniques would be preferable if piezoelectric discs with finite diameter to thickness ratios are of interest, and the analysis of complicated transducers is required. The experimental results by the previous researchers have shown that the vibration modes in piezoelectric disc could be very complicated, and accurate analyses are necessary

The brief study of transient responses of transducers by the one dimensional analytical model (Laplace transform method) has shown the effect of the backing on the response of the ultrasonic transducers, and that matched backing or backing with close values of acoustic impedance to that of the piezoelectric element are preferably in most applications. It has been shown that when the transducers are excited by voltage pulses, the short circuit mechanical response of the transducer is very complicated due to piezoelectric intercoupling effects.

The finite element method and modal analysis techniques have been used to analyse the vibration characteristics of piezoelectric discs with finite D/T ratios. The analysis uses a direct eigenvalue solution scheme treating the electrical potential of each node of piezoelectric structures exactly as an extra conventional displacement degree of freedom, and avoids the fully populated matrices which could be caused by the mass condensation scheme used by previous researchers (Allik and Hughes, 1970; Naillon *et al.*, 1983).

A thorough investigation of piezoelectric discs with D/T ratios of 20, 10 and 0.5 has shown that vibration characteristics of piezoelectric discs are very complicated. There are many modes predicted in the frequency range of interest. Five types of modes, radial modes, edge modes, thickness shear modes, thickness extensional modes and high frequency radial modes, which were reported by previous experimental works (Shaw, 1954; Ikegami *et al.*, 1974; Ueha *et al.*, 1983), have been predicted by the finite element model. The mode shapes of these modes predicted by the FE model have shown that none of the modes predicted has the sort of piston-like motion pattern assumed by the one dimensional model. However, one of the thickness extensional modes for a disc with a D/T ratio of 20 has a resonant frequency very close to that of the first through thickness mode assumed by the one dimensional model, and it has a very large mean value (or "dc" value) of axial displacement over the surface of the disc. This mode is excited much more strongly than the other modes.

Although there is no single mode predicted by the finite element method which has the sort of piston-like motion assumed by the one dimensional model, the predicted transient mechanical response of piezoelectric discs by the modal solution has shown that it is possible for piezoelectric discs with large D/T ratios to vibrate with almost uniform surface displacement over the first couple of cycles of the first through thickness mode when voltage pulses are applied across the discs. This has been shown to be due to high mode density in the thickness frequency range and mode coupling effects among these thickness extensional modes.

A new parameter, the modal constant (or mode participation factor) (Ewins, 1984), has been defined and used to evaluate the strength of excitation at each vibration mode. It is believed that the modal constant is superior to the electromechanical coupling factor in evaluating the strength of excitation for discs having many vibration modes and having high modal density. The modal constant has been used to predict the frequency spectrum of piezoelectric PZT5A discs with D/T ratios from 0.1 to 20, and it has been shown that the most strongly excited modes by an applied voltage across the top and bottom surfaces are the thickness extensional modes, and the number of these thickness extensional modes that piezoelectric discs can have depends upon their D/T ratios.

The measurements of electrical impedance responses of piezoelectric discs have shown excellent agreement with the predicted ones. The measurement of the mode shapes of some modes by laser interferometry has also shown good agreement with the prediction for the lower order modes which have simple mode shapes, and qualitative agreement for

the thickness extensional modes. These measurements show that the finite element model has high accuracy for the three dimensional analysis of piezoelectric discs.

The application of the model to piezoelectric discs with an addition has shown that the addition has significant effects on the vibration characteristics of the piezoelectric discs, in particular a large number of extra modes are predicted. The effect of the addition depends very much on its material properties compared with those of the piezoelectric disc, such as mass density, stiffness, acoustic impedance, and loss factor.

The flexibility of the finite element method and modal analysis has been demonstrated by the application of the model to partially electroded piezoelectric discs. This has shown that the three dimensional model has potential to provide an invaluable tool for the accurate analysis and design of piezoelectric transducers with complicated structures.

8.2 Further work recommended

The current work could be extended to the analysis of complete piezoelectric transducers, including the piezoelectric disc, backing, matching layer, etc., and also the interaction with the coupling fluid.

The major damping source in transducers is the backing. The damping included in the current model is modal damping. An analysis with uniform damping is justified for piezoelectric discs alone, and for discs with an addition of low loss factor. However, to analyse accurately damping effects in real transducers, non-uniform damping must be taken into account in the finite element analysis. If the damping is included in the eigenvalue solution, complex matrices must be introduced, and complex eigenvalues and eigenvectors are obtained. This could make the solution procedure complicated and require larger storage.

The other source of damping of piezoelectric transducers is the interaction with fluid. The fluid effect can be modelled by acoustic radiation loading, which adds a specific acoustic matrix to the dynamic equation (Smith *et al.*, 1973). The dynamic problem of structure-fluid interaction has been solved by many authors, for example, Wilson and Khalvati (1983), Olson and Bathe (1985a, 1985b), and Sharan and Gladwell (1985). Usual solid elements are used to model the solid structure in terms of displacement, while the fluid is divided into two regions; one is the region surrounding the transducer which could be modelled by fluid finite elements in terms of velocity potential, and the other is the region further from the transducer which could be modelled by so called infinite elements

(Zienkiewicz *et al.*, 1982; Bettess and Bettess, 1984). The dynamic equation of the problem can therefore be written as (Olson and Bathe, 1985b)

$$\begin{bmatrix} M_{ss} & 0 \\ 0 & -M_{ff} \end{bmatrix} \begin{Bmatrix} \ddot{u}_s \\ \ddot{\phi}_f \end{Bmatrix} + \begin{bmatrix} 0 & C_{sf} \\ C_{fs} & -C_i \end{bmatrix} \begin{Bmatrix} \dot{u}_s \\ \dot{\phi}_f \end{Bmatrix} + \begin{bmatrix} K_{ss} & 0 \\ 0 & -K_{ff}-K_i \end{bmatrix} \begin{Bmatrix} u_s \\ \phi_f \end{Bmatrix} = \begin{Bmatrix} F_s \\ 0 \end{Bmatrix} \tag{8.1}$$

where u_s is the nodal displacement of the solid, ϕ_f is the velocity potential in the fluid, $[M_{ss}]$ and $[K_{ss}]$ are mass and stiffness matrices of the solid, $[M_{ff}]$ and $[K_{ff}]$ are mass and stiffness matrices of the inner region of the fluid, $[K_i]$ and $[C_i]$ are stiffness and damping matrices which account for the fluid remote from the transducer and $[C_{fs}]$ is the matrix coupling the fluid to the solid.

By using piezoelectric elements in the solid in the above equation, piezoelectric structure-fluid interactions can be solved. Recently Friedrich *et al.* (1989) has applied these equations to a piezoelectric bar vibrating in water, and the comparison between the prediction and the experiment showed the damping effect of the fluid on the vibration of a piezoelectric array. However, the dielectric effect in water must be considered if accurate modelling and comparison with experiments are sought. It would be very interesting to see the effects of fluid on the vibration characteristics of piezoelectric discs since they have many more modes than that of a bar.

For both modelling of backing and fluid interaction with discs, a direct time integration solution for transient response and step by step frequency sweeping for the frequency response solution are preferable since they can more efficiently deal with structures which have very large number of vibration modes in the frequency range of interest.

The other parts of piezoelectric transducers, such as the matching layer, wear plate, and bonding layer between discs and backing, and between discs and wear plate, together with the electrical components in matching network may also be taken into account. The sound field of the transducers, which has not been dealt with in this thesis, is also very important, this can be calculated by wave propagation theory in elastic solids and fluids by taking the source predicted by the accurate finite element model.

The further modelling of transducers may involve modelling whole ultrasonic testing systems (Ludwig and Lord, 1988). The whole testing process must be taken into consideration, including the elastic wave generated by applying voltage pulses across the transmitter, the interaction between the transducer and solid (Hsu *et al.*, 1987), and in some cases the interaction between the transducer and wedge (Atalar and Koymen, 1987),

the wave propagation and reflection in the testing medium, and the electrical signal output by the receiver when the wave comes back.

Work on the piezoelectric discs alone can be extended to analyse other piezoelectric discs with irregular geometries and properties, many of which have been claimed to be wideband even without any backing, for example, discs with one curved surface (Vopilkin, 1987). Other work includes analysis of piezoelectric discs with non-uniform excitation pattern, such as discs with non-uniform polarization field or the novel edge-wave-only transducer (Brittain and Weight, 1987), and discs with non-uniform electric field (Kazhis and Lukoshevichyus, 1976).

APPENDICES

A Material properties of piezoelectric ceramics

Piezoelectric ceramics are transversely isotropic materials. Table A.1 lists the material properties of the ceramics used in this thesis, PZT4, PZT5A and PZT5H. The subscripts 11, 22 and 33 represent the x, y and z directions, 44, 55, 66 represent the planes perpendicular to x, y and z. If z is taken as the thickness direction, and piezoelectric discs are polarised along the thickness direction, then 11=22, 44=55, 13=23.

Notations for material constants listed in Table A.1 are

- E electric field (or potential gradient), V/m
- D charge density (or displacement), C/m^2
- ε_0 Dielectric constants of free space, = 8.854×10^{-12} F/m
- $\varepsilon^T/\varepsilon_0$ relative dielectric constant, free
- $\varepsilon^S/\varepsilon_0$ relative dielectric constant, clamped
- $\tan \delta$ dissipation factor at 1 kHz, low electric field
- e piezoelectric constant, stress/electric field at constant charge, N/(mV); or charge density/strain at constant electric field, C/m^2
- h piezoelectric constant, electric field/strain at constant charge, V/m; or stress/charge density at constant strain, N/C
- c^E Elastic stiffness, N/m^2
- Q_M Mechanical quality factor
- k piezoelectric coupling factor
- N_1 frequency constant of a thin bar, resonant frequency x length, Hz.m
- N_{3t} frequency constant of a thin plate, resonant frequency x thickness, Hz.m
- ρ density kg/m^3
- v_3^D velocity of a compressional wave parallel to polar axis, m/s
- v_4^E velocity of a shear wave parallel to polar axis, m/s

Constants	PZT4	PZT5A	PZT5H
$\varepsilon_{33}^T/\varepsilon_0$	1300	1700	3400
$\varepsilon_{33}^S/\varepsilon_0$	635	830	1470
$\varepsilon_{11}^T/\varepsilon_0$	1475	1730	3130
$\varepsilon_{11}^S/\varepsilon_0$	730	916	1700
tan δ	0.004	0.02	0.02
c_{11}^E (10^{10} N/m^2)	13.9	12.1	12.6
c_{33}^E (10^{10} N/m^2)	11.5	11.1	11.7
c_{12}^E (10^{10} N/m^2)	7.78	7.54	7.95
c_{13}^E (10^{10} N/m^2)	7.43	7.52	8.41
c_{44}^E (10^{10} N/m^2)	2.56	2.11	2.30
c_{66}^E (10^{10} N/m^2)	3.06	2.26	2.35
v_3^D (m/s)	4600	4350	4560
v_4^D (m/s)	2630	2260	2375
v_4^E (m/s)	1850	1650	1750
e_{31} (C/m^2)	- 5.2	- 5.4	- 6.5
e_{33} (C/m^2)	15.1	15.8	23.3
e_{15} (C/m^2)	12.7	12.3	17.0
h_{31} (10^8 V/m)	- 9.2	- 7.3	- 5.05
h_{33} (10^8 V/m)	26.8	21.5	18.0
h_{15} (10^8 V/m)	19.7	15.2	11.3
k_P	- .58	- .60	- .65
k_{31}	- .33	- .34	- .38
k_{33}	.70	.70	.75
k_{15}	.71	.68	.67
k_t	.51	.48	.50
Q_M	500	75	65
N_1 (Hz.m)	1650	1400	1420
N_{3t} (Hz.m)	2000	1890	2000
ρ (10^3 kg/m^3)	7.5	7.75	7.5

Table A.1 Material properties of PZT4, PZT5A and PZT5H (From Venitron Ltd.)

B Lanczos method

The Lanczos method was originally proposed for the tridiagonalization of matrices (Bathe, 1983). Once the coefficient matrices of the generalized eigenproblem have been tridagonalized, the eigenvalues and vectors can be calculated effectively using the standard techniques for eigenproblems, such as vector iteration.

Consider the generalized eigenproblem as follows,

$$[K]\phi = \lambda[M]\phi \tag{B.1}$$

where [K], [M] are stiffness and mass matrices, λ and ϕ are eigenvalue and eigenvector. Let $\{x\}$ be an arbitrary starting vector, and let this vector be normalized with respect to the matrix [M] to obtain $\{x\}_1$,

$$\{x\}_1 = \frac{\{x\}}{\gamma} \quad \text{and} \quad \gamma = \sqrt{\{x\}^T [M] \{x\}} \tag{B.2}$$

In the Lanczos algorithm the vectors $x_2, x_3, \ldots\ldots, x_q$, are then calculated using the following equations for $i = 2, 3, \ldots\ldots, q$

$$\begin{aligned}
[K]\,\bar{x}_i &= [M]\,x_{i-1} \\
\alpha_{i-1} &= \bar{x}_i^T [M]\, x_{i-1} \\
\tilde{x}_i &= \bar{x}_i - \alpha_{i-1} x_{i-1} - \beta_{i-1} x_{i-2} \\
\beta_i &= \sqrt{\tilde{x}_i^T [M]\, \tilde{x}_i} \\
x_i &= \frac{\tilde{x}_i}{\beta_i}
\end{aligned} \tag{B.3}$$

where $\beta_1 = 0$.

The sequence of vectors x_i, $i = 1, 2, \ldots\ldots, q$, generated using the above relationship are M-orthonormal and the matrix $[X] = [\, x_1, x_2, \ldots\ldots, x_q \,]$ satisfies the following relationships

$$\begin{aligned}
&[X]^T [M] [X] = I \\
&[X]^T ([M][K]^{-1}[M])\, [X] = [T]_q
\end{aligned} \tag{B.4}$$

where $[T]_q$ is a tridiagonal matrix of order q,

$$[T]_q = \begin{bmatrix} \alpha_1 & \beta_2 & & & & \\ \beta_2 & \alpha_2 & \beta_3 & & & \\ & \cdot & \cdot & \cdot & & \\ & & \cdot & \cdot & \cdot & \\ & & & \beta_{q-1} & \alpha_{q-1} & \beta_q \\ & & & & \beta_q & \alpha_q \end{bmatrix} \tag{B.5}$$

Using (B.4) the eigenvalues and vectors of T_q can be related to the problem of (B.1). When q = n, (B.1) can be written as

$$\frac{1}{\lambda}[M]\,\phi = [M][K]^{-1}[M]\,\phi \tag{B.6}$$

and using the transformation matrix $[X] = [\, x_1, x_2, \ldots\ldots, x_q \,]$

$$\phi = [X]\,\phi^* \tag{B.7}$$

(B.6) can be written as

$$\frac{1}{\lambda}[X]^T[M][X]\,\phi^* = [X]^T([M][K]^{-1}[M])[X]\,\phi^*$$

Substitution of (B.4) into the above equation, gives

$$\frac{1}{\lambda}\phi^* = [T]_n\,\phi^* \tag{B.8}$$

Hence, (B.1) has been transformed into (B.8), which is a standard eigenvalue problem. The eigenvalues of $[T]_n$ are the reciprocals of the eigenvalues of the problem $[K]\phi = \lambda[M]\phi$, and the eigenvectors are related as given in (B.7).

C Bendent method to extract modal constants from the experimental data

A short description of the Bendent method and its application to extract modal constants from the measured electrical impedance of the piezoelectric discs is appended here. Detailed accounts can be found from Dobson (1985) and Ewins (1984).

A frequency response function in terms of receptance (displacement response/force excitation) between the j'th and k'th degrees of freedom is defined as

$$\alpha_{jk} = \frac{x_j}{f_k} = \sum_{r=1}^{N} \frac{{}_r(A+iB)_{jk}}{\omega_r^2 - \omega^2 + i\,\eta_r\omega_r^2} \qquad (C.1)$$

where x_j is the displacement response at the j'th degree of freedom; f_k is the force excitation at the k'th degree of freedom; ω_r is the natural frequency of the r'th mode; ω is the excitation frequency, η_r is the loss factor for the r'th mode; N is the total number of degrees of freedom and ${}_r(A+iB)_{jk}$ is the complex modal constant for the r'th mode.

Around the frequency band of the r'th mode, (C.1) can be written as a summation of a single term corresponding to the dominant r'th mode and a residual constant representing the contributions of the remaining modes,

$$\alpha_{jk} = \frac{{}_r(A+iB)_{jk}}{\omega_r^2 - \omega^2 + i\,\eta_r\omega_r^2} + \text{residual} \qquad (C.2)$$

The receptance at a selected frequency, Ω, within the frequency band from ω_L to ω_U around ω_r as shown in Fig A.1, can be written as

$$\alpha_\Omega = \frac{{}_r(A+iB)_{jk}}{\omega_r^2 - \Omega^2 + i\,\eta_r\omega_r^2} + \text{residual} \qquad (C.3)$$

Then the residual term can be eliminated by

$$\alpha - \alpha_\Omega = (A+iB)\left[\frac{1}{\omega_r^2 - \omega^2 + i\,\eta_r\omega_r^2} - \frac{1}{\omega_r^2 - \Omega^2 + i\,\eta_r\omega_r^2}\right] \qquad (C.4)$$

which can be rearranged as

$$\Delta = \frac{\omega^2-\Omega^2}{\alpha-\alpha_\Omega} = \frac{A-iB}{A^2+B^2}\left[(\omega_r^2-\omega^2)(\omega_r^2-\Omega^2) - \eta_r^2\omega_r^4 + i\,\eta_r\omega_r^2(2\omega_r^2-\omega^2-\Omega^2)\right] \qquad (C.5)$$

The quantity Δ is a linear function of ω^2, with real and imaginary parts,

$$\begin{aligned} Re(\Delta) &= m_R\omega^2 + c_R \\ Im(\Delta) &= m_I\omega^2 + c_I \end{aligned} \qquad (C.6)$$

where the slopes are given by

$$\begin{aligned} m_R &= \frac{-1}{A^2 + B^2}[A(\omega_r^2 - \Omega^2) + B\eta_r\omega_r^2] \\ m_I &= \frac{-1}{A^2 + B^2}[A\eta_r\omega_r^2 - B(\omega_r^2 - \Omega^2)] \end{aligned} \qquad (C.7)$$

By selecting (or sweeping) a series of "fixing" frequencies within the defined frequency band, a family of linear curves are obtained. These curves intersect at specific points defined by

$$\begin{aligned} m_R &= n_R\Omega^2 + d_R \\ m_I &= n_I\Omega^2 + d_I \end{aligned} \qquad (C.8)$$

where the slopes and intercepts are:

$$\begin{aligned} n_R &= \frac{A}{A^2 + B^2} \quad \text{and} \quad d_R = \frac{-\omega_r^2(A + B\eta_r)}{A^2 + B^2} \\ n_I &= \frac{-B}{A^2 + B^2} \quad \text{and} \quad d_R = \frac{-\omega_r^2(A\eta_r - B)}{A^2 + B^2} \end{aligned} \qquad (C.9)$$

Therefore modal parameters (A, B, ω_r, η_r) can be extracted from the above set of equations.

For the measured electrical impedance of piezoelectric discs, the response can be first converted into a receptance form as shown in (C.1), then the above procedure can be applied. From equation (3.70),

$$\alpha_Z = \frac{Q}{\varphi} = \sum_{r=1}^{N} \frac{{}_rA}{\omega_r^2 - \omega^2 + i\,\eta_r\omega_r^2} + H_{\varphi\varphi} \qquad (C.11)$$

where, Q, φ is the electrical charge and potential across the electrodes respectively, ${}_rA$ is the modal constant (real part only); $H_{\varphi\varphi}$, the static capacitance term in (C.11), can be regarded as an extra residual term.

The above receptance can be related to the measured electrical impedance as

$$\alpha_Z = \frac{1}{i\,\omega Z(\omega)} \qquad (C.12)$$

An example for extracting modal constants of the electrical FRF is shown in Fig A.2. The electrical frequency response function of the PZT5A disc with a D/T ratio of 20 in the frequency range 10 to 510 kHz was converted from the corresponding measured electrical impedance response and is plotted as dotted line in Fig A.2, together with the regenerated curve by using the extracted modal parameters. The excellent agreement between the measured and regenerated curves indicates that the analysis is very accurate. Fig A.3 shows the real and imaginary parts of Δ (delta) around resonant frequency of the first mode at 50 kHz as a function of ω^2.

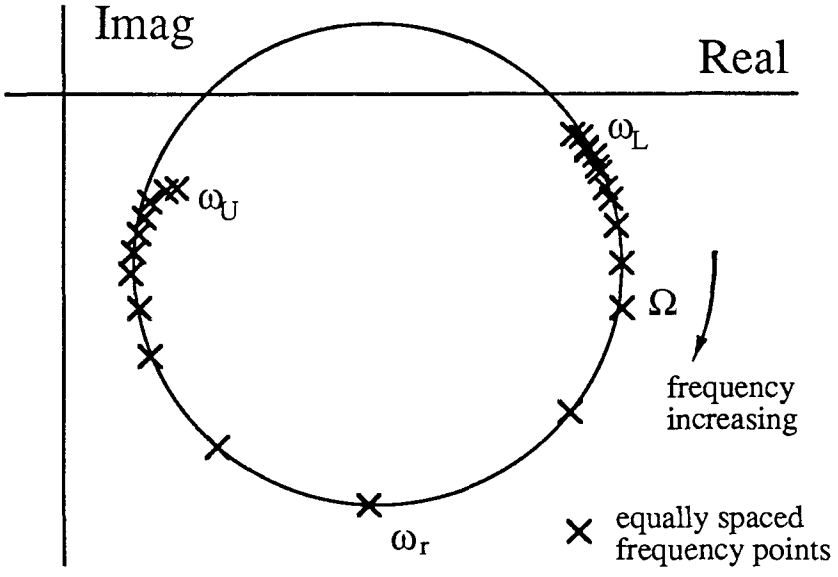

Fig A.1 Nyquist plot of the receptance around the frequency band of the resonance

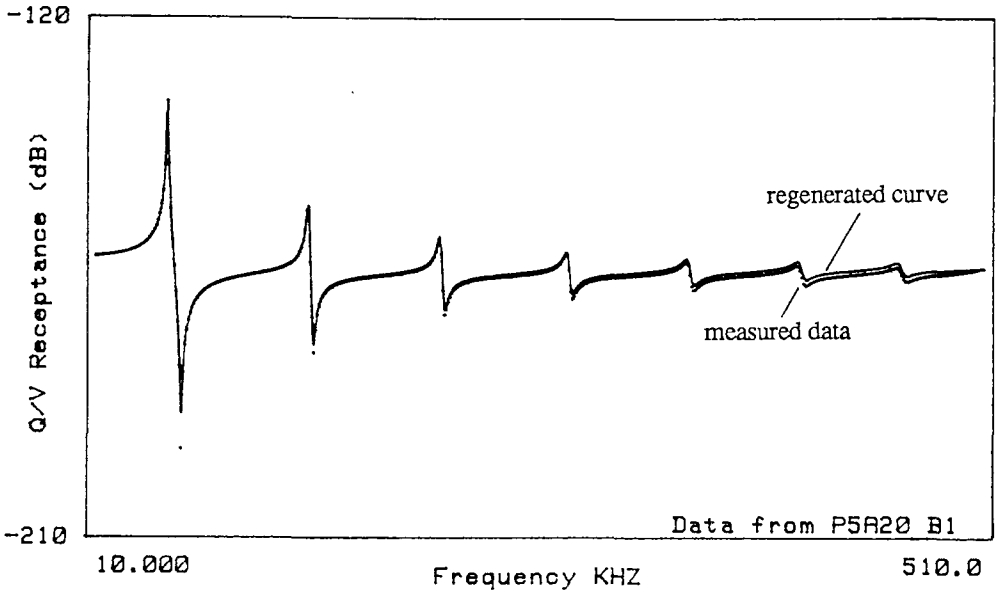

Fig A.2 The measured electrical receptance of a PZT5A disc with a D/T ratio of 20 from 10 to 510 kHz and the regenerated curve by using the extracted modal parameters (Dotted line: measured; Solid line: regenerated)

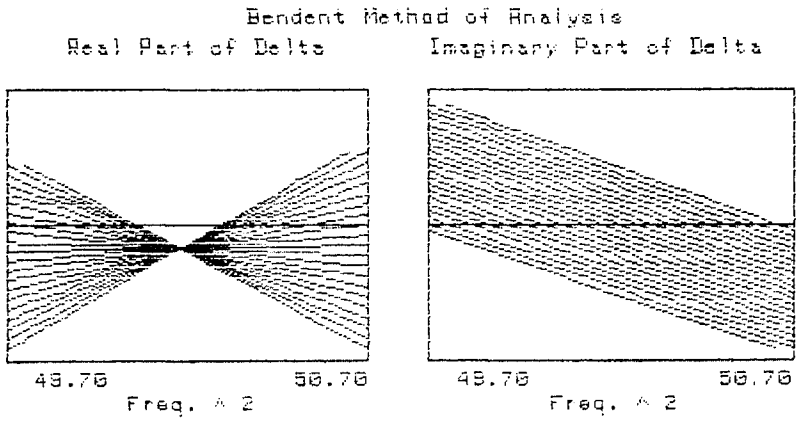

Fig A.3 The real and imaginary parts of Delta (as in (C.6)) as a function of ω^2 around the first resonant frequency at 50 kHz of the PZT5A disc with a D/T ratio of 20

Reference

Aggarwal, R.R., 1952a, "Axially symmetric vibrations of a finite isotropic disk. I", J. Acoust. Soc. Am., vol.24, pp463-467.

Aggarwal, R.R., 1952b, "Axially symmetric vibrations of a finite isotropic disk. II", J. Acoust. Soc. Am., vol.24, pp663-666.

Allik, H. and Hughes, T.J.R., 1970, "Finite element method for piezoelectric vibration" Int. J. Num. Meth. Eng., vol.2, pp151-157.

Allik, H. and Webman, K. M., Hunt, J.T., 1974, "Vibrational response of sonar transducers using piezoelectric finite elements", J. Acoust. Soc. Am., vol.56, pp1782-1791.

Allocca, J.A., and Stuart, A., 1984, "Transducers, theory and application", Reston Pub. Co., Virginia.

Armstrong, B.A., and McMahon, G.W., 1984, "Discussion of the finite-element modelling and performance of ring-shell projectors", IEE Proc., vol.131(3), pp275-279

Atalar, A. and Koymen, H., 1987, "Generation of focused surface waves with a solid wedge" Proc. IEEE Ultrasonic symposium, pp681-684.

Auld, B.A., 1973, "Acoustic fields and waves in solid", vols.I and II, Wiley, New York.

Baboux, J.C., Lakestani, F., and Perdrix, M., 1984, "Theoretical and experimental study of the contribution of radial modes to the pulsed ultrasonic field radiated by a thick piezoelectric disk", J. Acoust. Soc. Am., vol.75, pp1722-1731.

Banah, A.H., Korpel, A., and Vogel, R.F., 1983, "Feynman diagram analysis of transducer impulse response", J. Acoust. Soc. Am., vol.73, pp677-687.

Barker, J. R., 1964, "Mechanical and Electrical vibration", Methven & Co Ltd.

Barthe, P.G., and Benkeser, P.J., 1987, "A staircase model of tapered piezoelectric transducers", Proc. IEEE Ultrasonic symposium, pp697-700.

Bathe, H-J., 1982, "Finite element procedures in engineering analysis", Prentice-Hall., Inc., New Jersey.

Bechtel, S.E., and Bogy, D.B., 1984, "Interaction of a piezoelectric transducer with an elastic half-space", Int. J. Solids Structure, vol.20, pp809-828.

Bettess, P., and Bettess, J.A., 1984, "Infinite elements for static problems", Eng. Compt., vol.1, pp4-16.

Berlincourt, D.A., Curran, D.R., and Jaffe, H., 1964, "Piezoelectric and piezomagnetic materials and their function in transducers", Physical acoustics, vol.1A, pp169-270.

Bogy, D.B., and Miu, D.K-K., 1982, "Transient voltage across axisymmetrically loaded piezoelectric disks with electroded faces", J. Acoust. Soc. Am., vol.71, pp487-497.

Bogy, D.B., and Bechtel,S.E., 1982, "Electromechanical analysis of nonaxisymmetrically loaded piezoelectric disks with electroded faces", J. Acoust. Soc. Am., vol.72, pp1498-1507.

Bond, L.J., Jayasundere, N., Sinclair, D.A. and Smith, I.R., 1982, "Investigation of Ultrasonic Transducers as used for Non-Destructive Testing", Review of Progress in Quantitative NDE, vol.1, pp691-699.

Boucher, D., Lagier, M., and Maerfeld, C., 1981, "Computation of the vibrational modes for piezoelectric array transducers using a mixed finite element-perturbation method", IEEE Trans. Son. Ultrason., SU-28(5), pp318-330.

Brittain, R.H., and Weight, J.P., 1987, "Fabrication of non-uniformly excited wide-band ultrasonic transducers", Ultrasonics, vol.25, pp100-106.

Bugdayci, N., and Bogy, D.B., 1981, "A two-dimensional theory for piezoelectric layers used in electro-mechanical transducers-I Derivation", Int. J. Solids Structure, vol.17, pp1159-1178.

Challis, R.E., and Harrison, J.A., 1983, "Rapid solutions to the transient response of piezoelectric elements by Z-transform techniques", J. Acoust. Soc. Am., vol.74, pp1673-1680.

Desilets, C.S., Fraser, J.D. and Kino, G.S., 1978, "The design of efficient broad-band piezoelectric transducers", IEEE Trans. Son. Ultrason., vol.SU-25(3), pp115-125.

Dobson, B.J., 1987, "A straight-line technique for extracting model properties from frequency response data", Mech. Sys. & Sigl. Procs., vol.1(1), pp29-40.

Eer Nisse, Errol P., 1967a, "Resonances of one-dimensional composite piezoelectric and elastic structures", IEEE Trans. Son. Ultrason., SU-14(2), pp59-67.

Eer Nisse, Errol P., 1967b, "Variational method for electroelastic vibration analysis", IEEE Trans. Son. Ultrason., SU-14(4), pp153-160.

Ewins, D.J., 1984, "Modal testing theory and Practice", Research Studies Press, Letchworth, UK.

Filipczynski, L., 1975, "Transient, equivalent circuit and negative capacitance of a piezoelectric transducer performing thickness vibrations", J. Tech. Phys., vol.16, pp121-135.

Friedrich, W., Lerch, R., and Krammer, P., 1989, "Analysis of fluid-structural interaction for piezoelectric ultrasonic transducers using the finite element method", Proc. Ultrason. Int. '89, Spain.

Furgason, E.S., and Newhouse, V.L., 1973, "Convolution and Correlation using nonlinear interactions of Lamb waves", IEEE Trans. Son. Ultrason., SU-20(4), pp360-364.

Gazis, D.C., and Mindlin, R.D., 1960, "Extensional vibrations and waves in a circular disk and a semi-infinite plate", ASME J. Appl. Mechs., vol.27, pp541-547.

Guyott, C.C.H., Cawley, P., and Adams, R.D., 1986, "Vibration characteristics of the MK II Fokker Bonder Tester probe", Ultrasonics, vol.24, pp318-324.

Hayman, A.J., and Weight, J.P., 1979, "Transmission and reception of short ultrasonic pulses by circular and square transducers", J. Acoust. Soc. Am., vol.66, pp945-951.

Hayward, G., 1981, "Time and frequency domain modeling of the piezoelectric transducer", PhD thesis, University of Strathclyde, UK.

Hayward, G., MacLeod, C.J., and Durrani, T.S., 1984, "A systems model of the thickness mode piezoelectric transducer", J. Acoust. Soc. Am., vol.76, pp369-382.

Hilke, H.J., 1973, "Piezoelectric transducer vibrations in a one-dimensional approximation", Appl. Phys., vol.1, pp317-329.

Hitchings, D., 1984, "FINEL Reference manual", Imperial College, UK.

Hossack, J., Hayward, G., and Gillies, D., 1987, "A new method for element analysis in piezoceramic arrays", Proc. Ultrason. Int. '87, pp477-482.

Hsu, N.N., Chen, G., and Sansalone, M., 1987, "Characterization of a piezoelectric transducer coupled to a solid", Proc. IEEE Ultrasonic symposium, pp689-692.

Hutchins, D.A., Palmer, S.B., Bresse, L.F., and Mair, H.D., 1987, "Thick conical piezoelectric transducers for NDE", Proc. IEEE Ultrasonic symposium, pp685-688.

Ikegami, S., Ueda, I., and Kobayashi, S., 1974, "Frequency spectra of resonant vibration in disk plates of $PbTiO_3$ piezoelectric ceramics", J. Acoust. Soc. Am., vol.55, pp339-344.

Ikegami, S., Nagate, T., and Nakajima, Y., 1976, "Frequency spectra of extensional vibration in $Pb(ZrTi)O_3$ disks with Poisson's ratio larger than 1/3", J. Acoust. Soc. Am., vol.60, pp113-116.

IRE Standards on piezoelectric crystals, 1961, "Measurement of piezoelectric ceramics", Proc. IRE, vol.49, pp1161-1169.

Jacobsen, E.H., 1960, "Sources of sound in piezoelectric crystals", J. Acoust. Soc. Am., vol.32, pp949-953.

Jensen, H., 1986, "Calculations for piezoelectric ultrasonic transducers", Report, RISO-R-536.

Kagawa, Y., 1971, "A new approach to analysis and design of electromechanical filters by finite-element technique", J. Acoust. Soc. Am., vol.49, pp1348-1356.

Kagawa, Y. and Yamabuchi, T., 1976a, "A finite element approach to electromechanical problems with an application to energy-trapped and surface-wave devices", IEEE Trans. Son. Ultrason., SU-23(4), pp263-272.

Kagawa, Y. and Yamabuchi, T., 1976b, "Finite element approach for a piezoelectric circular rod" IEEE Trans. Son. Ultrason., SU-23(6), pp379-385.

Kane, T.R., and Mindlin, R.D., 1956, "High-Frequency extensional vibrations of plates", ASME J. App. Mechs., vol.23, pp277-283.

Kazhis, R.I., and Lukoshevichyus, A.I., 1976, "Wideband piezoelectric transducers with an inhomogeneous electric field", Sov. Phys. Acoust., vol.22(2), pp166-168.

Kossoff, G., 1966, "The effects of backing and matching in the performance of piezoelectric ceramic transducer", IEEE Trans. Son. Ultrason., SU-13(1), pp20-30.

Krammer, P., 1989, "Interferometric surface displacement measurements of piezoelectric transducers", Proc. Ultrason. Int. '89, Spain.

Krautkramer, J., Krautkramer, H, 1983, "Ultrasonic testing of materials", Third edition, Springer-Verlag, New York.

Krimholtz, R., Leedom, D.A., and Matthaei, G.L., 1970, "New equivalent circuits for elementary piezoelectric transducers", Electronics Letters, vol.6(13), pp398-399.

Kwun, H., Jolly, W.D., Light, G.M., and Wheeler, E., 1988, "Effects of variations in design parameters of ultrasonic transducers on performance characteristics", Ultrasonics, vol.26, pp65-72.

Lerch, R., and Kaarmann, H., 1987, "Three-dimensional finite element analysis of piezoelectric media", Proc. IEEE Ultrasonics Symposium, pp853-858.

Locke, S., Kunkel, H.A., and Pikeroen, B., 1987, "Finite element modelling of piezoelectric ceramic disks", Proc. IEEE Ultrasonics Symposium, pp701-706.

Low, G.C. and Jones, R.V., 1984, "Design and construction of short pulse ultrasonic probes for non-destructive testing", Ultrasonics, vol.22, pp85-95.

Low, G.C., 1980, "A simple computer method for predicting the transient response of ultrasonic NDT probes", NDT Int., vol.13, pp285-290.

Ludwig, R., and Lord, W, 1988, "A finite-element study of ultrasonic wave propagation and scattering in an aluminium block", Mat. Eval., vol.46, pp108-113.

Martin, R.W., 1975, "Force and electrical Thevenin equivalent circuits and simulations for thickness mode piezoelectric transducers", J. Acoust. Soc. Am., vol.58, pp475-489.

Mason, W.P., 1948, "Electromechanical transducers and wave filters", Second edition, D. Van. Nostrand Company Inc.

Meeker, T.R., 1972, "Thickness mode piezoelectric transducer", Ultrasonics, vol.10, pp26-36.

Meitzler, A.H., O'Bryan Jr, H.M., and Tiersten, H.F., 1973, "Definition and measurement of radial mode coupling factors in piezoelectric ceramic materials with large variations in Poisson's ratio" IEEE Trans. Son. Ultrason., SU-20(3), pp233-239.

Mindlin, R.D., and Medick, M.A., 1959, "Extensional vibrations of elastic plates", ASME J. Appl. Mechs., vol.26, pp561-569.

Moss, B.C., 1982, "Laser interferometry", AERE report No.10417.

Naillon, M., Coursant, R.H., and Besnier, F., 1983, "Analysis of piezoelectric structures by a finite element method", ACTA ELECTRONICA, vol.25, pp341-362.

O'Donnell, M., Busse, L.J., and Miller, J.G., 1981, "Piezoelectric transducers", Physical Acoustics, vol.15, pp29-65.

Olson, L.G., and Bathe, K.J., 1985, "An infinite element for analysis of transient fluid-structure interactions", Eng. Compt., vol.2, pp319-329.

Olson, L.G., and Bathe, K.J., 1985, "Analysis of fluid-structure interactions. A direct symmetric coupled formulation based on the fluid velocity potential", Computers & Structures, vol.21, pp21-32.

Onoe, M., and Tiersten, H.F., Meitzler, A.H., 1963, "Shift in the location of resonant frequencies caused by large electromechanical coupling in thickness-mode resonators", J. Acoust. Soc. Am., vol.35, pp36-42.

Ostergaard, D.F., and Pawlak, T.P., 1986, "Three-dimensional finite elements for analyzing piezoelectric structures" Proc. IEEE Ultrasonics Symposium, pp639-644.

Pialucha, T., Guyott, C.C.H., and Cawley, P., 1989, "Amplitude spectrum method for the measurement of phase velocity", Ultrasonics, vol.27, pp270-279.

Randall, R.B., 1977, "Frequency analysis", Application of B&K equipment, Bruel&Kjaer.

Redwood, M., 1961, "Transient performance of a piezoelectric transducer", J. Acoust. Soc. Am., vol.33, pp527-536.

Redwood, M., 1963, "A study of waveforms in the generation and detection of short ultrasonic pulses", Appl. Mater. Res., vol.2, pp76-84.

Redwood, M., 1964, "Experiments with the electrical analog of a piezoelectric transducer", J. Acoust. Soc. Am., vol.36, pp1872-1880.

Sachse, W., and Hsu, N.N., 1979, "Ultrasonic transducers for materials testing and their characterization", Physical acoustics, vol.14, pp277-406.

Sharan, S.K., and Gladwell, G.M.L., 1985, "A general method for the dynamic response analysis of fluid-structure systems", Computers & Structures, vol.21, pp937-943.

Shaw, E.A.G., 1956, "On the resonant vibrations o thick Barium Titanate Disks", J. Acoust. Soc. Am., vol.28 pp39-50.

Silk, M.G., 1983, "Predictions of the effect of some constructional variables on the performance of ultrasonic transducer", Ultrasonics, vol.21, pp27-33.

Silk, M.G., 1984, "Ultrasonic Transducers for Nondestructive Testing", Adam Hilger Ltd, Bristol.

Sittig, E.K., 1969, "Design and technology of piezoelectric transducers for frequencies above 100 MHz", Physical acoustics, vol.4, pp221-275.

Smith, R.R., Hunt, J.T., and Barach, D., 1973, "Finite element analysis of acoustically radiating structures with applications to sonar transducers", J. Acoust. Soc. Am., vol.54, pp1277-1288.

Smith, W.M.R., and Awojobi, A.O., 1979, "Factors in the design of ultrasonic probes", Ultrasonics, vol.17, pp20-26.

Solartron, 1987, "Manual, 1255 high frequency analyser".

Stepanishen, P.R., 1971, "Transient radiation from pistons in an infinite planar baffle", J. Acoust. Soc. Am., vol.49, pp1629-1638

Stuetzer, O.M., 1967, "Multiple reflections in a free piezoelectric plate", J. Acoust. Soc. Am., vol.42, pp502-508.

Stuetzer, O.M., 1968, "Impulse response measurement technique for piezoelectric transducer arrangements", IEEE Trans. Son. Ultrason., SU-15(1), pp13-17.

Tiersten, H.F., 1969, "Linear Piezoelectric Plate Vibrations", Plenum Press, New York.

Tiersten, H.F., 1970, "Electromechanical coupling factors and fundamental material constants of thickness vibrating piezoelectric plates", Ultrasonics, vol.8, pp19-23.

Ueha, S., Sakuma, S., and Mori, E., 1983, "Measurement of vibration velocity distributions and mode analysis in thick disks of Pb(Zr.Ti)O3", J. Acoust. Soc. Am., vol.73, pp1842-1847.

Uygur, E. M., 1979, "Nondestructive Dynamic Testing", Re.Tech. in NDT, vol.8, pp205-244.

Venitron Ltd., 1976, "Piezoelectric ceramic data".

Vopilkin, A.Kh., 1987, "Design and development of broadband axisymmetrical piezoelectric transducers of variable thickness", Sov. J. NDT, vol.23-4, pp265-273

Williams, J.H., and Doll, B., 1982, "A Simple wave propagation analysis of piezoelectric ultrasonic transducer response", Mat. Eval., vol.40, pp1374-1381.

Wilson, E.L., and Khalvati, M., 1983, "Finite elements for dynamic analysis of fluid-solid systems", Int. J. Num. Meth. Eng., vol.19, pp1657-1668.

Winnicki, R.T., and Auyer, S.E., 1977, "Geometric factors affecting hydrophone performance", J. Acoust. Soc. Am., vol.61, pp876-881.

Wustenberg, H., Rotter, B., Erhard, A., Mohrle, W., and Pitkanen, J., 1989, "A parametric study of ultrasonic probes with PVDF transducers", Proc. 12th WCNDT, pp691-698.

Ying, C.F., Li, M.X., and Zhang, H.L., 1981, "Computations and measurements of transient stress waves and electrical voltages generated by transmitting ultrasonic piezoelectric transducers", Ultrasonics, vol.19, pp155-158.

Zhang, H.L., Li, M.X., and Ying, C.F., 1983, "Complete solutions of the transient behaviour of a transmitting thickness-mode piezoelectric transducer and their physical interpretations", J. Acoust. Soc. Am., vol.74, pp1105-1114.

Zienkiewicz, O.C., 1971, "The finite element method in engineering science", Second edition, McGraw-Hill, New York.

Zienkiewicz, O.C., Emson, C., and Bettess, O., 1982, "A novel boundary infinite element", Int. J. Num. Meth. Eng., vol.19, pp393-404.